STRENGTHENING OF SHEAR CRITICAL REINFORCED CONCRETE COLUMNS BY STEEL-ROD COLLARS

Miss Phawe Suit Theint

จุฬาลงกรณ์มหาวิทยาลัย
CHULALONGKORN UNIVERSITY

A Dissertation Submitted in Partial Fulfillment of the Requirements
for the Degree of Doctor of Philosophy in Civil Engineering
Department of Civil Engineering
Faculty of Engineering
Chulalongkorn University
Academic Year 2018
Copyright of Chulalongkorn University

การเสริมกำลังเสาคอนกรีตเสริมเหล็กที่วิบัติแบบเฉือนโดยใช้ปลอกเหล็กชนิดเหล็กเส้น

น.ส.พาว์ สูท เทียน

Thesis Title	STRENGTHENING OF SHEAR CRITICAL REINFORCED CONCRETE COLUMNS BY STEEL-ROD COLLARS
By	Miss Phawe Suit Theint
Field of Study	Civil Engineering
Thesis Advisor	Associate Professor Anat Ruangrassamee

Accepted by the Faculty of Engineering, Chulalongkorn University in Partial Fulfillment of the Requirement for the Doctor of Philosophy

.... Dean of the Faculty of Engineering
(Associate Professor SUPOT TEACHAVORASINSKUN)

DISSERTATION COMMITTEE

.... Chairman
(Associate Professor TOSPOL PINKAEW, Ph.D.)

.... Thesis Advisor
(Associate Professor Anat Ruangrassamee)

.... Examiner
(Assistant Professor CHATPAN CHINTANAPAKDEE, Ph.D.)

.... Examiner
(Assistant Professor PITCHA JONGVIVATSAKUL, Ph.D.)

.... External Examiner
(Lecturer Jarun Srechai, Ph.D.)

จุฬาลงกรณ์มหาวิทยาลัย
CHULALONGKORN UNIVERSITY

พาว์ สูท เทียน :   การเสริมกำลังเสาคอนกรีตเสริมเหล็กที่วิบัติแบบเฉือนโดยใช้ปลอกเหล็กชนิด เหล็กเส้น. (STRENGTHENING OF SHEAR CRITICAL REINFORCED CONCRETE COLUMNS BY STEEL-ROD COLLARS) อ.ที่ปรึกษาหลัก : อาณัติ เรืองรัศมี

      กำลังรับแรงเฉือนที่ไม่เพียงพอสำหรับอาคารที่เก่าและตั้งอยู่ในพื้นที่เสี่ยงต่อแผ่นดินไหวส่งผลให้อาจเกิดการวิบัติแบบเฉือน ในการศึกษานี้ได้พัฒนาการเสริมกำลังของเสาคอนกรีตเสริมเหล็กด้วยปลอกเหล็กชนิดเหล็กเส้น โดยในชุดประกอบด้วยเหล็กรูปพรรณหน้าตัดฉากเสริมที่มุมเสาและยึดกันด้วยเหล็กเส้นเกลียว เสาทดสอบแบ่งเป็นเสาควบคุมที่ไม่มีการเสริมกำลัง 1 ต้น และเสาที่มีการเสริมกำลังอีก 2ต้น เสาตัวอย่างได้ทำการทดสอบโดยให้แรงในแนวดิ่งคงที่ และทำการให้การเคลื่อนที่ในแนวด้านข้างสลับไปมาเพื่อศึกษาผลของปริมาณของปลอกเหล็กชนิดเหล็กเส้นที่เสริมกำลัง จากการทดสอบพบว่าเสาที่ไม่มีการเสริมกำลังเกิดการวิบัติด้วยแรงเฉือน และมีอัตราการเคลื่อนที่ด้านข้าง 2% ส่วนเสาที่ทำการเสริมกำลัง มีการวิบัติในรูปแบบของแรงดัดและยังสามารถมีกำลังรับแรงทางด้านข้างที่สูงขึ้น รวมถึงคุณสมบัติด้านความเหนียวและการสลายพลังงานก็สูงขึ้น และรับการเคลื่อนที่ด้านข้างได้ 5% การศึกษานี้ยังได้พัฒนาแบบจำลองตัวอย่างทดสอบด้วยโปรแกรม OpenSees โดยได้เทียบกับผลการทดสอบ โดยพบว่าแบบจำลองได้ผลใกล้เคียงกับการทดสอบ

สาขาวิชา	วิศวกรรมโยธา	ลายมือชื่อนิสิต	
ปีการศึกษา	2561	ลายมือชื่อ อ.ที่ปรึกษาหลัก	

5571456021 : MAJOR CIVIL ENGINEERING
KEYWOR
D:

STRENGTHENING, REINFORCED CONCRETE COLUMNS,
STEEL JACKETING, NUMERICAL ANALYSIS

Phawe Suit Theint : STRENGTHENING OF SHEAR CRITICAL REINFORCED CONCRETE COLUMNS BY STEEL-ROD COLLARS. Advisor: Assoc. Prof. Anat Ruangrassamee

The inadequate shear strength of the existing old reinforced concrete columns located in the seismically active areas can lead the catastrophic shear failure. In this study, strengthening of shear-critical reinforced concrete columns by the steel-rod collar method is investigated. This proposed method is less intrusive to the existing building components. The steel-rod collar comprises the four sets of welded steel angles connected by steel-rods threaded at the ends. The three specimens were divided into one unstrengthened column, and the two strengthened columns. All the specimens were tested under the constant axial load and the reversed cyclic loadings. In addition, the specimens were the vertical cantilever type and used the same section properties. The number of steel-rod collar installed on the strengthened columns were the main parameter in this study. The unstrengthened column failed in shear failure mode and the diagonal shear cracks occurred at a drift ratio of 2%, whereas, the two strengthened columns failed in flexural mode and had an increase in the lateral load capacity, the ductility and the energy dissipation capacity than the unstrengthened column. The difference between the two strengthened specimens were the number of steel-rod collars mounted on the specimens. The spacing of steel-rod collars was 200 cm in the SC-200 specimen while that of the other strengthened specimen, SC-100 was 100 cm. After testing the strengthened columns failed in flexure and they had an increase in the lateral load capacity and the ductility. The drift ratio of both specimens reached 5%. Furthermore, the finite element models for all specimens were developed using the OpenSees program. The forced based beam column element with a shear spring was established to detect the behavior of the unstrengthened column. The lumped plasticity model was used to detect the behaviour of strengthened columns. The comparison results showed that the predicted numerical responses were in close agreement with test results.

Field of Study:	Civil Engineering	Student's Signature
		....
Academic Year:	2018	Advisor's Signature
		....

ACKNOWLEDGEMENTS

TABLE OF CONTENTS

Page

LIST OF TABLES

LIST OF FIGURES

Page

CHAPTER 1
INTRODUCTION

1.1. Background and Research Significant

Reinforced concrete columns require special design and detailing considerations to perform effectively when the earthquake exposure. Insufficient transverse reinforcements in reinforced concrete columns lead to the shear failure during earthquakes. Shear failure can cause a reduction in building lateral strength, loss of axial load carrying capacity and the building collapse. Existing reinforced concrete building columns constructed before 1970s were exposed to two major deficiencies: inadequate shear strength due to the low transverse reinforcement and inadequate flexural strength and ductility due to an inadequate lap splice in the longitudinal reinforcement (Aboutaha et al., 1999). A survey configuration irregularities of typical old existing multi-storey concrete building in Thailand in 2007 was conducted and it was found that shear failure had a higher tendency to occur in the lowest zone of mid-rise and high-rise building columns although the flexural failure was found in beam structures. Inspection of the transverse reinforcement ratio indicated that the columns in existing buildings in Thailand in 2007 have a very low confinement level, which was the rage of 0.006-0.009 for all zones of the building (Chaiyapat, 2007).

Reinforced concrete columns are the primary load bearing structural components in buildings. Therefore, there are needs to improve the strength, stiffness and ductility if they are seismically deficient columns. During the past decades, extensive experimental studies were carried out by many researchers using the strengthening methods such as concrete jacketing, steel jacketing, and fiber reinforced polymer jacketing (FRP) to increase the strength and ductility of the columns. Among them, a steel jacketing method is one of the least time consuming. Therefore, numerous researchers had focused on developing the steel jacketing methods in several ways during the decades.

Various kind of steel jacketing methods are steel plate or corrugated steel jacketing, batten and angle jacketing, rectified steel jacketing, precamnbered steel plate

jacketing and steel collar steel jacketing methods. The steel plate or corrugated steel jacketing method where the steel plates are installed in the plastic hinge regions or over the entire length of the column and the plates connected by welding (e.g. (Priestley et al., 1994), (Chai et al., 1994), (Tsai and Lin, 2002),(Ghobarah et al., 1997), (Aboutaha et al., 1999), (Griffith et al., 2005)). Without using the steel plate jacketing method, (Nagaprasad et al., 2009), (Adam et al., 2007), (Elsamny et al., 2013), (Belal et al., 2015), (Tarabia and Albakry, 2014), (Campione et al., 2017) investigated the behavior and the efficiency of reinforced concrete columns strengthened by using steel angles and battens. Unlike the other researchers, (Wang et al., 2017) studied the seismic behavior of preloaded rectangular RC columns strengthened with precambered steel plates under high axial load ratios and severe lateral reverse cyclic loading. To avoid the steel jacketing bulging in the plastic hinge area, (Xiao and Wu, 2003) proposed the rectified steel jacket technique which was adding stiffeners in the plastic hinge zones to the steel plate jacketing columns. According to their test results, retrofitting the columns by above steel jacketing methods exhibited the increase in strength and the ductility of the columns even though their methods had some drawbacks.

A relatively simple rehabilitation scheme for reinforced concrete column using external steel collars has been proposed by (Rodrigues et al., 2016), (Hussain and Driver, 2005) and (J. Liu et al., 2011). The experimental results showed excellent improvement in ductility, strength, and energy dissipation capacity of the columns due to the presence of the collars.

Although the abilities of various steel jacketing methods on strengthening the RC columns are confirmed by many researchers with experimental studies, some requirements are still needed (1) to be easy to install for rehabilitation (2) to be easy to install for the columns with masonry infilled walls (3) to be a cost effective method. In order to fulfil these requirements, the steel-rod collar jacketing method is introduced in the present study as the alternative shear reinforcement to improve the shear strength of the shear deficient columns and to provide additional confinement to the concrete core. The installation of the proposed method is simple not only for the isolated columns, but also for masonry-infilled frame structures. When the columns with infilled wall are strengthened by this method, no need to break the wall and just drilling the

wall and install the steel-rods simply. The steel collars are simply connected with the steel-rods which are attached level by level along the column height from the base of the column. Therefore, it can be said that the method is less intrusive to existing buildings The typical shear critical column strengthened with steel-rod collars is shown in Figure 1.1a. To fabricate a steel-rod collar, four sets of welded steel angles are prepared at column corners and connected by steel rods which tighten by bolts at the ends. Figure 1.1b shows the configuration of the steel-rod collars in the typical column. Figure 1.1c illustrates the installation of steel-rod collars to the columns with masonry infilled wall. Figure 1.2 demonstrated the masonry infilled wall with strengthened column. The aim of the study is to investigate the behavior of the shear critical columns strengthened by the steel-rod collars and to verify the effectiveness of the proposed strengthening method with The experimental program. Additionally, the finite element models for test specimens subjected to constant axial load and the lateral cyclic loading are established using the OpenSees program and then the numerical results are compared with the experimental results.
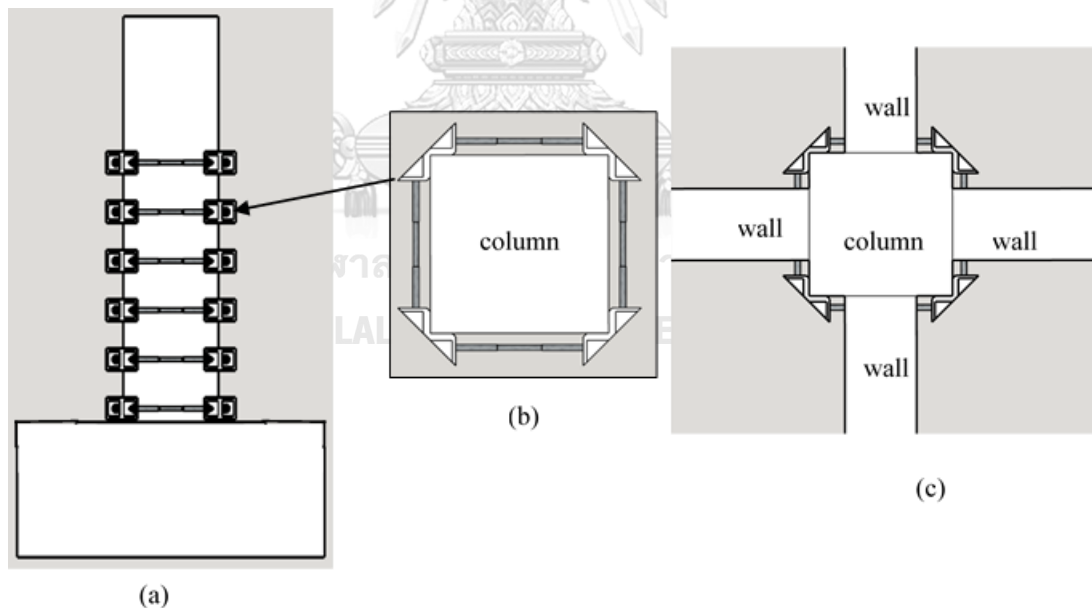
Figure 1.1 Typical strengthened column (b) steel rods-collars (c) Setting up
the steel-rod collars in the column with masonry infill wall
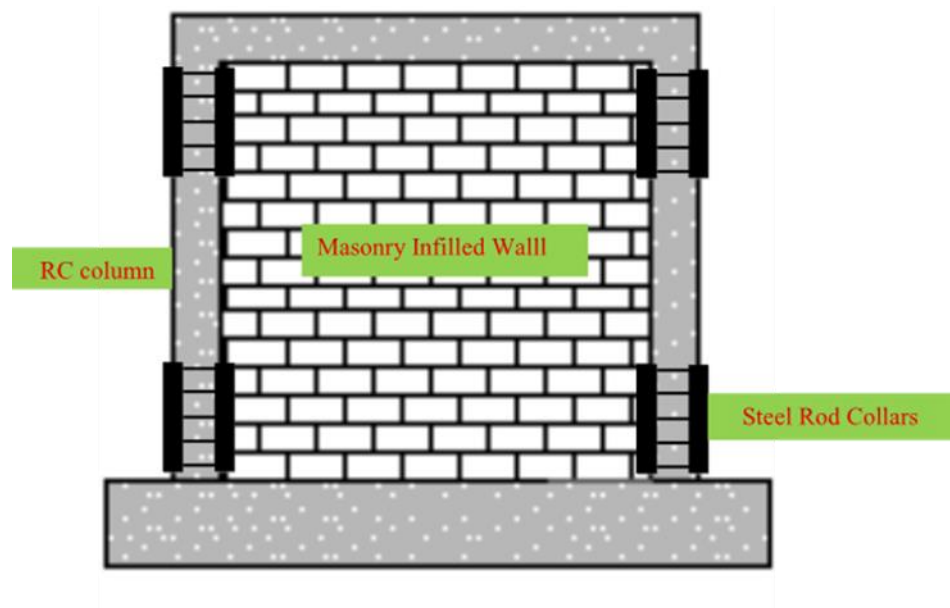
Figure 1.2 Masonry infilled wall with strengthened column by steel-rod collars

1.2. Objectives of the research

This research focuses on investigating the structural behaviour of the unstrengthened and strengthened columns with steel-rod collars under constant axial load and cyclic loading so as to utilize for seismic resistance. Although experimental studies are mainly emphasized, numerical analysis of the shear critical column and strengthening columns are also performed. Therefore, the main objectives of the research become;

1. To study the structural behaviour of unstengthened and strengthened reinforced concrete columns with steel-rod collar under constant and cyclic loading.

2. To perform the numerical analysis of unsterngthened column and strengthened columns which are implemented in OpenSees program.

3. To compare the accuracy of the numerical analysis results with experimental results of the unstrengthened column and strengthened columns.

1.3. Scope of the Research

The structural response of the unstrengthened column and strengthened columns is evaluated. Both experimental and numerical approaches are conducted in this research. In experimental approaches

1. Three columns are tested: one unstrengthened column and two strengthened columns.

2. Cantilever column type is chosen with the identical dimension for all the specimens.

3. Constant axial load and displacement controlled lateral cyclic loading are applied to all the tested specimen.

4. Same diameter of rods and same size of steel angles are used to make the steel rod collars and the number of steel rod collars in the strengthened columns are the main parameter.

5. Analytical study of the tested specimens will be accomplished with the aid of OpenSees program.

1.4. Research methodology

In order to achieve the objectives of the research mentioned above, the following procedures are conducted.

1. Review the background of steel jacketing methods and propose the appropriate jacketing method for the columns in this research.

2. Review the research building in Thailand which had been surveyed form one of the researcher to decide the structural parameters for columns.

3. Review the shear strength equations in order to apply the appropriate shear strength equation for unstrengthened columns and to propose the shear strength equation for strengthened columns.

4. Calculate the steel angle design and steel rods. And then steel rod collars are tested under tensile loading.

5. One unstrengthened specimen and two strengthened specimens with the proposed strengthening system are tested in the laboratory.

6. The experimental data were processed and the results are discussed.

7. Review the analytical models for reinforced concrete columns that failed in shear critical mode, flexural-shear mode and flexural mode.

8. An appropriate analytical model for unstrengtheend columns and strengthened columns are selected and the numerical analysis is performed in OpenSees program. The results from the numerical analysis are discussed and compared with the experimental results.

1.5. Outline of Dissertation

This thesis composed of six chapters which are briefly discussed as follows.

Chapter 1 gives the background of shear critical columns and various kinds of steel jacketing methods. This chapter also includes the research significance, objectives, scopes of the study and also research methodology.

Chapter 2 includes the literature review on steel jacketing methods, material model and the analytical modelling of the unstrngthened and strengthened columns.

Chapter 3 includes the test set up and discussion of experimental results.

Chapter 4 describes the comparison of three column specimens.

Chapter 5 presents the numerical analysis of the specimens in OpenSees program and the results are compared with experimental results.

Chapter 6 is the last chapter of this research which concludes the study results. Recommendation for future research are also described in this chapter.

CHAPTER 2

LITERATURE REVIEW

2.1. Introduction

This chapter provides an overview of previous experimental researches on strengthening of reinforced concrete columns using external steel jacketing methods and behavior of reinforced concrete columns and also presents the shear strength model to predict the strength of columns proposed by the previous researchers. In addition, analytical modeling of the reinforced concrete column also reviewed.

2.2. Study on the Previous Research of Strengthening Columns

Reinforced concrete jacketing is a traditional and one of the most common methods to retrofit and/or repair reinforced concrete columns. The additional cross-section area helps the column transfer more load while providing additional confinement. Reinforced concrete jackets can have multiple interface mechanisms to facilitate the transfer of loads from the original column to the jacket. According to the previous research and background, various types of steel jacketing methods are addressed. Generally, types of steel jacketing methods found in the literature are steel plate jacketing method, angle and batten jacketing methods, precambered steel plating method, corrugated steel jacketing method, rectified steel jacketing method, and steel collar jacketing method.

2.2.1. Steel plate jacketing methods

Many experimental research programs are needed to study the effect of the strengthening methods, especially steel jacketing method to the reinforced concrete columns. To fulfill these requirements, (Priestley et al., 1994) conducted a theoretical and experimental investigation to study the shear failure mode of reinforced concrete circular or rectangular bridge columns full-height retrofitted by circular or elliptical jackets as shown in Figure 2.1. The jacket was applied to the circular and rectangular

columns with cyclic load and different loads applied, aspect ratios, reinforcing, jacket thickness, and jacket strength. Test column details and summary of experimental results are shown in Table 2.1 and Table 2.2.
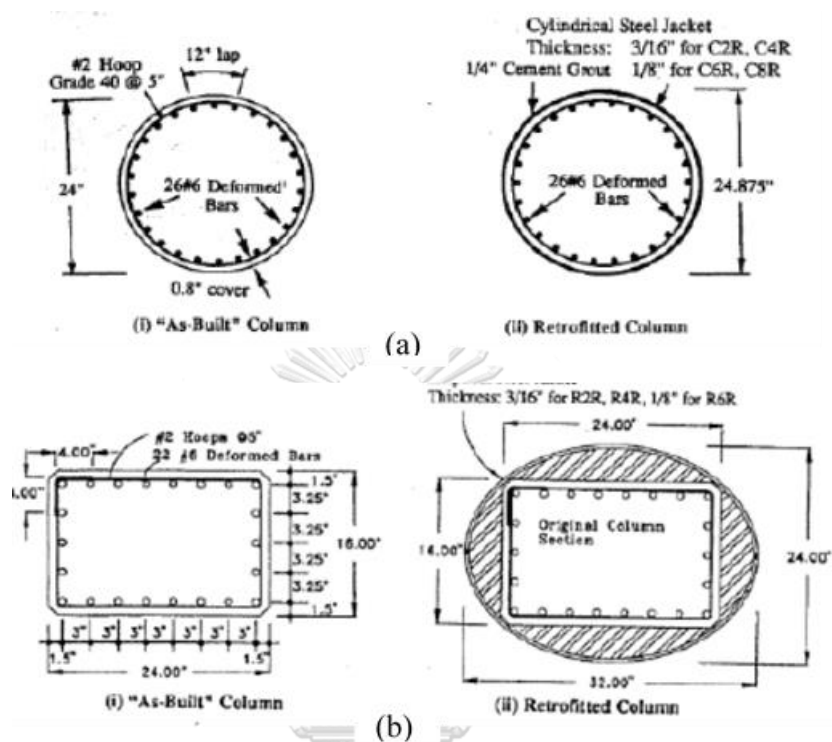
Figure 2.1 Reinforcement detail of test column (a) circular column

(b) rectangular column, (Priestley et al., 1994)

Table 2.1 Test column details (Priestley et al., 1994)

Test unit	Aspect ratio M/VD	Axial load P, kips	f'_c, ksi	Pf'_c/A_g	Longitudinal reinforcing bar (26 # 6) f_{yt}, ksi	Transverse reinforcing bar (#2 hoops) f_{yh}, ksi	Steel jacket details	V_{if}, kips	$\dfrac{V_{shear}}{\mu \leq 2}$, kips	$\dfrac{V_{shear}}{\mu \geq 4}$, kips
(a) Circular columns										
C1A	2.0	133	4.5	0.065	47	52		119	139.6	83.7
C2R	2.0	133	4.93	0.059	47	52	$f_{jy}=50.4$ ksi $t_j=3/16$ in.	127	774.3	718.4
C3A	2.0	400	5.0	0.177	47	47		151	197.6	138.7
C4R	2.0	400	5.1	0.173	47	47	$f_{jy}=50.4$ ksi $t_j=3/16$ in.	165	832.3	773.4
C5A	2.0	133	5.2	0.056	68	47		171	142	85.9
C6R	2.0	133	5.8	0.051	68	47	$f_{jy}=41.5$ ksi $t_j=1/8$ in.	175	489	432.9
C7A	1.5	133	4.45	0.066	68	47		222	148	92.7
C8R	1.5	133	4.52	0.065	68	47	$f_{jy}=41.5$ ksi $t_j=1/8$ in.	226	495	439.7
(b) Rectangular columns										
R1A	2.0	114	5.5	0.054	47	52	—	118	143.0	90.6
R2R	2.0	114	5.6	0.053	47	52	$f_{jy}=50.4$ ksi $t_j=3/16$ in.	123	1021	968.6
R3A	2.0	114	5.0	0.059	68	47		160	130.0	80.1
R4R	2.0	114	5.2	0.057	68	47	$f_{jy}=50.4$ ksi $t_j=3/16$ in.	169	1008	958.1
R5A	1.5	114	4.7	0.063	68	47		213	134.1	85.4
R6R	1.5	114	4.8	0.062	68	47	$f_{jy}=41.5$ ksi $t_j=1/8$ in.	226	614.5	565.4

Note: A = as-built; R = retrofitted.
1 kip = 4.5 kN; 1 ksi = 6.9 MPa; 1 in. = 25.4 mm.

Table 2.2 Summary of experimental results (Priestley et al., 1994)

Test unit	M/VD	$P/f'_c A_g$ [b]	V_y [c]	K_y [d]	V_{if} [e]	V_{exp} [f]	μ_{max} [g]	$\dfrac{V_{exp}}{V_{if}}$	$\dfrac{V_{exp}}{A_e\sqrt{f'_c}}$ [h]	θ [i]	Drift ratio [j]
Circular columns											
C1A	2	0.06	85	262	119	129	2.5	1.08	5.3	26	0.011
C2R	2	0.06	90	321	127	165	10	1.30	6.5		0.044
C3A	2	0.18	120	324	151	165	3	1.09	6.5	24	0.009
C4R	2	0.18	124	418	165	215	10	1.30	8.3	—	0.041
C5A[a]	2	0.06	120	234	171	138	1	0.81	5.3	25	0.007
C6R[a]	2	0.06	120	331	175	230	10	1.31	8.3		0.055
C7A[a]	1.5	0.06	165	398	222	178	1	0.80	7.4	20	0.008
C8R[a]	1.5	0.06	167	500	226	276	8	1.22	11.3	—	0.052
Rectangular columns											
R1A	2	0.06	90	271	118	127.2	3	1.08	5.6	32	0.014
R2R	2	0.06	90	388	122.5	149.2	11	1.22	6.5		0.036
R3A[a]	2	0.06	120	231	159.5	141	1.4	0.88	6.5	29	0.010
R4R[a]	2	0.06	120	375	169	221.2	8	1.31	9.9		0.038
R5A[a]	1.5	0.06	166	318	213	168	0.8	0.79	7.8	25	0.007
R6R[a]	1.5	0.06	166	595	226	294	7	1.36	13.9		0.037

According to the test results, retrofitting the circular columns by circular steel jackets and rectangular columns by elliptical steel jackets were extremely effective in enhancing shear strength and flexural ductility of shear deficient columns. Steel jackets increased the elastic stiffness of the columns by an average of 30 and 64 percent for circular and rectangular columns, respectively. Hysteresis loop for rectangular columns as built and retrofitted columns are shown in Figure 2.2. However, circular columns with a reduced jacket thickness of 1/5 in (3.18 mm) were unable to provide adequate confinement of the column in the plastic hinge at large ductility factors.
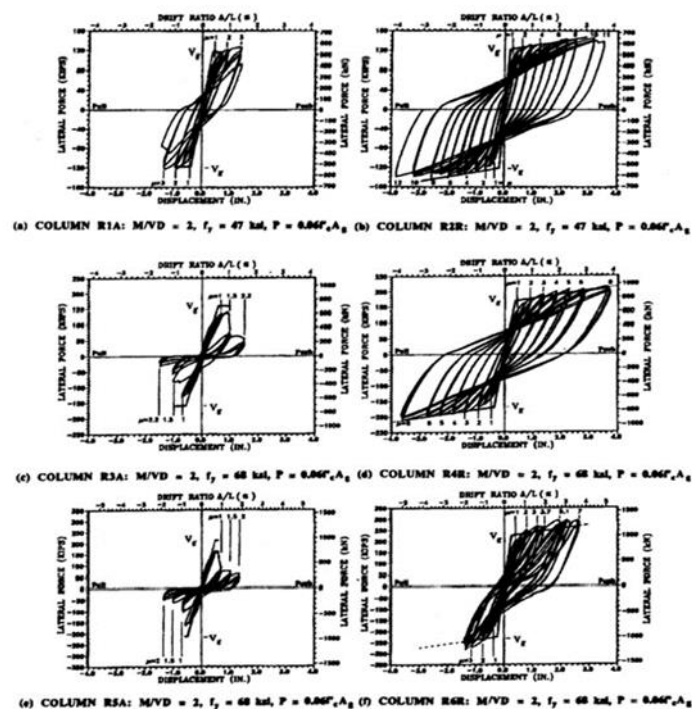
Figure 2.2 Hysteresis loops of rectangular column (Priestley et al., 1994)

Unlike the Priestley et al, (Chai et al., 1994) studied the analytical model for steel jacketed RC circular bridge columns that was tested in 1991. In testing the columns, the authors focused on the flexural performance of bridge columns by encasing the plastic hinge region with steel jacket. One of the reference specimen had lap splice and the other had continuous reinforcement in the plastic hinge region. While experimental testing has demonstrated, in case of flexural retrofit, the steel jacket needs not to be extended to the full height of the column. Figure 2.3 shows steel jacket circular bridge column and the hysteresis response of as built and retrofitted circular columns containing base lap-splices.
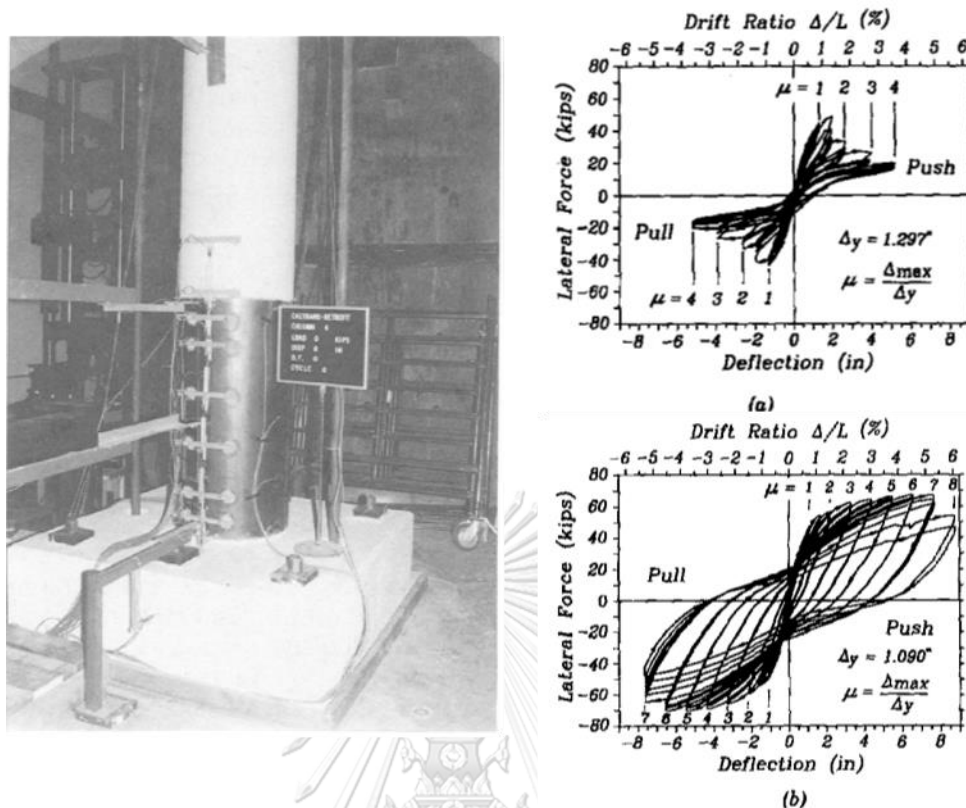
Figure 2.3 Steel jacket circular bridge column and the hysteresis response of as built and retrofitted circular columns (Chai et al., 1994)

According to the test result, the columns retrofitted with a steel jacket showed a significantly improved hysteresis behavior. On the other hand, bond failure that might develop in as built circular columns detailed with inadequately lapped longitudinal reinforcement were also prevented by steel jacketing.

(Tsai and Lin, 2002) performed the axial compression test of the square RC columns with various kinds of jacketing scheme such as circular or octagonal or square shapes as shown in Figure 2.4. The jacketing materials vary from steel plate to carbon fiber reinforced polymer composites. Among the retrofitted specimens, the steel jacketed specimen's exhibit not only greatly enhanced and carry capacity, but also excellent ductility performance as shown in Figure 2.5. Table 2.3 shows the specimen detail and test results. In rectangular steel jacketing RS45, its improvements in column axial strength and axial ductility are much less than those of other steel jacketed specimens due to premature outward bulging at a small column axial strain. Specimen

CS23 had the highest axial strength and circular retrofit scheme has excellent performance in axial strength and ductility.
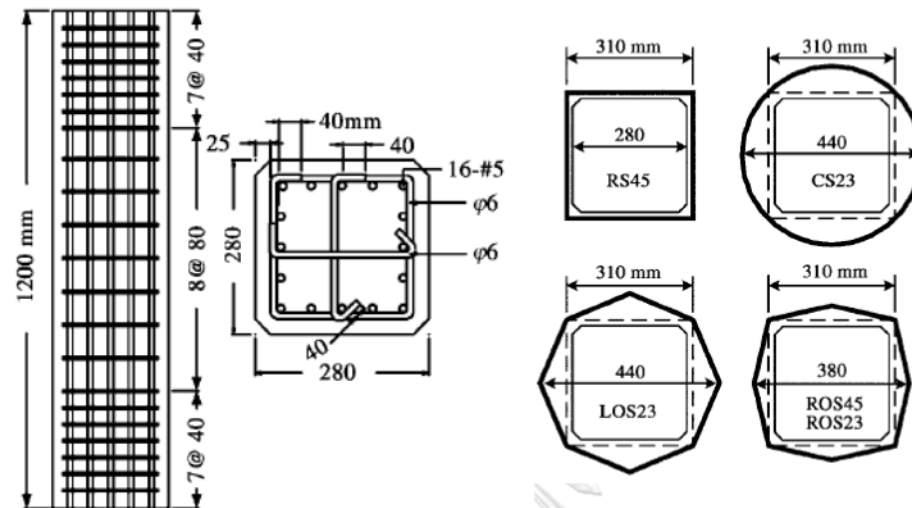
Figure 2.4 Detail of test specimen and steel jacketing schemes (Tsai and Lin, 2002)

Table 2.3 Specimen detail and test results (Tsai and Lin, 2002)

Specimen	Jacket Thickness (mm)	$Pmax$ (kN)	$Pmax/Pn$	ε_{Pmax} (%)	ε_{stop} (%)	Note
BM	NA	2960	1.03	0.41	1.43	Benchmark
RS45	4.5	4270	1.49	1.6	5.16	Rectangular Steel Jacketing
CS23	2.3	7340	2.56	4.73	4.99	Circular Steel Jacketing
LOS23A	2.3	6725	2.35	3.73	5.37	Large Octagonal Steel Jacketing
LOS23B		6485	2.27	4.84	5.30	
ROS45A	4.5	6310	2.20	3.82	5.27	Reduced Octagonal Steel Jacketing
ROS45B		6450	2.25	4.29	5.25	
ROS23	2.3	5710	2.00	3.61	5.12	Reduced Octagonal Steel Jacketing
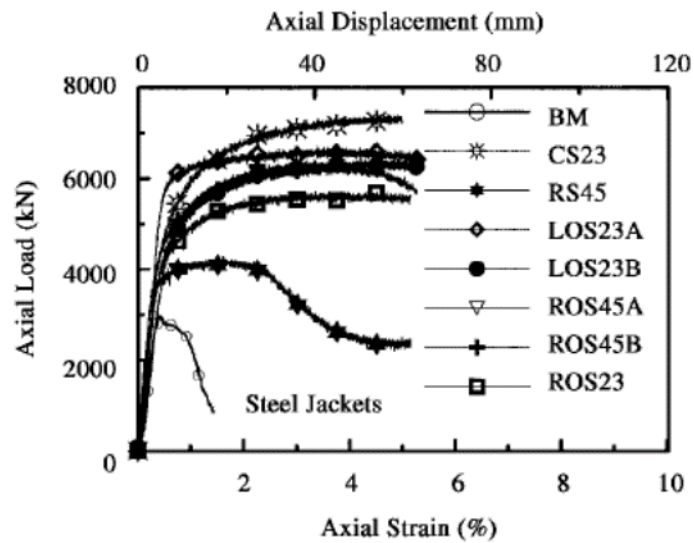
Figure 2.5 Axial force and strain relationship of steel jacketed columns

(Tsai and Lin, 2002)

As an extension study of previous research of Tsai and Lin, (Lin et al., 2010) investigated the behavior of lap splice deficient column subjected to cyclic lateral loads. One column is as built column and the other two specimens were retrofitted by steel jackets of elliptical and octagonal cross section. Test result reported that the octagonal steel jackets performed a little better than the elliptical steel jackets in terms of energy dissipation and lateral capacity. As the author expected, as built column showed brittle failure, while the retrofitted specimens exhibited ductile performance with the low cycle fatigue failure of longitudinal reinforcement. Table 2.4 shows the material and retrofitted properties. Figure 2.6 shows the test setup, jacket details and later load deformation of the specimens

Table 2.4 Material and retrofit properties (Lin et al., 2010)

Specimen	Description	Yield Strength of Steel (Mpa)		Yield Strength of Steel Jacket (Mpa)
		#6 rebar	#3 rebar	
BMRL 100	As built column	440	423	-
SRL1	Octagonal steel jacket	440	423	262
SRL2	Elliptical steel jacket	440	423	412

(a)

(b)
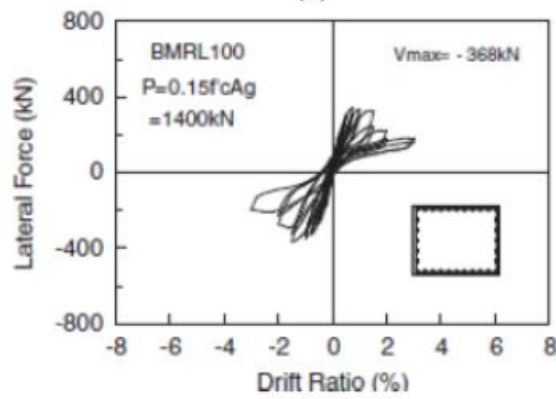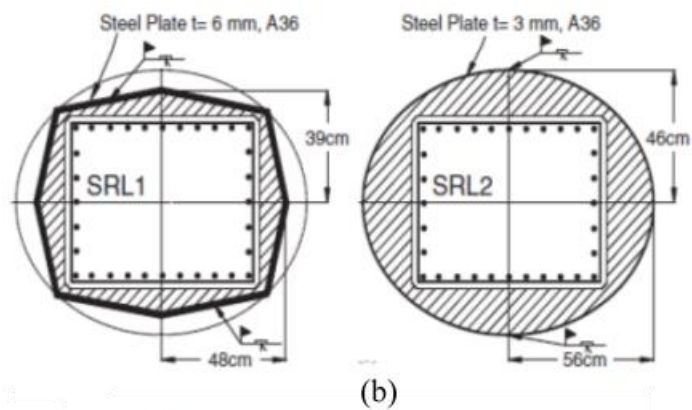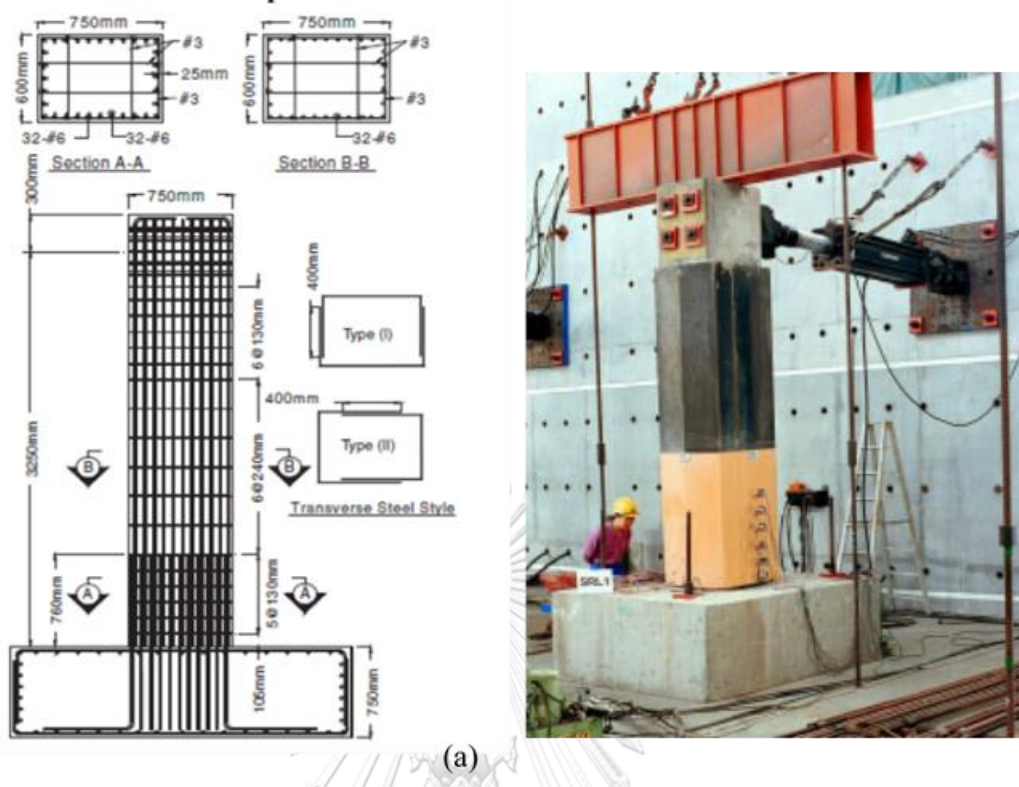
(c)
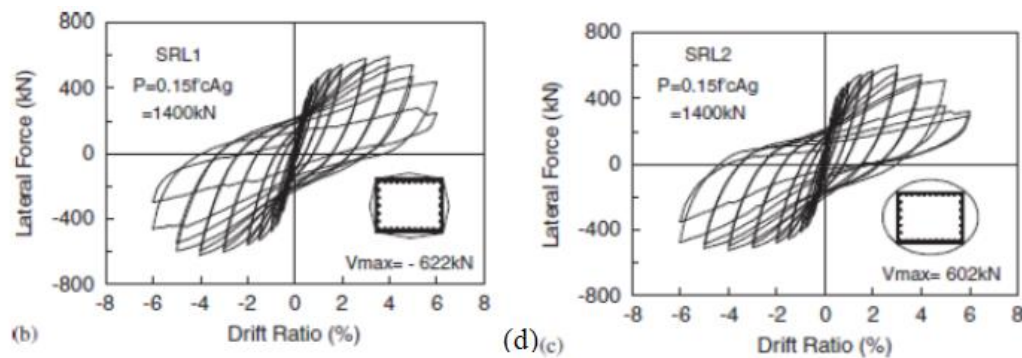
Figure 2.6 (a) Specimen detail and test set up (b) Jacket details (c) lateral load deformation of as build specimen (d) Lateral load deformation of retrofitted specimens (Lin et al., 2010)

The author concluded that the seismic performance of the rectangular RC bridge columns can be significantly enhanced by the elliptical or octagonal steel jacket. Octagonal steel jackets could be cost effective and space saving. Octagonal steel jackets have a smaller cross-section area requirement while slightly improving strength and energy dissipation performance over the elliptical steel jacketing scheme.

As a state of the art new steel jacketing technique, (Choi et al., 2010) proposed a technique wherein steel jackets are installed using the external pressure, without the application of grout. Four test columns were subjected to constant axial load and the lateral loading; two of them are un-jacketed columns such as one was with lap splice and another one was with continuous reinforcement. Another two of them are confined by steel jackets with external pressure; one is single layer jacket and the other is the double layer jacket. The proposed steel jacketing methods increased the ductility of the lap splices RC columns. Jacketing procedures and cross section of the column are shown in Figure 2.7. The load displacement response of the column is shown in Figure 2.8. Retrofit results are shown in Table 2.5.
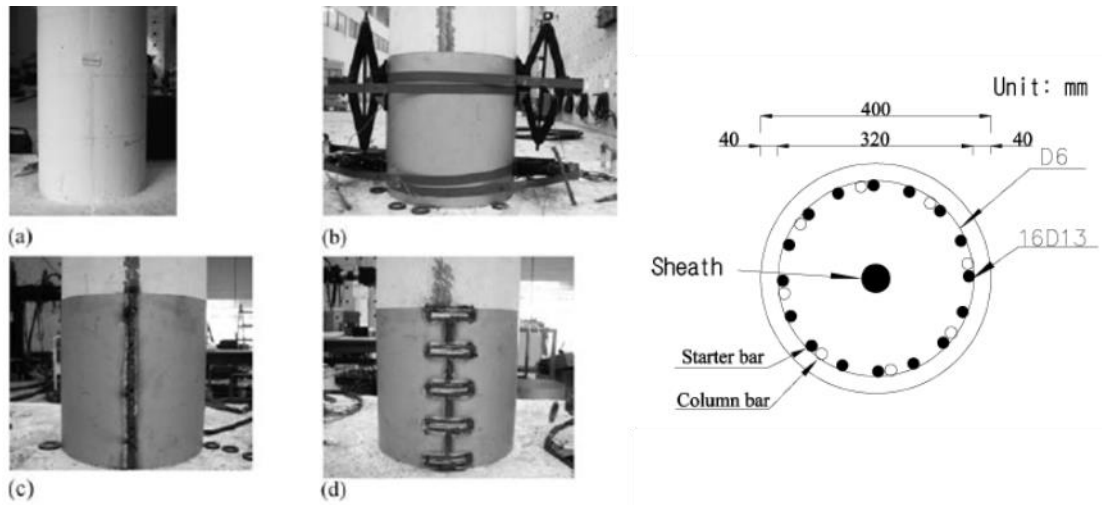
Figure 2.7 Jacketing procedures and cross section of the column (a) As build column (b) Apply external pressure on steel jacket (c) Weld overlap line and (d) Weld lateral strip bands , (Choi et al., 2010)
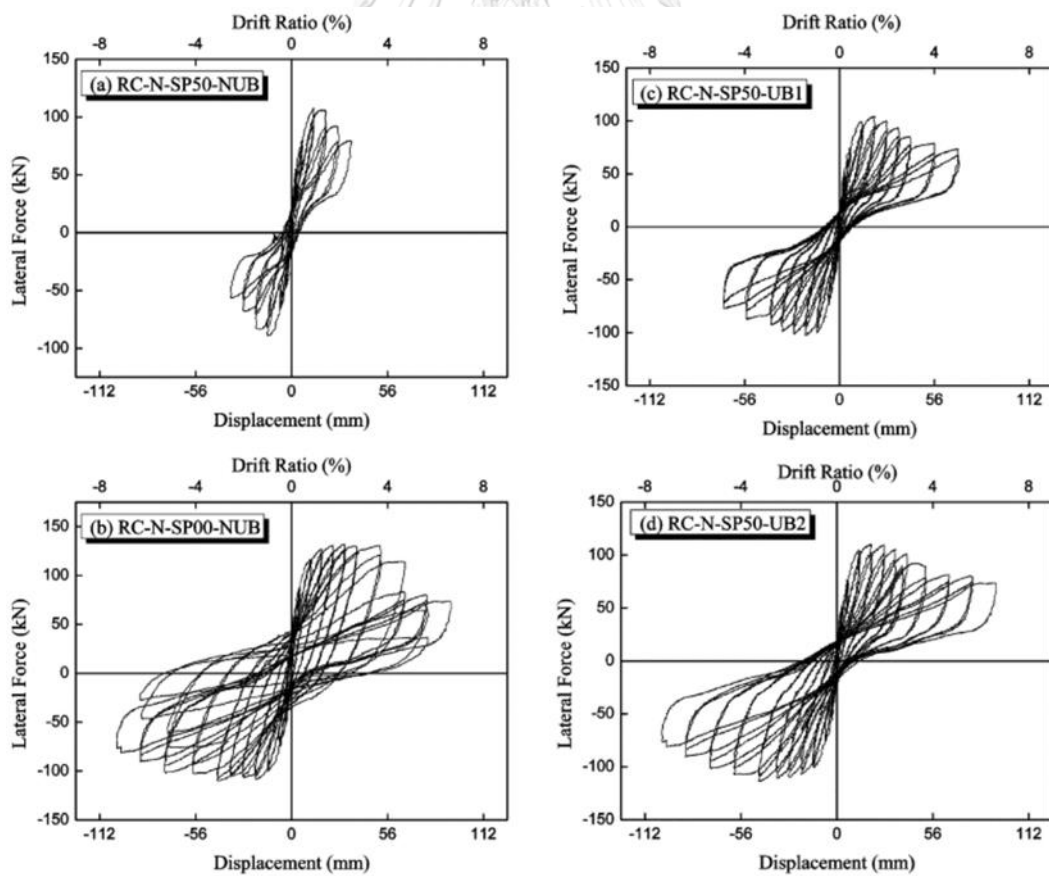
Figure 2.8 Load displacement response of the columns (Choi et al., 2010)

Table 2.5 Retrofitted column results (Choi et al., 2010)

Column Designation	Peak		Displacement Ductility
	Force (KN)	Displ, mm	
RC-N-SP00-NUB	112.4/-93.3	65.6/-61.9	-
RC-N-SP50-NUB	91.6/-75.9	27/-23.3	6.97/5.01
RC-N-SP50-UB1	88.4/-86.7	39/-54.5	3.19/2.69
RC-N-SP50-UB2	93.5/-96.5	45.3/-80	4.08/5.65

The author concluded that the new steel jackets enhanced the displacement ductility and energy dissipation capacity of the RC columns with lap splice. The jacket did not increase the flexural strength; this seemed to be from the imperfect installation of the jackets with not enough external pressure. The effective stiffness of the columns did not increase because the jackets did not induce the composite behavior between the jackets and the concrete. However, it was beneficial because it does not disturb the original stiffness of the column. The newly proposed steel-jacketing method can be used to easily install steel jackets at any location (bottom, middle, top). The performance of the double-layered jacket was better than the single-layered jacket.

(Aboutaha et al., 1999) tested rectangular steel jackets on 11 non-ductile reinforced concrete frame columns with inadequate shear strength for seismic retrofit. Different types of steel jackets were tested, including rectangular solid steel jackets and partial steel jackets. Cyclic lateral forces were applied to the half scale column. The column was cantilevered and framed into a fixed end large footing. For retrofitting of columns with inadequate shear strength, four columns were tested as basic retrofitted specimens. The remaining seven columns were tested after being strengthened with steel jackets. Eight columns were loaded in weak direction and three columns were loaded in a strong direction. Summary of the shear columns is shown in Table 2.6. Details of steel jackets are shown in Figure 2.9. Basic unretrofitted columns and retrofitted column are shown in Figure 2.10. Envelopes of cyclic response of test columns are shown in Figure 2.11.

Table 2.6 Summary of shear columns (Aboutaha et al., 1999)

Column no.	Type	Cross ties	Cross section type	Retrofit type	Direction of loading	Concrete* f_c, psi	Footing[†]
SC1	Basic	EB	B	N/A	Weak	5040	F3
SC2	Strengthened	EB	B	Collars	Weak	5040	F4
SC3	Basic	EOB	A	N/A	Weak	3170	F3
SC4	Basic	EB	B	N/A	Weak	3170	F4
SC5	Strengthened	EOB	A	Collars	Weak	2240	F3
SC6	Strengthened	EOB	A	W-SJ	Weak	2255	F4
SC7	Strengthened	EOB	A	B-SJ	Weak	2940	F7
SC8	Strengthened	EOB	A	U-PSJ	Weak	2785	F8
SC9	Basic	EOB	C	N/A	Strong	2325	F3
SC10	Strengthened	EOB	C	W-SJ	Strong	2390	F7
SC11	Strengthened	EOB	C	C-PSJ	Strong	2360	F8

(a) Welded steel jacket   (b) Steel collars

(c) U shaped partial steel jacket   (d) C shaped partial steel jacket
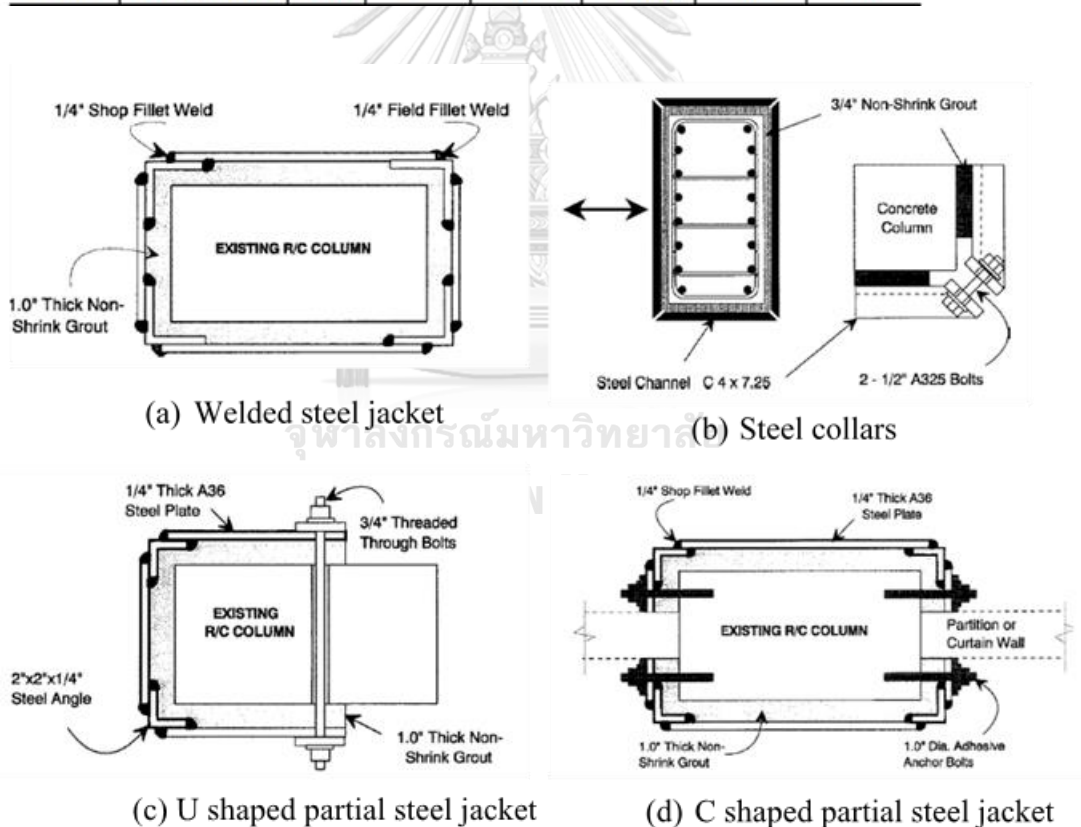
Figure 2.9 Details of steel jacket (Aboutaha et al., 1999)
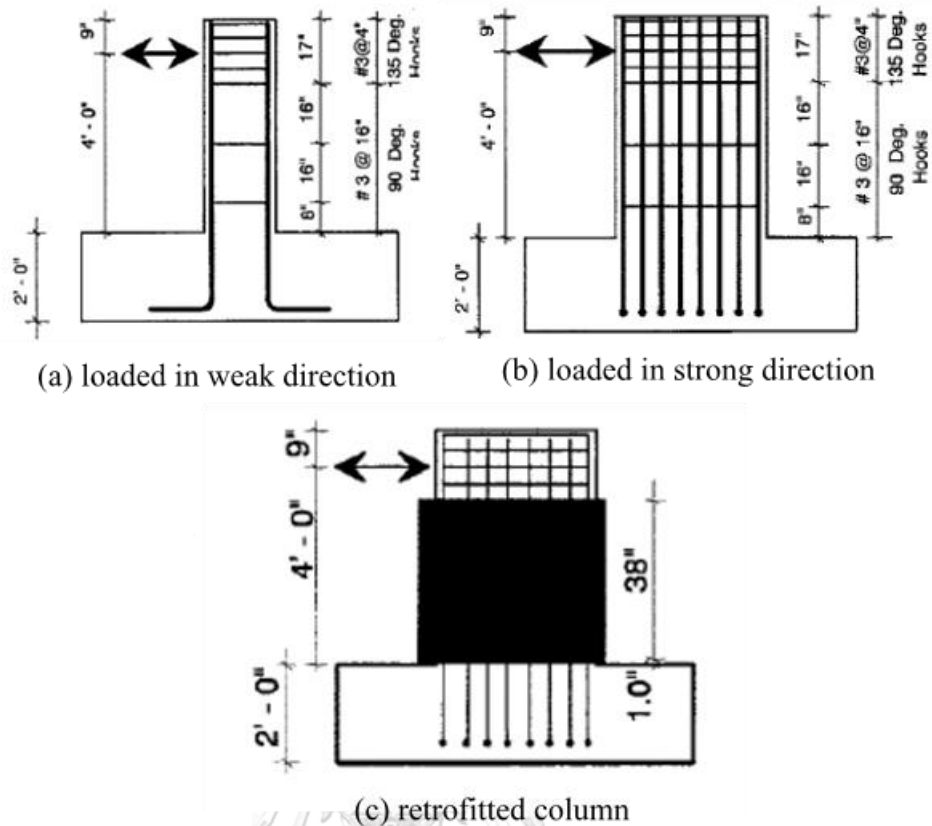
Figure 2.10 Unretrofitted column and retrofitted column (Aboutaha et al., 1999)
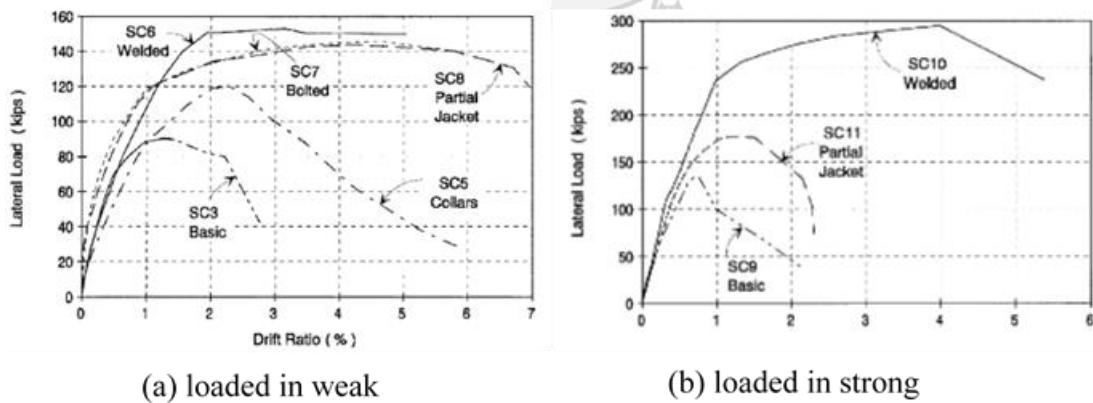
Figure 2.11 Envelopes of cyclic response of test columns (Aboutaha et al., 1999)

According to the test results, the author concluded that thin rectangular steel jacket can be highly effective at retrofitting reinforced concrete columns with inadequate shear strength. The steel jackets were effective at improving flexural yield capacity, improving ductility, and having a higher energy dissipation. Despite large

lateral displacements, the steel jackets had low maximum strains due to the confinement preventing major shear cracks from opening. Yielding in the steel jacket may reduce stiffness and strength with more crack openings; thus, jacket yielding should be prevented for better performance. Welded or bolted connections at the jacket corners adequately developed the forces in the ties.

Instead of jacketing the column with plates on the four faces of the column, (Griffith et al., 2005) approached a new technique which consists of attaching steel plates to the flexural faces of a concrete column using bolts. That technique would be suitable mainly for rectangular columns in which lateral loading includes predominately a single plane of bending. This technique had been demonstrated by experimental study and numerical simulations. Steel plate in the shaped of an "L" were bolted to the tension and compression face of the column and also to the foundation. Schematic of retrofit scheme is shown in Figure 2.12. The retrofit scheme of the test columns is shown in Table 2.7. Three columns are tested under monotonic loading and two columns are tested under cyclic loading.
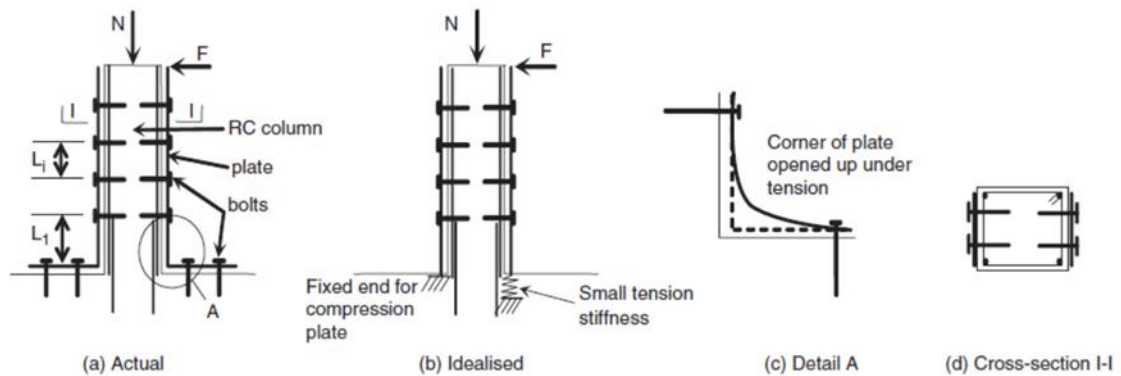
Figure 2.12 Schematic of retrofit scheme (Griffith et al., 2005)

Table 2.7 Retrofit scheme of the test columns (Griffith et al., 2005)

Name	Plate Thickness	Connection Details
1AMR	None	None
1BMP6	6 mm	12 mm bolts at 100 mm spacing
2AMF12	12 mm	12 mm bolts at 100 mm spacing plus epoxy adhesive
3ACR	None	None
4ACP6	6 mm	12 mm bolts at 100 mm

According to the observation on the test results, plated column was significantly more ductile than the bare reinforced concrete column. The retrofitted system delayed the crushing of concrete by bolting plates to the compression face of the column. The connection detail at the base of the column allows the plate to carry the large compression forces in the plastic hinge region. Load and displacement results for monotonic test is shown in Figure 2.13 and load and displacement result of cyclic loading is shown in Figure 2.14.
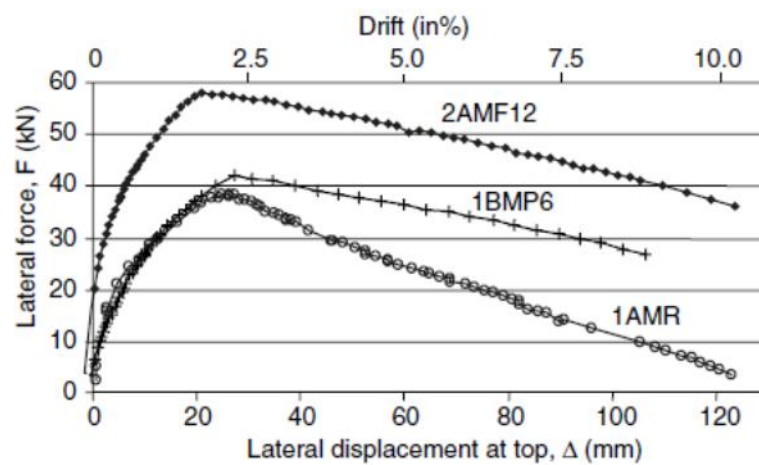
Figure 2.13 Load and displacement result for monotonic tests (Griffith et al., 2005)
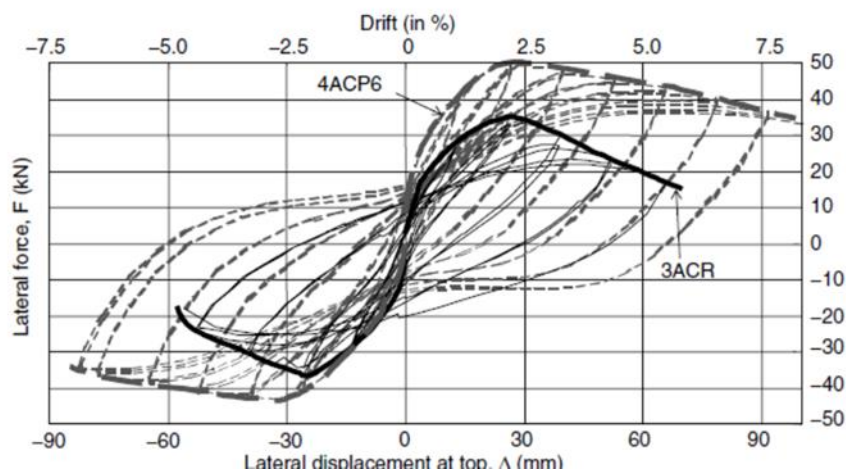
Figure 2.14 Load and displacement result for cyclic tests (Griffith et al., 2005)

In addition, the plated columns for different plate thickness (from 0 to 30 mm) and different bolt stiffness were also examined. Response of columns with different plate thickness is shown in Figure 2.15. Response of columns with different bolt stiffness (Kb = 0, 0.75, 5.75, 11.5, 23, 46, ∞) is shown in Figure 2.16.
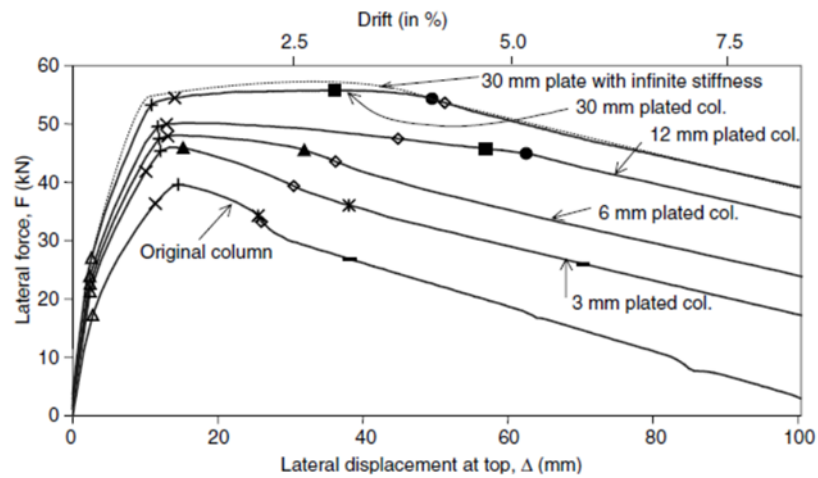
Figure 2.15 Response of the column with different plate thickness

(Griffith et al., 2005)
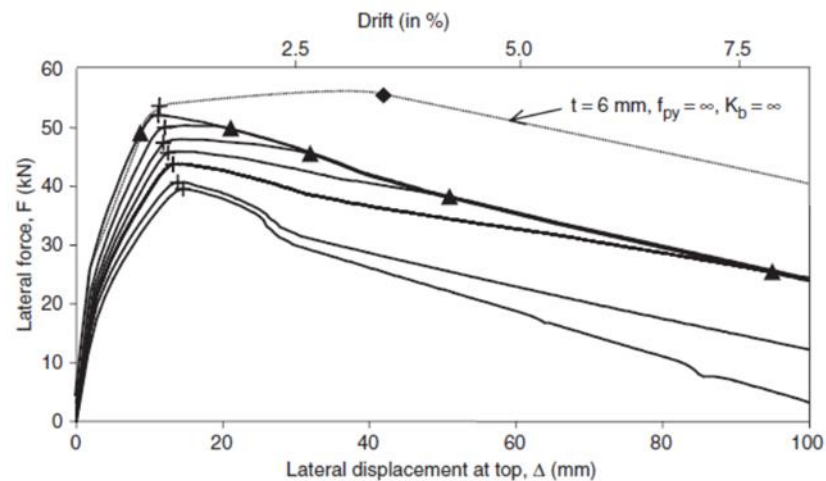
Figure 2.16 Response of the column with different bolt thickness

(Griffith et al., 2005)

Regrading to the test results, the author concluded that increasing plate thickness or bolt stiffness does not always increase the ductility of the column. The response curve had a larger ductility factor when the yield of the plates or bolts was delayed. The author suggested that larger improvements in ductility could be achieved with this retrofitted method by using FRP plates and bolts which do not yield, instead of steel. Nonetheless, this may require a greater plate thickness and /or decreased bolt spacing to prevent the buckling of the steel plate.

2.2.1.1. Summary

Concerning with the steel plate jacketing methods, the following conclusions were made by some of the researchers. Regardless of elliptical or octagonal jackets were used, the column width is significantly enlarged after retrofitting, thus resulting in the occupation of extra space which prevents the wide application of these methods (Wang et al., 2017). Regarding the effective parameter of rectangular steel jackets for retrofitting, the rectangular steel jacket are not effective in providing lateral confinement for concrete due to the out of plane bulging of the steel jacket (Tsai and Lin, 2002). In addition, in a conventional steel jacketing method, the gap between the steel and concrete has to be filled with pure cement, cement mortar or epoxy resin in order to transfer passive confining pressure to the existing concrete; this is called grouting and the method affects the speed of installation. However, the conventional steel jacketing method presents other drawbacks besides grouting. The grout induces a composite behaviour between the steel jacket and the concrete, and also increases flexural stiffness (Choi et al., 2013). Changing square or rectangular shaped column sections to circular or elliptical jacketing is not always desirable or practical in engineering, especially where space is limited as in building structures (Griffith et al., 2005). Although the rectangular steel jacketing can still be effective in certain circumstances, the relative poor performance of rectangular jackets in confining the concrete core has been experimentally verified (Griffith et al., 2005).

2.2.2. Angle and batten jacketing methods

In order to avoid the bugling of the steel plate and the increasing of the initial stiffness, (Nagaprasad et al., 2009) investigated the steel caging technique which consisted of steel angles at the corners of RC columns and steel battens along the height of the columns which was the theoretical model of (Masri and Goel, 1996). The moment capacity of a strengthened RC column was taken as a sum total of moment capacities of the confined RC column section and steel angle sections of the steel cage. That theoretical concept was shown in Figure 2.17. The compressive strength of the confined concrete with steel cage depended on the spacing and size of the battens and number of battens. Wider battens were placed in the expected plastic hinge region of the steel cage.

The method appeared effective in increasing concrete confinement and reducing the likelihood of local buckling of steel angles. Three test specimens were investigated under constant axial compressive load and gradually increased cyclic lateral displacements. Two specimens were strengthened using longitudinal steel angles and welded transverse battens. Three specimens were designed as RCO, RCS1 and RCS2. Detail of test specimens is shown in Figure 2.18. Material properties of concrete and steel are shown inTable 2.8.
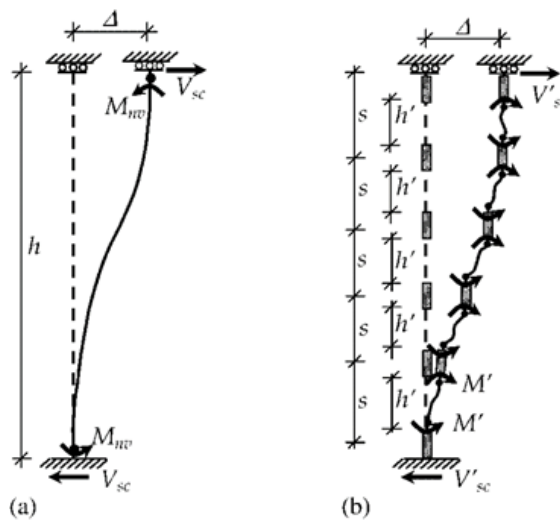
Figure 2.17 Theoretical design mode of steel cages (a) original model

(b) refined model (Masri and Goel, 1996)
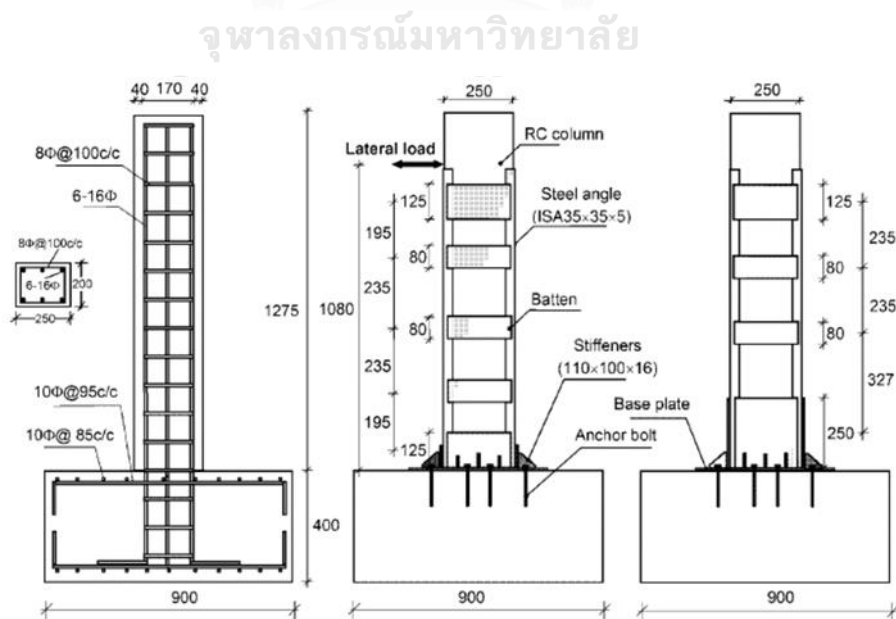
Figure 2.18 Detail of test specimens (Nagaprasad et al., 2009)

Table 2.8 Material Properties of the concrete and steel (Nagaprasad et al., 2009)

Specimen	Concrete strength (MPa)	Axial load (kN)	Longitudinal reinforcement ratio (ρ_l)	Transverse reinforcement ratio (ρ_s)	Yield strength of longitudinal bar (f_y)	Yield strength of transverse bar (f_{sh})
RCO	38	450				
RCS1	45.5	450	0.025	0.005	468.4	438.5
RCS2	39.9	450				

This investigation found that detailing of the end batten of the steel cages located in the potential plastic hinge region of RC columns plays an important role in improving its overall behavior under lateral loads. The increase in width of end battens of steel cage significantly enhanced the plastic rotational capacity and its resistance to lateral loads; however, it had a minor effect on overall energy dissipation potential. It was concluded that the correct choice of width of end battens depends largely on the target moment and plastic rotation capacity of strengthening column. In addition, this method requires an intermediate level of skilled labors since it demands drilling of holes in the foundation. Damage state and hysteretic response of the test columns are shown in Figure 2.19. Comparison of energy dissipation capacity is shown in Figure 2.20
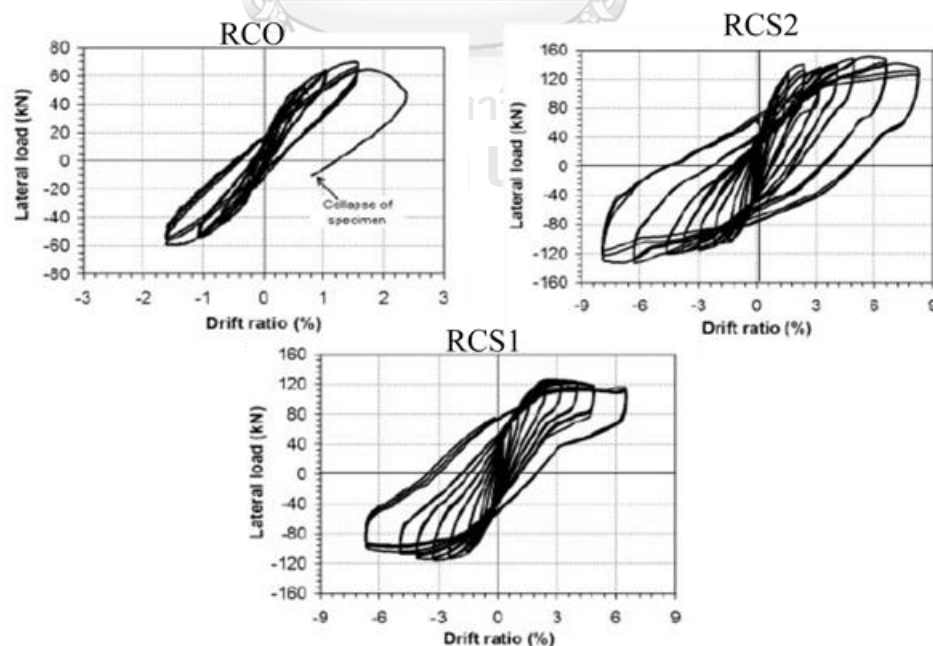
Figure 2.19 Hysteresis response of the tested specimens (Nagaprasad et al., 2009)
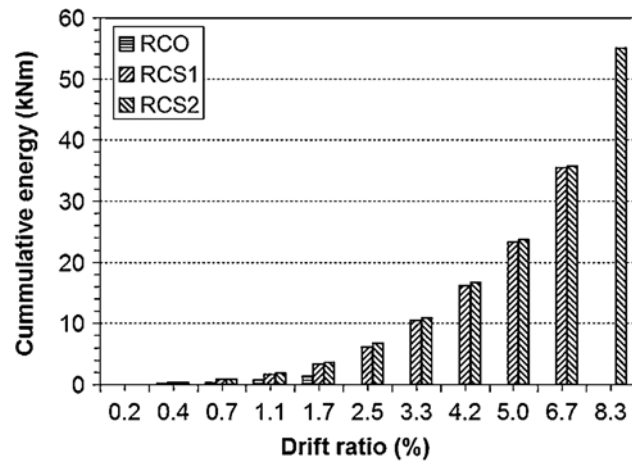
Figure 2.20 Energy dissipation capacity of the tested specimens

(Nagaprasad et al., 2009)

Unlike the Natgaprasad et al, three variables were considered such as shape of strengthening system, size and number of batten plates to study the behavior of strengthened reinforced concrete column by the (Belal et al., 2015). Seven specimens; two un-strengthened columns and five strengthened ones with a different steel jacketing configuration, such as the angle with battens, channel with battens and plates only on four sides. An axial load of 5000 kN was applied to all the tested specimens. Specimen dimension and steel jacket configuration are shown in Figure 2.21. Strengthened specimens after casting and jacket erection are shown in Figure 2.22.
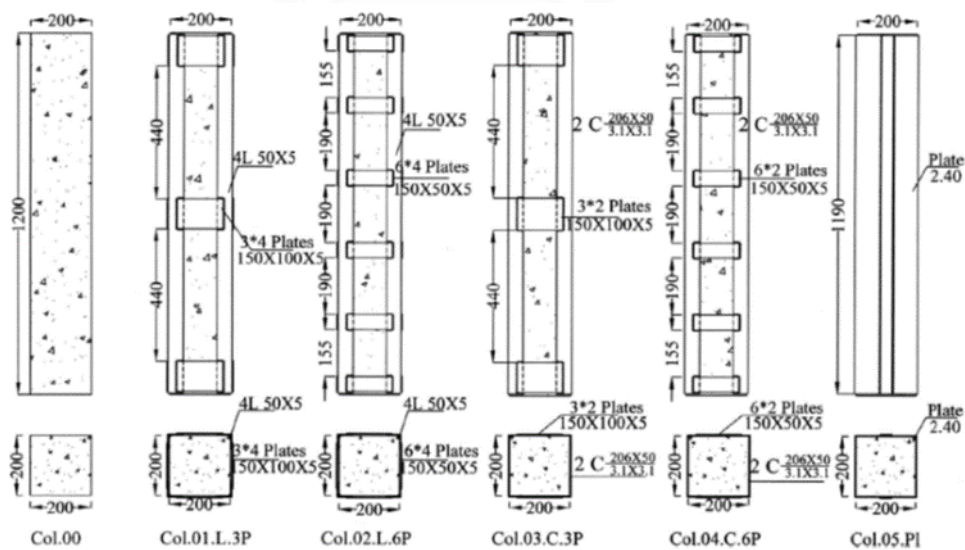
Figure 2.21 Specimen dimension and steel jacket configuration

(Belal et al., 2015)

Figure 2.22 Strengthened specimens after casting and jacket erection

(Belal et al., 2015)

The aforementioned studies have found that the size of batten had a significant effect on the failure load for specimens strengthened with angles, whereas the number of batten was more effective for specimens strengthened with C-channels. In addition, based on the test results, the author concluded that steel jacketing techniques for strengthening RC columns increased the column capacity to a minimum of 20%. The load displacement relationships are shown for each specimen during testing in Figure 2.23.
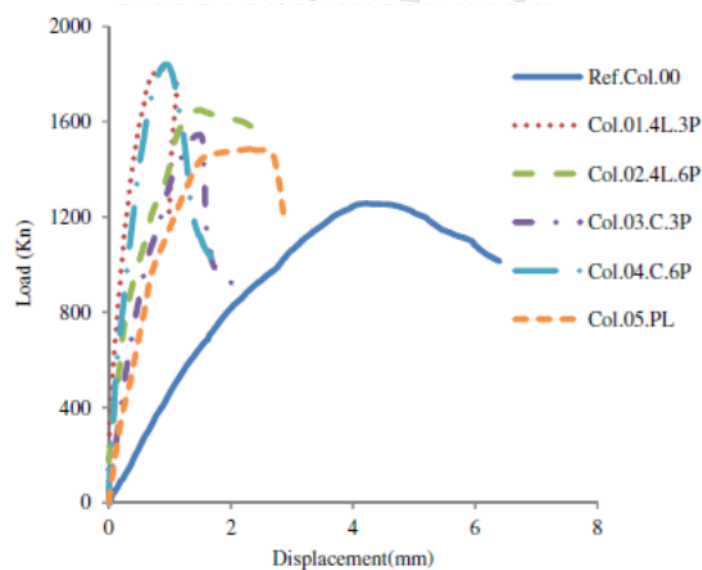
Figure 2.23 Load displacement relationship for all specimens (Belal et al., 2015)

Different strengthening methods, including angles, channels and plates only on four sides of columns have a significant impact on the failure load of columns. The effectiveness of specimens using angles or channels is insignificant. On the other hand, the specimen strengthened with angles or channel sections with battens recorded a higher failure load than that strengthened with plates only. Steel plates had a significantly less capacity due to the thinness of the plates. C sections, with battens or plates only in strengthening concrete column needs cautions due to buckling consideration of their thin thickness. The simulation results of strengthened columns using ANSYS program were much closed those measured during experimental testing.

In the situation where it was not feasible to connect the vertical angles to the roof of slabs and beams, steel heads were placed at the ends of the specimens in order to get the indirectly loaded case. This kind of strengthening technique was investigated by (Tarabia and Albakry, 2014). Ten square columns were prepared with two different cube strength. The test columns were divided into two groups. Reinforcement detail of the concrete column specimens is shown in Figure 2.24. Detail of some strengthened specimens is shown in Figure 2.25. Detail of the test specimens is shown in Table 2.9.
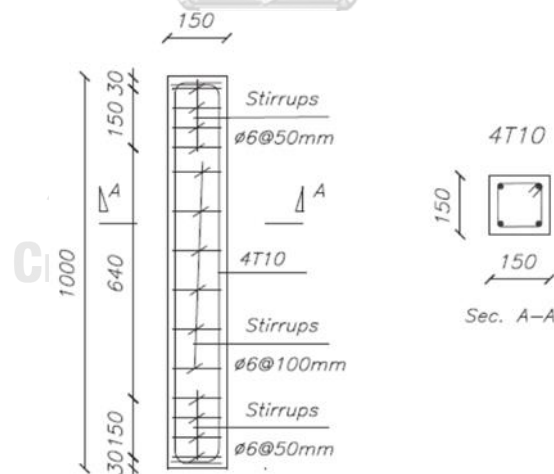
Figure 2.24 Reinforcement detail of concrete specimen (Tarabia and Albakry, 2014)
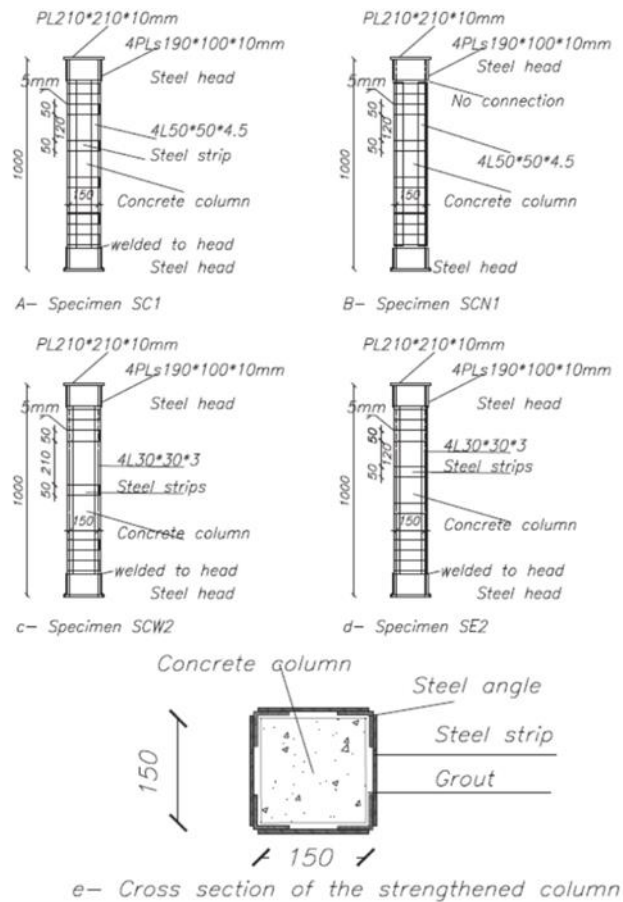
Figure 2.25 Detail of some strengthened specimens (Tarabia and Albakry, 2014)

Table 2.9 Detail of the test specimen (Tarabia and Albakry, 2014)

Specimen	Group	Spacing of strips (mm)	Corner angles	Grout type	Angle-head connection	f_{cu} (N/mm^2)
N1 (reference)	1	N.A.	N.A.	N.A.	N.A.	57.80
SC1	1	170.00	4L50*50*4.5	Cement	Connected	57.80
SCN1	1	170.00	4L50*50*4.5	Cement	Not connected	57.80
SCW1	1	260.00	4L50*50*4.5	Cement	Connected	57.80
SE1	1	170.00	4L50*50*4.5	Epoxy	Connected	57.80
N2 (reference)	2	N.A.	N.A.	N.A.	N.A.	47.50
SC2	2	170.00	4L30*30*3	Cement	Connected	47.50
SCN2	2	170.00	4L30*30*3	Cement	Not connected	47.50
SCW2	2	260.00	4L30*30*3	Cement	Connected	47.50
SE2	2	170.00	4L30*30*3	Epoxy	Connected	47.50

According to the test results, the initial stiffens of the strengthened specimens was higher than that of the reference column of the same group. Generally, all strengthened columns had higher maximum axial shortening than those of the reference columns without axial steel cages. Axial load and axial shortening of Group 1 and Group 2 are shown in Figure 2.26.
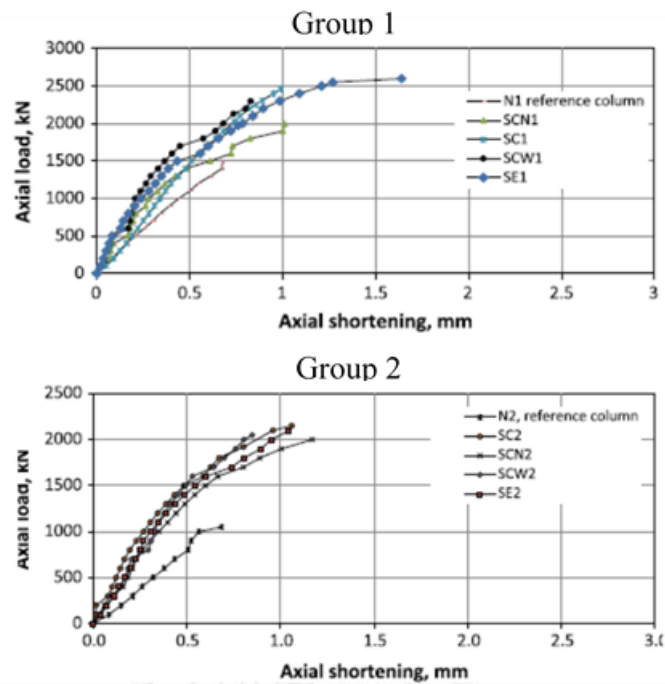
Figure 2.26 Axial load and axial shortening of Group 1 and Group 2

(Tarabia and Albakry, 2014)

The author also occurred some facts from the tests, the failure in most of the unstrengthened was due to the buckling of the steel angle after their yielding followed by the crushing of the concrete column. No yielding of horizontal strip was observed because of the relatively large size of the horizontal strips with respect to the vertical angles. Directly connected vertical angels on the head of the columns showed that all angles yielded before failure of strengthening column. On the other hand, in the case of indirectly loaded vertical angles to the head of the columns, the angel did not reached yielding.

For practical reason, steel angles are arranged, leaving a gap with end beams or slabs in several cases. Despite this disconnection, the angles are still able to carry a portion of load because of the frictional interaction forces developed long the column angles contact surface. (Campione et al., 2017) studied the friction effects in structural behaviour of connected angle and battens jacketed RC columns subjected to axial compressive tests and eccentric compressive tests. A total of sixteen number of specimens was tested. Design detail of the specimen with and without steel jacketing is shown in Figure 2.27. Test set up for compressive test and the eccentric compressive

test is shown in Figure 2.28. Displacement controlled maximum loading capacity of 4,000 kN was applied. Matrix test specimens is shown in Table 2.10.
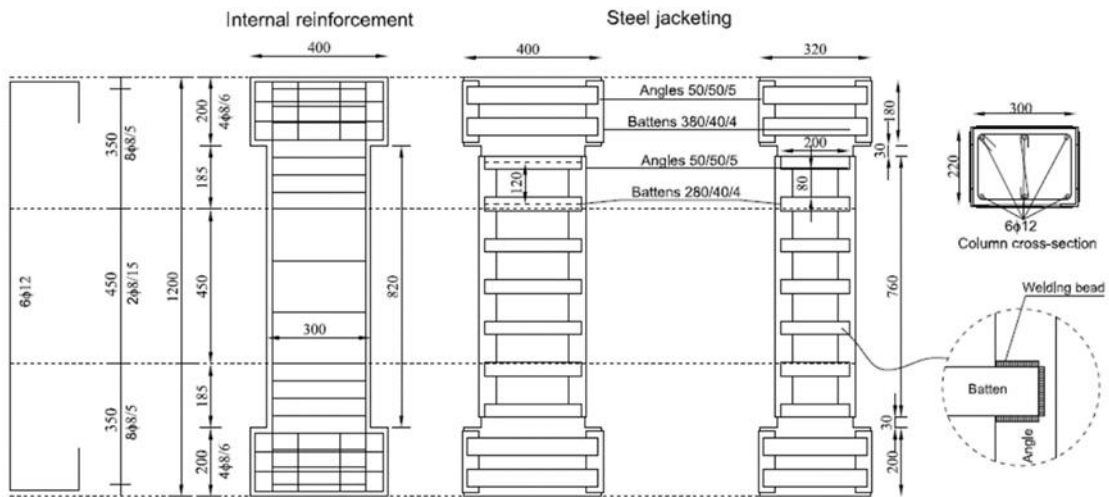
Figure 2.27 Design detail of specimens with and without steel jacketing

(Campione et al., 2017)
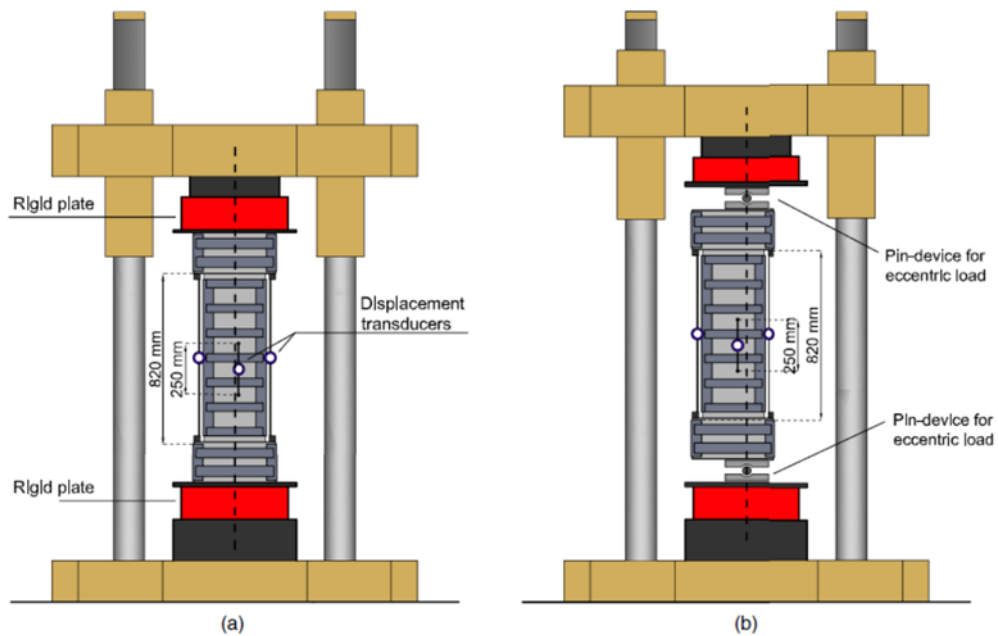
Figure 2.28 Test set up (a) axial compressive test (b) eccentric compressive test

(Campione et al., 2017)

Table 2.10 Matrix of test specimens (Campione et al., 2017)

Specimen	Concrete type	Concrete average strength (MPa)	Steel jacketing	Load eccentricity (mm)
CA1	A	12.65	No	—
CA2	A	12.65	No	—
CAEX1	A	12.65	No	65
CAEY1	A	12.65	No	55
RCA1	A	12.65	Yes	—
RCA2	A	12.65	Yes	—
RCA3	A	12.65	Yes	—
RCAEX1	A	12.65	Yes	65
RCAEY1	A	12.65	Yes	55
CB1	B	24.00	No	—
CB2	B	24.00	No	—
CBEX1	B	24.00	No	65
CBEY1	B	24.00	No	55
RCB1	B	24.00	Yes	—
RCBEX1	B	24.00	Yes	65
RCBEY1	B	24.00	Yes	55

From the results obtained, the author concluded that significant increase of bearing and deformation capacity was observed for steel jackets in axial compressive tests. Also for the eccentric compressive tests, a large load increased in steel jacketing columns even in the case of low strength concrete specimens. For both axial and eccentric compressive tests on the unjacketed specimens, the damage was occurred in the central zones of the columns as well as the large width cracks. Cover spalling and buckling of longitudinal reinforcement also happened. For the jacketed specimens, the damage was less evident and spread out over the entire length of the column. Concrete spalling and buckling of longitudinal reinforcement were escaped by the confinement action. For compressive axial tests, the collapse of the specimens occurred because of the failure of the welding at very large deformations. The results of the axial compressive test for unretrofitted and retrofitted columns are shown in Figure 2.29. The results of the eccentric compressive test for unretrofitted and retrofitted columns are shown in Figure 2.30.
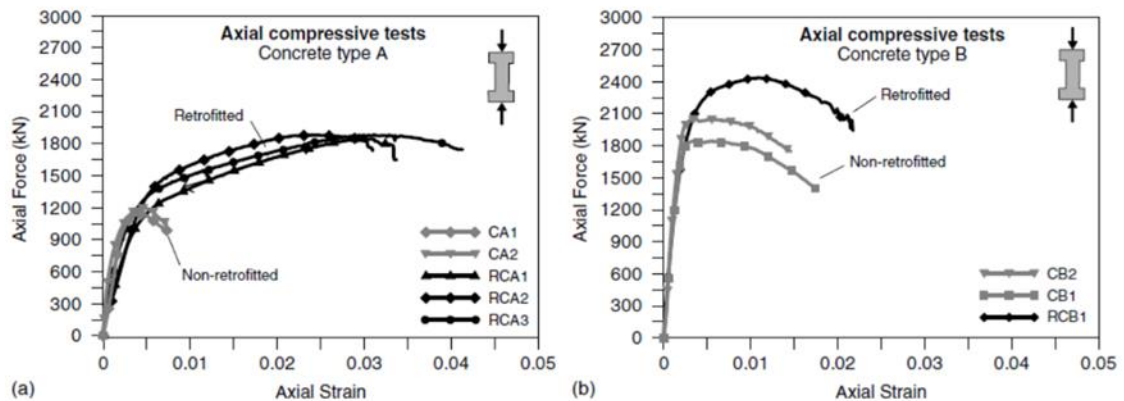
Figure 2.29 Result of axial compressive test for retrofitted and unretrofitted specimens
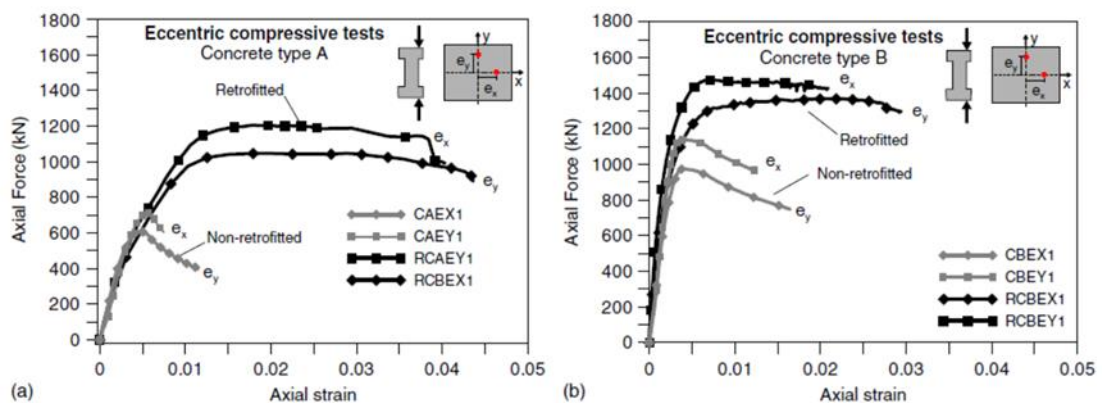
(Campione et al., 2017)

Figure 2.30 Result of eccentric compressive test for retrofitted and unretrofitted specimens (Campione et al., 2017)

Similar to the Campionee et al (2017), the increase in axial capacity and enhancement in ductility of column between unstrengthened and strengthened specimens under displacement controlled eccentric loading was studied by (Montuori and Piluso, 2009). Experimental tests had been performed on 13 specimens. Load transmission system made of steel plates and reinforcing and stiffening had been adopted to apply different eccentricities which had been hinge the specimen ends of the testing machine. Strengthened and unstrengthened specimen model is shown in Figure 2.31. Geometry of the test specimen is shown in Table 2.11
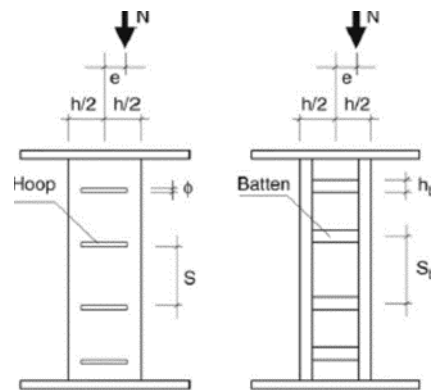
Figure 2.31 . Strengthened and unstrengthened specimens models

(Montuori and Piluso, 2009)

Table 2.11 Geometry of test specimens (Montuori and Piluso, 2009)

Beam Name	Long Bars	Angles (mm)	Battens (mm)	Ties (mm)	Eccentricity, e (mm)	Hoop Spacing, s (mm)	c/c Battens, b (mm)
A-NR	8 φ10	-	-	-	71	125	-
B-NR	8 φ10	-	-	-	44.5	101.3	-
C-NR	8 φ10	-	-	6	73	102.5	-
D-NR	4 φ16	-	-	-	80	102.5	-
E-NR	4 φ16	-	-	-	44	116	-
A-R1 (CT)	8 φ10	30 x 30 x 3	15 x 3	-	73	111.2	135
B-R1a (CT)	8 φ10	30 x 30 x 3	15 x 3	-	47.5	106	130
B-R1b (CT)	8 φ10	30 x 30 x 3	15 x 3	-	50.7	100	130
C-R1 (CT)	8 φ10	30 x 30 x 3	15 x 3	6	79.3	105	130
D-R1 (CT)	4 φ16	30 x 30 x 3	15 x 3	-	78.6	100	127
E-R1 (CT)	4 φ16	30 x 30 x 3	15 x 3	-	54.7	116.5	130
D-R2 (CO)	4 φ16	30 x 30 x 3	15 x 3	-	71.2	105	130
D-R3 (CA)	4 φ16	30 x 30 x 3	15 x 3	-	69.7	105	130

CT = angles resisting both compression and tensions

CO = angels resisting in compression by cutting the angles in tension

CA = angles acting as confinement only by cutting the angles in compression and tension

The results of the test indicated that the strengthened specimens had load capacity, nearly twice that of the unstrengthened specimen and with higher buckling resistance. Peak axial load with less displacement is exhibited for angles resisting load in both compression and tension, while highest ductility is obtained for a specimen with angles as confinement elements only. This method provides effective lateral restraint to columns thus preventing buckling of bars. Axial load and load displacement curves resulting from experimental tests are shown in Figure 2.32. The technique is most suitable for a corner column of a building with poor lateral confinement for longitudinal bars.
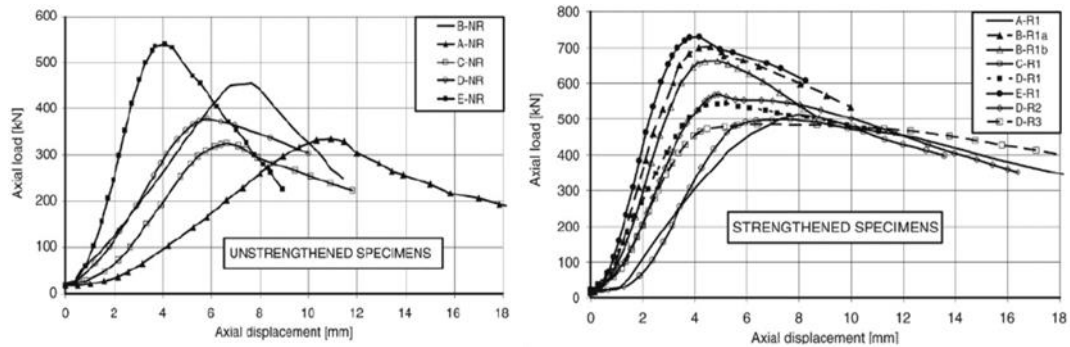
Figure 2.32 Axial load and displacement curves of the test specimens

(Montuori and Piluso, 2009)

(Adam et al., 2008) explored the laboratory tested study of beam-column joints in axially loaded RC columns strengthened by steel cages and strips. Direct load transmission method was used to transmit the load from the beam column joints to the cage in two ways such as capitals (AxL.C) and steel tube (AxL.T). Specimen geometry and reinforcement is shown in Figure 2.33. A total of eight specimens was tested, including two specimens without strengthening and a total of three specimens of AxL.C and AxL.T. Detail of strengthened specimens is shown in Figure 2.34. The general view of the test column is shown in Figure 2.35.
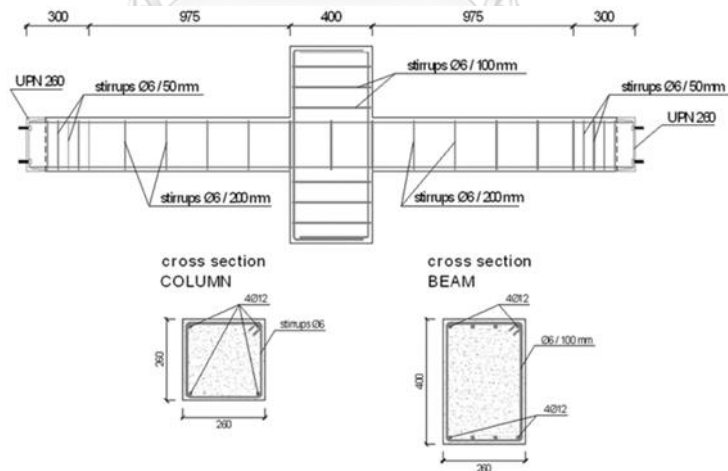
Figure 2.33 Specimen geometry and reinforcement (Adam et al., 2008)
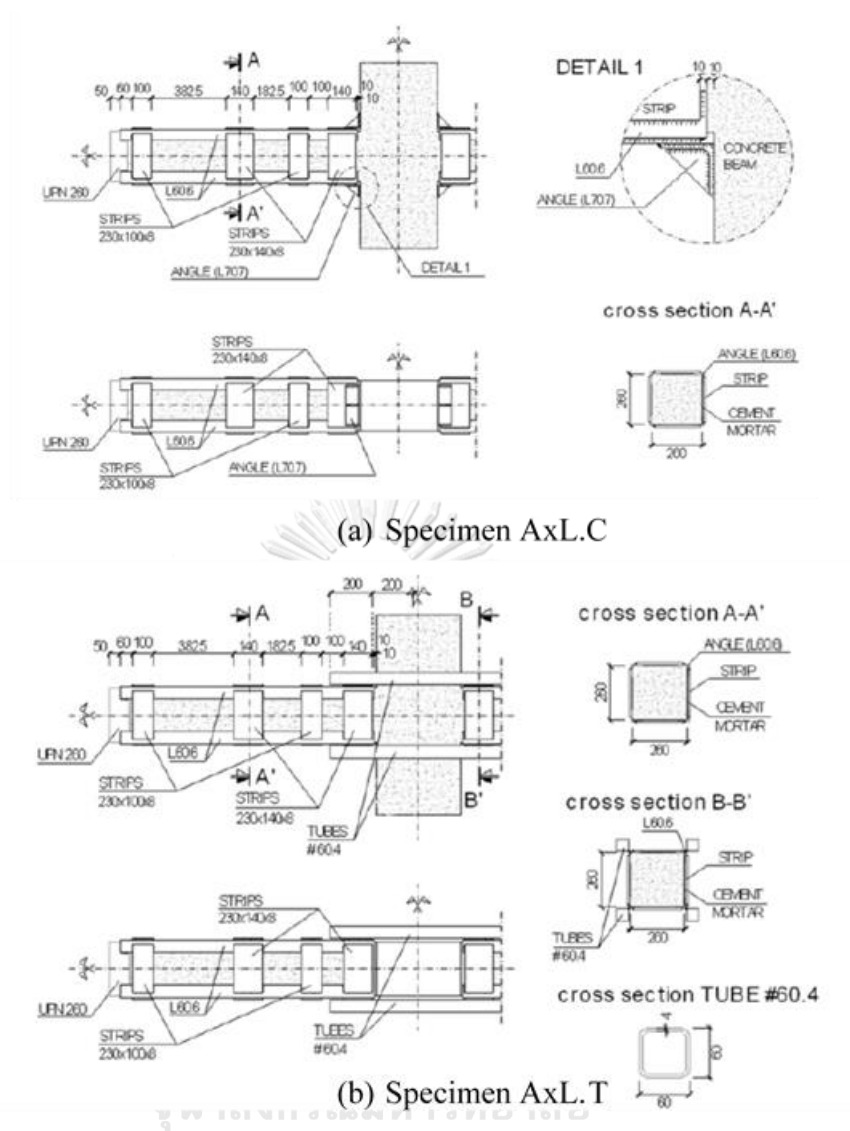
Figure 2.34 Detail of Strengthened columns (Adam et al., 2008)
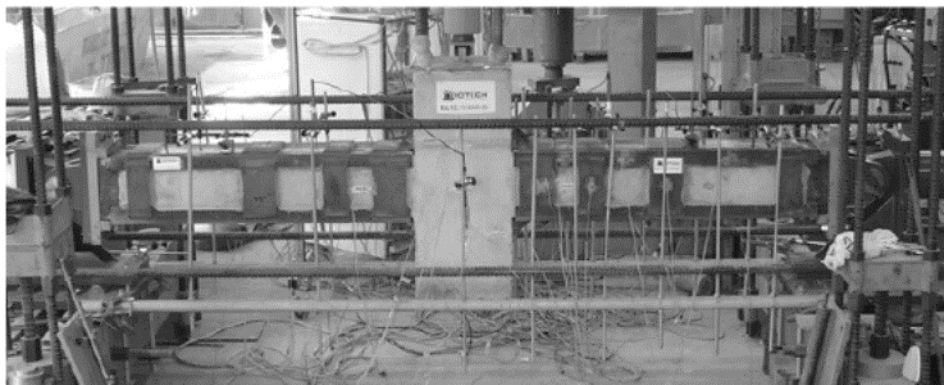
Figure 2.35 General view of the test specimen (Adam et al., 2008)

As stated by the test results, it can be seen that the strengthened columns have a considerable increase in ultimate load compared to the non-strengthened specimens as shown in Figure 2.36. In the case of two strengthened columns, the use of steel tube increase the ductility and ultimate load in strengthened columns more than that of using capital steel cage. The mean ultimate load value for Axl. Ref specimens were 937.5 on failure occurring near to one of the column ends. The mean ultimate load value for Axl.C specimens was 1618.1kN. The mean ultimate load value for Axl.T specimens was 1684.3 kN. The author concluded that the failure mode of the strengthened specimens AxL.T occurred in a confined zone of the concrete, indicating that the failure mechanism was ductile due to the behaviour of the concrete itself when subjected to triaxial compressive loads. Failure in specimen Axl.C was in a zone with low confinement and was caused by a more brittle failure mechanism.
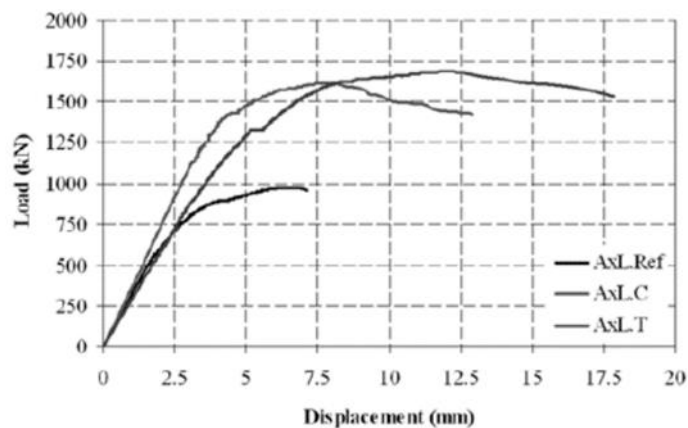
Figure 2.36 Load shortening curve (Adam et al., 2008)

2.2.2.1. Summary

Concerning with the angle and batten jacketing methods, the following summaries were generally drawn. The correct choice of width of end battens depends largely on the target moment and plastic rotation capacity of strengthened column. In addition, intermediate level of skilled labor is required for wider end battens in the plastic hinge region since it demands drilling of holes in the foundation (Nagaprasad et al., 2009). The failure was initiated by the buckling of the vertical angles after yielding in most cases (Tarabia and Albakry, 2014). For compressive axial test, the collapse of the specimen occurred because of the failure of welding in correspondence with very large deformation (Campione et al., 2017).

2.2.3. Precambered steel plate jacketing method

Precambered steel plates are a unique method of steel retrofit for columns. The process consists of placing a steel plate larger than the available space for the column and providing a spacer to plates. Then the spacer is removed and the cambered plate is anchored to the column to relief the column stress. (Wang and Su, 2012) tested precambered steel plates on RC column under axial loading with varying plate thickness, eccentricities, and initial precamber displacements. It was confirmed again that controlling the precamber profile can relief the stress lagging effects. Increasing initial precamber also resulted in more load sharing and higher ultimate load capacity from post compressive stress. Furthermore, (Wang and Su, 2012) studied the seismic behavior of preloaded rectangular RC columns strengthened with precambered steel plates under high axial load ratios and severe lateral reverse cyclic loading. A sufficient amount of shear reinforcement was provided to the specimens to avoid shear failure. A total of six specimens was fabricated and tested. This approach allowed the steel plates to share the existing column axial loads with the original column. The post - stressing procedure was adopted to decompress the RC column and the precambered plates were pressed to achieve a high order buckling mode by tightening the bolts at mid height of the specimens. Layout of the strengthened specimens is shown in Figure 2.37. Summary of the strengthening details is shown in Table 2.12.
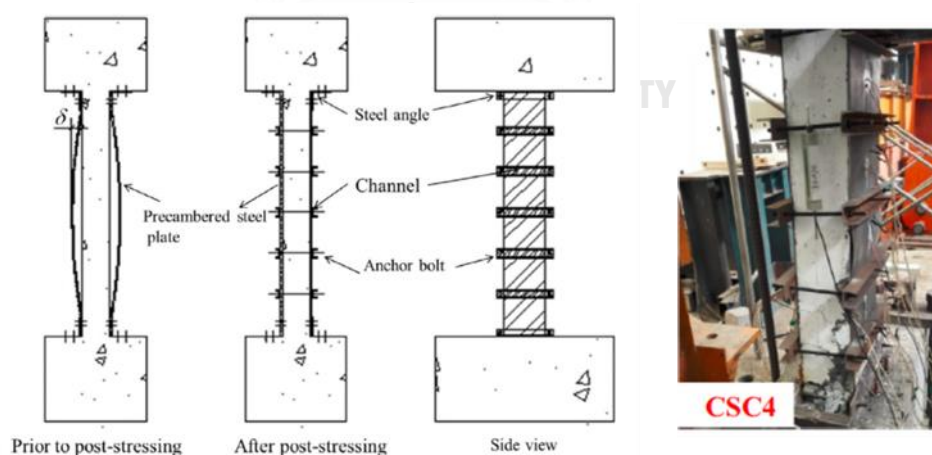
Figure 2.37 Layout of strengthened columns (Wang and Su, 2012)

Table 2.12 Summary of strengthening detail (Wang and Su, 2012)

Specimen	f_{cu} (MPa)	f_c' (MPa)	t_p (mm)	δ (mm)	P_{pl} (kN)	φ
CSC1	42.3	37.6	-	-	960	0.6
CSC2	41.3	34.8	6	0	960	0.6
CSC3	41.9	35.9	3	16	960	0.6
CSC4	42.7	36.5	6	8	960	0.6
CSC5	42.5	37.3	6	16	960	0.6
CSC6	42.0	36.2	6	16	1120	0.7

Then, the testing results demonstrated that the post compressed approach is effective in increasing the level of lateral displacement ductility while maintaining columns high axial load carrying capacity. The external steel plates can considerably improve the lateral force and ductility of the strengthened columns under reversed cyclic lateral loading. Occurrence of brittle failure can be achieved with the use of thicker steel plates. The reason is that the thicker steel plates can provide much more resistance to the applied load. This evidence can be seen in CSC4, CSC5 and CSC6 specimens. Envelope curves of lateral force and drift ratio of columns are shown in Figure 2.38.
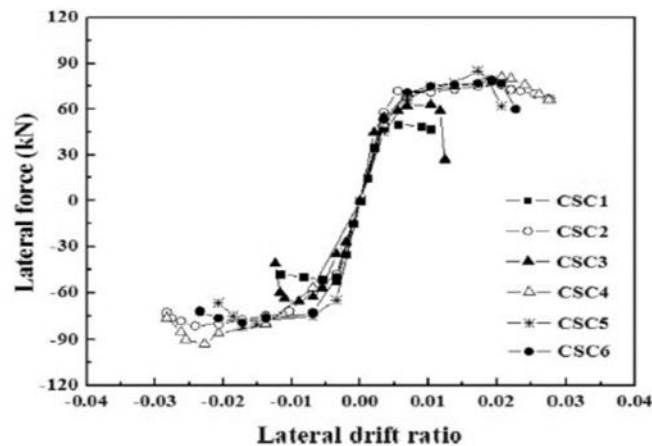
Figure 2.38 Envelope curve of load drift ratio (Wang and Su, 2012)

2.2.4. Corrugated steel jacketing method

Using corrugated steel jackets, (Ghobarah et al., 1997) conducted an experimental investigation to provide the confining pressure by passive restraint in the hinge region to the columns designed during the 1960s. The corrugated steel jacket was found to be effective in the rehabilitation of the selected existing structures. Three specimens were tested, but the first specimen and second specimen were detailed to

represent the existing reinforced concrete frame. The specimen S2 was rehabilitated using the corrugated steel jacket around the column to enhance its seismic behavior. Detail of reinforcement of specimen S1 and S2 and rehabilitation system is shown in Figure 2.39.

(a) Specimen S1 and   (b) Rehabilitation system
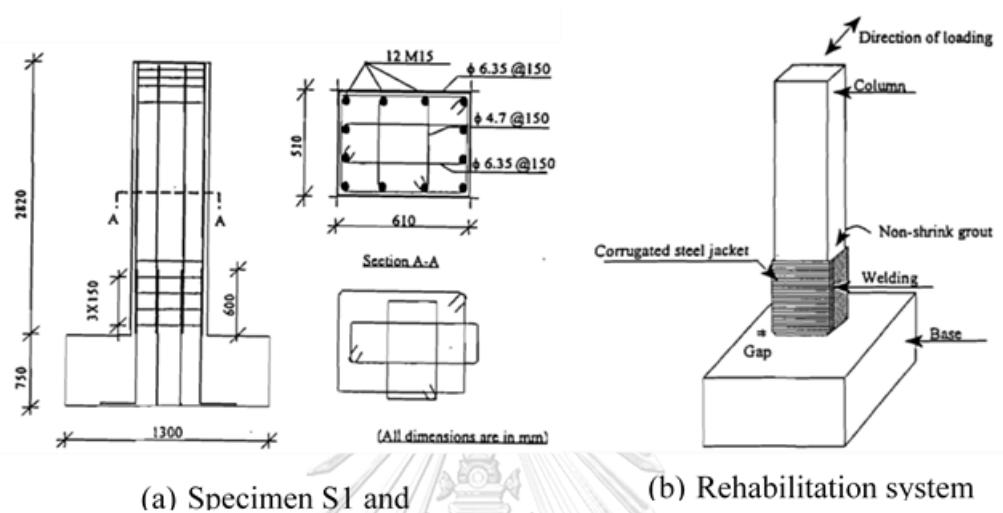
Figure 2.39 Detail of reinforcement of specimens (Ghobarah et al., 1997)

The results of the tests showed that corrugated steel jacket rehabilitation system was beneficial in inhibiting the bond slip failure of lap splices and restraining the buckling of longitudinal steel. Therefore, this method was preferred for lap splice columns. Specimen S2 with corrugated steel jacket improved energy dissipation and slower stiffness degradation. Nevertheless, the jacket dimensions should allow the use of non-shrink ground of a thickness not less than 25 mm for ease of grout pouring. In addition, a 25 to 50 mm gap between the column base and the column jacket was proposed to avoid the unnecessary flexural strength degradation, which may adversely cause excessive moment demands on foundation. The load displacement relationship of the two specimens is shown in Figure 2.40.
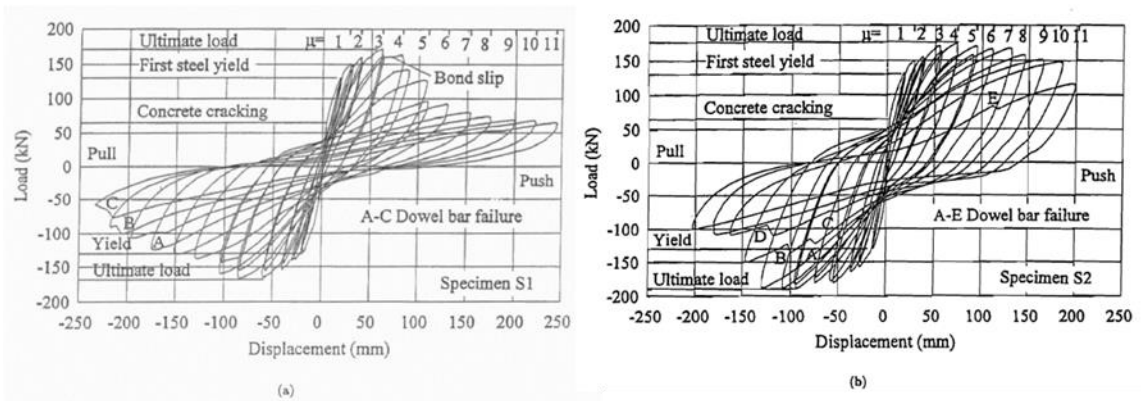
Figure 2.40 Load displacement relationship of two specimens (Ghobarah et al., 1997)

2.2.5. Partially stiffened steel jacketing methods

In order to avoid the steel plate jacketing bugling in the plastic hinge area, (Xiao and Wu, 2003) proposed the rectified steel jacket technique which was adding stiffeners in the plastic zones to the steel plate jacketing columns in order to show the improvement of the stiffeners under the seismic behavior of existing damaged columns. Five rectangular RC columns and a control specimen of 1/3 scale model were tested under constant axial load and cyclic loads. Detail of the column specimens is shown in Figure 2.41. Column test parameters are shown in Table 2.13. Detail of retrofitted specimens is shown in Figure 2.42.
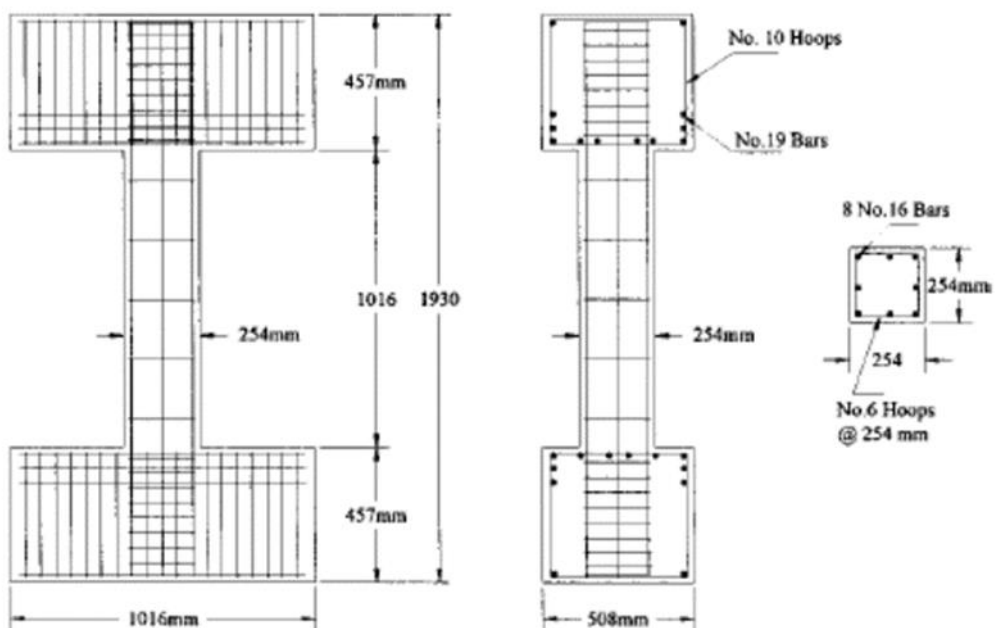
Figure 2.41 Detail of the column specimens (Xiao and Wu, 2003)

Table 2.13 Detail of the column specimens (Xiao and Wu, 2003)

Test Unit	fc' (Mpa)	Axial Load (kN)	Retrofit Details
RC-1A	45	930	As built
RC-2R	57	1112	3.175 mm rec. jacket fyj = 393 Mpa
RC-3R	57	1112	3.175 mm rec. jacket with 15.9mm plate fyj = 328 Mpa
RC-4R	57	1112	3.175 mm rec. jacket with 31.8 x 31.8 x 6.4 mm angles as stiffeners, fyj = 367 Mpa
RC-5R	60	1157	3.175 mm rec. jacket with 31.8 x 31.8 x 6.4 mm square tubes as stiffeners, fyj = 491 Mpa
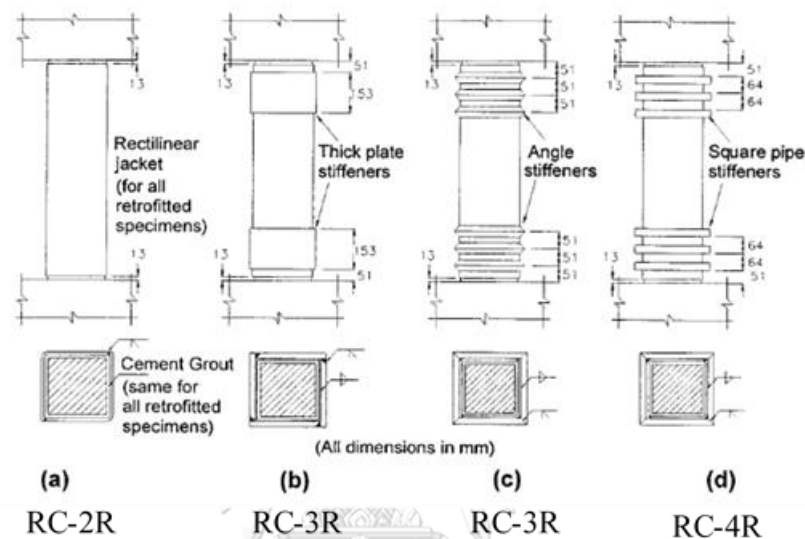
Figure 2.42 Detail of the retrofitted specimens (Xiao and Wu, 2003)

In relation to the test results, the partially stiffened rectilinear steel jacketing not only prevented the brittle shear failure, but also improved the ductility of the column with achieving an ultimate drift ratio of more than 8%. However, for retrofitted columns with rectilinear steel jacket only, the stiffness of the jacket in out of plane direction was insufficient to effectively confine the concrete. The column failure was initiated by bulging out of the steel jacket near the column ends followed by rupture of welded corners. Meanwhile, longitudinal steel buckled. Conversely, the steel jacketed column with stiffeners had no physical damage was observed except concentrated wide opening of the flexural cracks at the column ends. Angle stiffeners may be the most feasible, since they are more readily available and easy to install. The geometric shape of stiffness does not have a drastic effect on the hysteretic behavior of retrofitted column (Abedi et al., 2010). The load drift hysteresis response of the retrofitted specimens is shown in Figure 2.43.
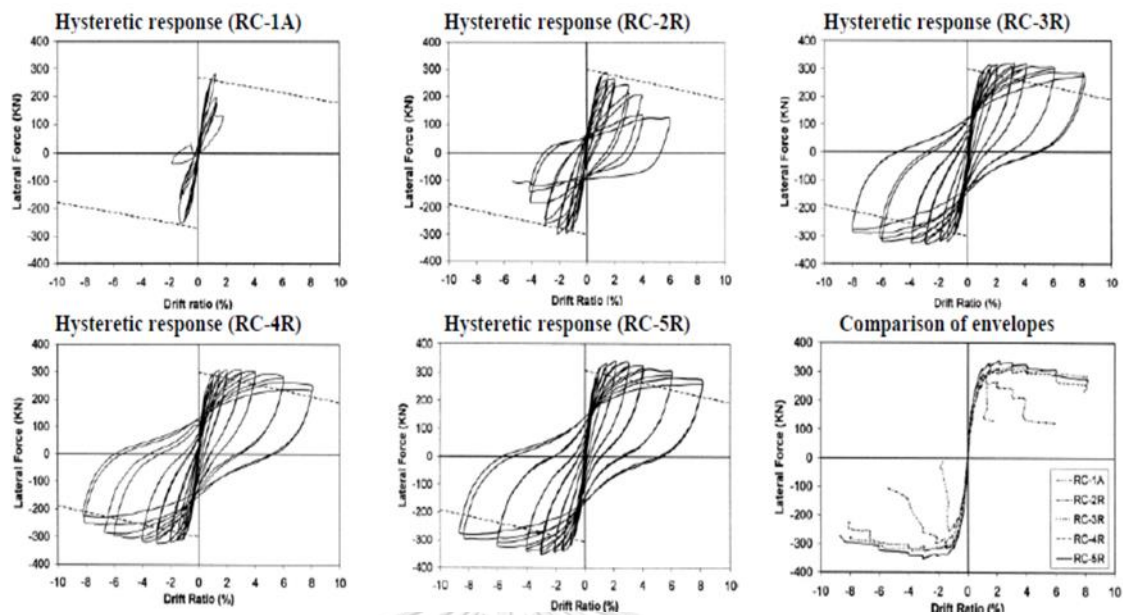
Figure 2.43 The load drift hysteresis response of the retrofitted specimens (Abedi et al., 2010)

2.2.6. Steel collar jacketing methods

(Rodrigues et al., 2016) studied the numerical modelling of RC columns strengthened with CFRP jacketing and steel plates jacketing under biaxial loading and compared with test results. The steel plate was L shaped folded, bonded to the column with epoxy resin and welded in situ in two corners to complete the collar. The plates were placed in three defined levels at increasing distances from the footing. After the wedding, the void between the plates and the concrete were filled with injection of epoxy resin in order to ensure full contact and early efficiency of the external strengthening. Three specimens were strengthened with steel jacketing and four specimens were strengthened with CFRP jacketing. The test result was compared with numerical results for evaluating the numerical modelling efficiency. A constant axial load of 300 kN was maintained and cyclic bi-axial horizontal loading (diagonal 45 and diamond pattern were imposed on the top of the columns. The numerical modelling of the specimens were performed in the computer program of SeismoStruct. Steel jacketing specimen details and test setup the specimen is shown in Figure 2.44. Three steel jacketing columns detail is shown in Table 2.14.
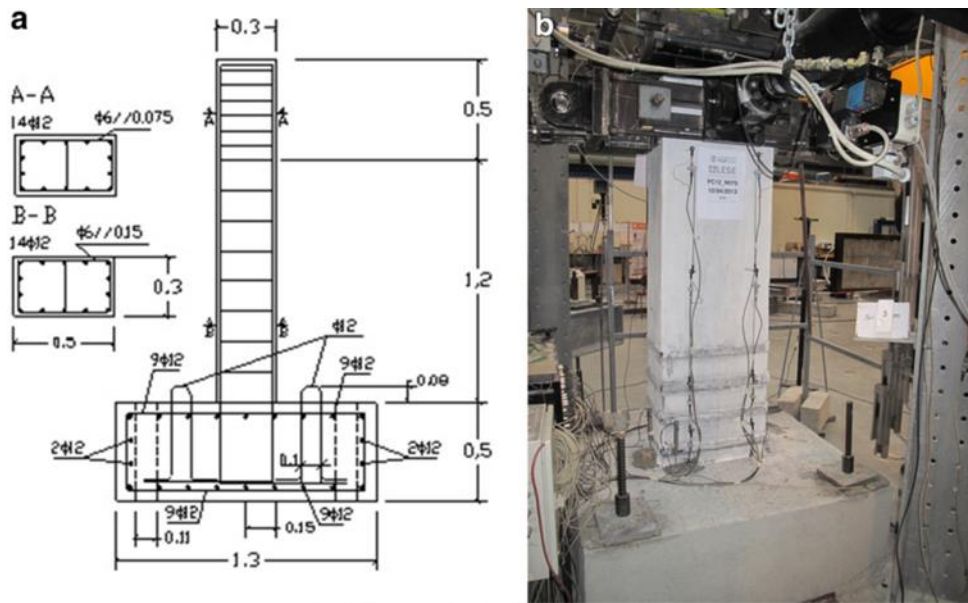
Figure 2.44 Specimen detail and test set up of specimen (Rodrigues et al., 2016)

Table 2.14 Jacketing specimens detail (Rodrigues et al., 2016)

Group	Samples	Compressive strength f_c (kPa)	Elasticity modulus E_{steel} (GPa)	Strain at peak strength ε_c (‰)	P_{steel}
2	PC12-N11S	8400	210	4.5	0.0013
	PC12-N15S	15,950			
	PC12-N16S				

Experimental results demonstrated that a good hysteresis behaviour of collar strengthened column. Also the numerical model represented very satisfactory the maximum strength of the experimental results. The shear drift response of experimental result and numerical results is shown in Figure 2.45.
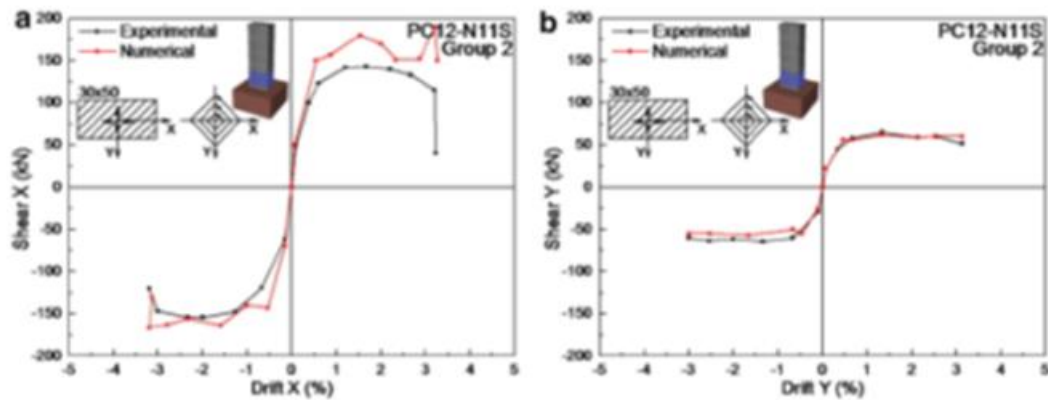
(a)
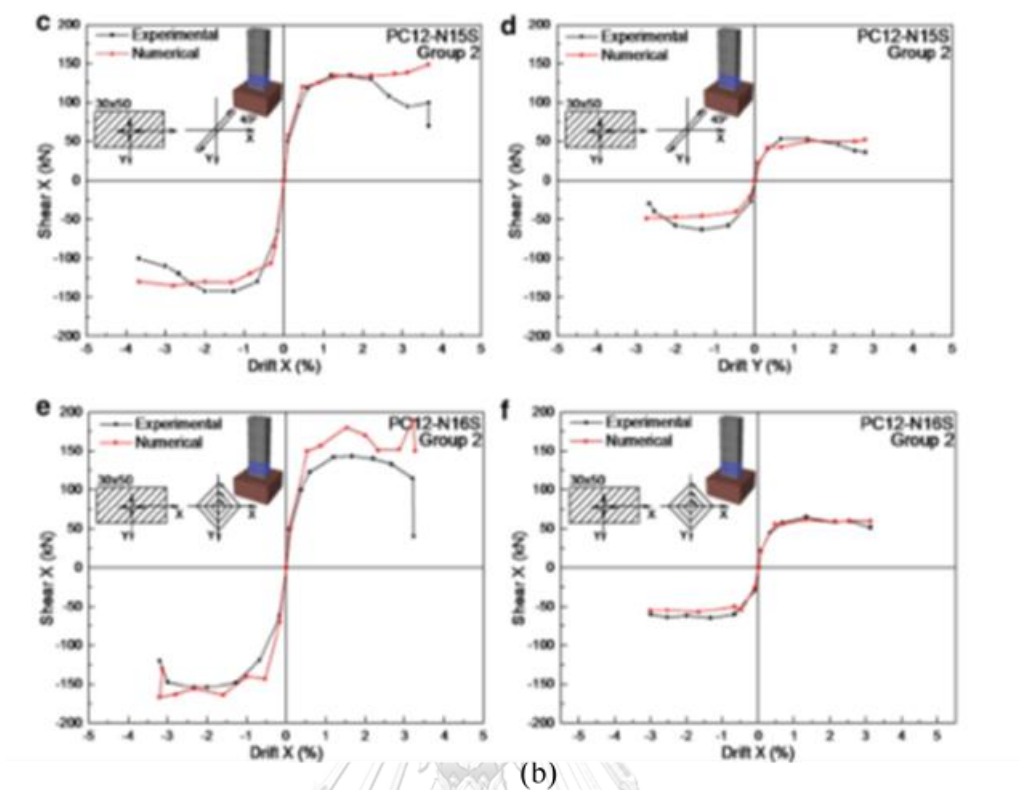
Figure 2.45 (a) and (b) Shear drift hysteresis response (Rodrigues et al., 2016)

As another approach of collar jacketing, (Hussain and Driver, 2005) proposed a relatively simple scheme that confines the concrete, externally with hollow structural section (HSS) collars that possess a combination of significant flexural and axial stiffness. These collars do not only provide the benefits of efficient confinement, but also inhabit spalling of the outer concrete shell and provide additional shear reinforcement. Typical collars made from HSS sections with bolted or welded corner connections as shown in Figure 2.46. In the case of the collars with bolted corner connections, 25.4 mm diameter high strength threaded rods were used
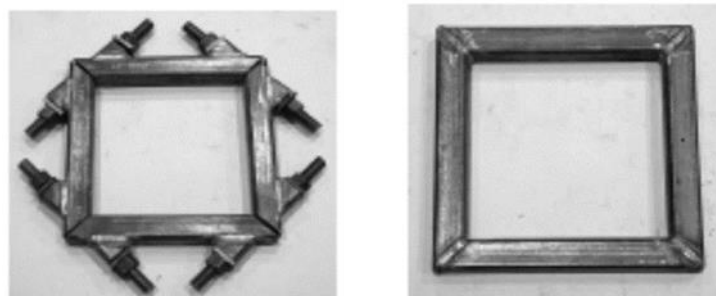
Figure 2.46 Bolted collar and welded collar (Hussain and Driver, 2005)

In the case of the collar with welded corner connection, a partial penetration single- V groove weld was deposited all around the corner joints and welded. A total of 11 columns was tested; two columns with conventional reinforcement was control columns and the remainders had external steel collars. For those columns which had external steel collars, no tie reinforcement was provided in the test region in order to study the effect of external confinement. Column reinforcement details and typical test specimen with welded collars in the test region is shown in Figure 2.47. Description of the column specimens is shown in Table 2.15
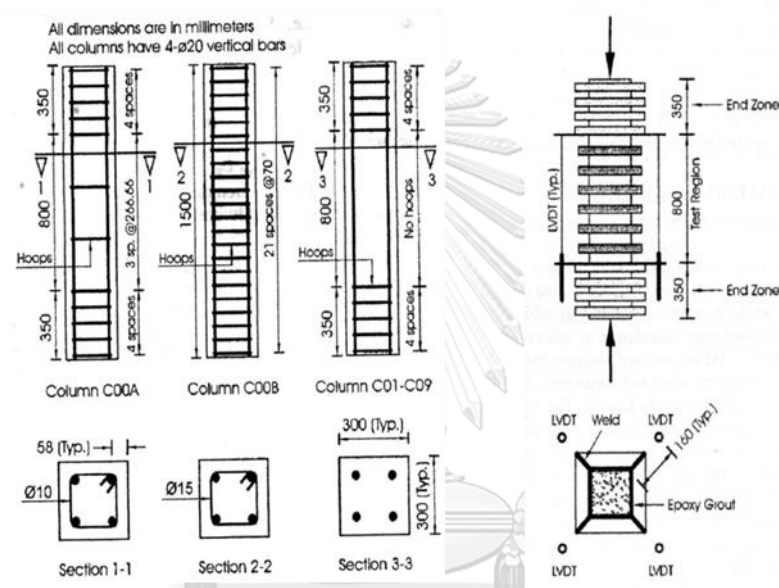
Figure 2.47 Column reinforcement details and typical test specimen

(Hussain and Driver, 2005)

Table 2.15 Description of the column specimen (Hussain and Driver, 2005)

Specimen	Type	Size, mm	Spacing on centers, mm	Type of corner connection	Cross-sectional area, mm²	Volumetric ratio ρ_t, %
C00A	Conventional reinforcing bars	ϕ10	267	—	100	0.70
C00B		ϕ15	70	—	200	5.19
C01	Collars made from hollow structural sections (HSS)	HSS 51 x 51 x 6.35	122	Bolted	375[*]	4.81[*]
C02		HSS 76 x 51 x 6.35	122	Bolted	375[*]	5.15[*]
C03		HSS 76 x 51 x 6.35	122	Bolted	375[*]	5.15[*]
C04		HSS 76 x 51 x 6.35	170	Bolted	375[*]	3.68[*]
C05		HSS 76 x 51 x 6.35	95	Bolted	375[*]	6.63[*]
C06		HSS 51 x 51 x 6.35	122	Welded	1085	13.92
C07		HSS 76 x 51 x 6.35	122	Welded	1375	18.90
C08		HSS 102 x 51 x 6.35	122	Welded	1734	25.48
C09		HSS 76 x 51 x 6.35	170	Welded	1375	13.50

As the author expected, column C00A showed the brittle failure because of the relatively wide spacing of the ties and the degree of confinement was very low and the column behaviour wss unconfined concrete. Column C00B showed brittle failure because of the closely spaced hoops in the test region. Column C01, C02, C03, C04 with bolted collars showed ductile failure. The ductility of the column C04 was lower because of the large collar spacing. Column C05 was not failed completely, terminated prematurely and the failure strain was not known. Column C06, C07, C08 and C09 with welded collars exhibited brittle failure that had fractured at the corners weld in one or more of the collars. Generally, the provision of HSS collars results in considerable enhancement in strength as well as ductile. The effective core area of externally confined is larger than the conventional columns. However, the hollow structural section (HSS) collars were not cost effective and it may not be easy to install the collars are heavy weight. The load displacement relationship of the test columns is shown in Figure 2.48
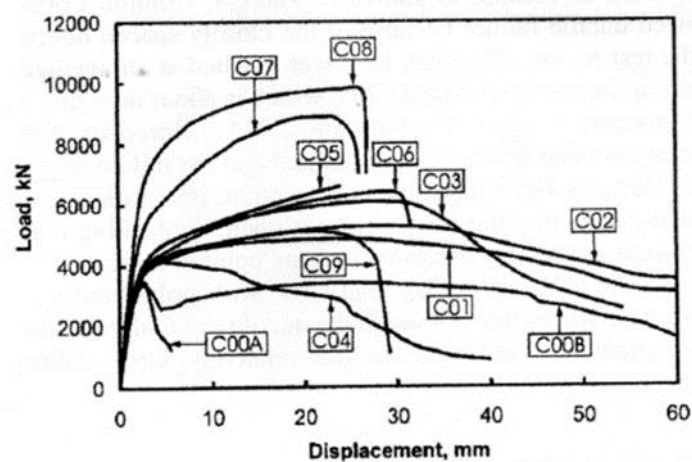
Figure 2.48 Load displacement relationship of the test columns

(Hussain and Driver, 2005)

Similar to the Husssian and Driver, (J. Liu et al., 2011) investigated reinforced concrete columns strengthened by the steel collar jacketing method. The collars consisted of two L-shaped pieces cut from a 50 mm thick steel plate in a commercial fabrication shop using a conventional computer controlled Oxy-gas cutting table which is cost effective in comparison to build-up a hollow structural section (HSS) collars of Hussain and Driver (2005). The purpose of this method is to confine the concrete with

significant flexural and axial stiffness. Ten cantilever column including two control columns and eight rehabilitated columns tested under combined axial load and cyclic load through full scale experiment. Specimen reinforcement details are shown in Figure 2.49. Test specimen detail is shown in Table 2.16. Fabrication and assembled view of the steel collar is shown in Figure 2.50. Test set up of the retrofitted column is shown in Figure 2.51.
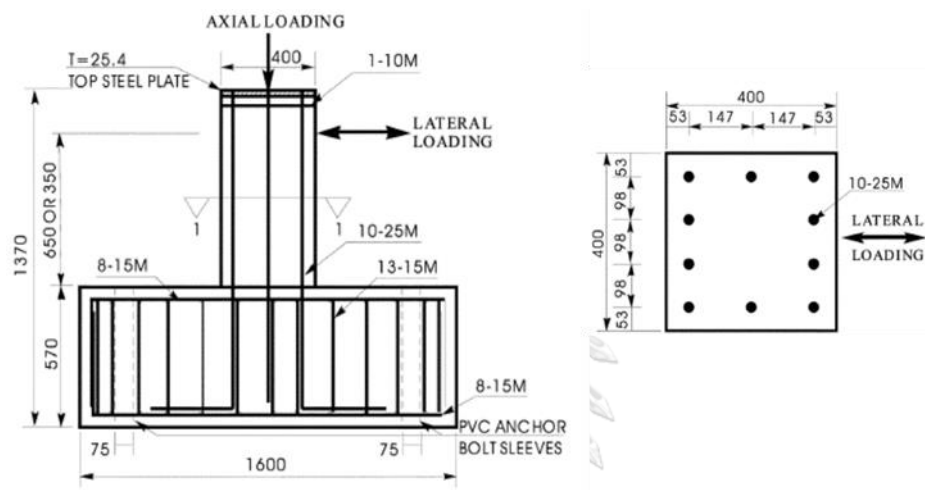
Figure 2.49 Specimen reinforcement details (J. Liu et al., 2011)

Table 2.16 Detail of test specimens (J. Liu et al., 2011)

Specimen	Aspect ratio $M/(VD)$	Collar cross section,* mm x mm	Collar center-to-center spacing,† mm	Axial compression index $P/(f'_c A_g)$	Longitudinal reinforcement ratio‡ ρ	P/T in collar bolt, kN
CV0A	1.63	—	400	0.3	3.13%	—
CV0AR	1.63	30 x 50	150	0.3	3.13%	10
CV0B	1.63	—	100	0.3	3.13%	—
CV1	1.63	30 x 50	150	0.3	3.13%	9
CV2	1.63	30 x 50	200	0.3	3.13%	12
CV3	1.63	30 x 50	95	0.3	3.13%	12
CV4	1.63	30 x 50	150	0.3	1.88%	12
CV5	0.88	30 x 50	150	0.3	3.13%	11
CV6	1.63	30 x 50	150	0	3.13%	11
CV7	1.63	30 x 50	150	0.3	3.13%	144
CV8	1.63	50 x 50	150	0.3	3.13%	13
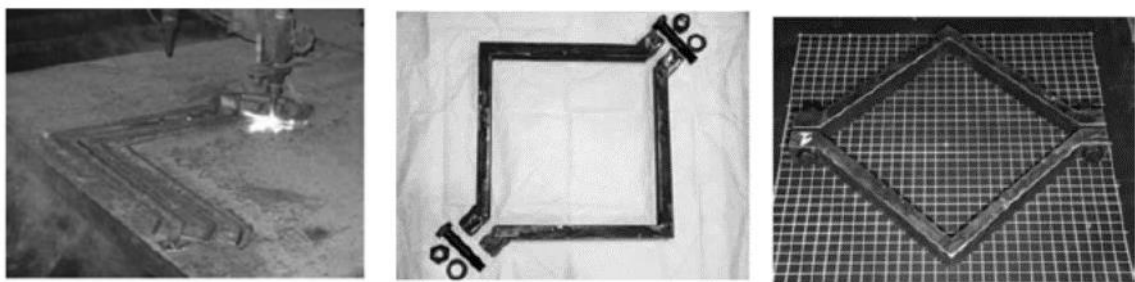
Figure 2.50 Fabrication and assembled view of the steel collars (J. Liu et al., 2011)
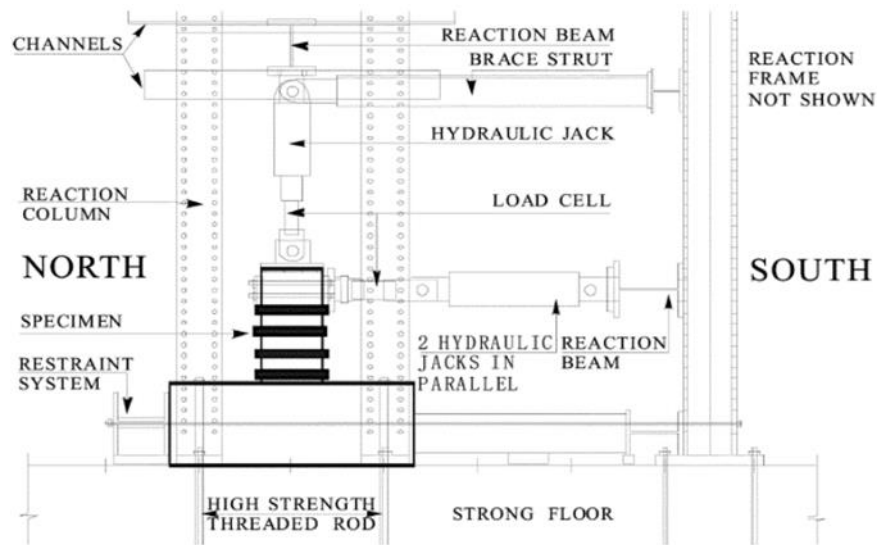
Figure 2.51 Test set up of typical retrofitted specimen (J. Liu et al., 2011)

Based on the test results, the author concluded that all columns exhibited flexural failure except the specimen without axial load. Generally, the experimental results showed excellent improvement in ductility, strength, and energy dissipation capacity of the columns due to the presence of the collars. With no slippage of the collars was observed except plastically outward to some degree. No concrete spalling occurred directly under the collars. In general, the steel collars allowed a more general degradation of strength after the peak load, as compared to the control columns without collars. The experiments showed that the collar columns had stable hysteresis behaviour as shown in Figure 2.52. Force displacement envelopes for retrofitted test specimens is shown inFigure 2.53.
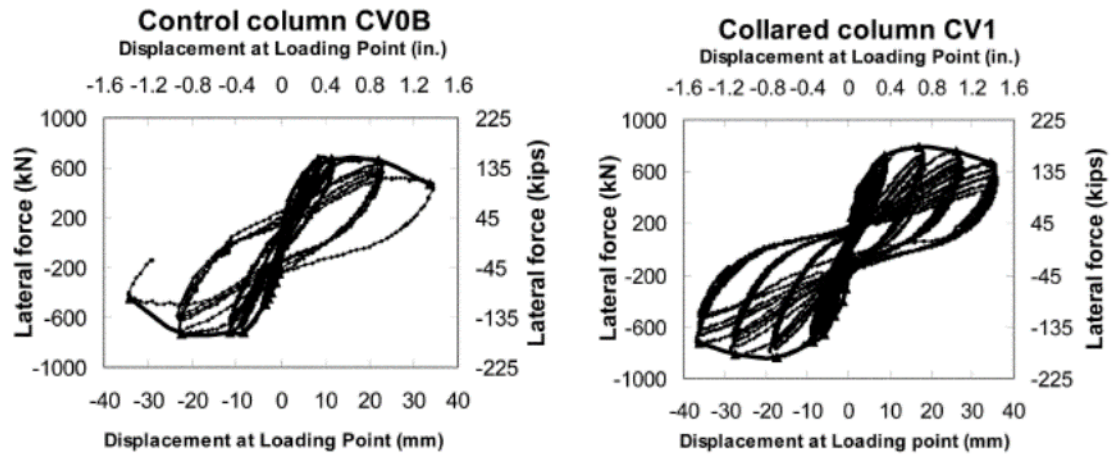
Figure 2.52 Hysteresis behavior of retrofitted specimen (J. Liu et al., 2011)
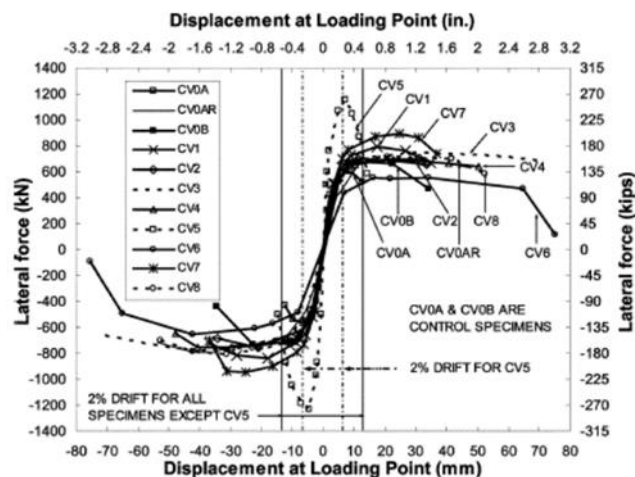
Figure 2.53 Force displacement envelopes for retrofitted test specimens

(J. Liu et al., 2011)

2.2.6.1. Summary

The steel collars jacketing methods were able to confine the concrete as a confinement effectiveness and gave the excellent improvement in ductility, strength, and energy dissipation capacity of the columns. Due to the presence of the collars, no concrete spalling which was under the collars were occurred. However, it can be cost ineffective if the columns is retrofitted by HSS collars. HSS collars or bolted collars seem to be satisfactory for deficient short reinforced concrete columns.

2.3. Review of Modelling Strategies of Reinforced Concrete Columns

The earthquake performance of RC buildings has been well documented from the observation of past seismic events. Ten most common causes of failure or damage in RC buildings: (1) lack of stirrups/hoops, confinement and ductility; (2) bond/anchorage/lap-splices slipping and bond splitting; (3) inadequate shear capacity; (4) inadequate flexural capacity; (5) inadequate shear strength of the joints; (6) influence of the infill masonry on the seismic behaviour of frames; (7) vertical and horizontal irregularities, abrupt change in structural and/or element properties; (8) higher modes' effects; (9) strong-beam weak-column mechanisms; and finally, (10) structural deficiencies due to architectural requirements. The collapse of an RC building is mainly caused by the failure of the vertical members in the majority of cases. Failure of a reinforced concrete column are classified into three major types: shear, bond splitting of the longitudinal reinforcement and flexural modes. In recent years, many researchers had attempted to study the behavior of the reinforced concrete columns experimentally under combined axial and cyclic lateral loading. In addition, the analytical and numerical modeling strategies for reinforced concrete columns had been studied for many decades that is capable of simulating the behaviour of reinforced concrete members subjected to seismic loading. The modelling strategies are built in Open System for Earthquake Engineering Simulation (OpenSees) program for simulating the seismic response of structure.

2.3.1. Force based beam column element model

In this strategy, the column element is modeled using the force based fiber beam column elements. The consecutive stress, strain relationship of concrete and steel that is assigned to the fiber section. It is assumed that column are fixed to the ground and each column is represented by a single fiber element which can be seen in Figure 2.54.
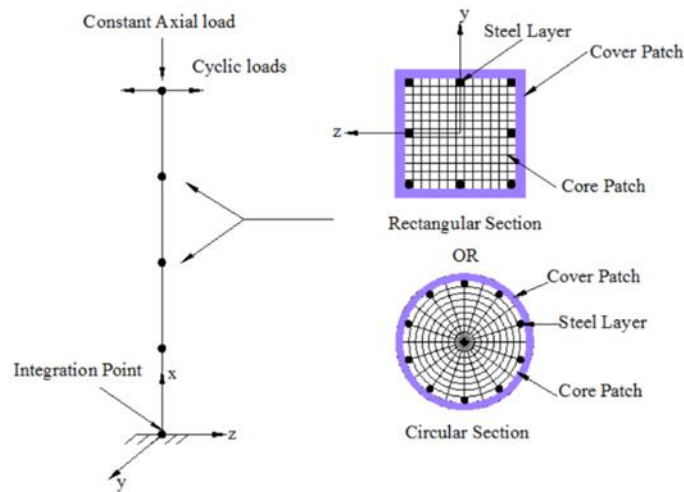
Figure 2.54 Forced based beam column element model (Huang, 2012)

Force based beam column element allows the plasticity to spread along the length of the column by using number of integration points. Since the column ends are considered to be critical, integration points are placed at the end of the element. The number of integration points are not sensitive to the global response, but local behavior is very significant. (Berry and Eberhard, 2006) had carried out the investigation on the influence of the number of integration points. Then, it is found that for hardening behaviour of columns, global and local responses do not vary when at least four integration points are assigned. However, the softening behavior of the columns, the number of integration points have a great impact on both local and global responses. In addition, a proper number of fiber is also important to minimize the computational demands without reducing the accuracy. Significant errors are only produced when very crude fiber mesh are used (Huang and Kwon, 2015).

2.3.2. Lumped plasticity column model

(Scott and Fenves, 2006) developed a lumped-plasticity formulation suitable for implementation in a standard displacement-based finite-element environment. The formulation utilizes the force-based fiber beam column element formulation, and introduces a modified integration scheme, in which inelastic deformations are confined to an assigned plastic-hinge length. The curvature distribution is linear above the plastic-hinge, and within the plastic-hinge the curvature is calculated with moment-

curvature analysis similar to the force-based beam-column element. The lumped plasticity model is shown in Figure 2.55.
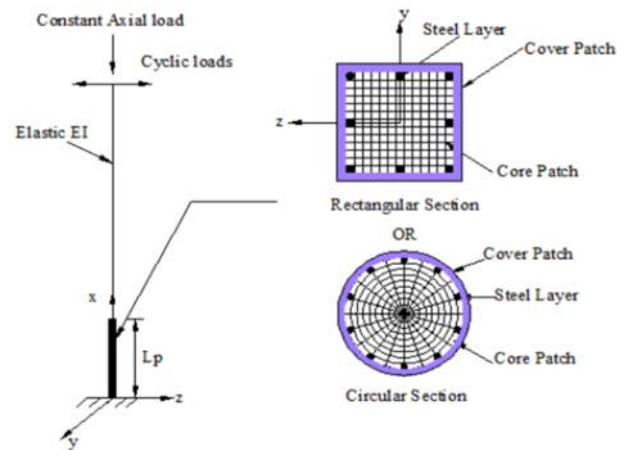
Figure 2.55 Lumped plasticity column model (Huang, 2012)

The lumped plasticity model allows the user modify the stiffness by changing elastic modulus (E_c) and initial stiffness (I_c) of the elastic segment. The accuracy of the model mainly relies on proper definition of the stiffness and plastic hinge length.

2.3.3. Numerical models of RC columns

During the recent years, many of the researchers focused on predicting the inelastic hysteretic behavior of flexural failure columns, flexural shear failure columns and the pure shear failure columns. (Del Vecchio et al., 2013) studied the numerical model for flexural reinforced concrete columns subjected to cyclic loading by using fiber element in OpenSees. Lumped plasticity model is adopted. A column of (Tanaka, 1990) was used to valid the proposed numerical model as shown in Figure 2.56. Five integration points were used. In the fiber model, the unconfined concrete and confined concrete were simulated with the nonlinear Concrete02 material. Longitudinal reinforcement was modelled with the Steel02 material model. Mechanical properties of concrete core were formulated (Mander et al., 1988) model. It had shown that the close match of experimental hysteresis response with the OpenSees fiber model numerical results as shown in Figure 2.57.
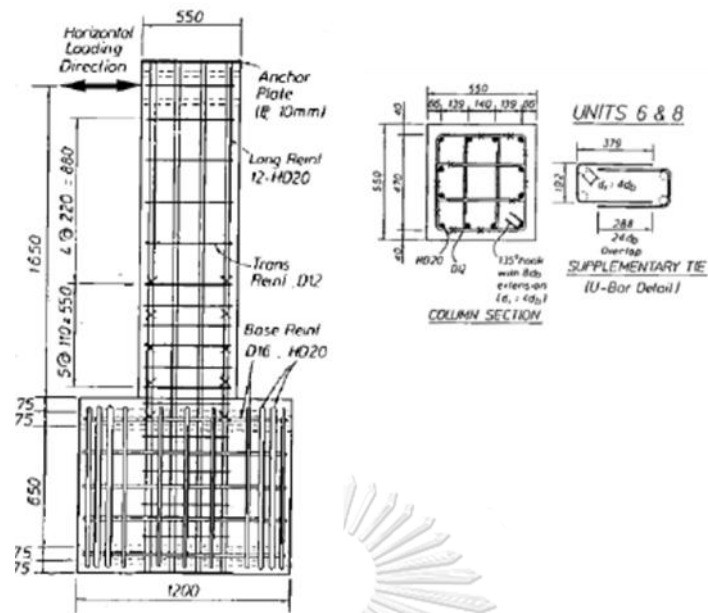
Figure 2.56. Detail of column specimen (Tenaka, 1990)
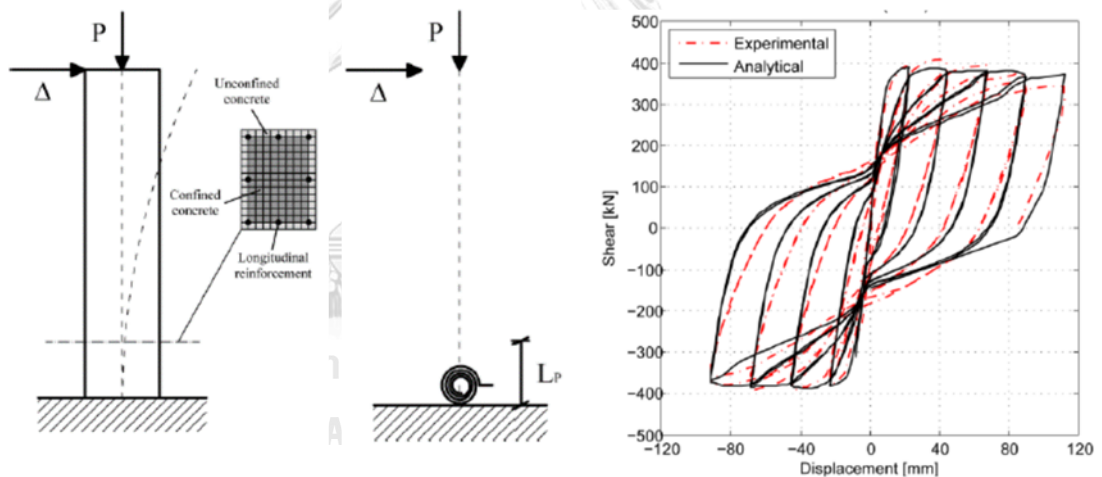
Figure 2.57 (a) Analytical model for flexural failure column

(b) Experimental and Analytical result (Del Vecchio et al., 2013)

The reinforced concrete column with widely spaced transverse reinforcement are vulnerable to shear failure. Even though there have been many years of experimental and analytical investigation, imitating the hysteretic behaviour of flexural shear critical RC column is still challenging task. Therefore, numerical study on the flexural shear critical reinforced concrete RC columns were studied by (Wang and Oh-Sung, 2014). The specimens have a sectional dimension of 200 mm x 200 mm and height of 800 mm as shown in Figure 2.58
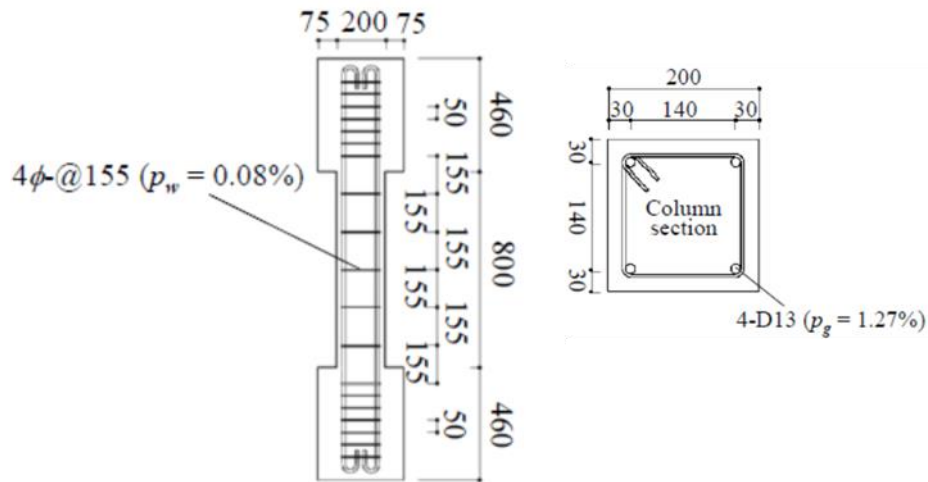
Figure 2.58 Detail of column specimen (Wen and Oh-Sung, 2014)

The numerical element composed of a two dimensional nonlinear beam column with fiber section located at the integration points. The specimen was modeled three nodes and each node had three degrees of freedom as shown in Figure 2.59 Five integration points are defined along the nonlinear beam column element. The Concrete04 material model is simulated for confined and unconfined concrete and hysteretic material model is used for longitudinal reinforcement.
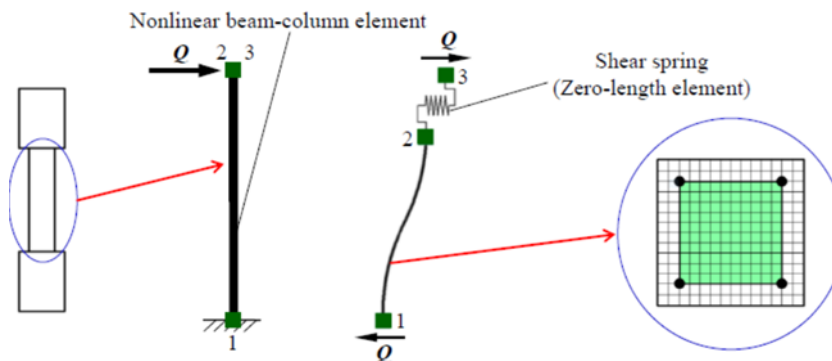
Figure 2.59 Numerical element in OpenSees (Wen and Oh-Sung, 2014)

To capture the shear strength degradation of the, a shear spring was assigned using the zero length element as shown in above figure. The shear spring was defined by the limit state material with shear limit curve based on the work of (Elwood, 2004). The cyclic analysis was carried out at the top of the column. Then, the author concluded that it was possible to detect the shear failure of the specimen using OpenSees by introducing a shear spring element and shear limit curve. The numerical result almost

agreed with the experimental ones before detection of shear failure. Comparison of the hysteretic response of experimental and numerical result is shown Figure 2.60.
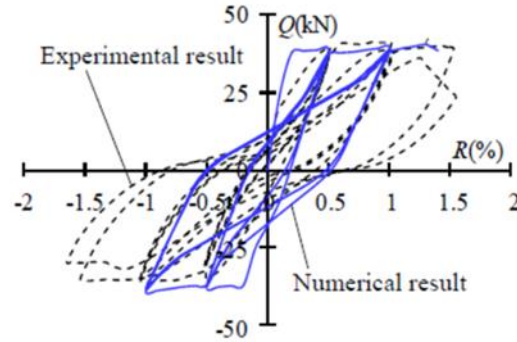
Figure 2.60 Comparison of experimental and numerical result

(Wen and Oh-Sung,2014)

In order to provide a guideline for the numerical modelling of RC frame element for the seismic performance assessment of a structure, (Huang and Kwon, 2015) investigated the numerical analysis of flexural critical columns and shear critical column.. Two sample reinforced concrete columns were selected from the PEER column data base. Reinforcement detail of two sample reinforced concrete columns is shown in Figure 2.61.
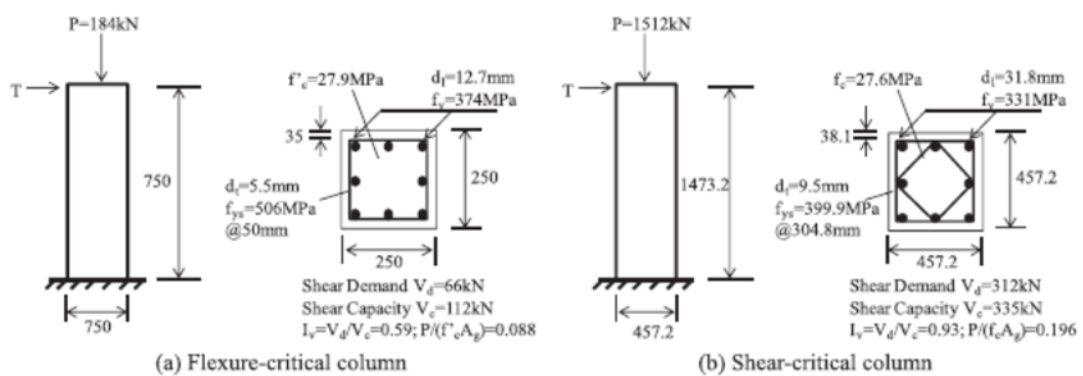
Figure 2.61 Reinforcement details of two sample RC columns

(Huang and Kwon, 2015)

Forced based beam column element and lumped plasticity model was used in OpenSees program to analyze the columns. This can be seen in Figure 2.62. Five integration points are used to efficiently compare the global response of the RC columns. The shear spring was added to detect the elastic shear deformation ($K_{shear}=$

GA$_g$/L) at the bottom of the column. The Concrete01 material model (Kent and Park concrete material) was defined in unconfined concrete in the fiber section. The Confinedconcrete01 (Mender et al, 1988) concrete material model was used to define the confine concrete material. Longitudinal reinforcement was characterized by a Steel02 material model (uniaxial Giuffre-Menegotto-Pinto steel material).
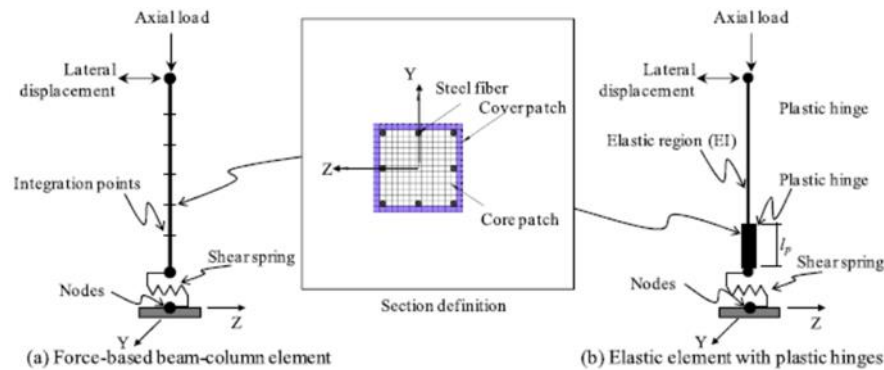
Figure 2.62 Fiber section element (Huang and Kwon, 2015)

Based on the analyzing results, the author concluded that the computationally efficient fiber section model using forced based beam column element model or lumped plasticity model could be used for flexural critical column. The analysis result well matched with the experimental results. However, fiber section model characterized by uniaxial material alone could not capture the shear failure behaviour. Comparison of experimental result and numerical result is shown in Figure 2.63
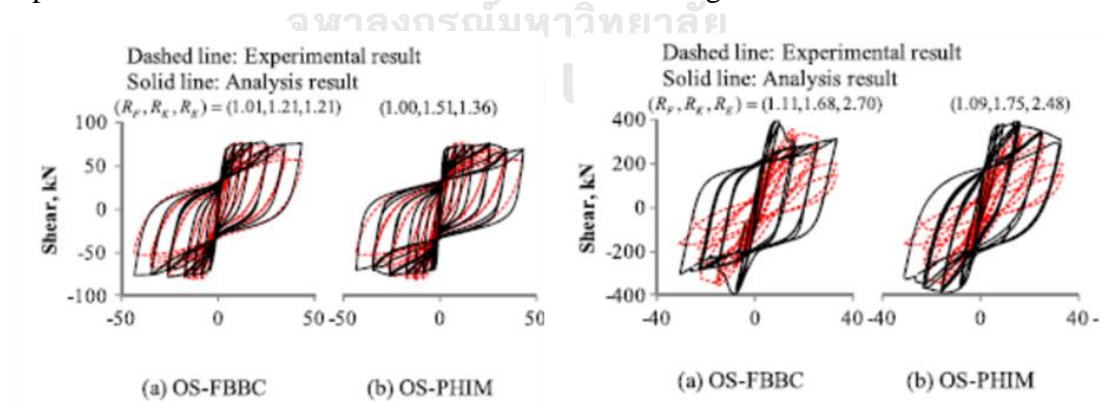
Figure 2.63 Comparison of experimental results and numerical results (Huang and Kwon,2015)

(K.Y. Liu et al., 2015) proposed the composed models for RC bridge piers that can accommodate flexure failure, flexure shear failure and pure shear failure. To check

the accuracy of the analytical models, the author used the data from the static cyclic-loading experiments of 16 single columns and one multi-column bent and dynamical experiment from two pseudo-dynamic tests. The column data base is shown in Table 2.17.

Table 2.17 Column data base (K.Y. Liu et al., 2015)

Number	Failure type	Specimen	b (mm)	h (mm)	d (mm)	a/d	fc (MPa)	ξ	f_{ye} (MPa) Longitudinal reinforcement	f_{ye} (MPa) Transverse reinforcement	ξ	P/(fc.Ag)	Test type	Maximum displacement (mm)	Dissipated energy (kN·m)
								Rectangular section							
1	F	TANEEB1* [44]	1200	1800	1729.4	4.9	39.2	0.0149	432	449	0.0069	0.061	C	423.9	6783.9
2		LDEC2* [45]	600	870	814.6	3.4	41.3	0.0214	475	479.5	0.0062	0.083	C	224.3	1122.3
3		Wehbe A1** [46]	380	610	566.1	4.1	27.2	0.0221	448	428	0.0036	0.098	C	162.9	265.4
4		RCF* [47]	600	600	534.6	6.7	42.2	0.0226	451	335	0.0127	0.1	DC	321.1	4048.5
6	PS	Chang C* [48]	600	750	705.92	4.6	23	0.0202	500	350	0.0053	0.066	C	146.5	92.3
7		BMR2* [49]	600	750	707.52	4.6	26.0	0.0141	343.2	490.3	0.0041	0.079	C	162.3	336.7
8		BMR4* [50]	600	750	707.52	4.6	20.5	0.0141	387.1	451.1	0.0023	0.152	C	162.7	309.0
9		Lynn 3CLH18** [51]	457.2	457.2	393.7	3.7	26.9	0.0313	331	399.9	0.0008	0.09	DC	61.6	35.0
10		ISCE4** [52]	400	400	360	3.5	35.9	0.0161	363	368	0.0024	0.027	C	75.6	160.7
11	S	808BM* [53]	450	450	389.37	2.9	25	0.0229	491	354	0.0016	0.168	DC	45	48.9
12		Umehara CUW** [54]	410	230	189.45	2.4	34.9	0.0301	441	414	0.0036	0.162	DC	14.3	9.3
13		Imai No.1 ** [55]	400	500	454.9	1.8	27.1	0.0271	318	336	0.0037	0.072	DC	18.6	13.1
								Circular section							
1	F	Niu-Dou Bridge P2* [56]	1800		60	1440	6.3	33.4	0.0097	365.4	340.9	0.0024	0.036	C	513.1	911.1
2		Niu-Dou Bridge P3* [56]	1800		60	1440	7.1	36.8	0.0097	471.8	424.5	0.0024	0.033	C	512.8	1822.2
3		Henry 41.5** [57]	609.6		19	487.7	5.0	37.2	0.015	462.0	606.8	0.007	0.060	C	179.1	381.6
4	PS	BMC2* [50]	760		25	608	5.3	25.5	0.0131	343.2	490.3	0.0031	0.121	C	162.6	292.9
5		BMC3* [50]	760		25	608	5.3	21.3	0.0131	387.1	451.1	0.0018	0.145	C	163	266.4
6	S	BMCS* [50]	760		25	608	2.9	16.7	0.0188	425.5	426.5	0.0014	0.15	C	26.2	35.8

The composed analytical models are relatively complex models with nonlinear fiber elements to represent the pier columns and springs in series at the ends of the columns to simulate the bond slip, shear strength degradation. The composed analytical models are shown in Figure 2.64. The 'Concrete04' material model in OpenSees was chosen to represent the Mander model. 'Hysteretic' material model in OpenSees was chosen to represent the bilinear steel model.
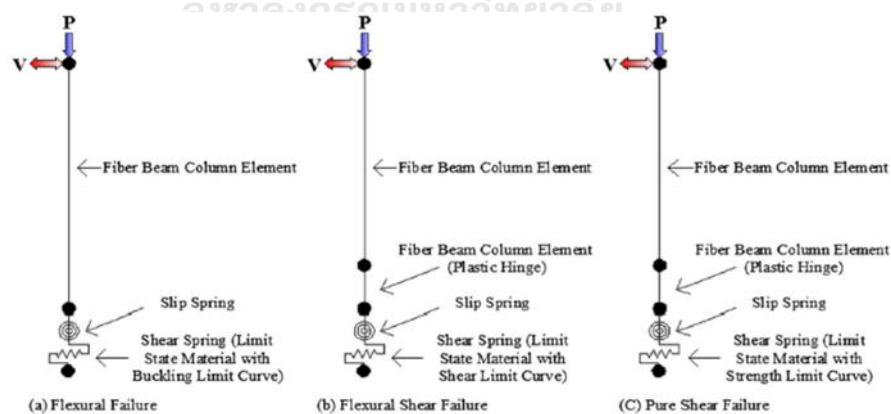
Figure 2.64 Composed analytical models (K.Y. Liu et al., 2015)

To check the accuracy of each models, the author selected the corresponding specimens from the data for each model and then the results were compared with the test results. Four flexural failure specimens were selected to verify the accuracy of the

analytical models. The comparison of hysterics loop between the analytical and experimental results are shown in Figure 2.65.
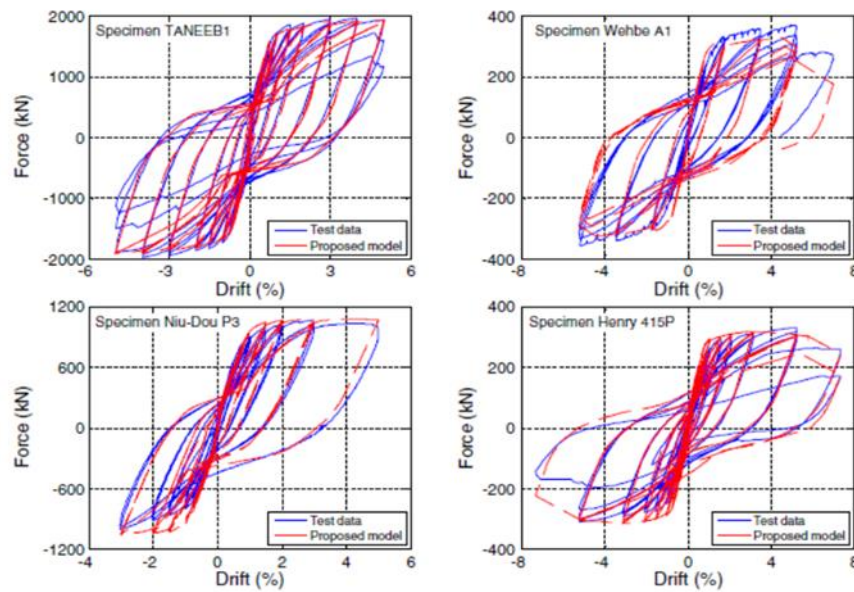
Figure 2.65 Experimental and analytical result of flexural failure specimens

(K.Y. Liu et al., 2015)

For flexural failure specimens, the hysteretic loops from the analytical model were generally consistent with the experiment test results. The initial stiffness, maximum force, and nonlinear flexural behavior were accurately.

To verify the accuracy of the analytical model of flexural shear critical model, four flexure-shear failure columns were used. The comparison of hysterics loop between the analytical and experimental results are shown in Figure 2.66. All results of the linear or nonlinear behaviour were similar to the experiments. In most cases, the analytical model derived a slightly higher rate of strength degradation beyond the shear failure point than the experiments.
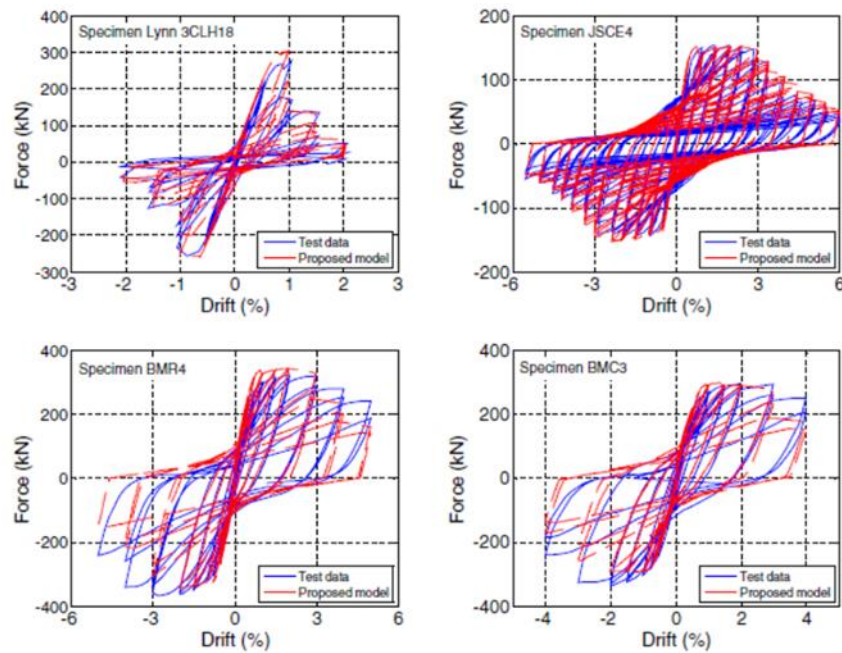
Figure 2.66 Experimental and analytical result of flexural-shear failure specimens

(K.Y. Liu et al., 2015)

To verify the accuracy of the analytical model of pure shear failure model, four pure shear failure columns were used. The comparison of hysterics loop between the analytical and experimental results are shown in Figure 2.67. In specimen RO8BM and CUV, the backbone curve was consistent with the experimental results. However, Imai and MNCS, the backbone curve did not correspond well.
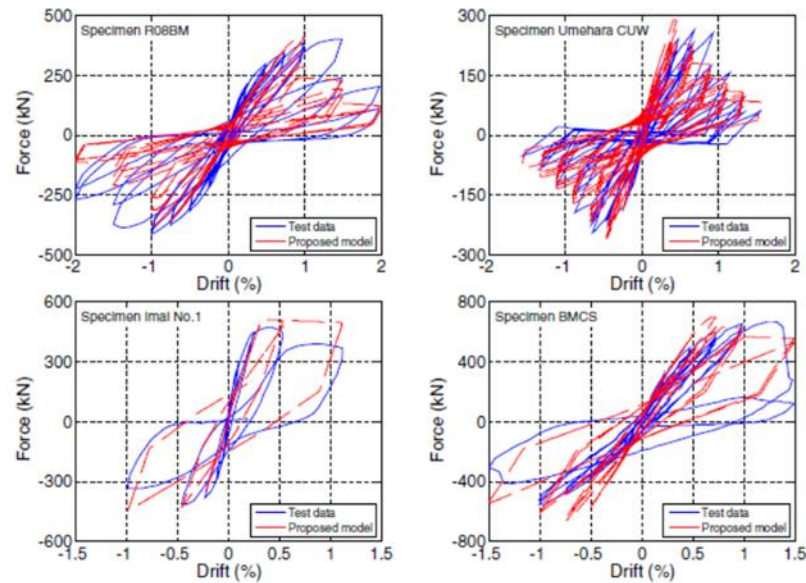
Figure 2.67 Experimental and analytical result of pure shear failure specimens

(K.Y. Liu et al., 2015)

2.4. Limit State Uniaxial Material Model and Column Failures

(Elwood, 2004) introduced a uniaxial material model that incorporates the failure surfaces and subsequent strength degradation. When used in series with a beam-column element, the uniaxial material model can capture the response of the reinforced concrete column during shear and axial load failure. The limit state uniaxial material model was developed based on the existing material model in OpenSees. For modelling the shear strength degradation of the shear critical columns, the limit state material model is used to define the force deformation relationship of a shear spring in series with beam column element as shown in Figure 2.68.
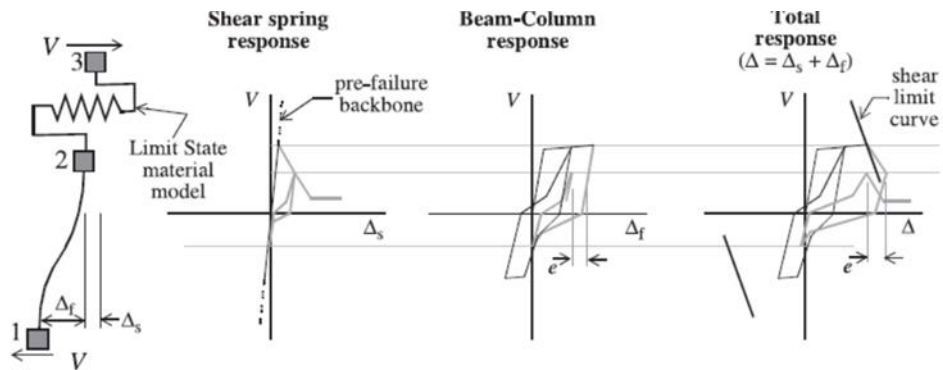
Figure 2.68 Shear spring in series model using limit state uniaxial material model

(Elwood , 2004)

When the beam column response reach the limit curve for the first time the back bone of the shear was redefined to include the degradation slope Kdeg and residual strength Fres . After the failure was detected the response will follow the Kdeg slope. To define the shear limit curve, it is important to define the slope of the third branch in the post failure backbone curve (Kdeg) as shown in Figure 2.69.
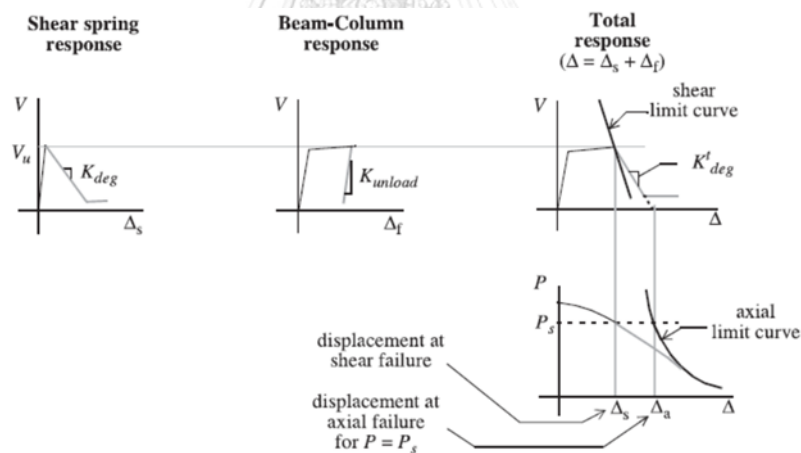
Figure 2.69 Determination of the Kdeg (Elwood,2004)

When the shear failure is detected the degrading slope for the total response K^t_{deg} can be estimated as follows.

$$K^t_{\ deg} = \frac{V_u}{\Delta_a - \Delta_s} \tag{2-1}$$

where,

V_u = the ultimate capacity of the RC column

Δ_s = the calculated displacement at shear failure

Δ_a = the calculated displacement at axial failure

Since the shear spring and the beam column element are in series, the total flexibility is equal to the sum of the flexibilities of shear spring and the beam-column element. Hence, K_{deg} can be determined as follows,

$$K_{deg} = \left(\frac{1}{K^t_{deg}} - \frac{1}{K_{unload}} \right)^{-1} \tag{2-2}$$

where,

K_{unload} = the unloading stiffness of the beam column element

If the column is vulnerable to shear failure after flexural yielding, the drift capacity model was proposed by Elwood (2004) to define the shear limit curve. Then, the displacement at shear failure can be calculated as follows.

$$\frac{\Delta_s}{L} = \frac{3}{100} + 4\rho_v - \frac{1}{40}\frac{v}{\sqrt{f'_c}} - \frac{1}{40}\frac{P}{A_g f'_c} \geq \frac{1}{100} \quad \text{Mpa} \tag{2-3}$$

where,

$\dfrac{\Delta_s}{L}$ = drift ratio at shear failure

ρ_v = transverse reinforcement ratio

v = nominal shear stress

Axial load capacity model also was modelled by Elwood and Moehle(2003) and the drift at axial load failure can be calculated as,

$$\frac{\Delta_a}{L} = \frac{4}{100} \times \frac{1+(\tan\theta)^2}{\tan\theta + P(s/A_v f_{yh} d_c \tan\theta)} \quad \text{Mpa} \tag{2-4}$$

where,

$\dfrac{\Delta_a}{L}$ = drift at axial failure

s = spacing of the transverse reinforcement

$A_v and f_{yh}$ = area and yield strength of the transverse reinforcment

P = axial load

The limit state uniaxial material model can also be used to model the axial failure where the limit curve is defined by an axial capacity model for shear damaged columns. In the axial capacity model, it was assumed that the axil failure has already occurred and that axial failure result from sliding along a critical inclined shear crack. The model is illustrated in Figure 2.70.
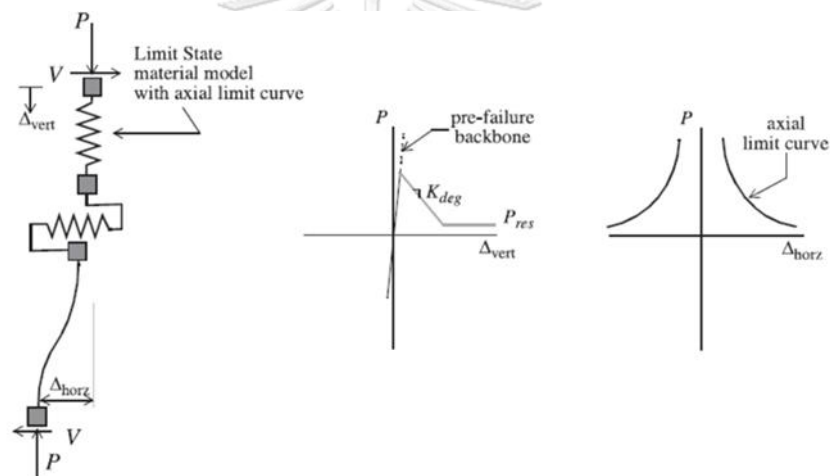
Figure 2.70 Axial spring in series model (Elwood, 2004)

CHAPTER 3

EXPERIMENTAL CONFIGURATIONS AND TEST RESULTS OF THE SPECIMENS

3.1. Introduction

In order to investigate the seismic response of the shear critical columns and strengthened shear columns, the experimental program was conducted. Three specimens were tested under constant axial load and cyclic loading. Structural parameters, test specimen configuration, test setup and strengthening system are discussed in this chapter.

3.2. Specimens and Parameters used in the current research

The size of the specimen, rebar diameter and spacing of the transverse reinforcement, axial load ratio, shear span ratio, longitudinal reinforcement ratio and transverse steel ratio are used based on the inadequate shear strength column buildings in Thailand. The summary of these parameters is shown in the following Table 3.1

Table 3.1Summary of parameters used in the current research

Type of specimens		CC	SC-100	SC-200
External steel cages		Without	@100 mm	@200 mm
Concrete compression strength (MPa)		31.5		
Specimen size	Width	0.40 m		
	Depth	0.40 m		
	Length	1.65 m		
Steel reinforcement	no of steel/bar size	16-DB20		
	Longitudinal steel (%)	3.14%$		
	Longitudinal steel yeild strength (MPa)	514.85		
Reinforcement according to area	no of steel/spacing	3-RB9@300		
	Transverse steel (%)	0.18%		
	Transverse steel yeild strength (MPa)	229		

3.3. Test Specimens

The specimens were the vertical cantilever types fixed to the strong ground tested frame. The column section size was 400×400 mm square columns. Sixteen longitudinal reinforcement bars with a diameter of 20 mm were placed around the parameter of the section. The transverse steel hoops were 9 mm diameter with the spacing of 300 mm for all specimens. Two cross tie bars were used with 9 mm diameter. The specimen geometry and reinforcement details were shown in Figure 3.1. A constant axial load of $0.16 f_c' A_g$ was exerted by manually controlled hydraulic jacks. All the specimens are tested under a constant axial load and the cyclic loading applied at the 1450 mm from the column base, resulting in shear span to depth ratio of 3.6.
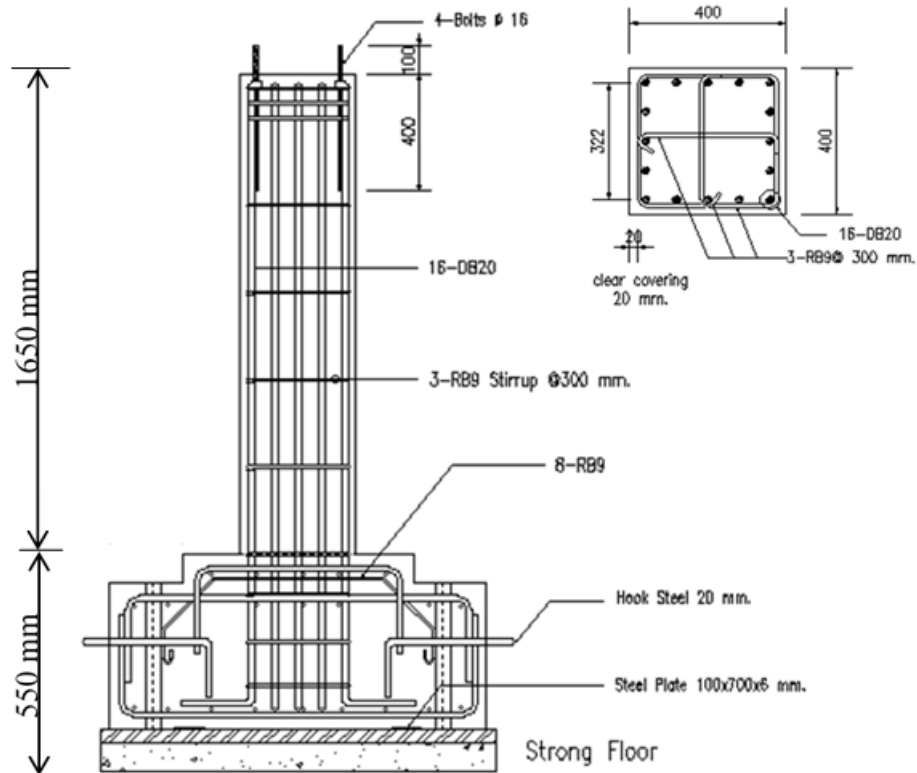
Figure 3.1 Specimen geometry and reinforcement details

3.4 Concept of Steel-Rod Collars

The existing reinforced concrete columns which have low transverse reinforcement ratios can have the shear failure under the seismic loading. To prevent the shear failure of the columns, additional transverse reinforcement ratio is needed to increase the shear capacity of the columns. In order to fulfil this requirement, the external steel rods were used to create the additional reinforcement ratio in the columns as shown in Figure 3.2a. The threaded bars were used as the steel rods. The steel rods were designed to be thinner section in the middle of the rod in order to tear out at the center when tensile force are suffered because if the rods tear out at the end, the nuts will throw away and it becomes dangerous to the people. The tensile strength of steel rods was tested by computer control tensile testing machine.

In selecting the steel rod diameter, firstly the shear capacity of the unstrengthened column was calculated using the column section analysis. Then, the

additional shear strength carried by the steel rods was calculated again using the ACI equation, shear strength carried by transverse reinforcements. The diameter of steel rods such as 10 mm, 12 mm, 14 mm and the spacing of steel rods such as 100 mm, 150 mm and 200 mm were considered as the main parameters. In the calculation, selecting the installing length of the steel rods was needed to consider to define the number of steel rods. Therefore, the plastic hinge lengths were calculated based on the plastic hinge length equations from the previous literature review. However, the plastic hinge length values from the various equations was too small and did not cover to install the steel-rod collars in the strengthened column. For the fact that the length for installing the retrofit was finally selected based on the diagonal shear crack length of the tested shear failure columns the previous research. The diagonal shear crack length was within 1m length and so the length for installing the retrofit for the strengthened columns was chosen 2.5d. Then, every parameters such as diameter of steel rods, number of the steel rods were assigned to the equation of shear strength carried by the steel rods. Next, the shear capacity of steel rods was simply added to the shear capacity of unstrengthened column. The shear capacity and the failure mode the strengthened columns were checked. After the trials, the results of 14 mm diameter steel rods with spacing of 100 mm, 150 mm and 200 mm gave the satisfactory condition with the flexural failure mode. However, it was decided that only two columns with the retrofit spacing of 100 mm and 200 mm to test in practice in order to investigate how the two intervals of 100 mm and 200 mm effect of lateral confinement to the columns and how will be the damage of the columns in the real case.

Applying the steel rods around the columns without any connectors is not possible. Therefore, steel collar with fasteners was also designed to connect the steel rods around the columns as shown in Figure 3.2b. Firstly, assume the size of the steel angle and then the moment capacity of the steel angles with fastener was calculated. Later, tensile moment strength of steel rods was calculated and which was compared to the moment capacity carried by steel angles as demonstrated in Figure 3.2c. Then, the size of the steel angles was decided for connecting the steel rods. Three steel angles were used to create one steel collar and the angles are connected by welding. While the middle steel angle is used to confine the column at the corner and the other two flanges of the two angels were used to connect the steel rods. Steel-rod collar method is

practical not only for the isolated columns, but also for the columns connected with masonry infill wall. No need to break the wall to install the steel-rod collars and just drilling the hole in the masonry wall is needed as shown in **Figure 3.3.**
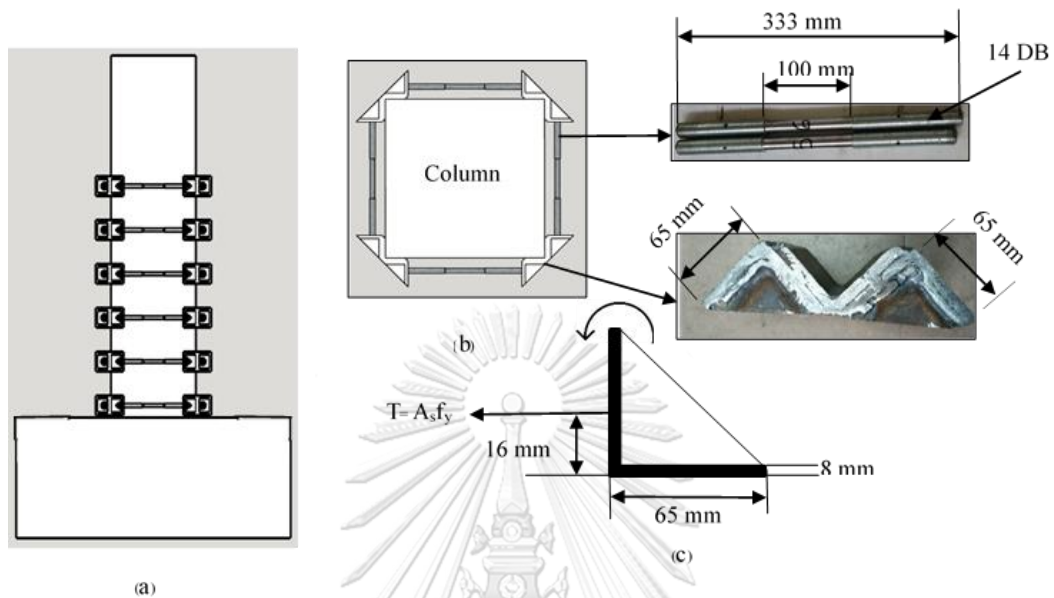
Figure 3.2 (a) Typical strengthened column (b) Steel rods and steel collars (c) Applying tensile moment of steel rods and moment capacity carried by steel angles and fastener
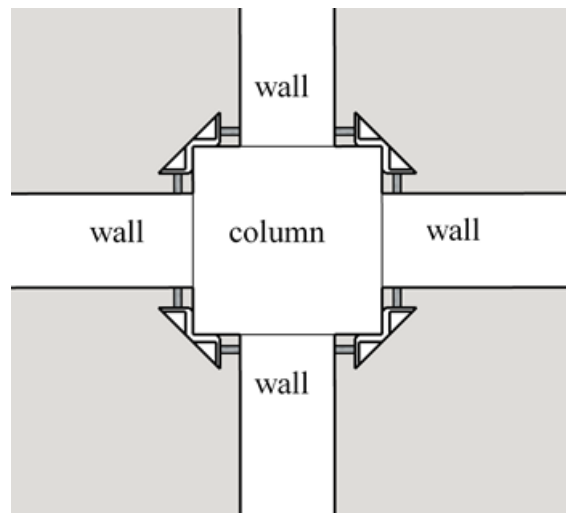
Figure 3.3 Setting up the steel-rod collars in the column with masonry infill wall

3.4.1 Installation of steel rod collars

To install the steel-rod collars, firstly the four sets of steel collars were placed at the corners of the columns. Then the steel rods are connected to the steel collars by nuts. The nuts were tightened by torque wrench. The first steel cage was placed 10 mm from the top face of the strengthening column footing to get some rotation and to prevent the damage on the face of the column footing. After installing the first steel-rod collar to the column, the nuts were checked again whether it was tightened or not. Then the steel rod collars were installed level by level with the specified spacing within the retrofit length. The steel rod collars were set up to the columns with 200 mm spacing for SC-200 and 100 mm spacing for SC-100. Epoxy resin was applied between the gap of the steel angle and the corner of concrete column faces. Typical steel rod collar strengthened to column is illustrated in Figure 3.4.
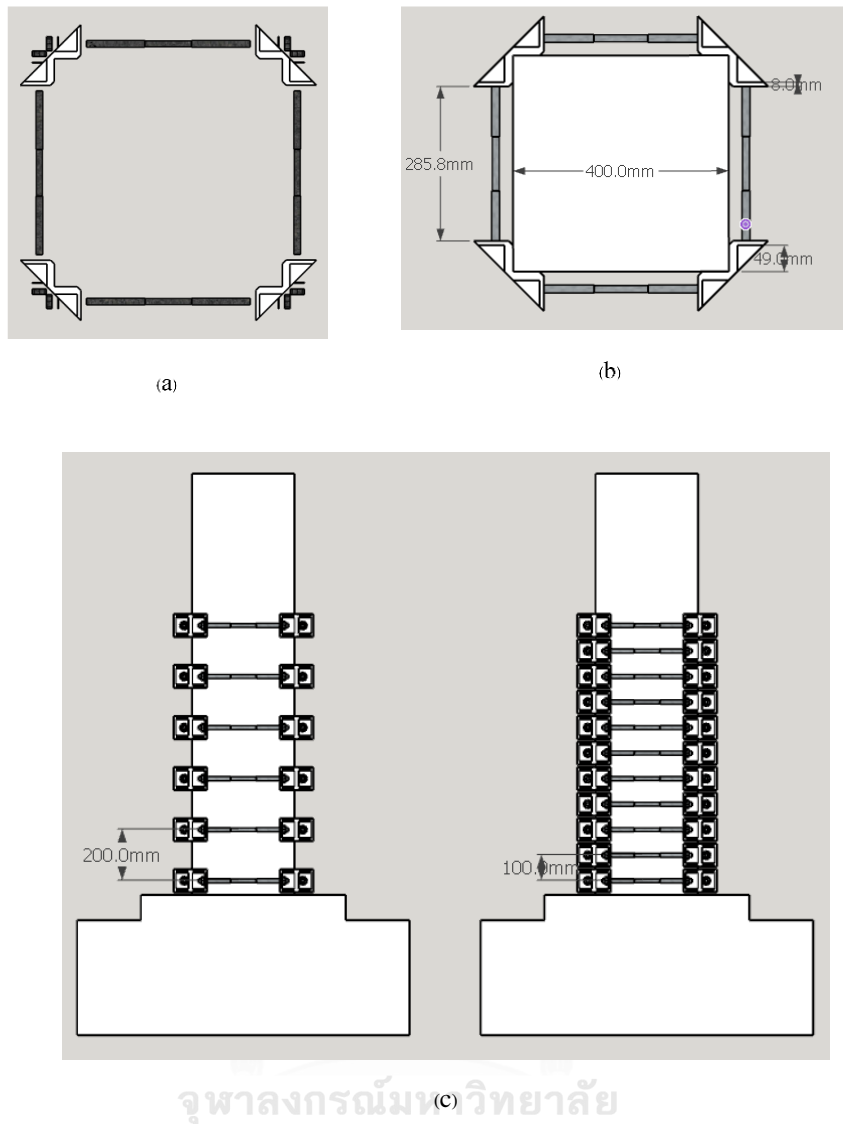
Figure 3.4 (a) Preparing the steel-rod collars (b) Installing the steel-rod collar to the column (c) Two strengthened columns with steel-rod collars

3.4.2 Testing of the steel rods

Tensile test is the one of the most common test of steel. Before testing the steel rods, the original length of the steel rod was measured. Four numbers of 14 mm diameter steel rods were prepared to test the tensile strength. Two steel rods were attached to the steel angles respectively. Next, the prepared steel-rod collar is put in place in the tensile test machine as shown in Figure 3.5. The tensile strength of the steel rods was recorded by the computer connecting to the tensile test machine. The steel rods were tested until it failed. After the test, the final gauge length of the steel rods was

measured. The final condition of the one set of steel rods is shown in Figure 3.6. According to the test result, the maximum load for the two rods were 120 kN. The yield load for the two bars were 100 kN. Yield load for one bar was 50 kN. Therefore, the yield stress of one rod was 442 MPa. The yield stress of the rod was calculated by dividing the yield load to the steel rod area.
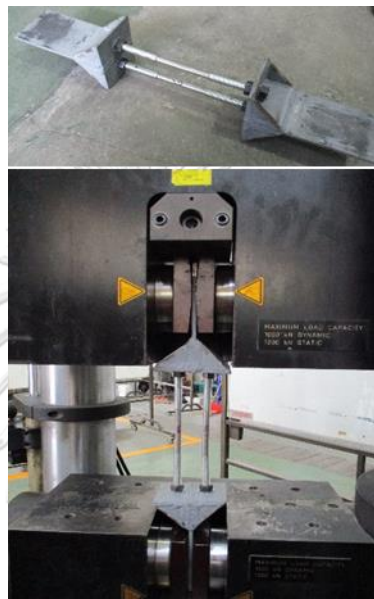
Figure 3.5 Setting up the steel-rod cage in the testing machine

Figure 3.6. Final condition of the steel rod

3.5. Material properties

ASTM standard was followed to estimate the mean concrete strength of cylinder specimens. The compressive strength of the concrete was determined by tests on cylindrical specimens 150 mm in diameter and 300 mm long. The average cylinder compressive strength of all the eight specimens was 31.5 MPa. Also, ASTM standard was followed by testing the tensile strength of the longitudinal reinforcement, transverse reinforcement and the steel rods. The longitudinal steel has a yield strength, fy_l of 515 MPa and the transverse steel has a yield strength, fy_h of 299 MPa. The yield strength of the steel rod in the steel-rod collar, fy_{collar} is 442 MPa. The size of the steel angle is L $65\times 65\times 8$ mm and the yield strength of the steel angle is 235 MPa.

3.6. Instrumentation

A number of twelve strain gauges were used to measure the strain in the transverse reinforcements and four strain gauge locations were used. The strain gauge for transverse reinforcement were put every 30 cm from the column footing surface. The strain gauges were placed in the middle of the steel rods around the four faces of the column specimens. Figure 3.7a shows the location of the strain gauges on the transverse reinforcements and Figure 3.7b shows the location of the strain gauge on the longitudinal reinforcements.

A number of twenty strain gauges were used for longitudinal reinforcements and five strain gauge locations were used. The first level was put inside the column footing, the second level was put at the column footing surface level, the third level was put 1.5 cm from the column-footing surface, and the fourth and fifth level was put 30 cm spacing from the third level. Locations of all the strain gauges were the same for the three specimens. The first two levels were for measuring the yield strain penetration. The third and the fourth level was within the predicted plastic hinge length.

Four strain gauge locations were used for SC-100 with spacing 20 cm and three strain gauge locations were used for SC-200 with spacing 20 cm. All levels are within the predicted plastic hinged length. The strain gauges at every level were placed in the middle of the steel rods around the four faces of the column specimens. Figure 3.8 shows the location of strain gauges on the steel-rod cages in SC-200 and SC-100

specimens. All of the strain gauges in the specimens were connected to the data logger. All the data are recorded by the computer monitor connected to the data logger. Data logger equipped with personal computer was used to record the data of every strain gauges during the applying of the lateral loading cycles as shown in Figure 3.9.

(a)

(b)
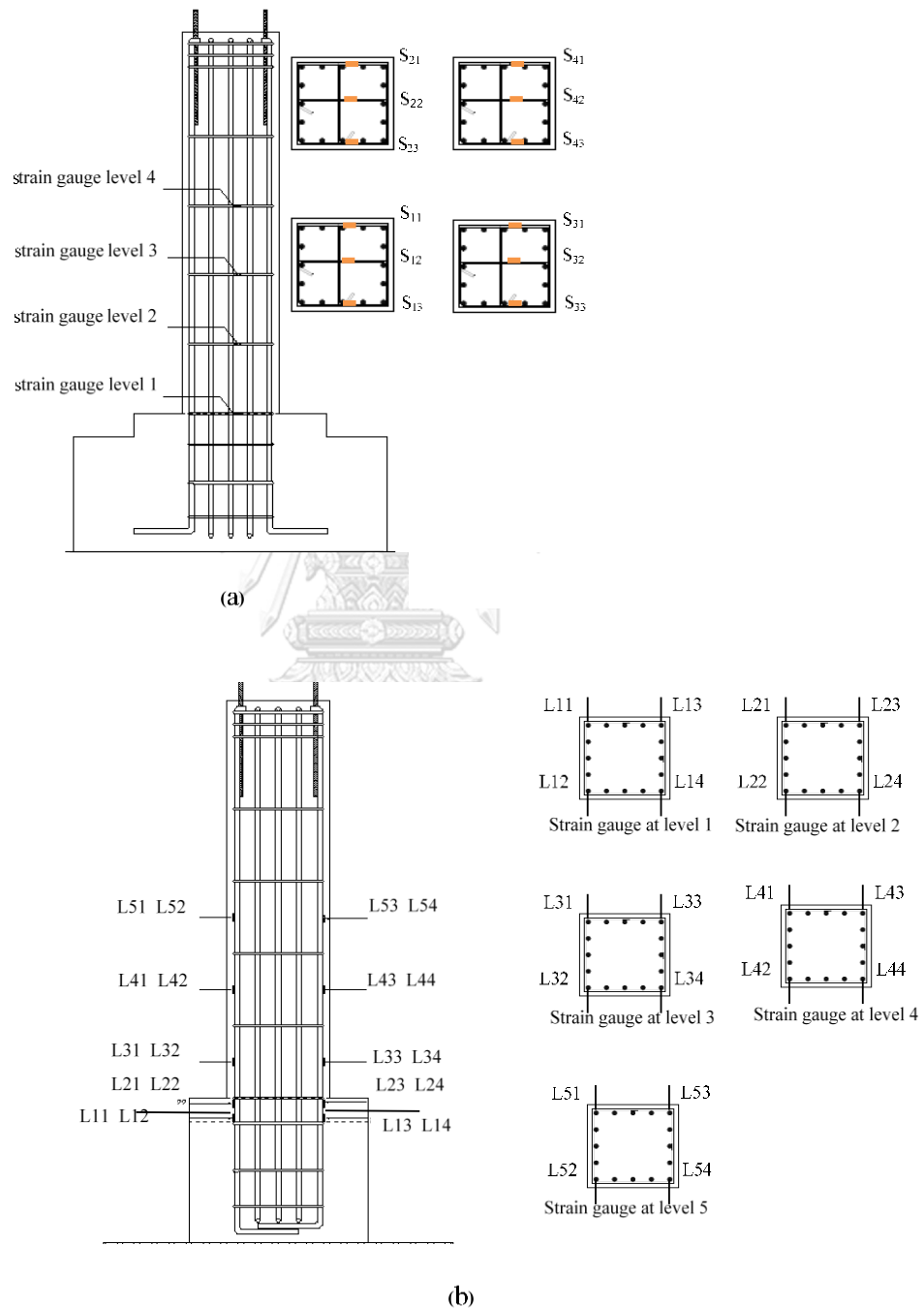
Figure 3.7 (a) Placement of strain gauge on transverse reinforcements

(b) Placement of strain gauge on longitudinal reinforcements
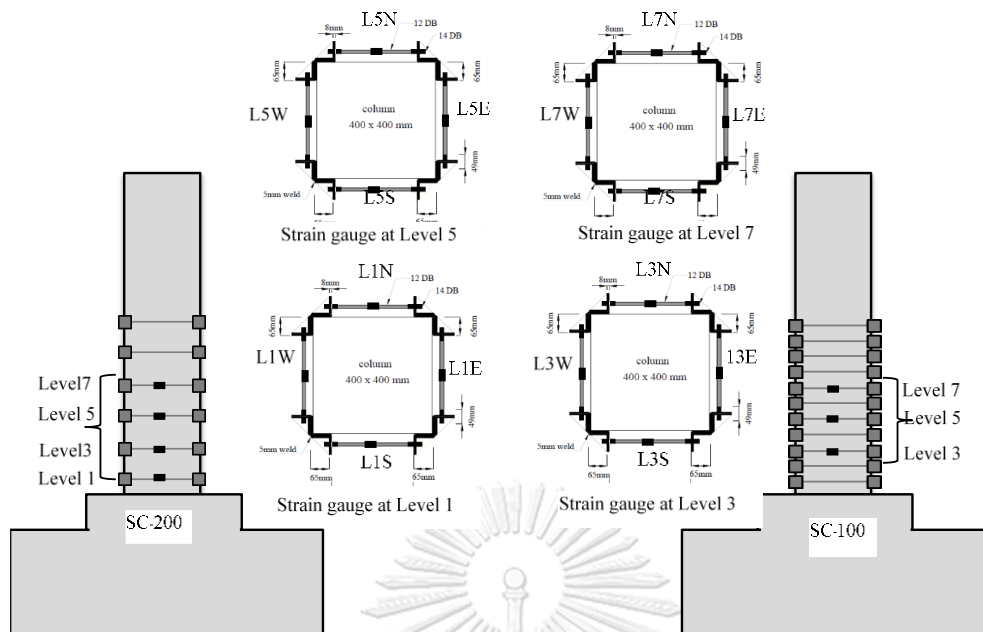
Figure 3.8 Location of strain gauges on the steel-rod collars for specimens SC-200 and SC-100

Figure 3.9 Recording the data from data logger

3.7. Test Setup and Loading System

The specimens were applied by the lateral load by means of MTS 1000 KN hydraulic actuator, and a stroke of ± 300 mm that was horizontally supported by a strong reaction wall. A constant axial load of 0.16 $f_c' A_g$ was exerted by manually controlled hydraulic jacks. The displacement control loading sequences consisted of two cycles at each lateral drift. The lateral displacement increased 0.25 % until 2% drift and then

followed by an increase of 0.5%. The test specimen is as shown in Figure 3.10 and the displacement scheme is shown in Figure 3.11.
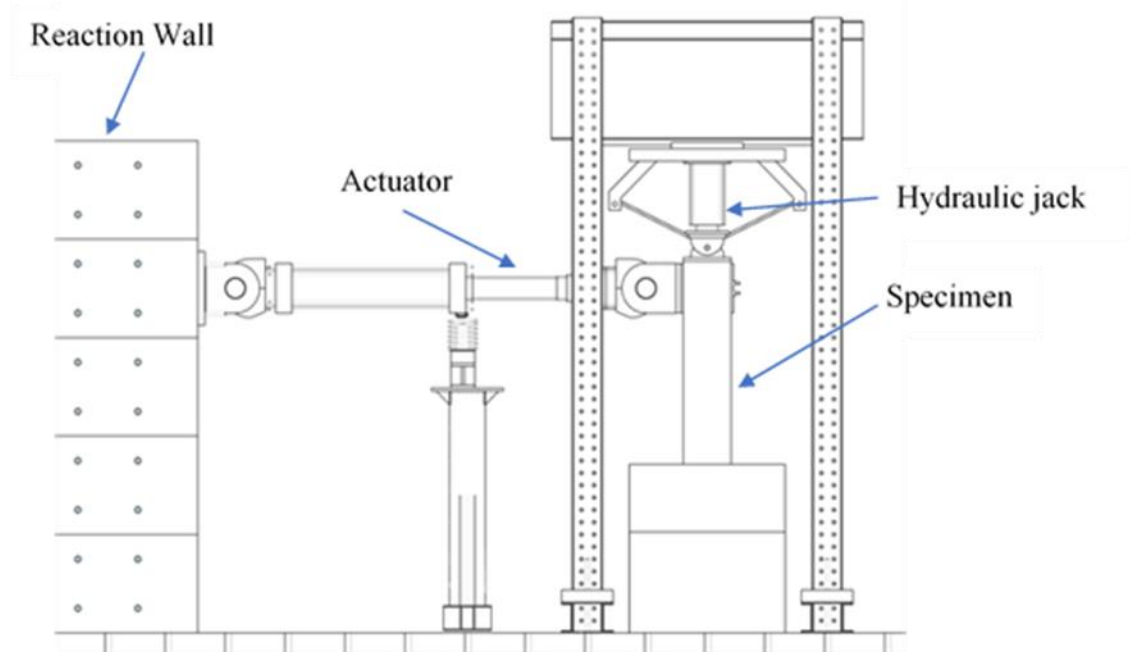
Figure 3.10 Test set up of the specimen
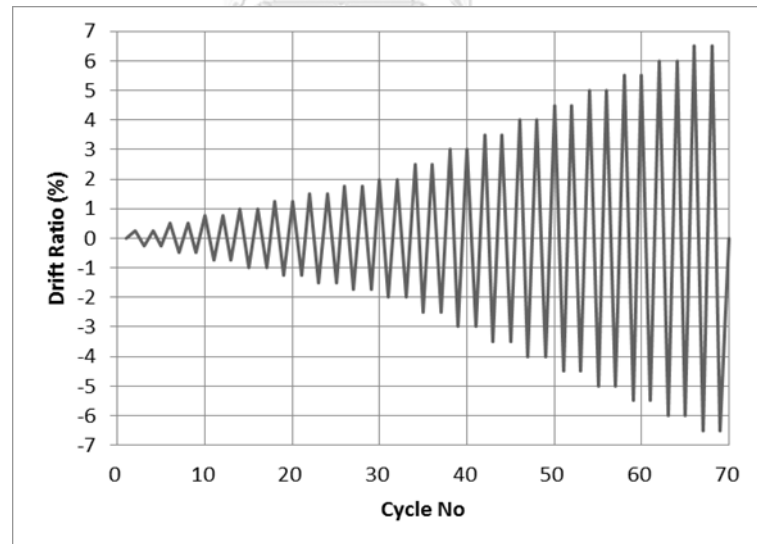
Figure 3.11 Displacement history for the tested specimen

3.8 Strengthening Configurations

Three specimens are tested under a constant axial load along with the cyclic displacement. The three specimens are named as CC for the unstrengthened specimen, SC-200 for the strengthened specimen with steel-rod collars spaced at 200 mm, and

SC-100 for the strengthened specimen with steel-rod collars spaced at 100 mm. All the steel-rod collars are installed within 1 m from the column bases. Strengthening configurations are shown in Figure 3.12.
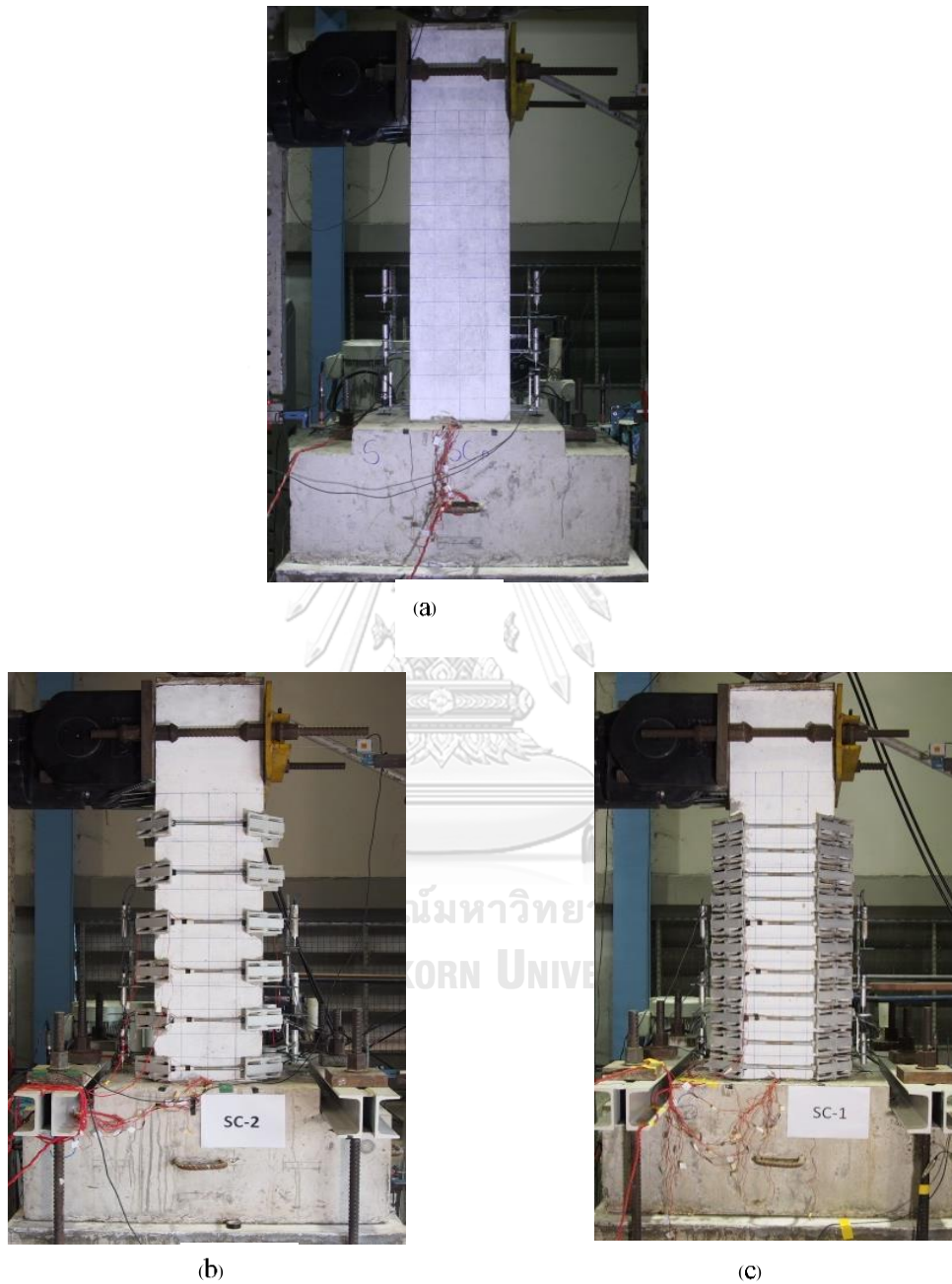
Figure 3.12. Specimens (a) Unstrengthened column CC

(b) Strengthened column, SC-200 (c) Strengthened column, SC-100

3.9. Experimental Results of CC, SC-200 and SC-100

In this section experimental results of control column CC, two strengthened columns SC-200 and SC-100 are presented. Detailed descriptions of the hysteretic behavior of each specimen are also provided. During testing the specimens, the sliding of the foundation against the strong floor, the rotation of the foundation against the strong floor and the displacement of the reaction wall which is mounted an actuator are observed as shown in Figure 3.13. Therefore, it is important to understand how these factors affected experimental results and it is necessary doing the data correction of the recorded test results to get the usable data. The corrected displacement values are calculated as follows equation.
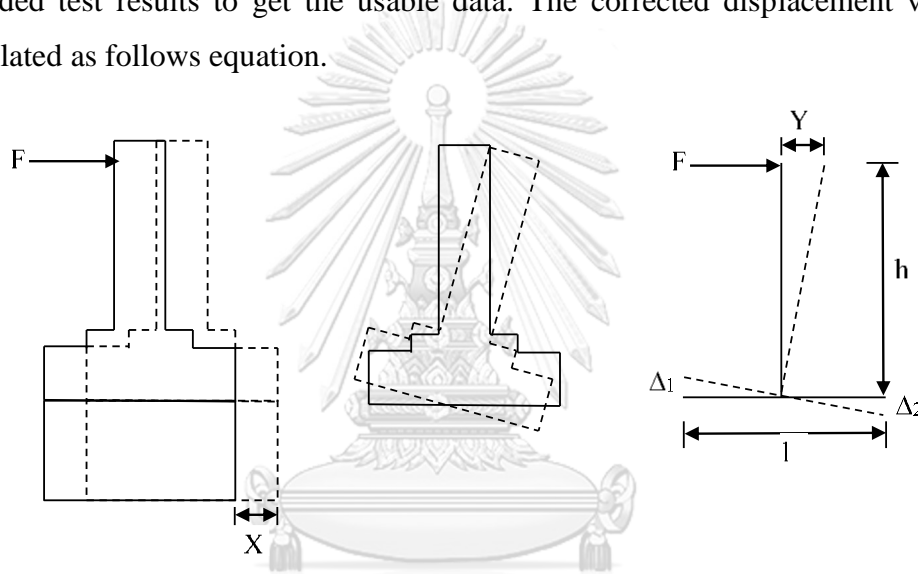
Figure 3.13 Displacement due to sliding, footing rotation

$$\Delta_{real} = \Delta_{record} - X - Y - Z$$

$$Y = \frac{\Delta_1 - \Delta_2}{l}.h$$

Where,

X = Footing rotation (mm)

Y = Displacement due to sliding (mm)

Z = Displacement of the reaction wall

Δ_1 = Data recorded from LVDT FR-L

Δ_2 = Data recorded from LVDT FR-R

3.10. Experimental Results of CC

This section describes the experimental results of the CC specimen such as damage and hysteresis of the CC specimen in each loading cycle, strain in the longitudinal reinforcements, and strain in the transverse reinforcement

3.10.1. Progressive damage of specimen CC

Progresses of the cracks of the CC specimen under testing were recorded in the crack pattern drawing. No cracks were occurred from 0.25% drift to until after 0.5% drift cycles. Small hairline cracks appeared at 0.75 % drift at about 150 mm and 300 mm above the column base. When the loading is increased gradually from 0.75% to 1% and then until 1.25% drift, no cracks progression were increased. When the loading is increased to 1.5% drift, many flexural cracks were appearing on the column specimen. At 1.75% second cycle drifts, small diagonal shear crack started to develop. With increasing lateral load, shear cracks propagate to be a big diagonal shear crack. At 2% drift cycle, many shear cracks were propagated and all propagated shear cracks connected each other. At first cycle of push 2.5% drift, the lateral strength reached the peak strength of 280 kN and a diagonal shear crack developed obviously. The next cycle of 2.5% drift, the lateral strength started to drop. At 3% drift cycles, the lateral strength of the column dropped continuously and finally the column failed by shear failure mode. The basic of the un-strengthened column CC was dominated by shear. In this study, the ultimate displacement was defined at the stage at which the shear strength dropped to 80% of the maximum lateral load capacity. Therefore, the shear capacity at the 80% of the maximum load was about 224 kN. The hysteretic response of the lateral load displacement diagram is shown in Figure 3.14. Progressions of damage of CC are shown in the following Figure 3.15 (a),(b) and (c). Crack pattern on each four faces of the column are illustrated in Figure 3.16 (a) and (b).
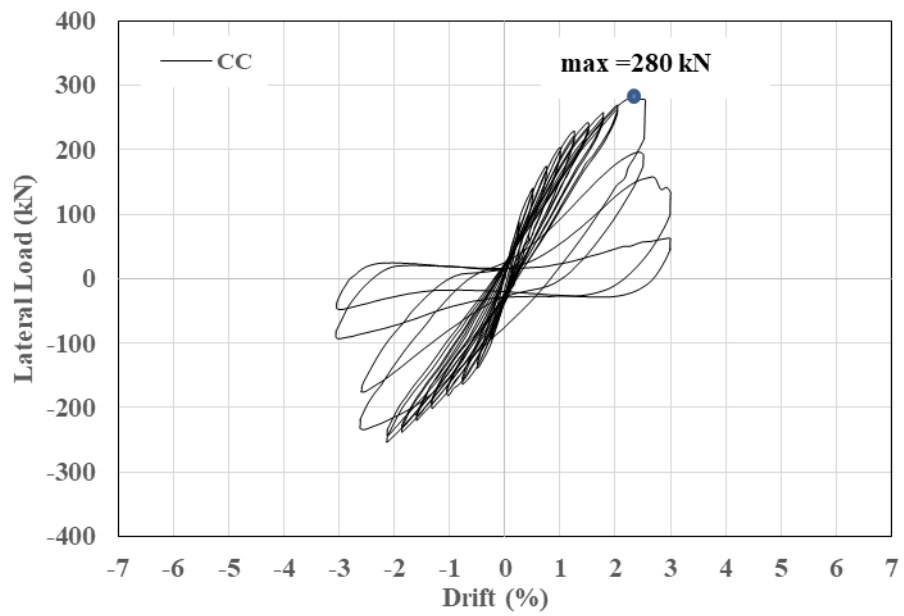
Figure 3.14 Hysteretic behavior of the CC specimen

(a)

(b)
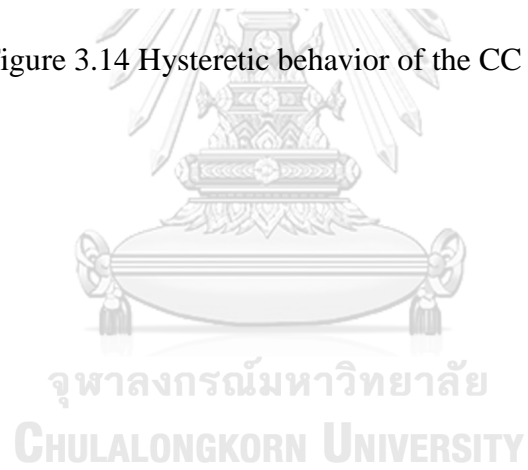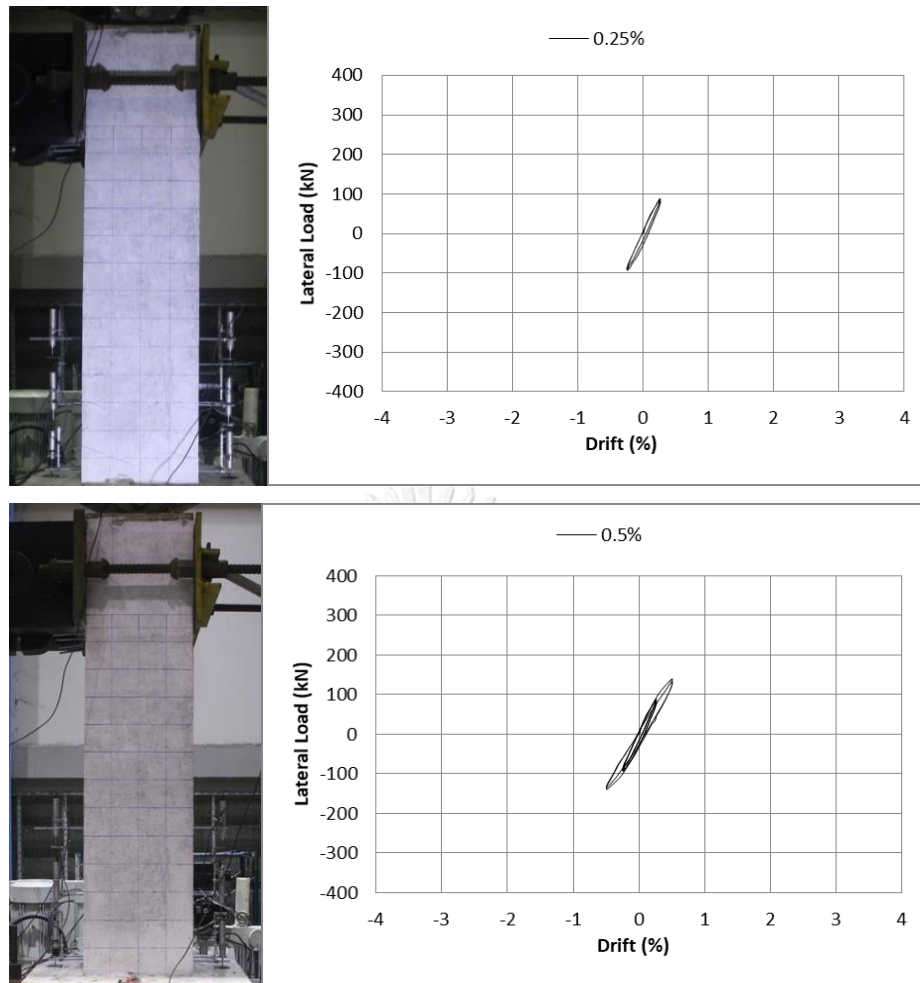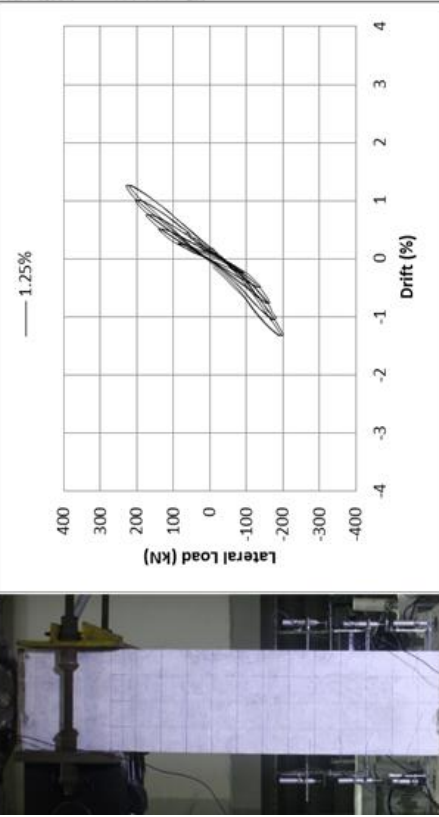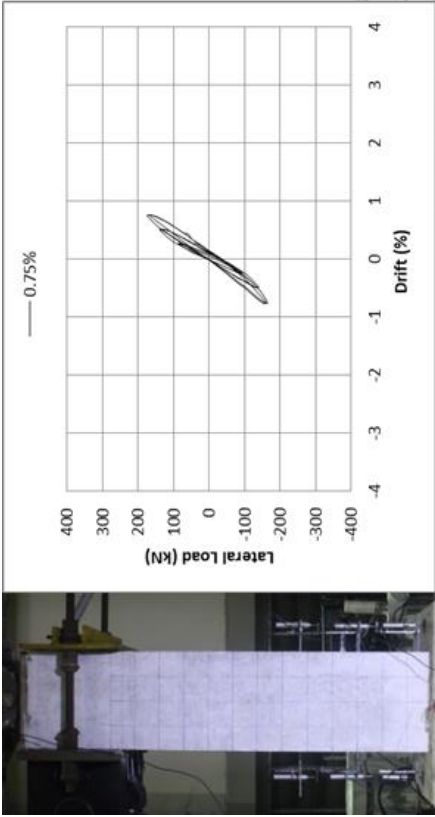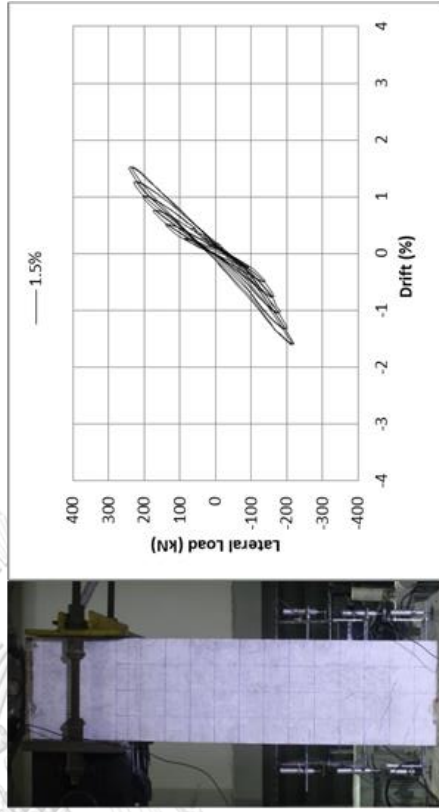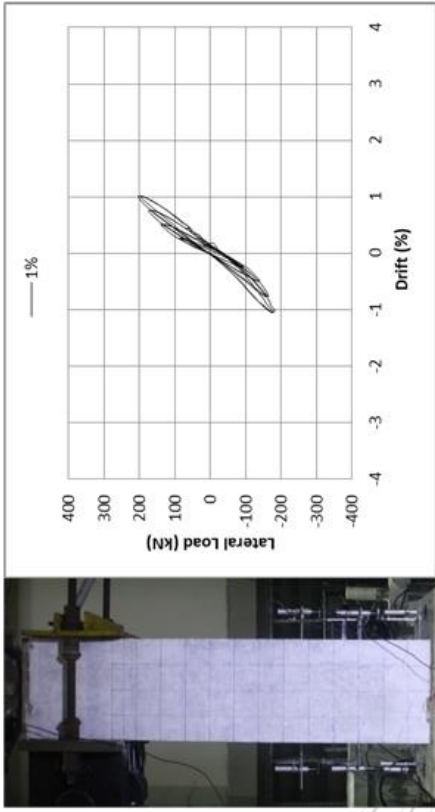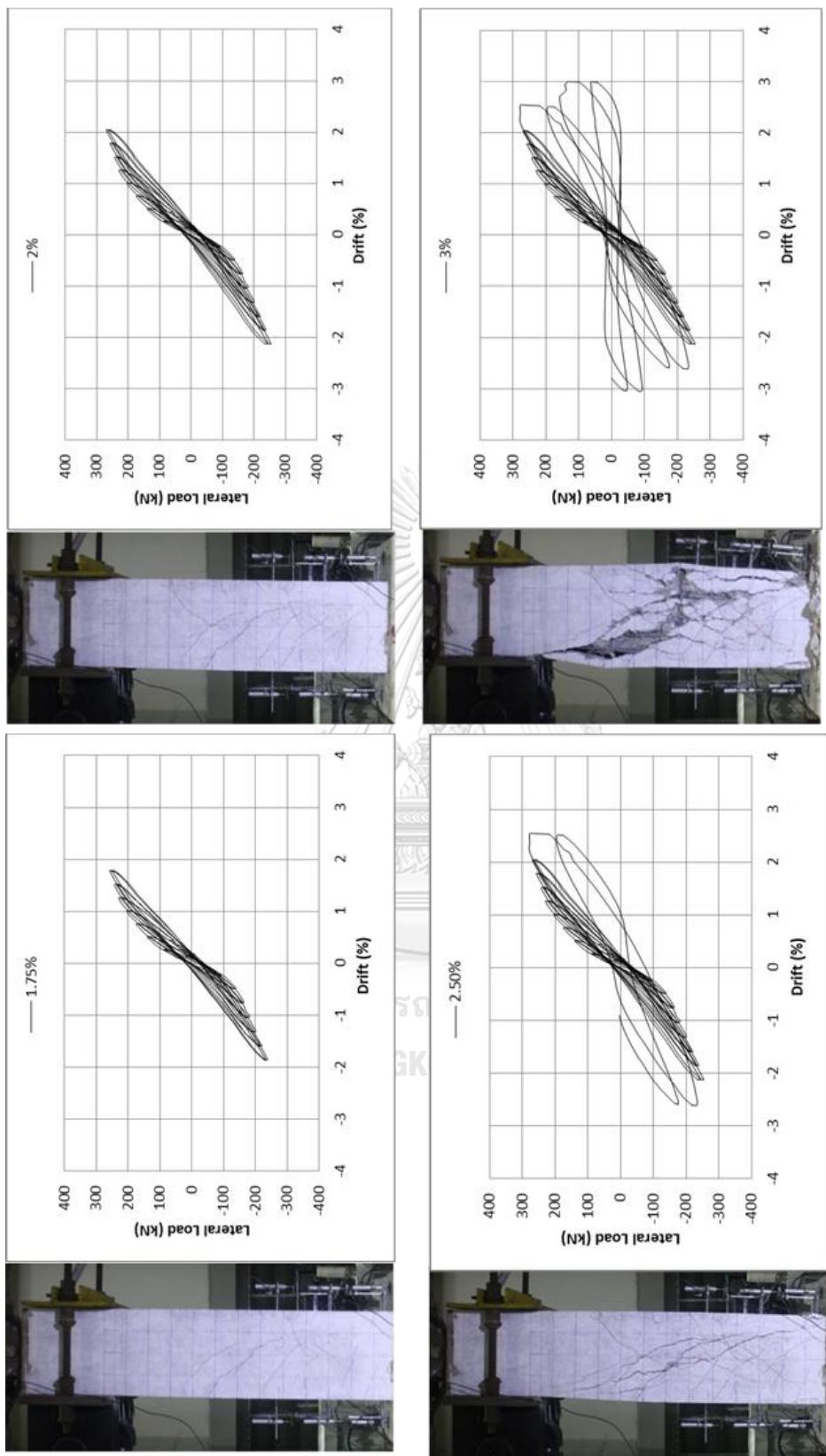
Figure 3.15 (a), (b) and (c) Progression of damage specimen, CC

(c)
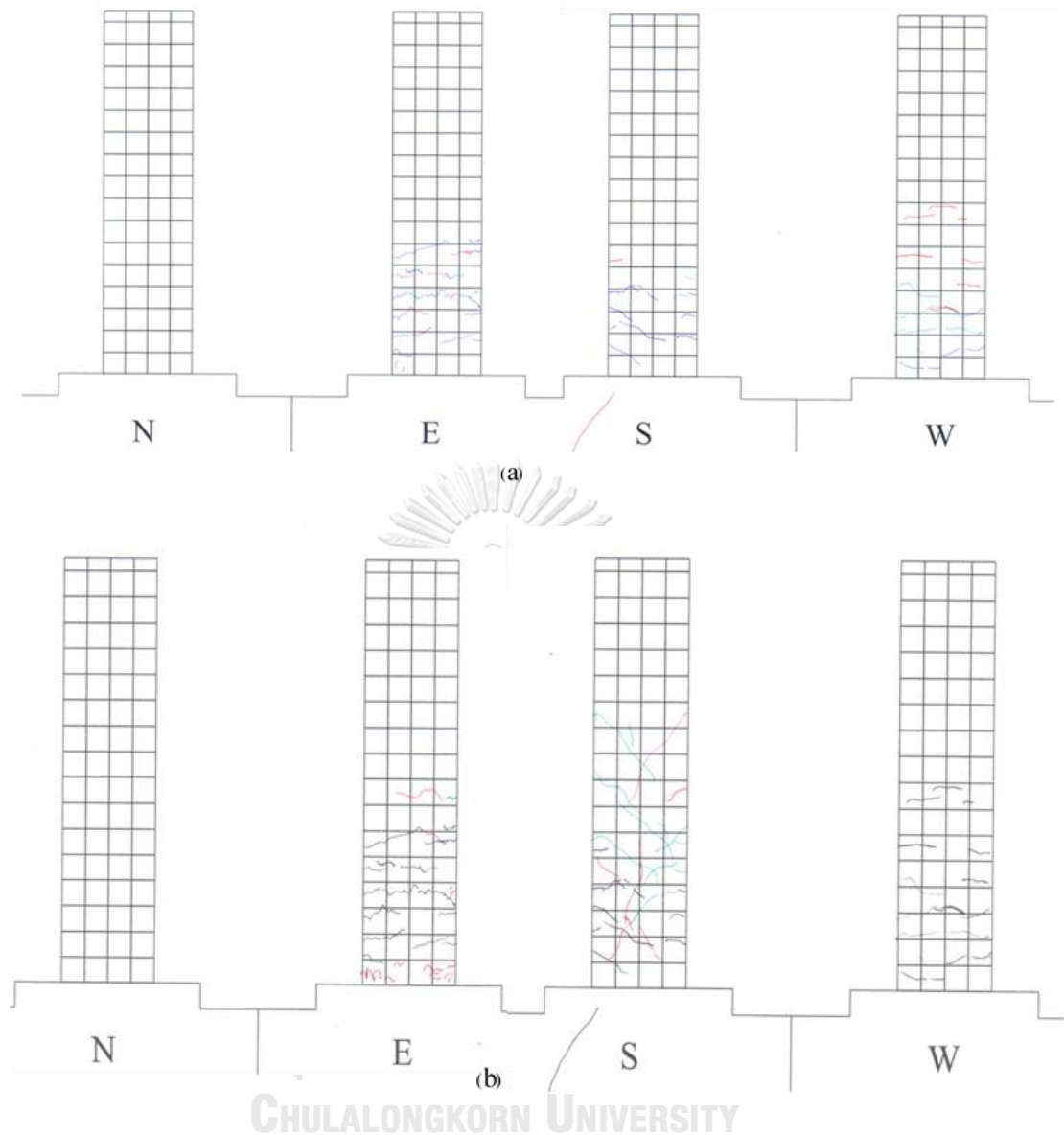
Figure 3.16 (a) Crack Pattern of CC from ±0.25% to until ±1.5%

(b) Crack Pattern of CC from ±1.75% to until ±2.5%

3.10.2. Strain in the longitudinal steel of CC

The maximum yield strain of the longitudinal steel is 2574 micro strain for all tested specimens because all specimen configurations were almost identical. The four numbers of strain gauge wires were attached at the four corners of longitudinal reinforcement in one level. The total of twenty numbers strain gauge was attached to the face of longitudinal steel in five levels. At the level1, only L11 strain gauge recorded the strain in the longitudinal steel until the complete loading cycle. After the 2.5% drift

cycle, there was a sudden increase of strain in longitudinal steel at the location of L12 and L14. At this stage, the lateral loading reached the maximum value and the diagonal shear crack appeared. Strain in the longitudinal steel at the level 1 is shown in Figure 3.17.

At level 2, only L23 strain gauge could record the strain in the steel until the complete loading cycle, whereas, the value of stain in the any other strain gauge cannot record the available data because the L21, L22 and L24 strain gauges were damaged before the loading test. Strain in the longitudinal steel at level 2 is shown in Figure 3.18.

At level 3, only L31 recorded the strain in the longitudinal steel until the complete cycles. When the loading cycle was increased to 2.5% drift, there was also an increase in strain value in any other L32, L33, and L34 because the buckling of longitudinal steel occurred in that level and also the column was in the stage of failure by shear. The results of strain in the longitudinal steel at level 3 are shown in Figure 3.19.

At level 4, the stain value reached the yield during the 2 % loading cycle in general. After the 2.5% drift, the stain value increased suddenly in all stain gauge L41, L42, L43 and L44. The results of strain in the longitudinal steel at level 3 are shown in Figure 3.20.

At level 5, after the 2% drift, all the strain value was increased significantly. Strain in L51, L52 and L53 strain gauge were over yield limit and strain in the L54 was within yield limit until the loading reached the 2% drift. The results of strain in the longitudinal steel at level 3 are shown in Figure 3.21.

In conclusion, strain value recorded at each level reached the yield limit. Both CC specimens failed by shear and longitudinal steel reached yield. After the column failure, buckling of longitudinal steel occurred in some reinforcements.
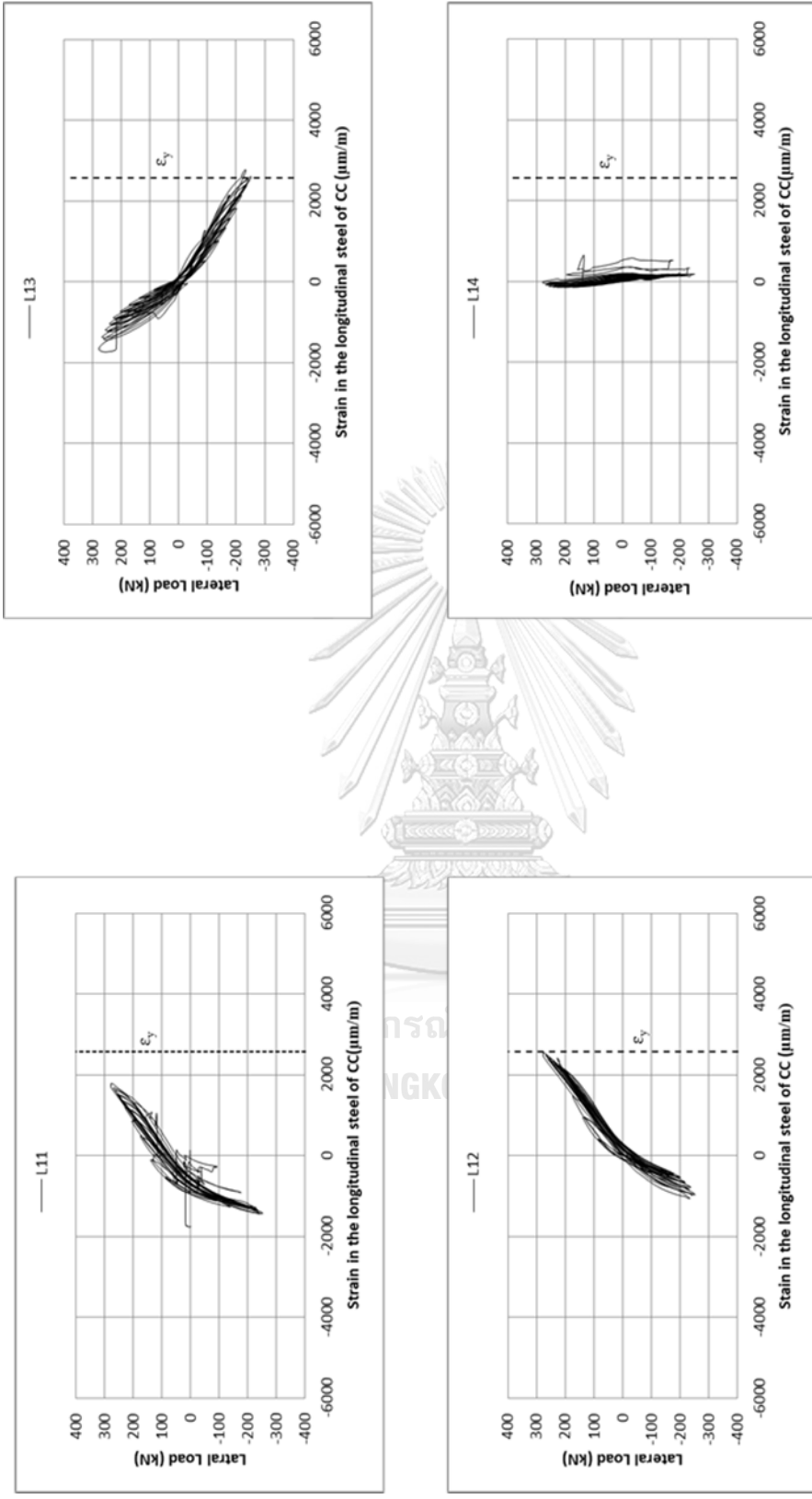
Figure 3.17 Strain in the longitudinal steel of CC at level 1

88
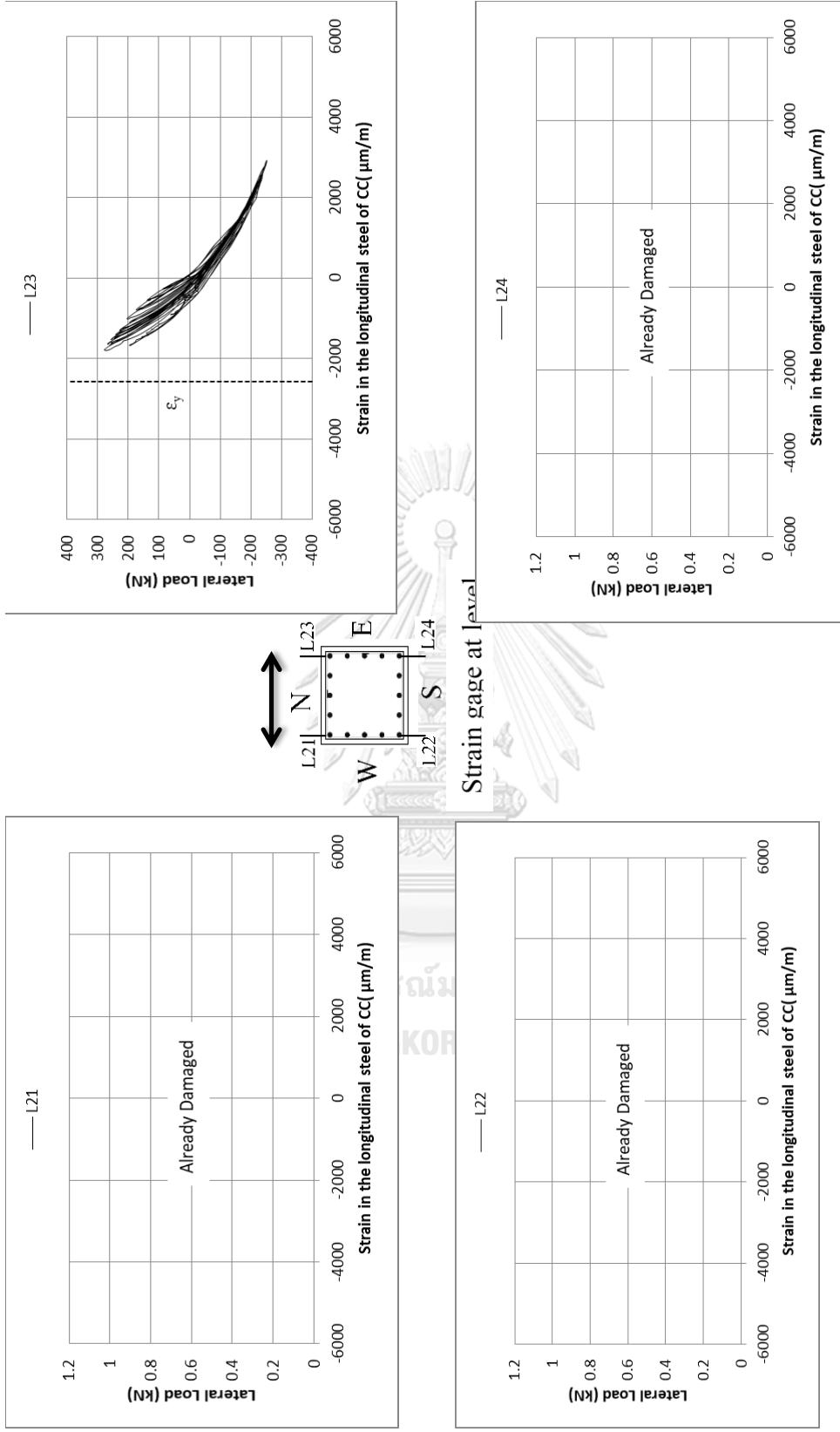
Figure 3.18 Strain in the longitudinal steel of CC at level 2
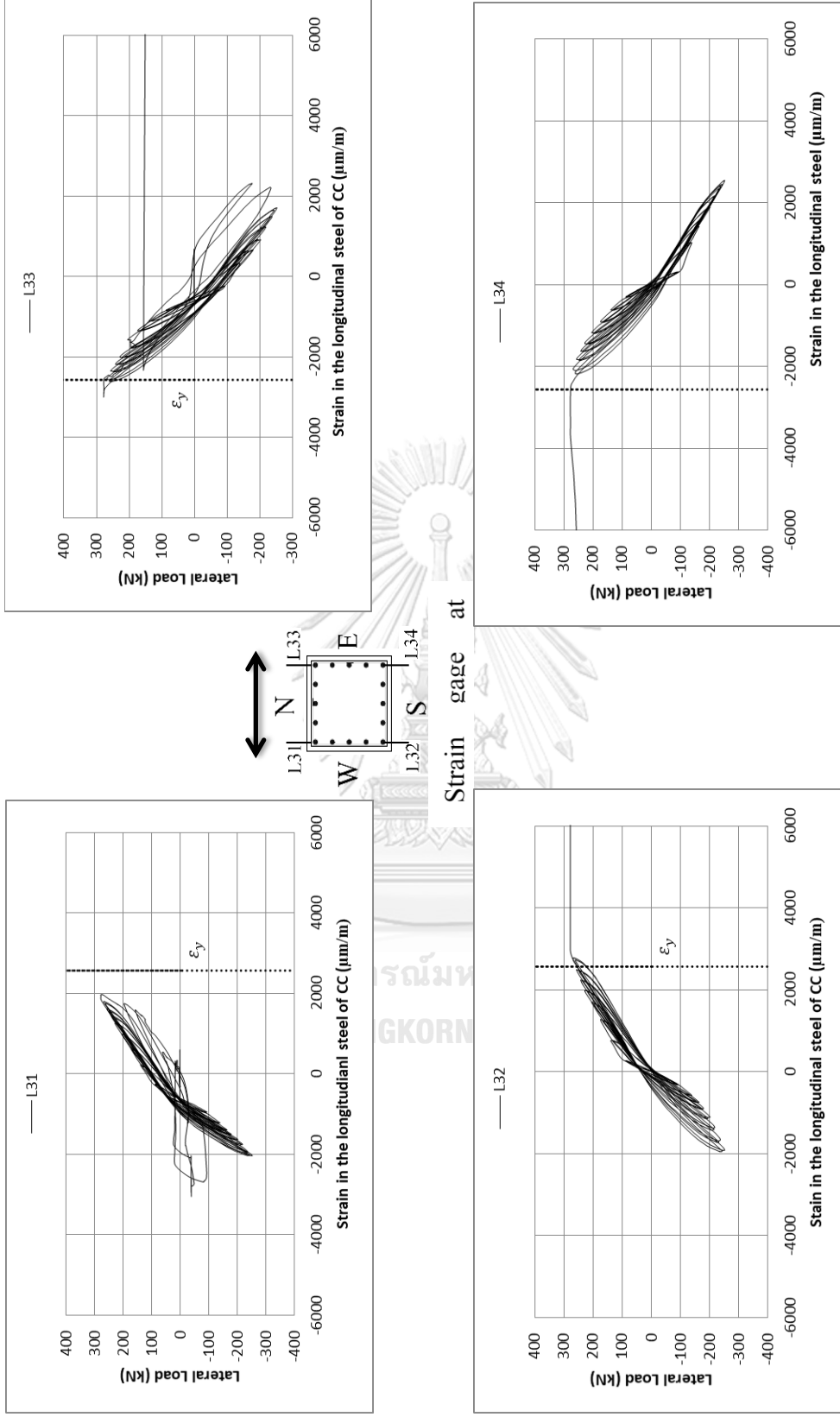
Figure 3.19 Strain in the longitudinal steel of CC at level 3
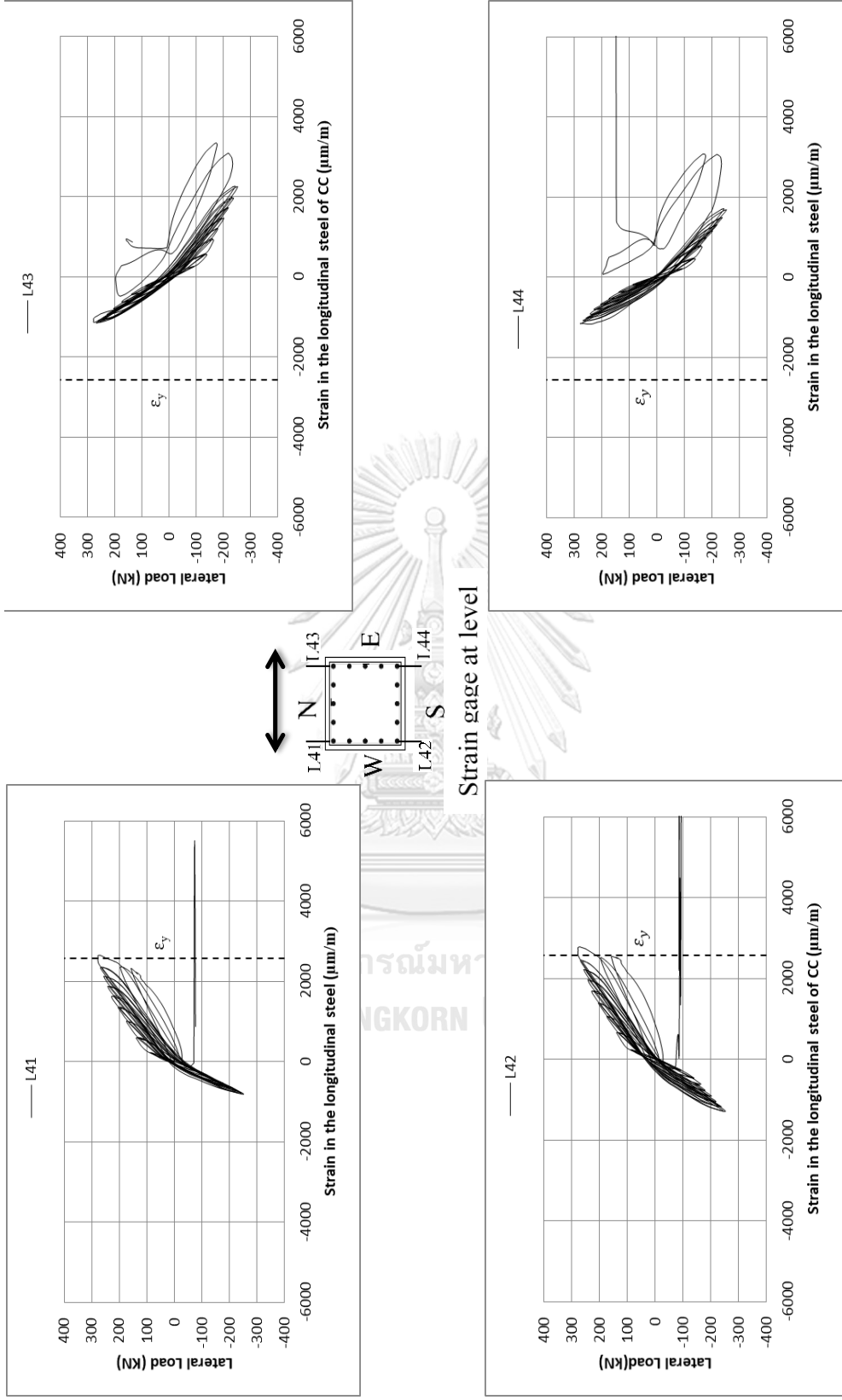
Figure 3.20 Strain in the longitudinal steel of CC at level 4
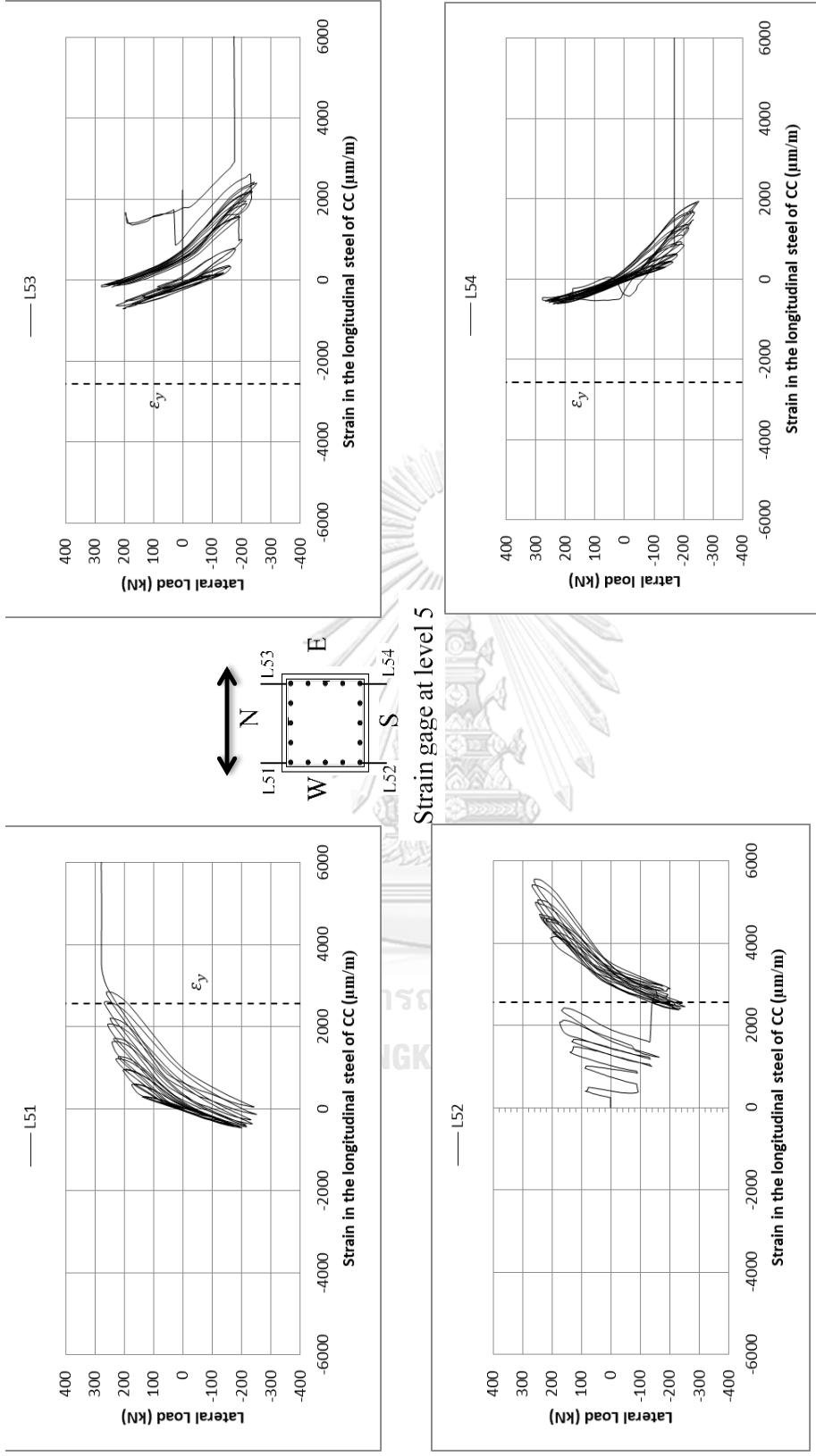
Figure 3.21 Strain in the longitudinal steel of CC at level 5

3.10.3. Strain in the transverse steel of CC specimen

To capture the strain in the transverse steel, twelve number of strain gauge was used for the four levels and three numbers of strain gauges were put on one level. The yield strain of the transverse steel was 1495 micro strain.

Strain gauge Level 1 is located at the top of the column footing level and strain gauge did not work properly and the records were not captured effectively as shown in Figure 3.22. It has some noise. In the level 2, S21 strain gauge had been already damaged before the loading test and it was not available to record the strain value. The transverse reinforcement, S22 and the cross tie, S23 reached yielded when the loading was increased to 2.5 % drift. It can be seen in Figure 3.23.

At this level, the S32 strain gauge was damaged before the loading test when it was checked. Therefore, the S32 strain gauge was not available to record the strain value. Strain in the S31 strain gauge was over 2000 micro strain when the loading reached at 2.5% drift ratio. Stain in the S33 was increased suddenly after the 1.5% drift cycle. Before the 1.5% loading cycle, the strain value was around 500 micro strains. It was shown in Figure 3.24.

At this level 4, strain gauge S41 damaged after the 2% drift cycle and the recorded data was unit 2% drift. At 1.75% drift cycle, the strain value reached the yield and after 2.5% drift, it was beyond the yield limit. Strain gauge S42 and S43 recorded the data until the complete loading cycles. Strain gauge S42 reached the yield at 2.5% drift in positive loading and it was beyond the yield in the negative loading cycle. Strain gauge S43 reached the yield at the 3 % drift in the negative loading cycle. It is illustrated in Figure 3.25.

Figure 3.22 Strain in the transverse steel of CC at level 1

Figure 3.23 Strain in the transverse steel of CC at level 2
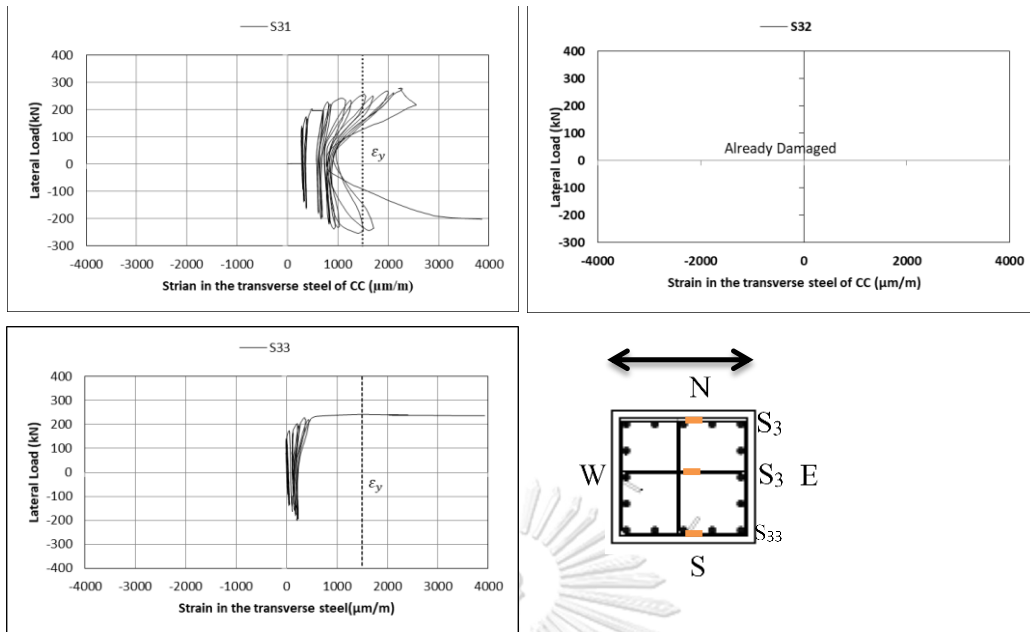
Figure 3.24. Strain in the transverse steel of CC at level 3

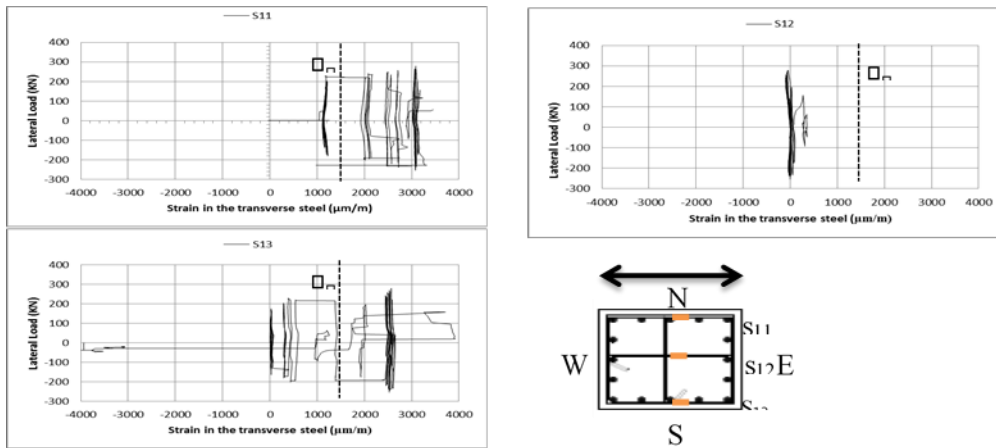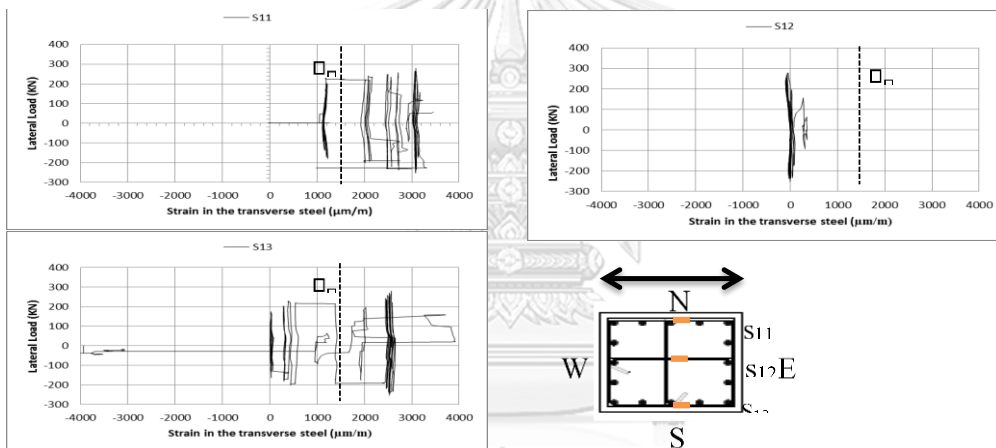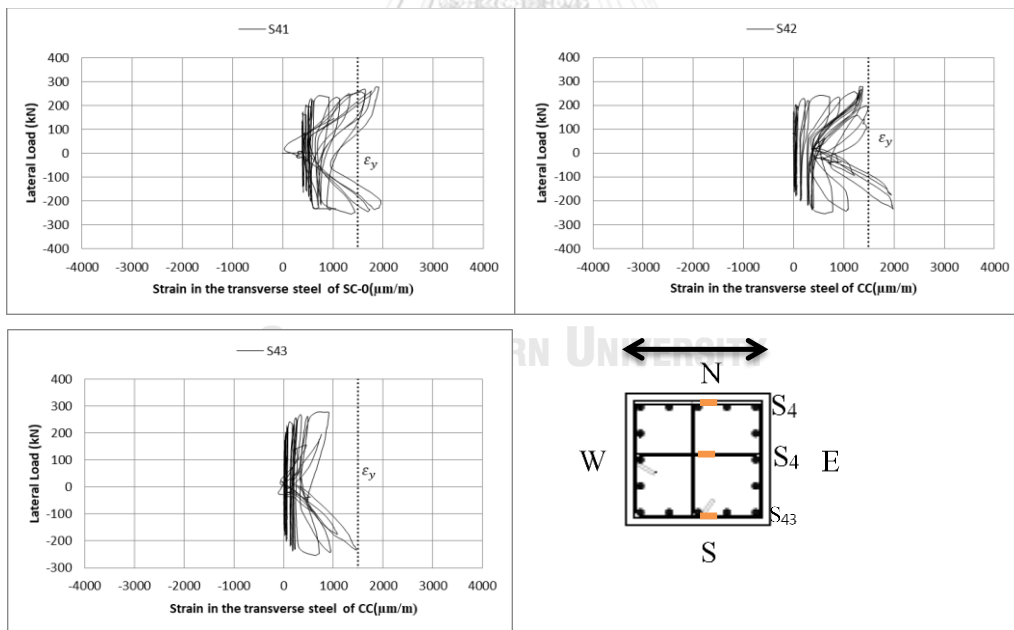Figure 3.25 Strain in the transverse steel of CC at level 4

3.11. Experimental Results of SC-200

This section describes the experimental results of the SC-200 specimen such as damage conditions at every loading cycles and hysteresis behavior of SC-200 specimen in each loading cycle, strain in the longitudinal reinforcements, and strain in the transverse reinforcement

3.11.1. Progression of damage of SC-200

SC-200 specimen is the strengthened column with the external steel rod collars having a 200 mm spacing of steel rods. Until 0.5% drift, no cracks were occurred. At the first cycle pull of 0.75% drift, the first horizontal hair line cracks were observed at 150 mm elevation. At 1% drift cycle, no cracks were increased. At 1.25% small amount of flexural cracks was increased. First flexural–shear crack appeared at second cycle of 1.5 % drift at elevation 400 mm and 600 mm. At 1.75 % and 2% drifts, the cracks were connected each other from end to end. At 2.5% drift, no more cracks were increased. At 3% drift, expansion of the cover concrete was observed on between 100mm and 200mm from the base. This happened because of the longitudinal reinforcement buckled a little. At 3% drift, the lateral loading reached the maximum of 340 kN. At the 4% drift, the cover concrete cracked horizontally between the elevation 100 mm and 200 mm from the column base.

At the 5% drift and 5.5% drift, the damage was more serious. The corner concrete cover significantly crushed and spalled off. At this stage, buckling of the longitudinal steel occurred clearly between 100 mm and 200 mm. When the loading cycle reached the final stage of 6.5% drift, the cover concrete totally damaged on the four faces between lower portions of two steel cages. Finally, the column failed by flexure with spalling of concrete cover around the column specimen. Also, buckling of longitudinal reinforcement occurred on the two sides between 300 mm height from the base of the column specimen. This is the effect of larger spacing of steel cages. The lateral strength at the 80% of the maximum load was 272 kN. The Hysteretic behavior of SC-200 specimen is shown in Figure 3.26 and the progression of damage state Figure 3.27. Crack patterns are shown in Figure 3.28 (a), (b) and (c).
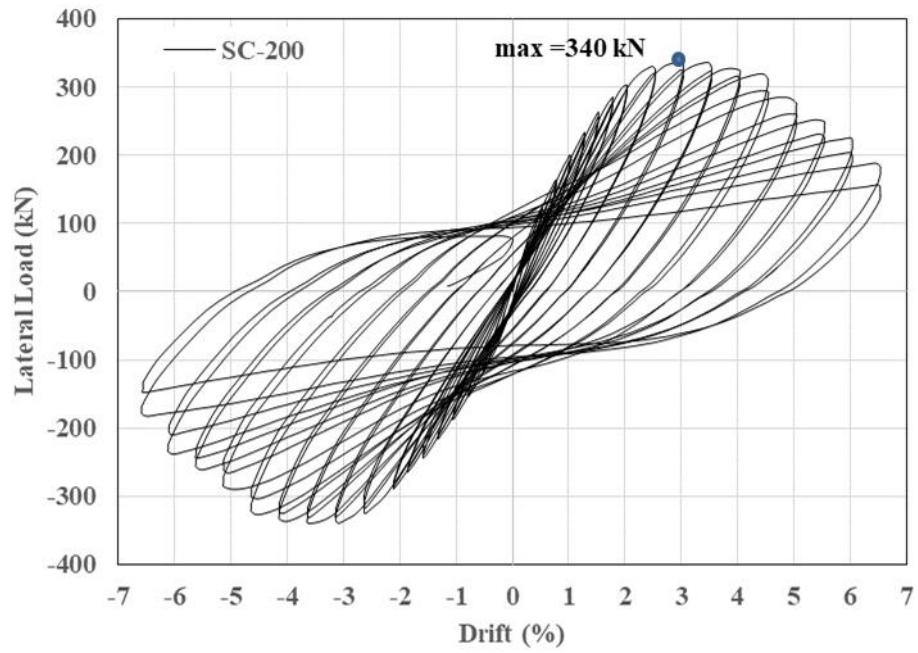
Figure 3.26 Hysteresis behaviour of SC-200

(a)

(b)
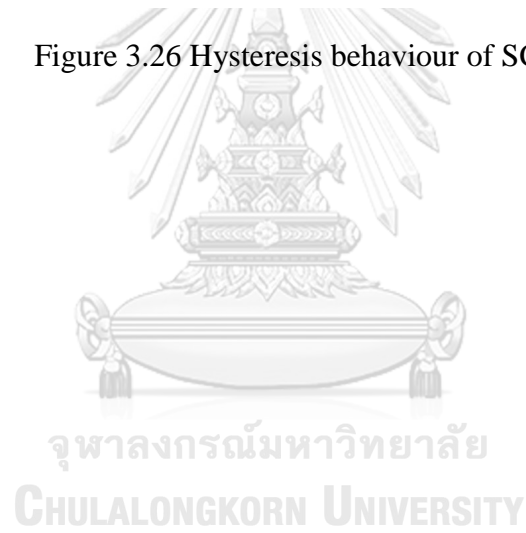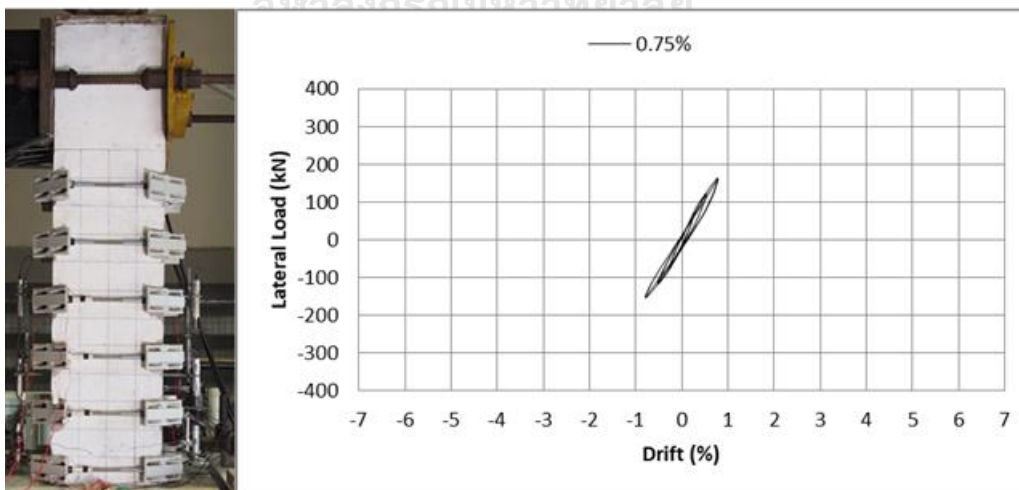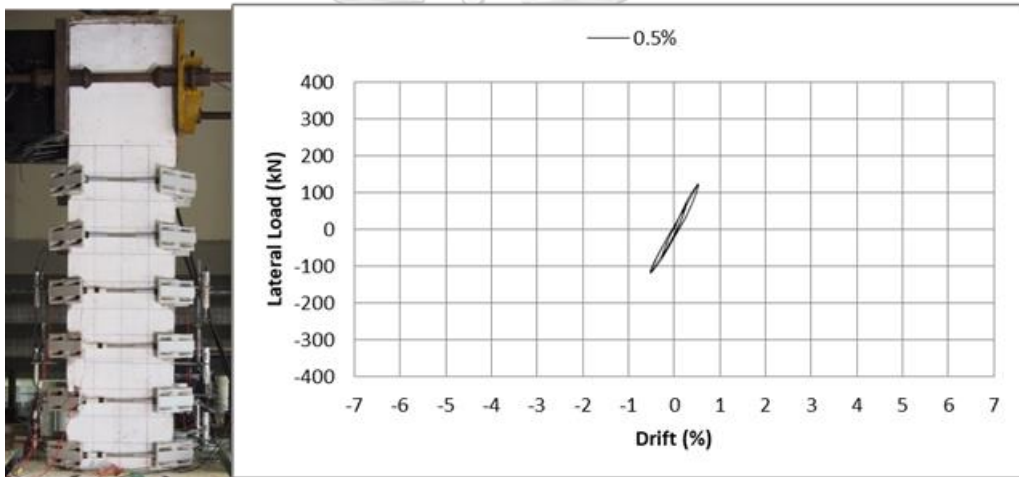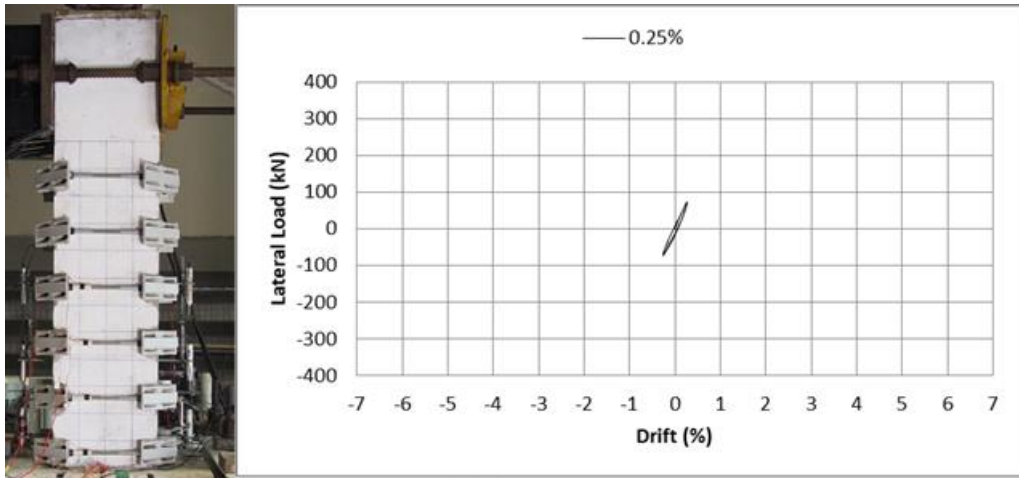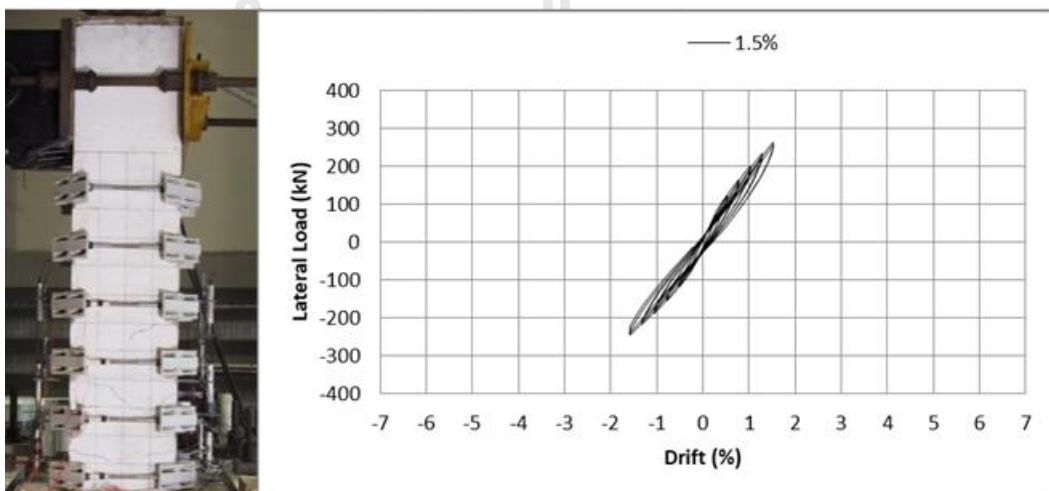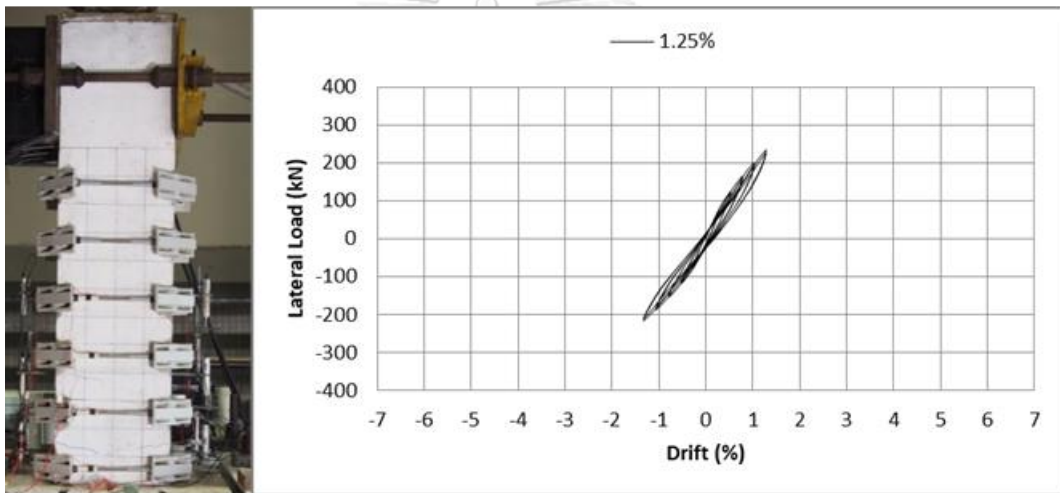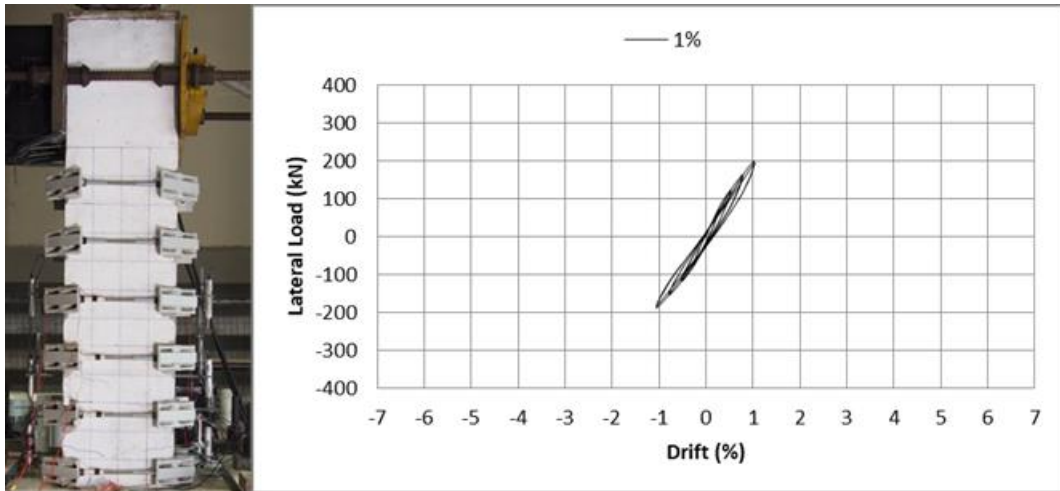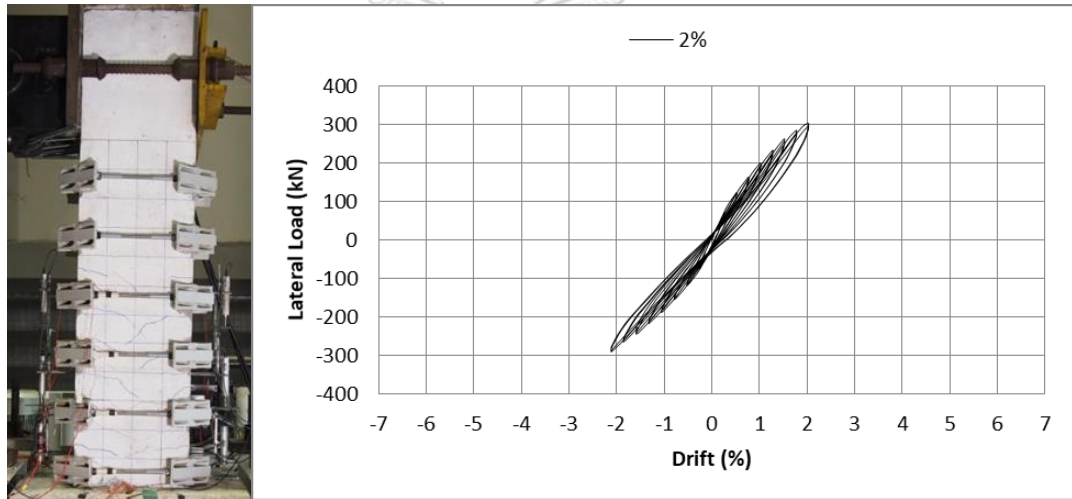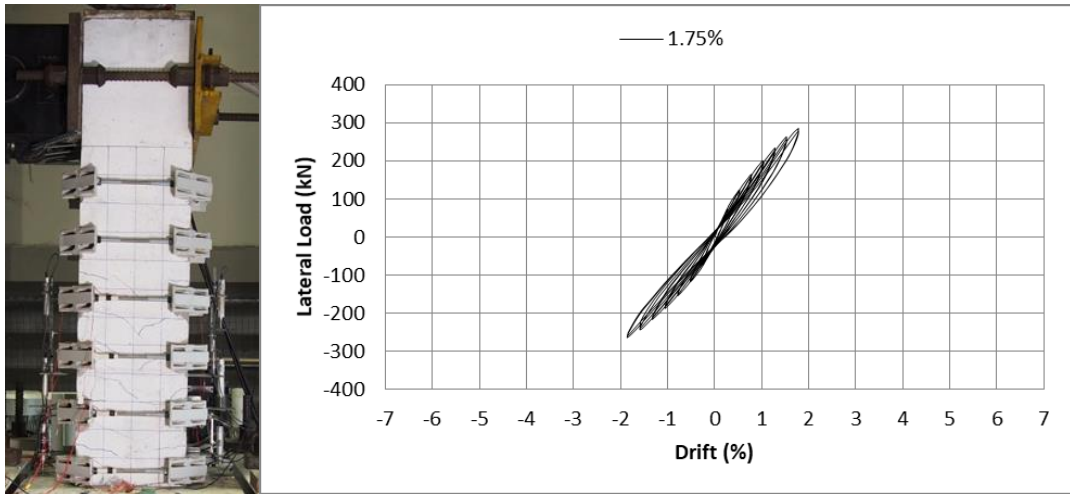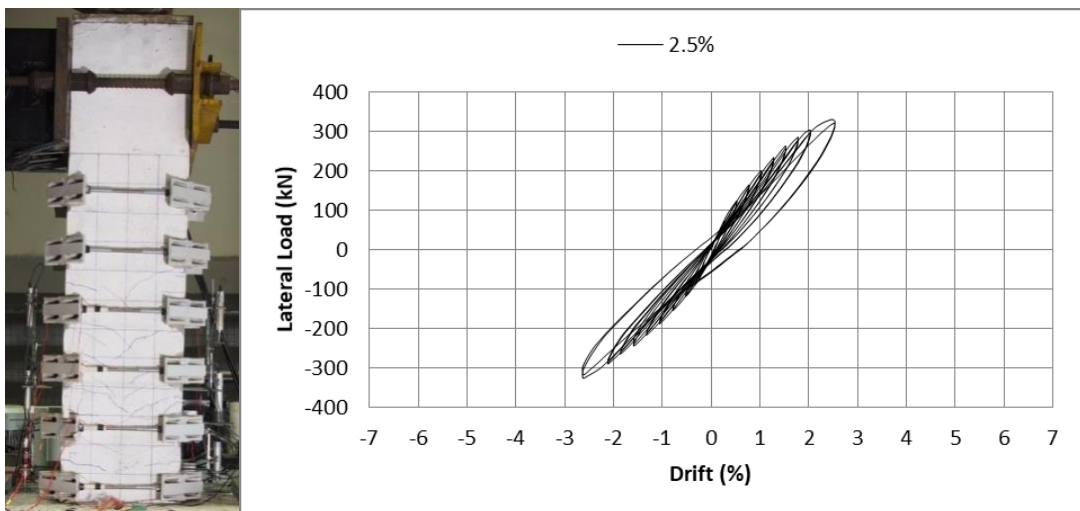
(c)
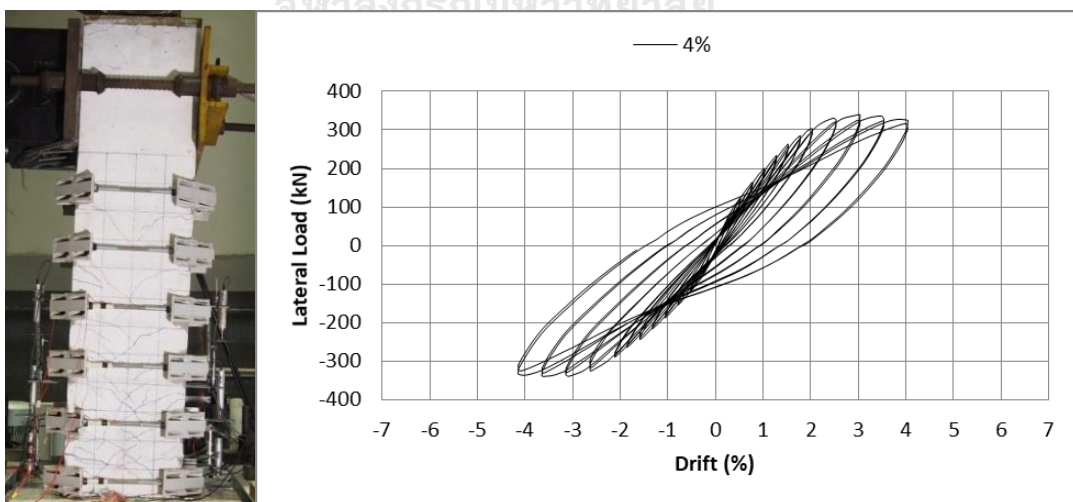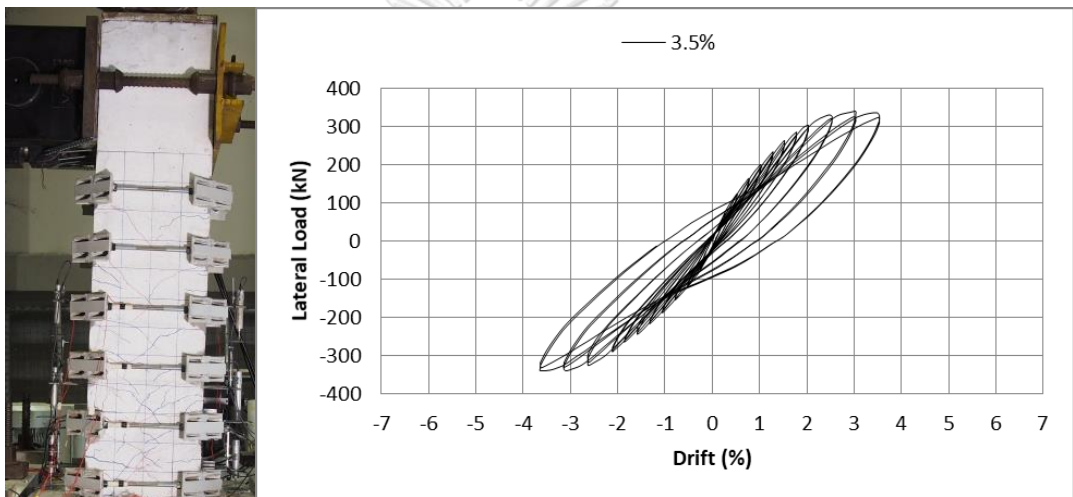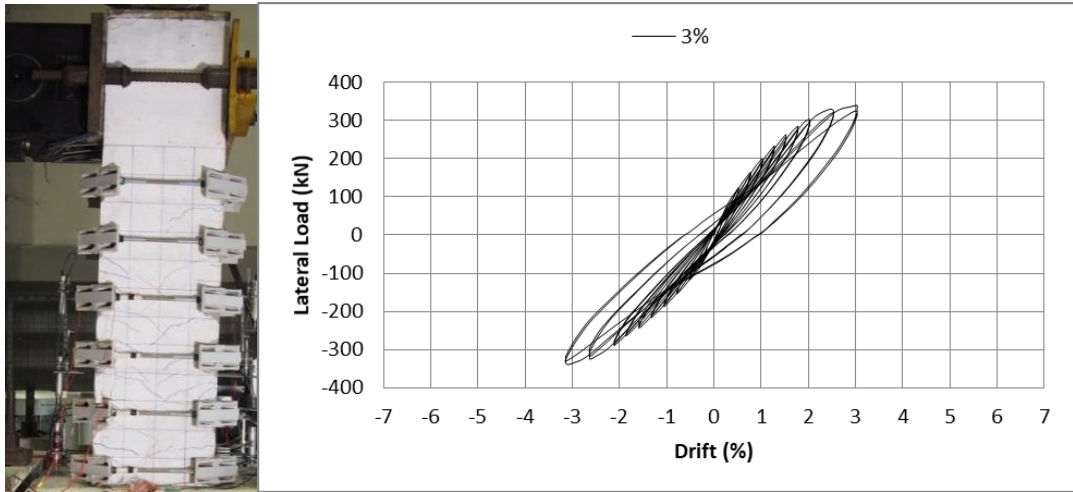
(d)
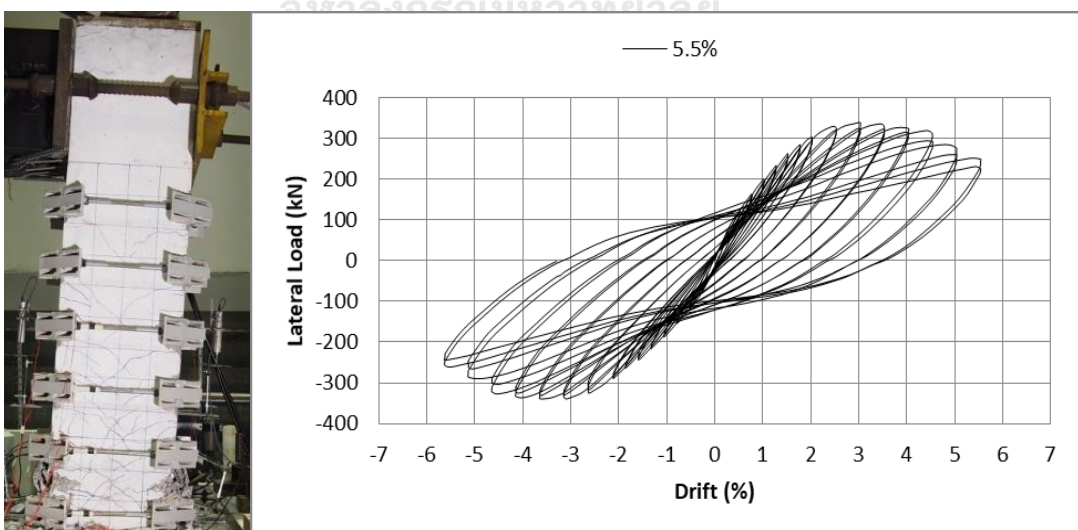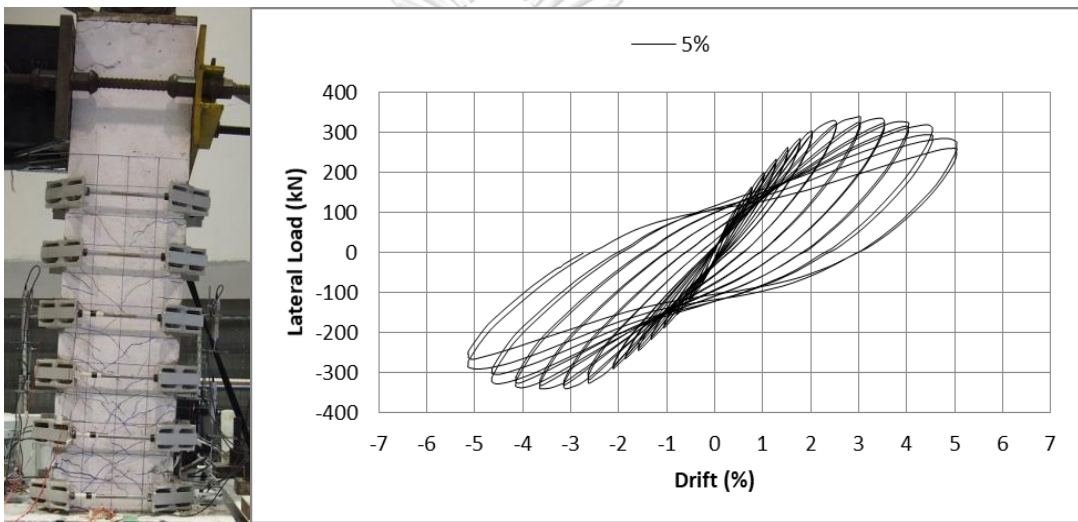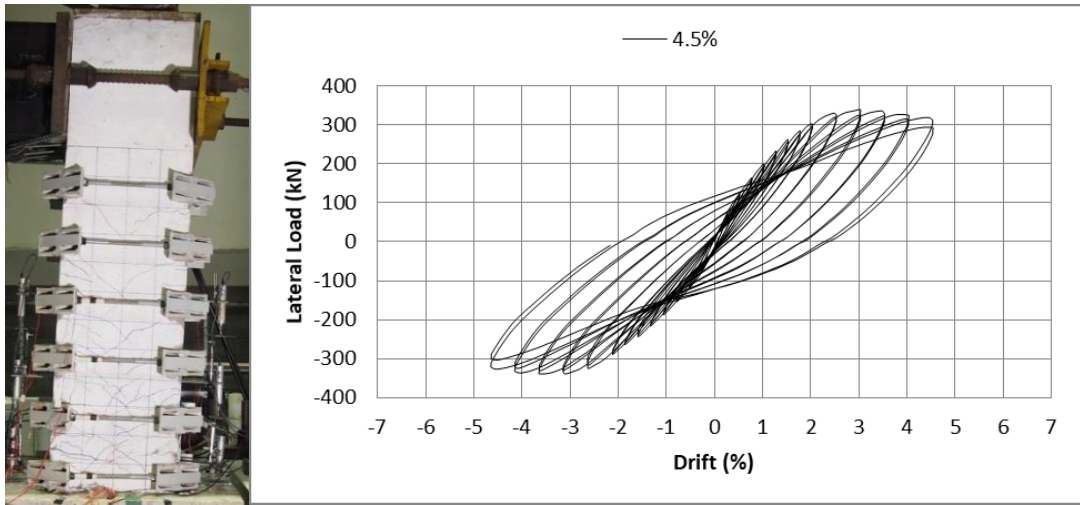
(e)
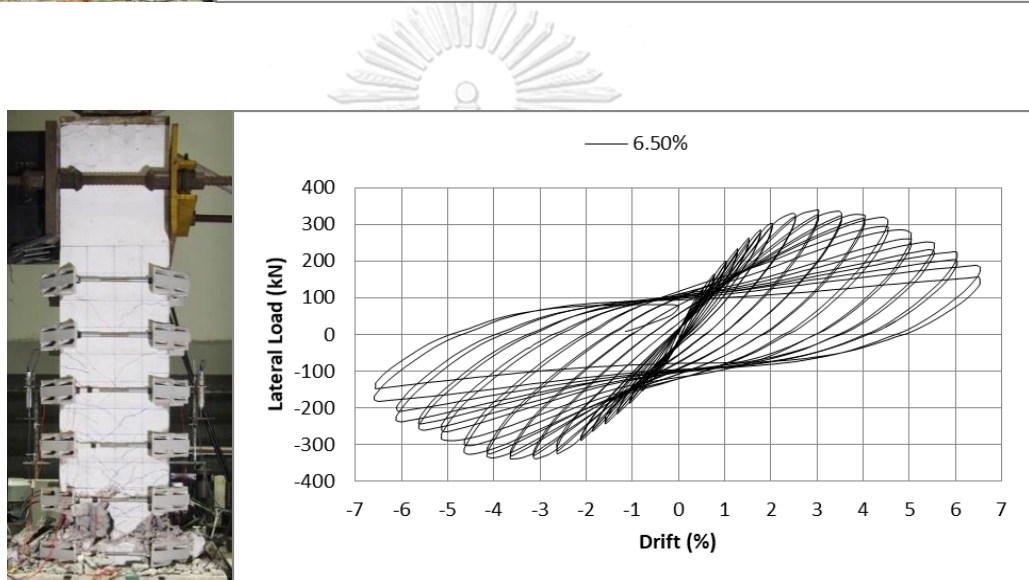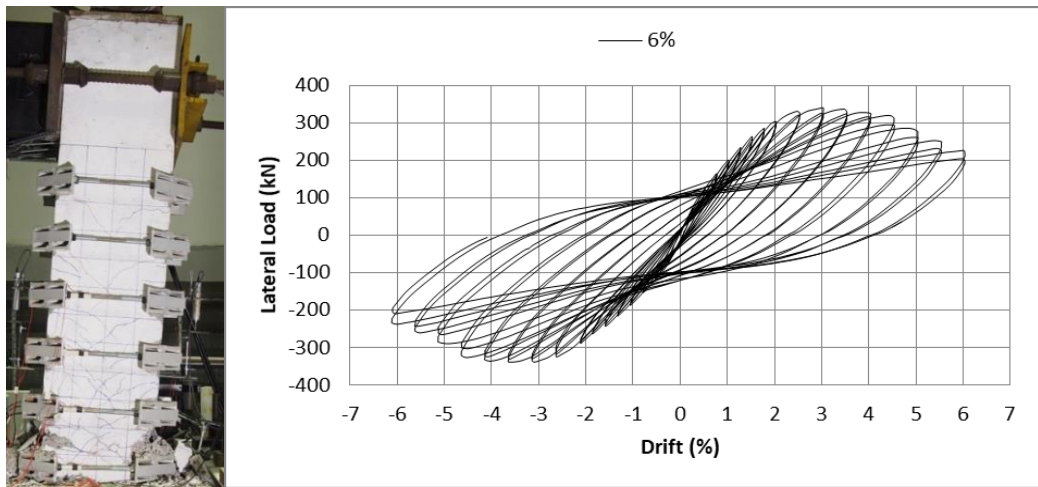
Figure 3.27 (a), (b), (c), (d), (e) and (f) Progressive damage stage of SC-200

(a)
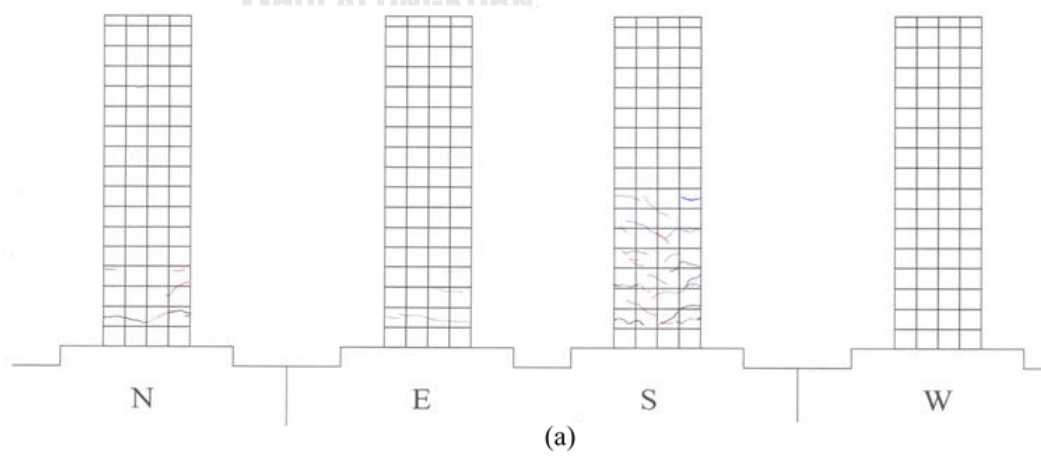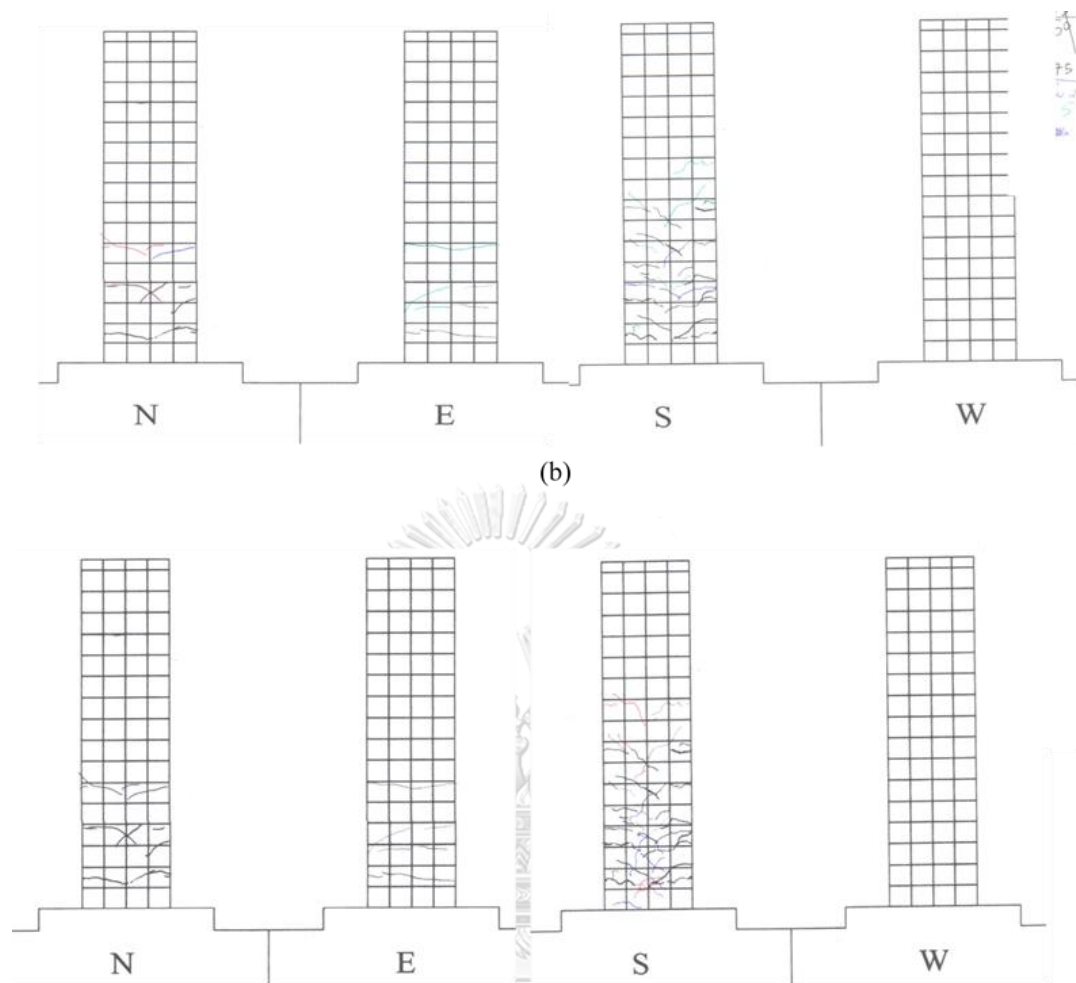
Figure 3.28 (a) Crack Pattern SC-200 from ±0.25% to ±1.5%

(b) Crack Pattern SC-200 from ±1.75%% to

(c) Crack Pattern SC-200 from ±3%% to ±3.5%

3.11.2 Strain in the longitudinal steel

Tension steels L31 yield at the first cycle of 2% drift and L32 yielded the first cycle of 3% drift respectively. In contrast, the compression steel L33 began to yield at the first cycle of 3% drift and L34 yielded at the second cycle of 2.5% drift. At the time of all longitudinal reinforcement yielded, the lateral load capacity of the SC-200 also reached the peak point. At the end of the loading cycles, all corner longitudinal steel buckled within the plastic hinge region. In comparison of specimens CC, SC-200 reached the yielding of longitudinal reinforcements at the higher loading cycles than CC. It can be said that the ductility of the column increased because of the additional confinement effect of steel rod collars and SC-200 specimen was dominated by flexural failure mode. Strain in the longitudinal steel of SC-200 within the plastic hinge region is also shown in Figure 3.29.
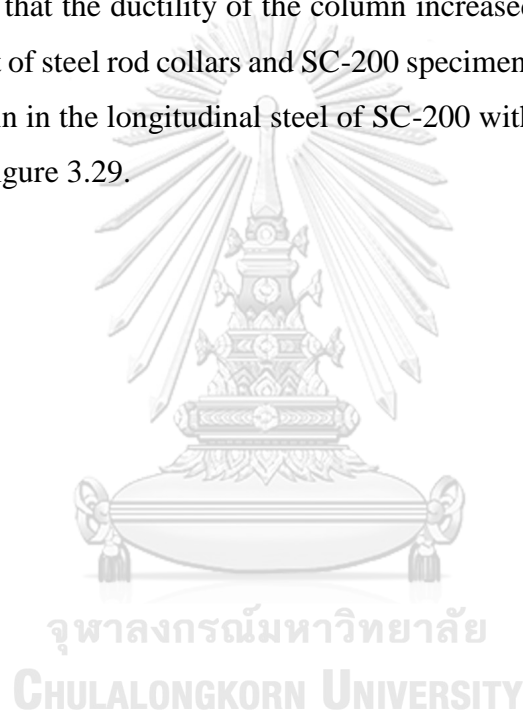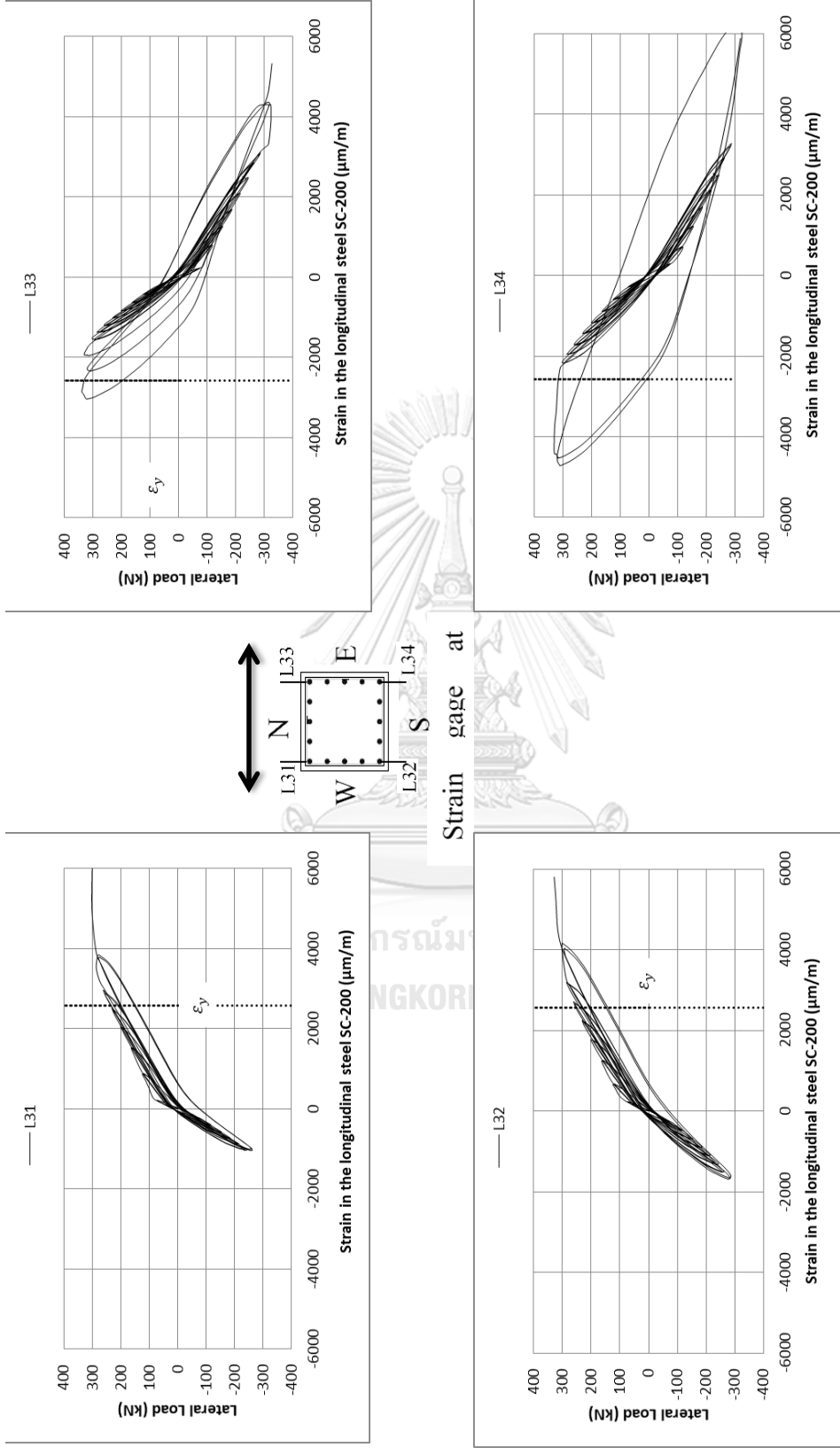
Figure 3.29 Strain in the longitudinal reinforcement of SC-200 at level 1

3.11.3. Strain in the transverse steel

To capture the strain in the transverse steel, twelve number of strain gauge was used for the four levels and three numbers of strain gauges were put on one level. The first level, all the strains in the transverse steel were within the yield limit. Strain in the cross ties was higher than the transverse reinforcement. Strains in the transverse steel at level 1 are shown in Figure 3.30.

At level 2, only strain in the S21 was within the yield limit. S22 and S23 were over the yield limit near the end of the loading cycles. On the other hands, the strain in the transverse reinforcement and cross ties was beyond the yield limit. This was the effect of longitudinal steel buckling. Longitudinal steel buckled between the elevations of 100 mm to 200 mm. Strains in the transverse steel at level 2 are shown in Figure 3.31.

At this level, transverse reinforcement reached the yield limit at the loading 6.5% drift, but a strain cross tie was still within the yield limit until the end of loading. After the flexural shear cracks had appeared on the south faces, the shear was carried by transverse reinforcement by some amount. Therefore, strain in the transverse steel in this level reached the yield. Strains in the transverse steel at level 3 are shown in Figure 3.32.   At level 4, strain in transverse reinforcement was within the yield limit. No serious damage occurred at this level. Strain in the transverse reinforcement in this level was lower than that of any other level. Strains in the transverse steel at level 4 are shown in Figure 3.33. Strain in the transverse steel was recorded and discussed at each level as follows.

In conclusion, strain in the transverse reinforcement at level 2 was the maximum than any other levels because longitudinal reinforced buckled and the cover concrete spalled off seriously. This effected to the transverse reinforcement to be more than yield limit.
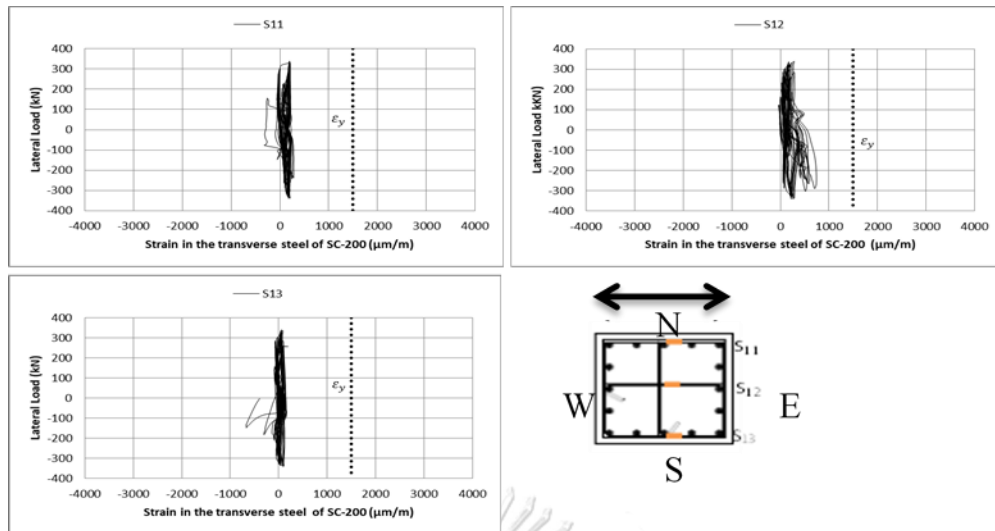
Figure 3.30 Strain in the transverse steel of SC-200 at level 1
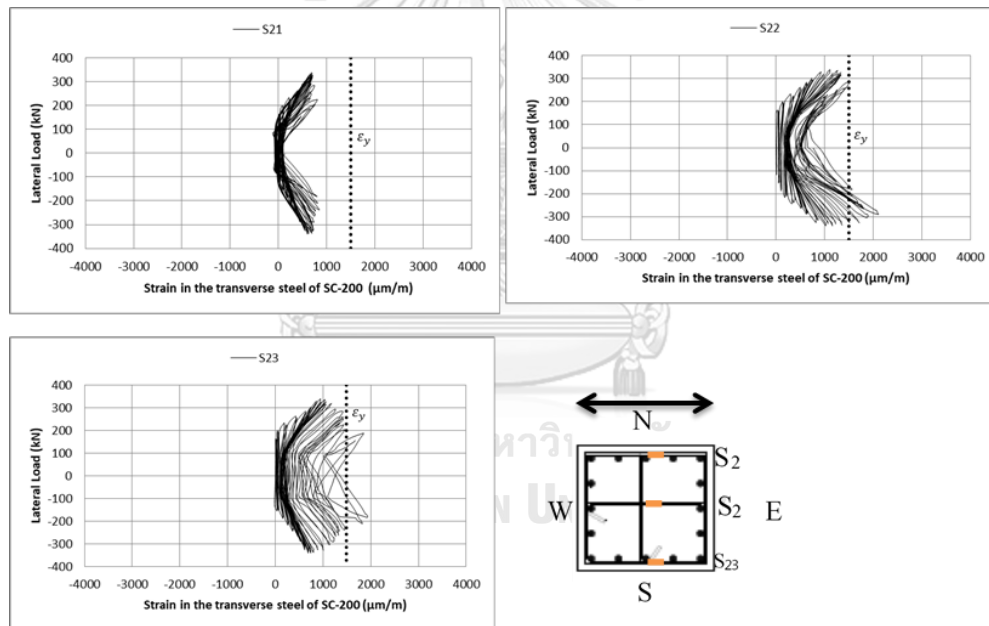
Figure 3.31 Strain in the transverse steel of SC-200 at level 2
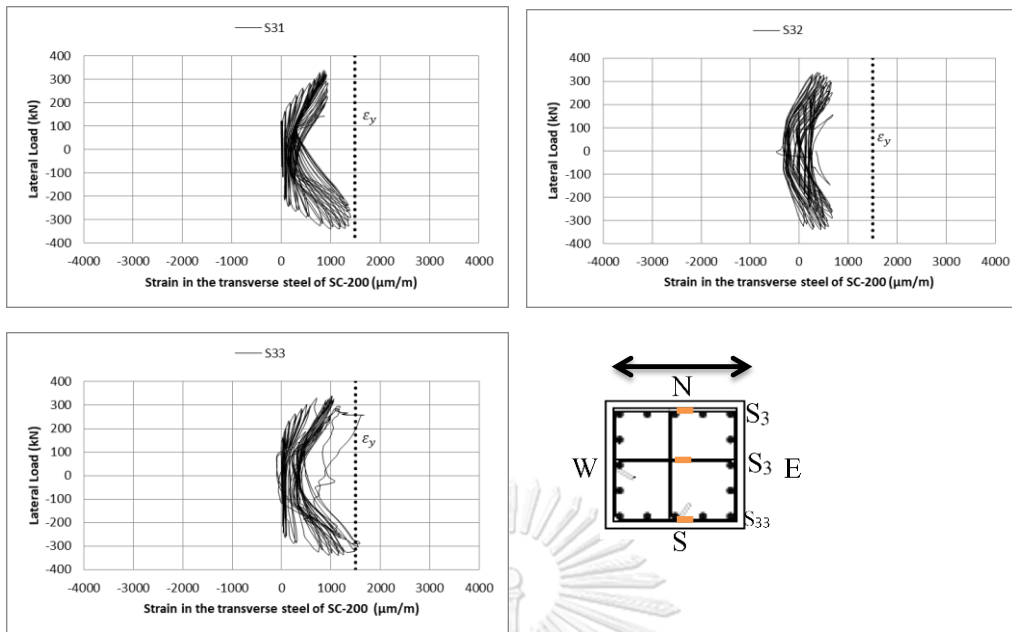
Figure 3.32 Strain in the transverse steel of SC-200 at level 3
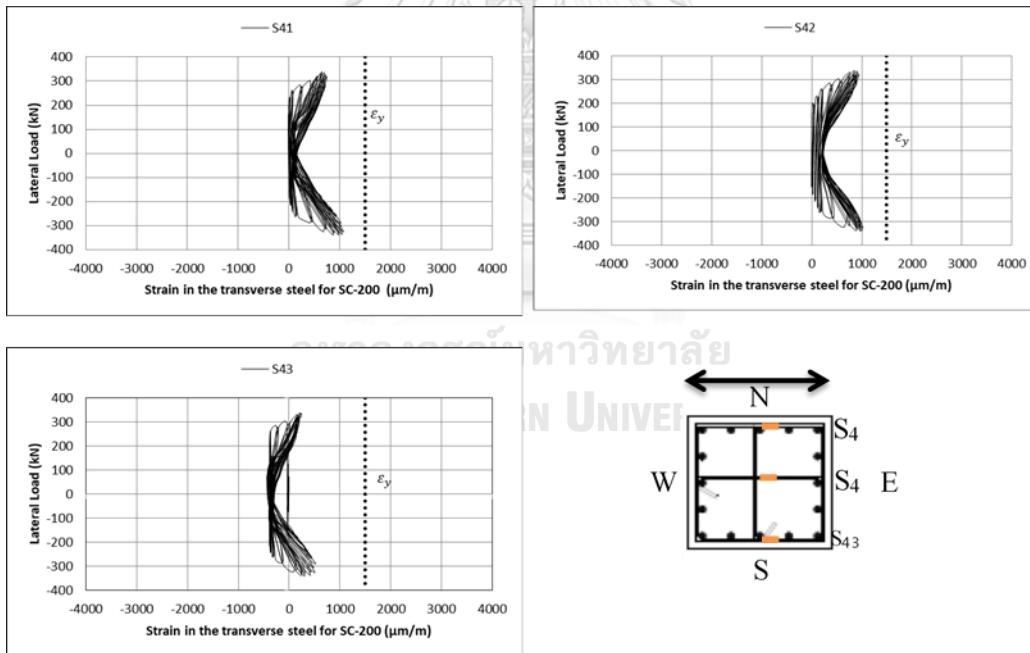
Figure 3.33 Strain in the transverse steel of SC-200 at level 4

3.11.4. Strain in the external steel rods of SC-200

A total of fourteen numbers of strain gauges is fixed on the steel rods around the four faces of the columns at the level of 3, 5 and 7 as shown in Figure 3.34. However, only two numbers of strain gauges were put at the level 1. The maximum yield strain of the steel cage bars was 2210 micro strain. Strains in the steel rods at each level are shown in Figure 3.35 (a), (b), (c) and (d).
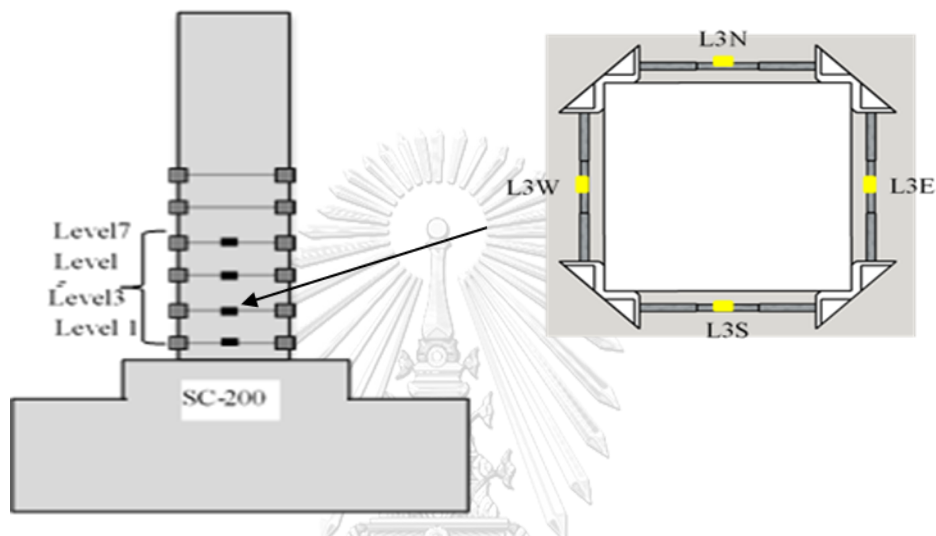
Figure 3.34 Location of the stain gauge on the external steel rods of SC-200

At level 1, strain in the steel rod in north direction increased to the yield limit after the maximum loading reached and also buckling of the longitudinal steel was observed after maximum loading cycle. At level 3, strain in the steel rods yielded at 6.5 % drift in the north direction and 6% drift at in the south direction. At level 5, strain in the steel rods yielded at 5.5 % drift in north and south direction. Strain in the steel rods in the east and west direction was still within the yield limit until the end of loading cycles. At level 7, strain in the steel rods was within the yield limit.

In conclusion, strains in steel cage bars at level 3 and level 5 at the North and South direction were more than any other two directions. The steel cage bars yielded at the North and reached beyond the yield limit at the South direction because the longitudinal reinforcement buckled and then followed by crushing of the cover concrete.

(a)

(b)
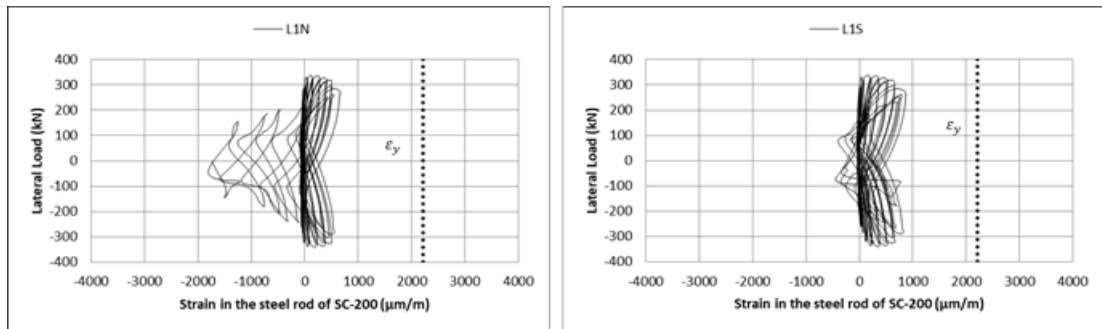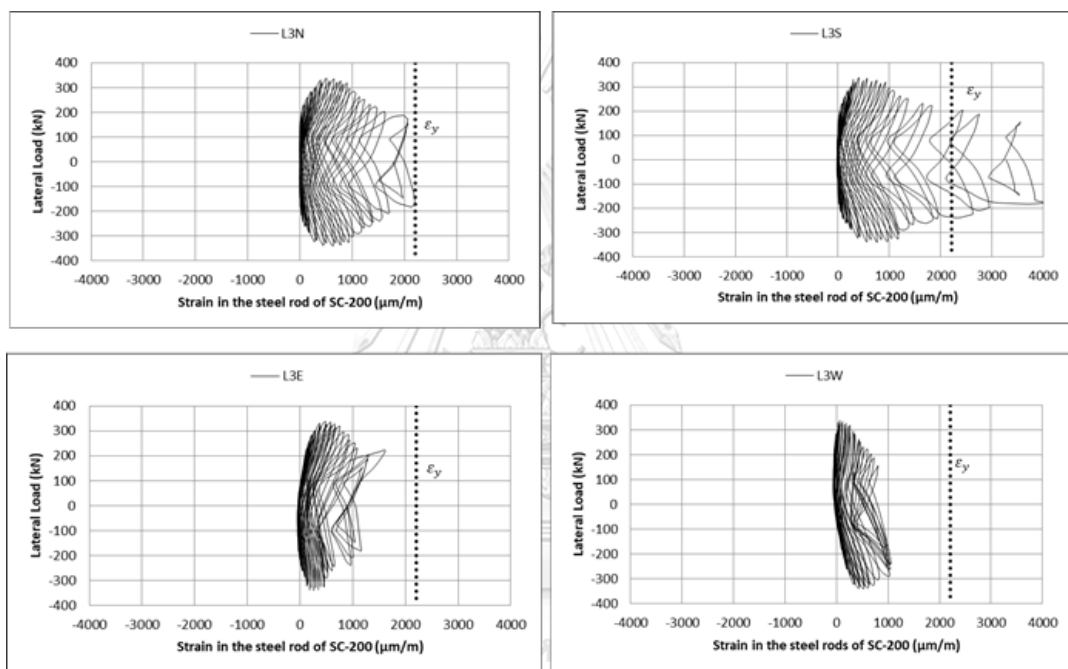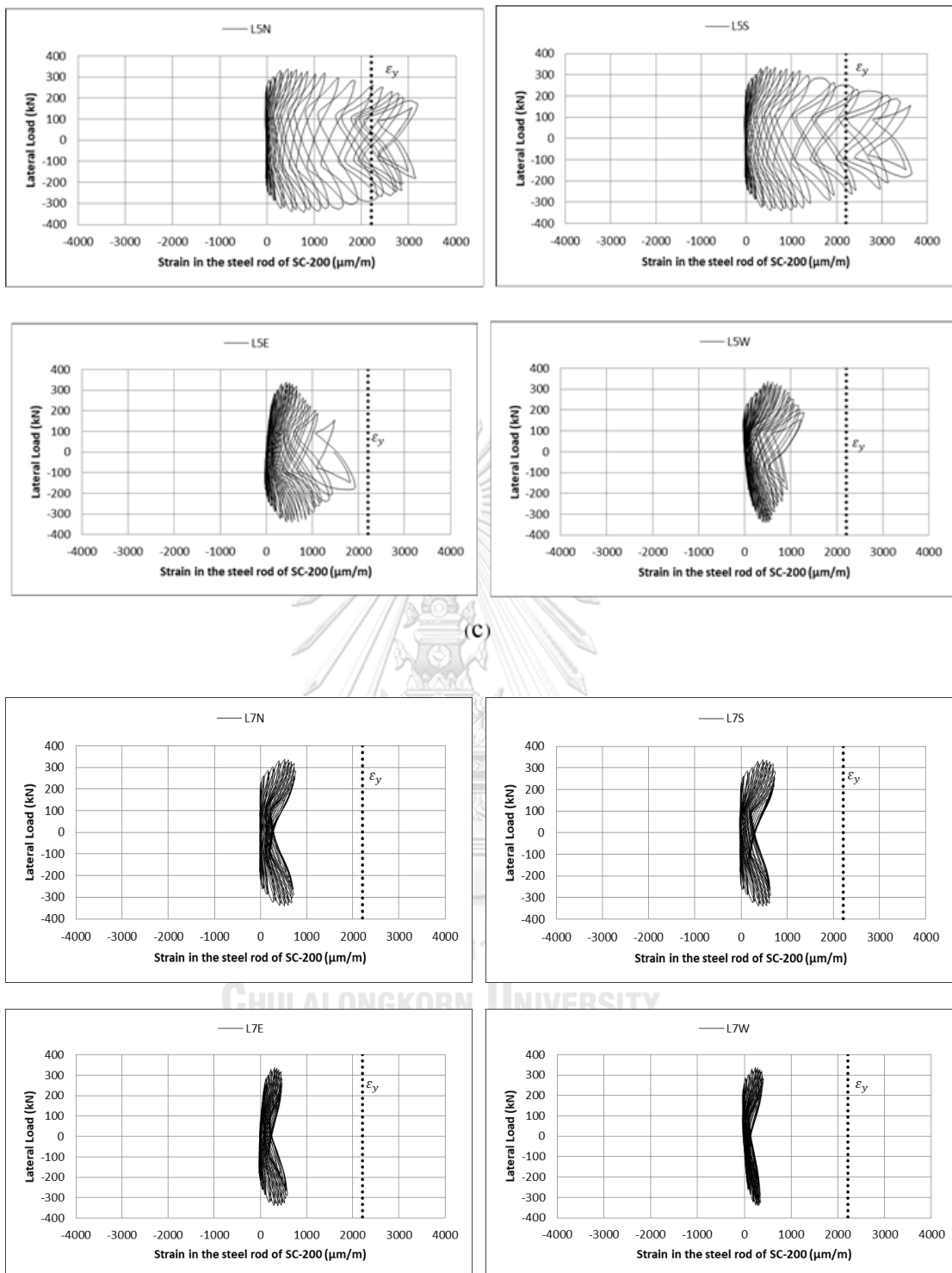
Figure 3.35 (a) Strain in the steel rods of SC-200 at level 1

(b) Strain in the steel rods of SC-200 at level 3

(c) Strain in the steel rods of SC-200 at level 5

(d) Strain in the steel rods of SC-200 at level 7

3.12. Progression of Damage of SC-100

SC-100 specimen is the strengthened column with steel rod collars having the spacing of 100 mm. When the strengthened column is applied the cyclic loading, until 0.25% drift no crack occurred around the column faces. At 0.5% drift, small hair line cracks were observed at 100 mm and 400 mm elevation form the base of the column, and no cracks were propagated until 0.75% drift From 0.75 % drift to until 1.5% drift, small flexural cracks occurred and the cracks propagated more and more with the increasing lateral drift cycles.

The small flexural shear cracks were observed with 1.75% drift and 2.5 % drift. At 3% loading drift, the lateral loading reached the maximum capacity of 335 kN and the lateral load capacity decreased gradually in the next loading cycles. At 4% drift, crushing of the cover concrete were occurring on the west face of the column between the 100mm elevation from the base of the column. At the 6% drift cycle, the cover concrete spalled off at the west and the east face of the column around 300 mm elevation from the base and the buckling of the longitudinal steel observed. At 6.5% drift, the lateral strength dropped continuously and the lateral loading cycles were stopped after 6.5% drift. The lateral load capacity was 268 kN at the 80% of maximum loading. The hysteresis behaviour of the SC-100 specimen under lateral loading is shown in Figure 3.36. And the progression of the damage level at each stage was shown in Figure 3.37 (a), (b), (c), (d), (e) and (f). The crack pattern of SC-100 is also shown in Figure 3.38 (a), (b), (c) and (d).
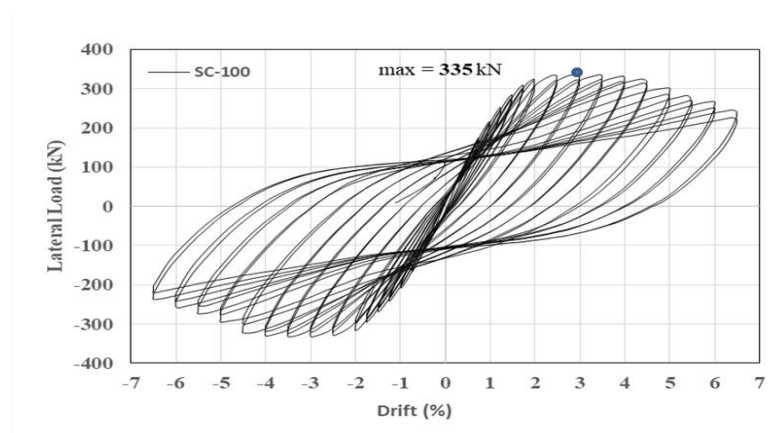
Figure 3.36 Hysteresis behaviour of SC-100
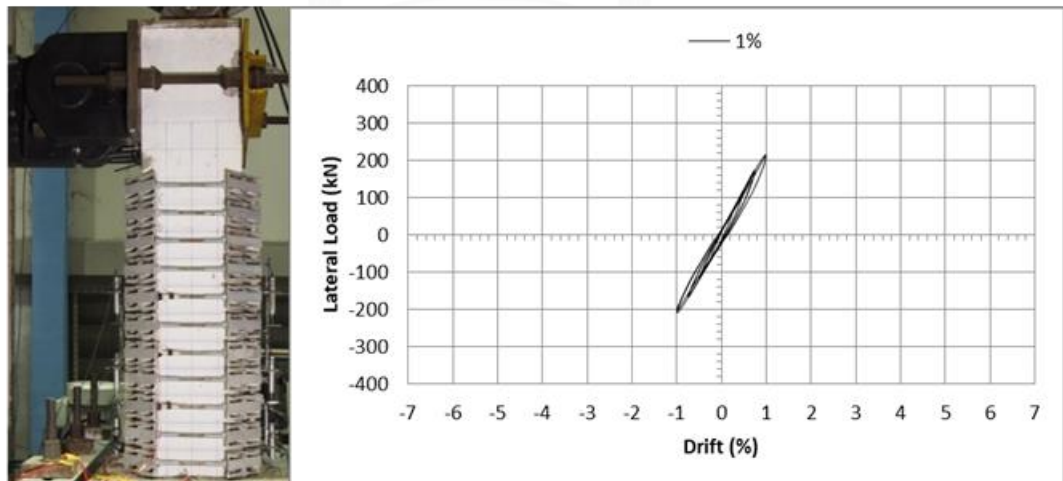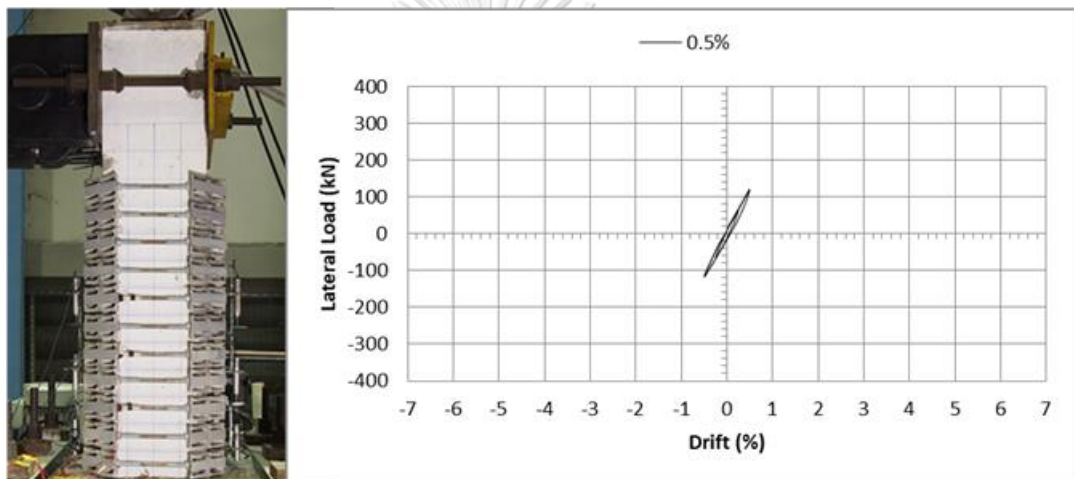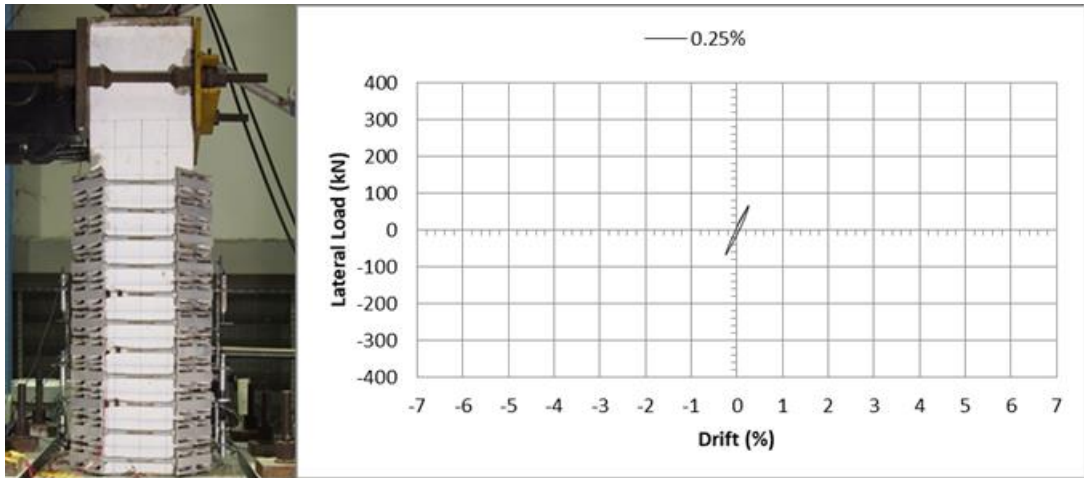
(a)
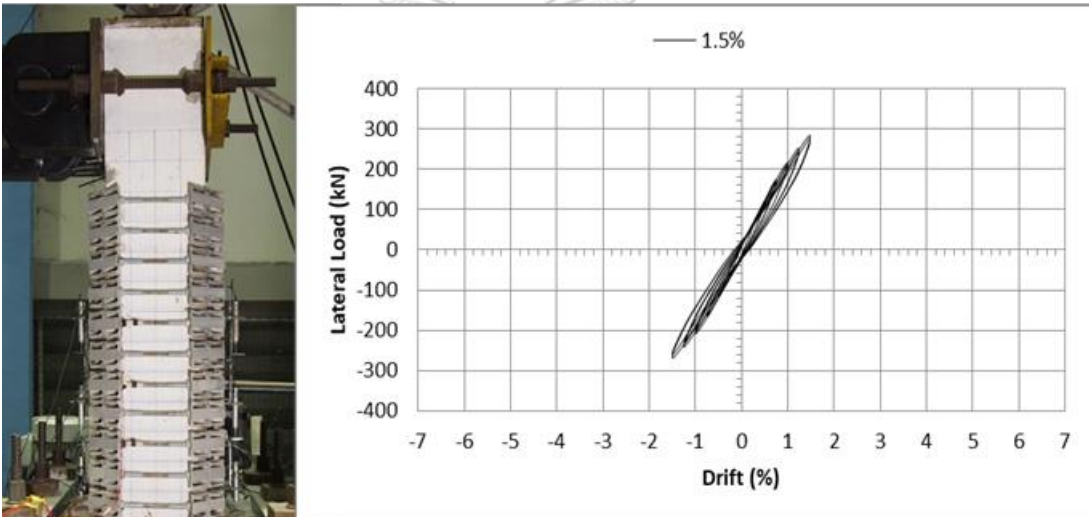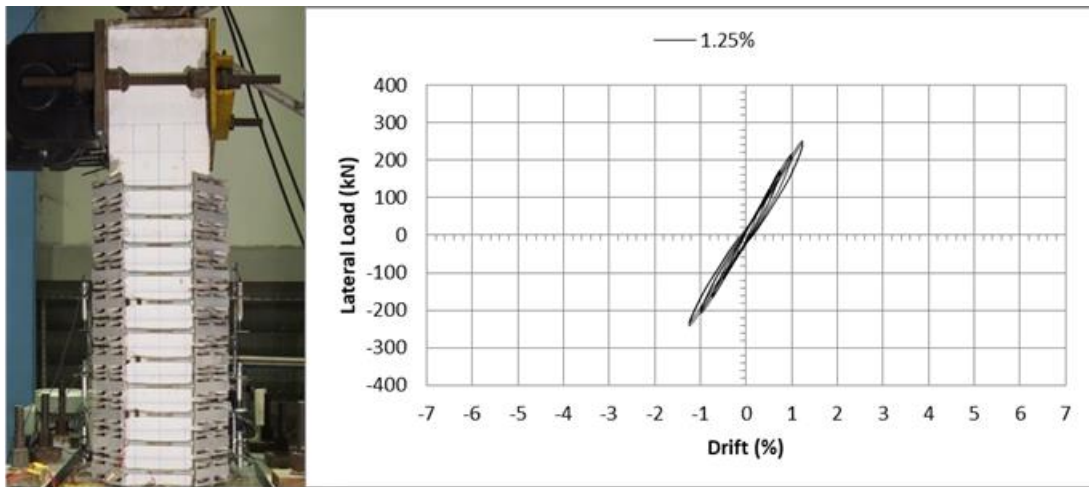
(b)

(c)

(d)

(e)

(f)
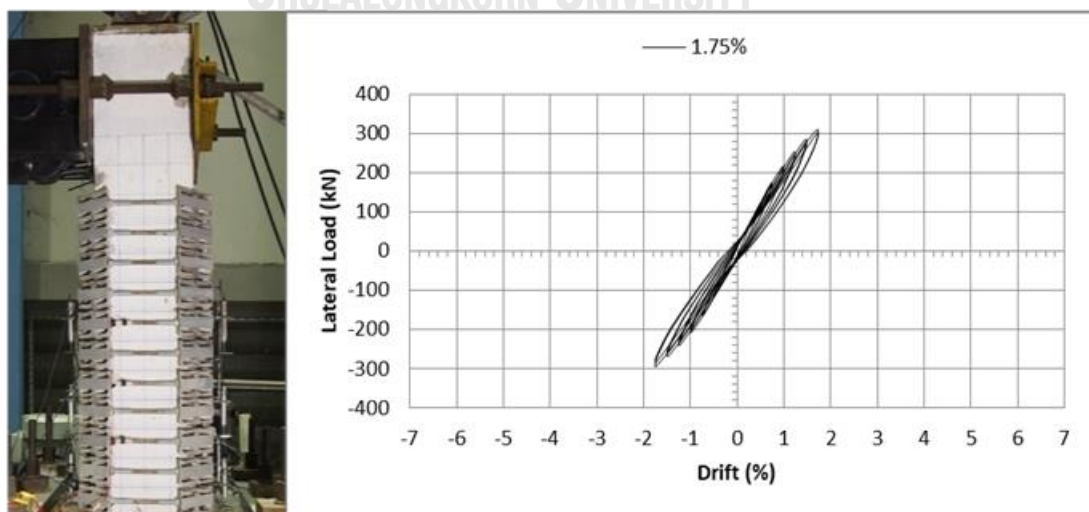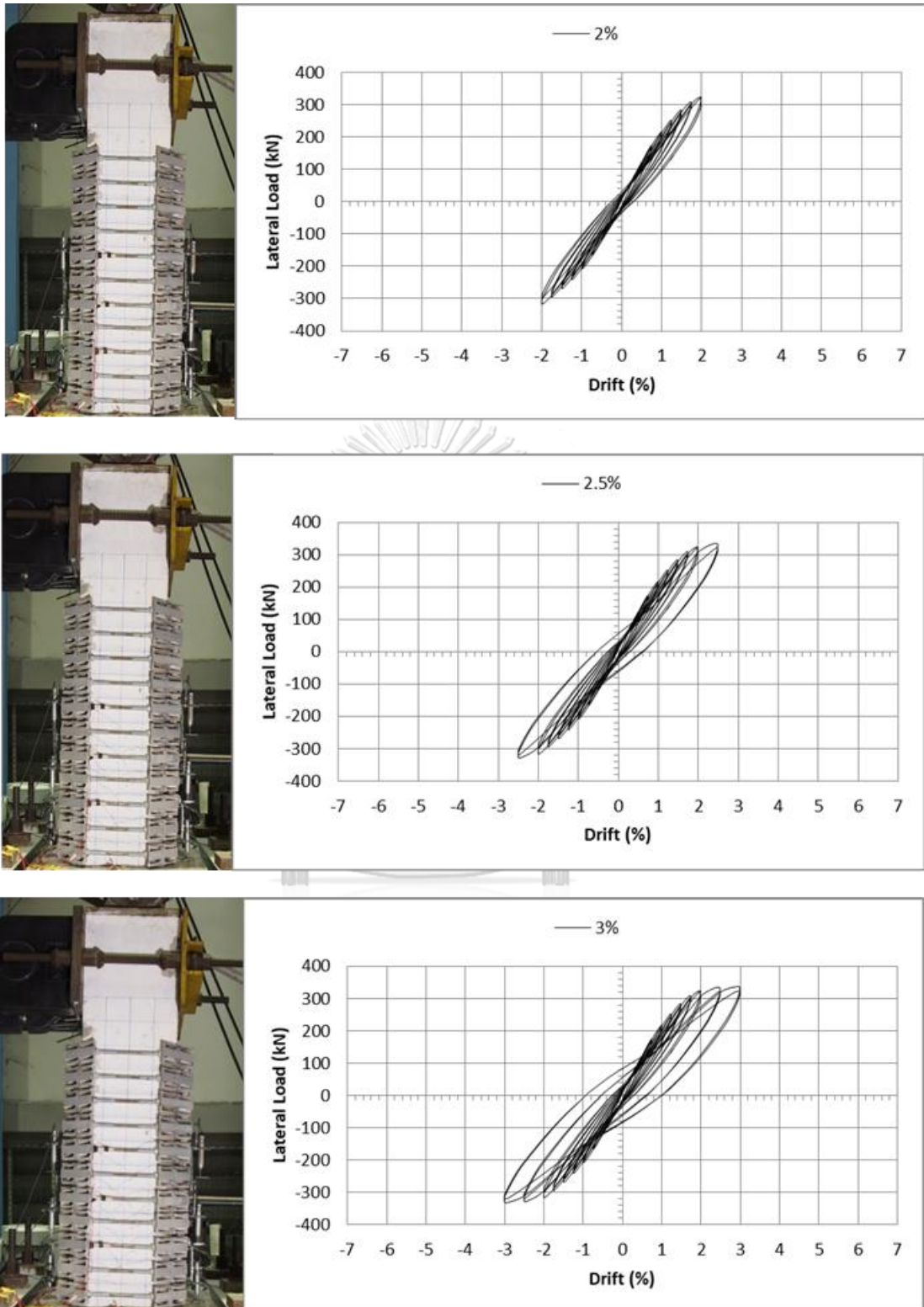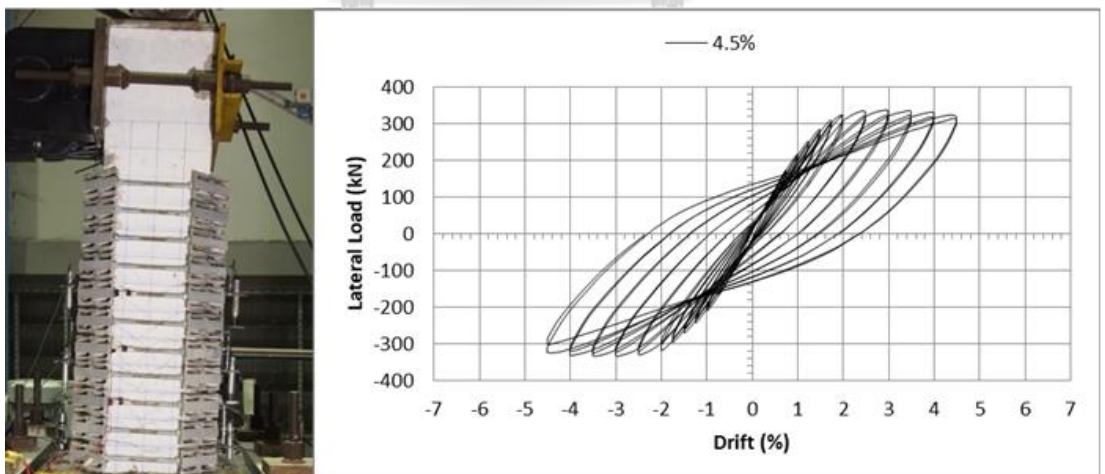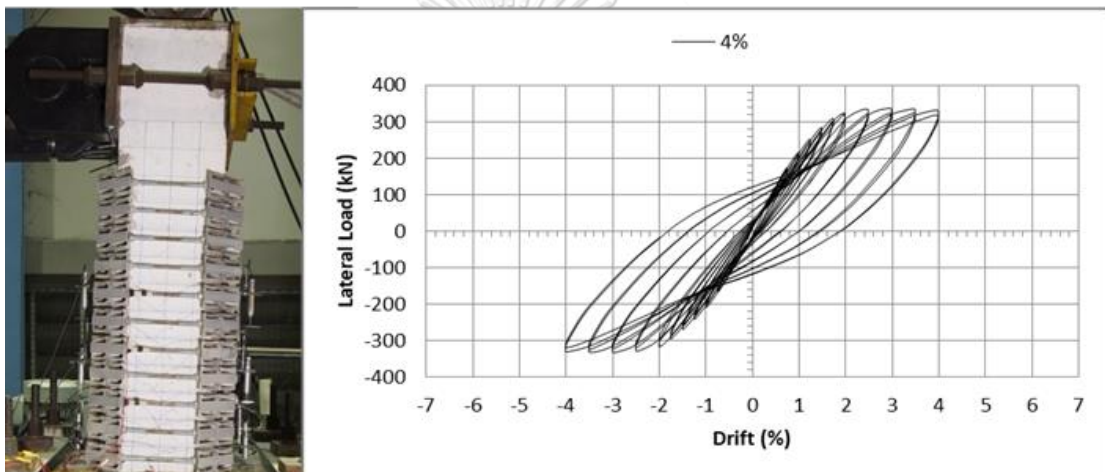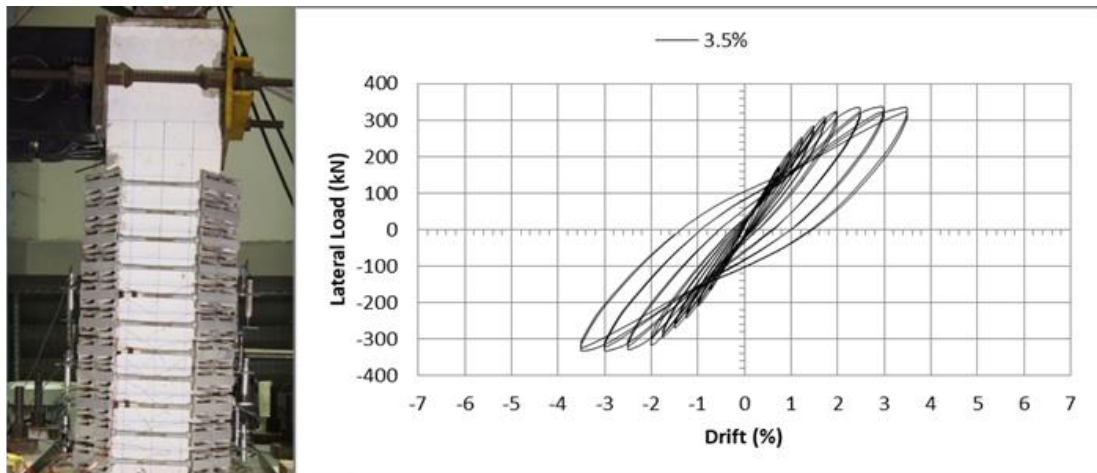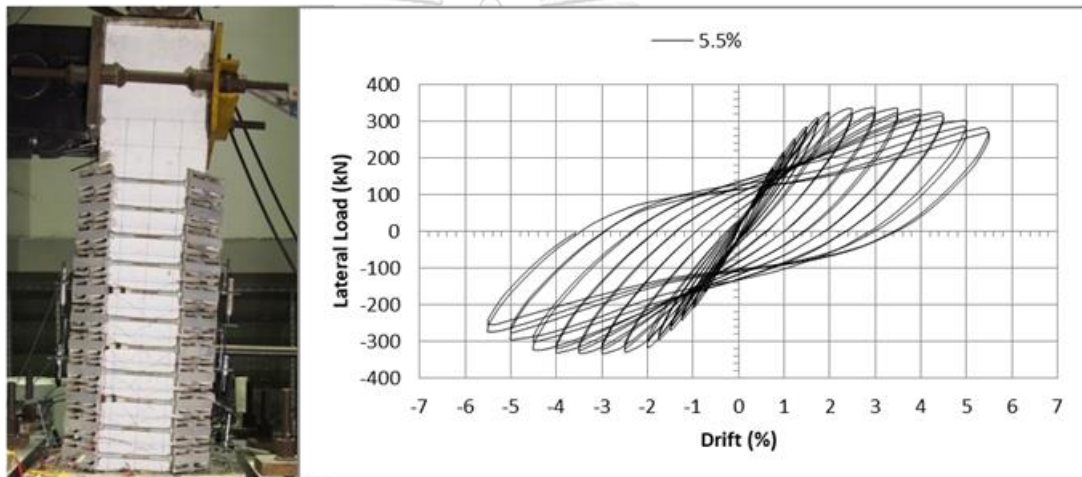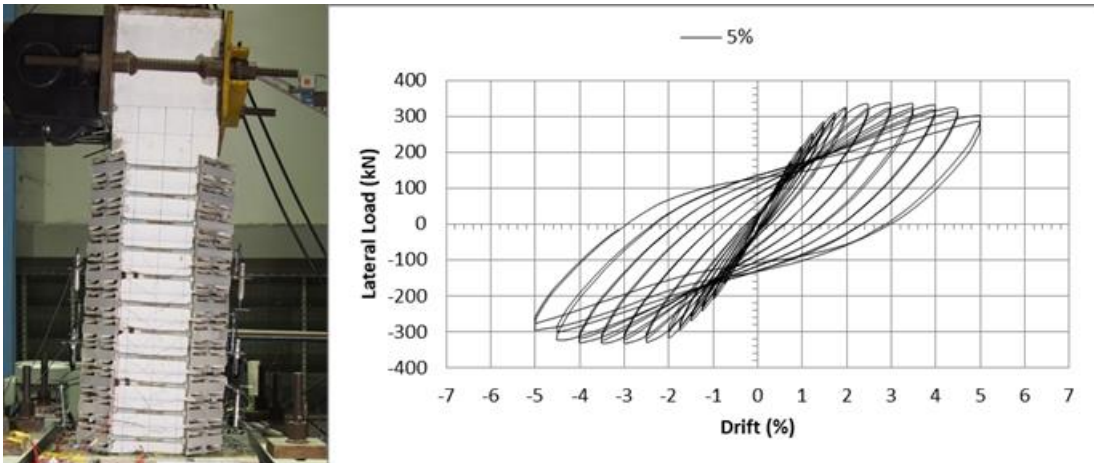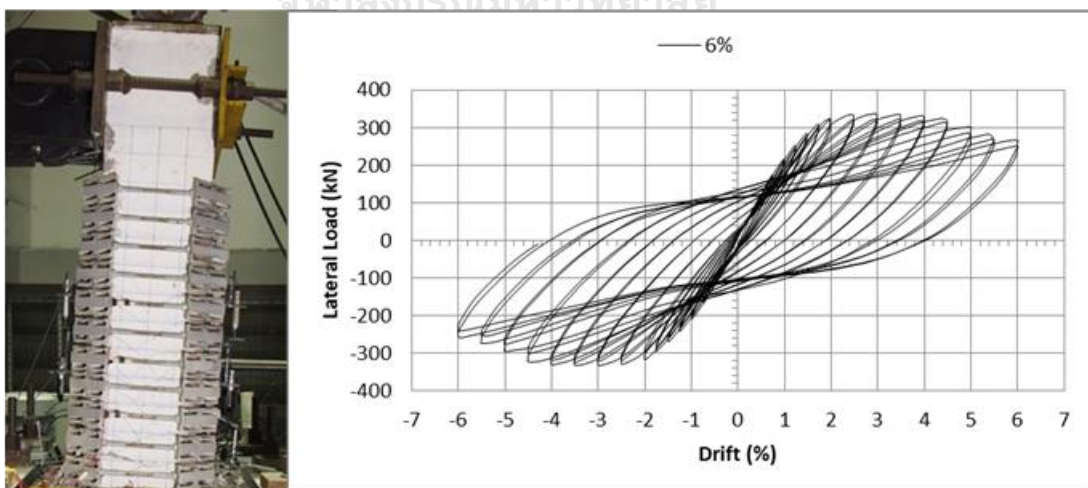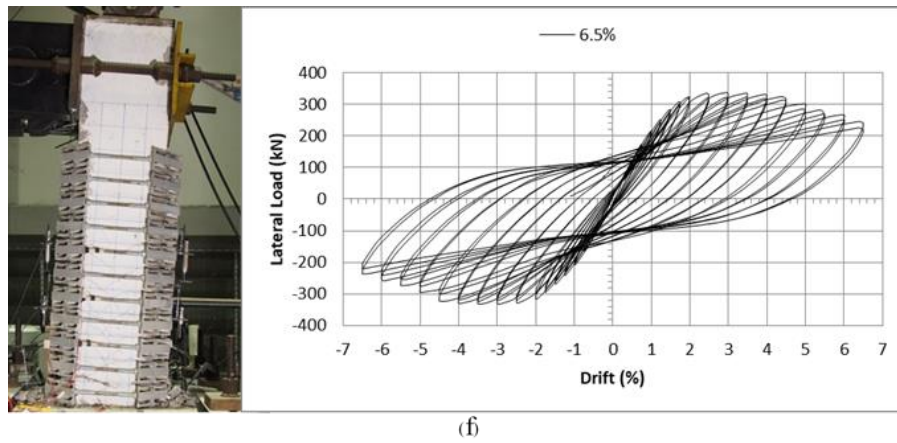
Figure 3.37. (a), (b), (c), (d), (e) and (f) Progression of damage specimen of SC-100

(a)

(b)

(c)
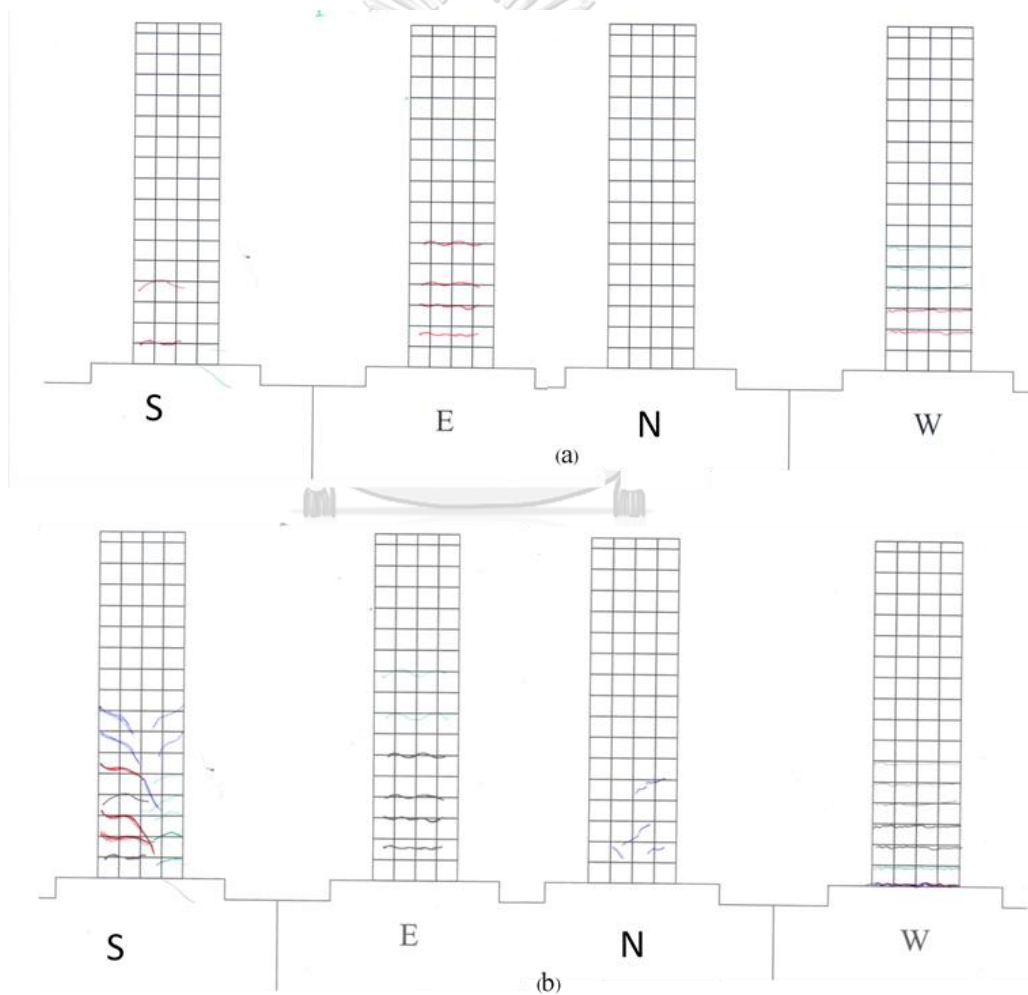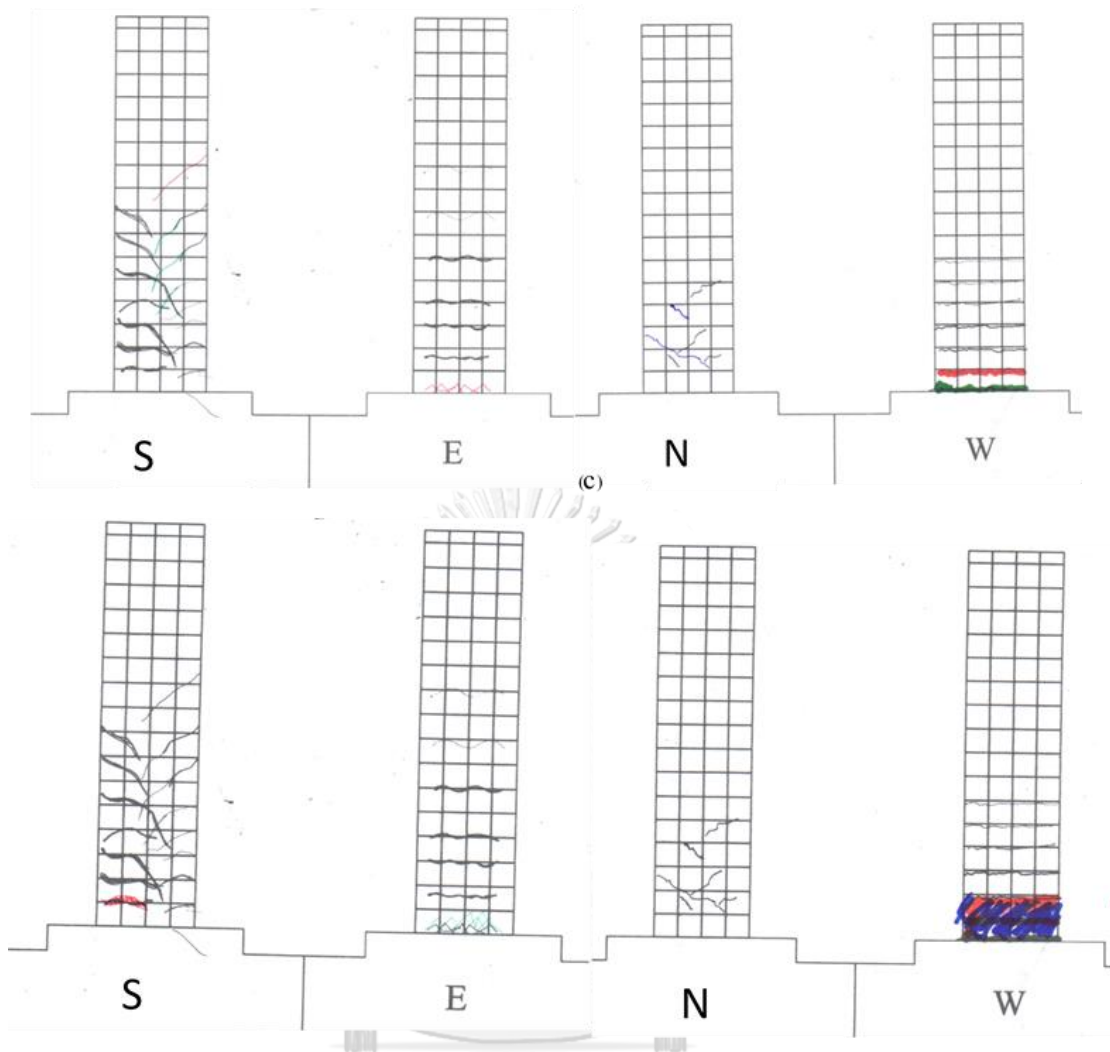
Figure 3.38 (a) Crack Pattern of SC-100 from ±0.25% to until ±1.5%

(b) Crack Pattern of SC-100 from ±1.75% to until± 2.5%

(c) Crack Pattern of SC-100 from ±3% to until ±4%

(d) Crack Pattern of SC-100 from ±5%

3.12.1. Strain in the longitudinal reinforcement of SC-100

In order to measure the strain in the longitudinal reinforcement, strain gauge located at level 3 which is in the plastic hinge region were connected the data logger and strain value were recorded by the monitor. Tension reinforcement, L31 reached the yield strain at the first 3% drift and L32 reached the maximum yield strain at the second loading cycle of 3.5% drift. Similarly, compression steel L33 also started to yield at the first cycle of 3% drift whereas the L34 rebar yielded at the first cycle of 3.5% drift. All the longitudinal reinforcement in the plastic hinge region yielded when the lateral load capacity reached the peak point. On failure of the specimen, longitudinal reinforcements in the plastic hinge region buckled slightly. The SC-100 specimen was controlled by flexural failure mode. Strain in the longitudinal steels of SC-100 within plastic hinge region was shown in Figure 3.39
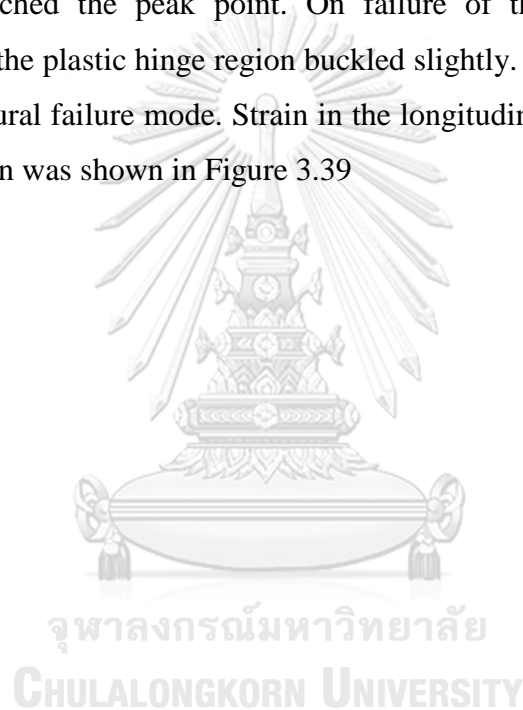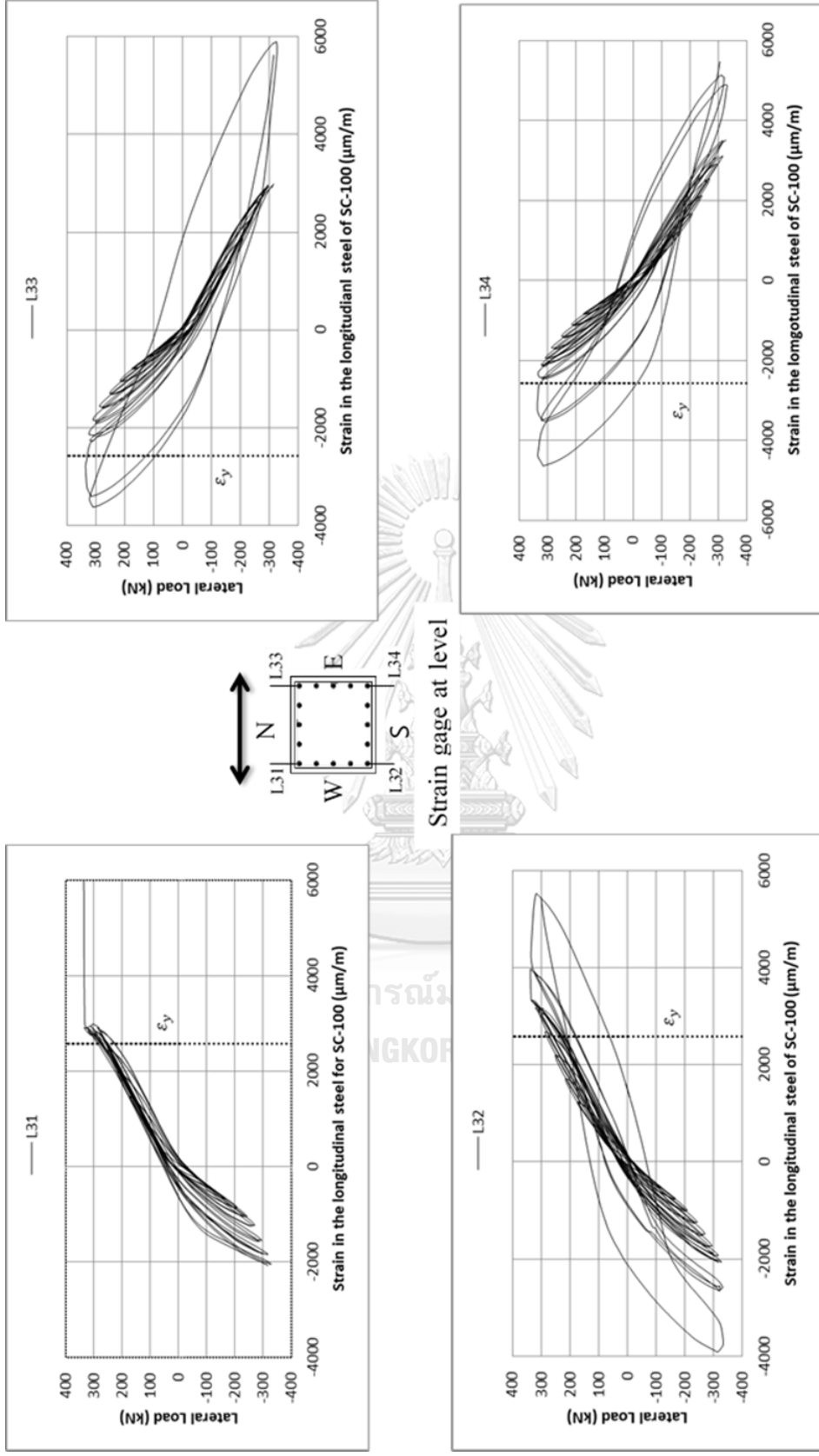
Figure 3.39 Strain in the longitudinal steel at level 3 of SC-10

3.12.2. Strain in the transverse reinforcement

To capture the strain in the transverse reinforcement, twelve number of strain gauges were used at four levels. At this level, strain gauge S11 recorded the strain data until the complete loading cycle. The strain value in S11 stain gage is less the yield value. The strain gage S12 was over after the 2% drift loading cycle. S13 strain gauge also recorded the data for all complete cycles. Strain value in S12 strain gauge was also less than the yield limit. According to test data, the transverse reinforcement located in the level 1 was within the yield limit. The maximum strain was about 800 micro strains. Strains in the transverse reinforcement at level 1 are shown in Figure 3.40. In the level 2, S21 and S23 strain gauge recorded the strain data until the end of loading cycles, whereas S22 strain gauge recorded the data until the 6% drift. After 6% drift cycle, the strain gauge was not available to record the data anymore. According to the test data, strain in the transverse reinforcements at this level was less than the yield limit. The maximum strain was about 1000 micro strain. Strains in the transverse steel at level 2 are shown in Figure 3.41.

In the level 3, there was a sudden increase in strain value in the strain gauge S31 about over 9000 micro strain at the loading of 6.5% drift. This was very near to end the loading test. Also the stain in the strain gauge S32 reached over 9000 micro strain at 4.5% loading cycle. Strain gauge S33 recorded the data for all complete loading cycles. According to the test data, the transverse reinforcement reached the yield at 6.5% loading cycle. The cross tie also reached the yield limit. Strains in the transverse steel at level 3 are shown in Figure 3.42. At level 4, S41 and S43 strain gauges recorded the data for the full loading cycles. Strain in the transverse steel was within the yield limit. The strain in strain gauge S42 increased suddenly at 6% drift and so the strain on the cross tie was over the yield. Strains in the transverse steel at level 4 are shown in Figure 3.43.
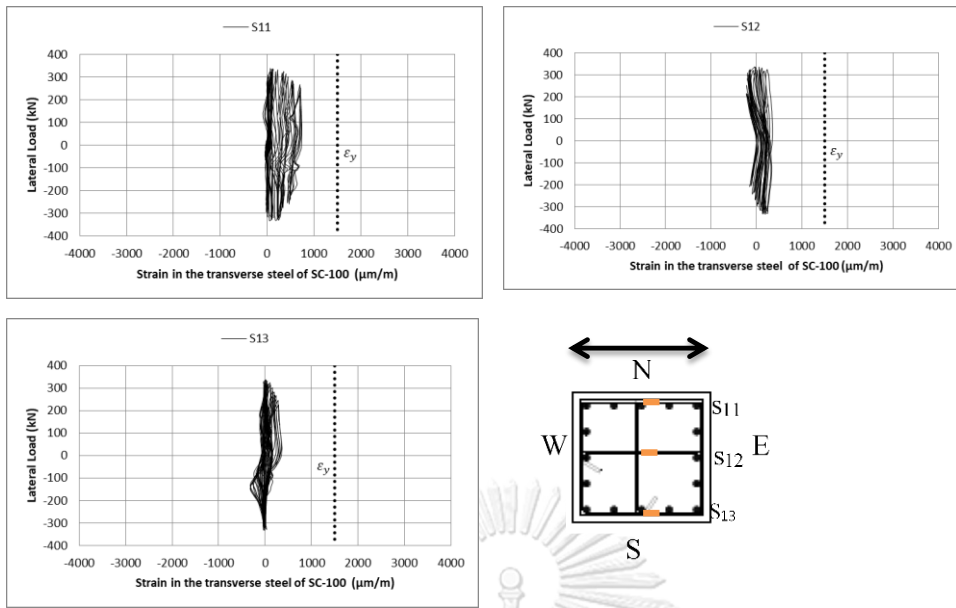
Figure 3.40 Strain in the transverse steel at level 1 of SC-100
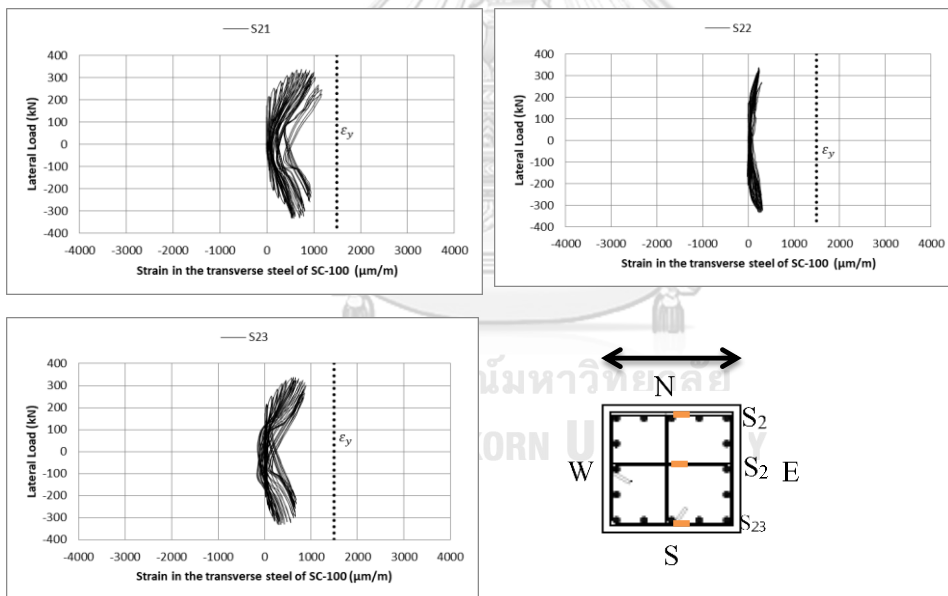
Figure 3.41 Strain in the transverse steel at level 2 of SC-100
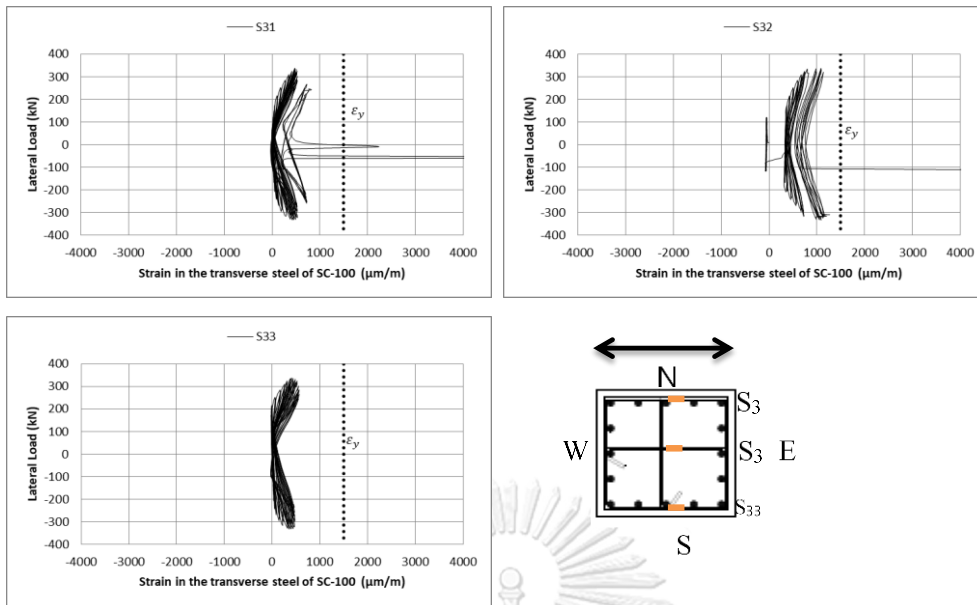
Figure 3.42 Strain in the transverse steel at level 3 of SC-100
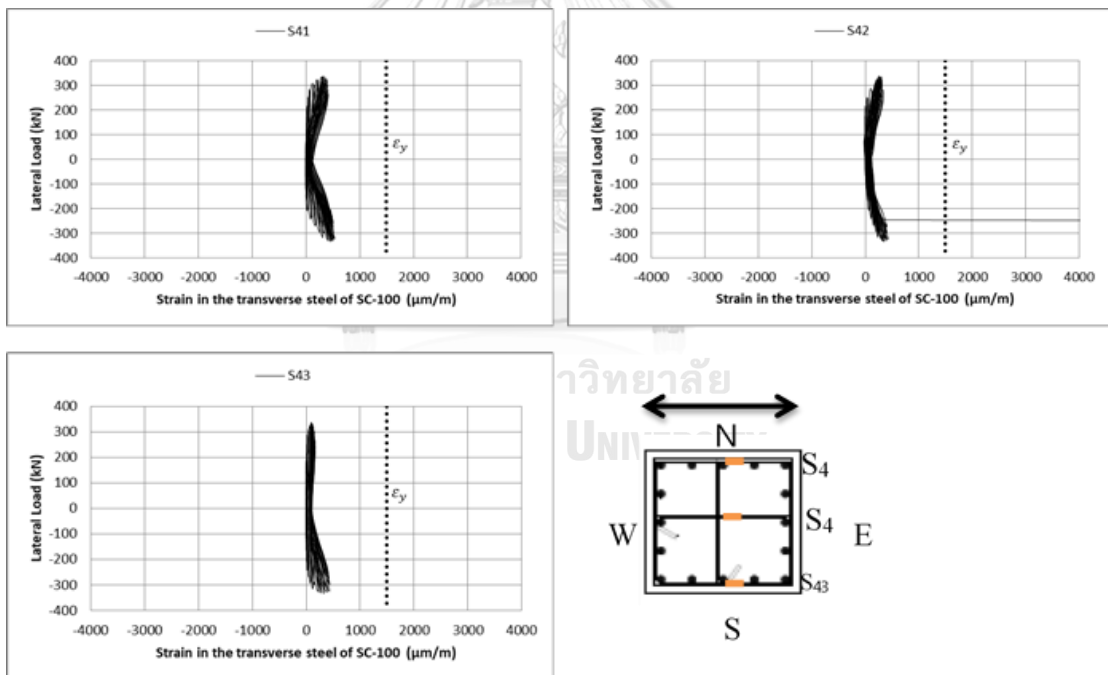
Figure 3.43 Strain in the transverse steel at level 4 of SC-100

3.12.3. Strain in the external steel rods SC-100
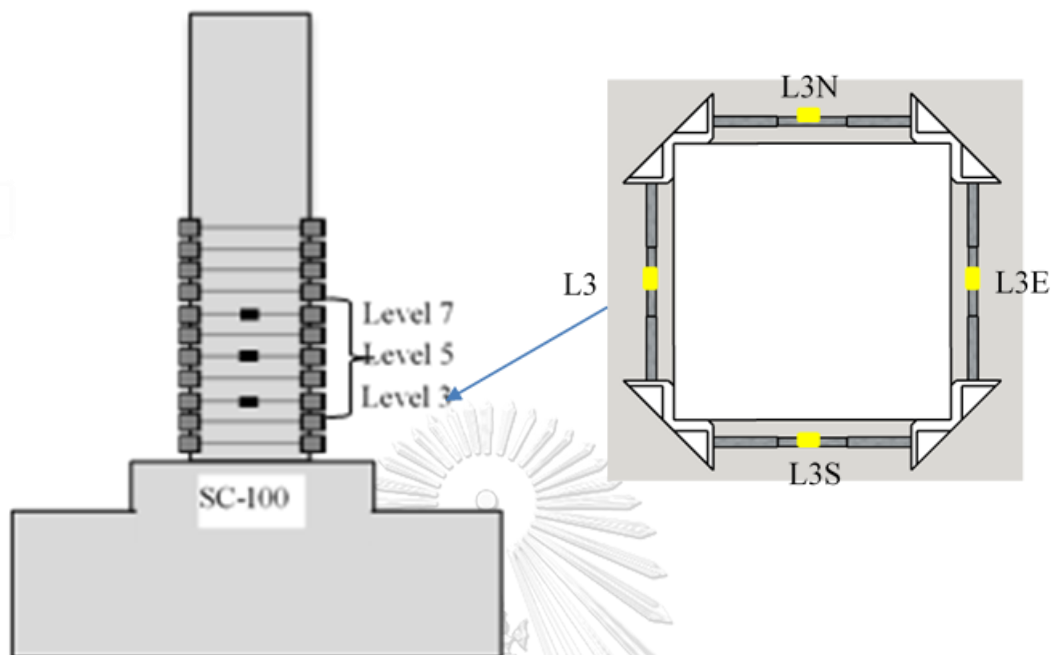
Figure 3.44 Location of the stain gauge on steel rods of the specimen SC-100

Twelve numbers of strain gauge on the steel rods were used for SC-100 specimens. The spacing between the steel rods was 100 mm. The strain gauges are positioned at the level of 3, 5 and 7 as shown in Figure 3.44. The maximum yield strain of the steel-rods were 2210 micro strain. According to the test data, strain in the steel rods at all levels was within the yield limit. This was because of the effect of sufficient confinement of the steel-rod collars to the column. The failure mode had changed from shear mode to flexure mode. After the SC-100 specimen had failed, no damages on the steel rod collars was found. Strain in the steel rods at each level in SC-100 specimen was shown in Figure 3.45 (a), (b) and (c).
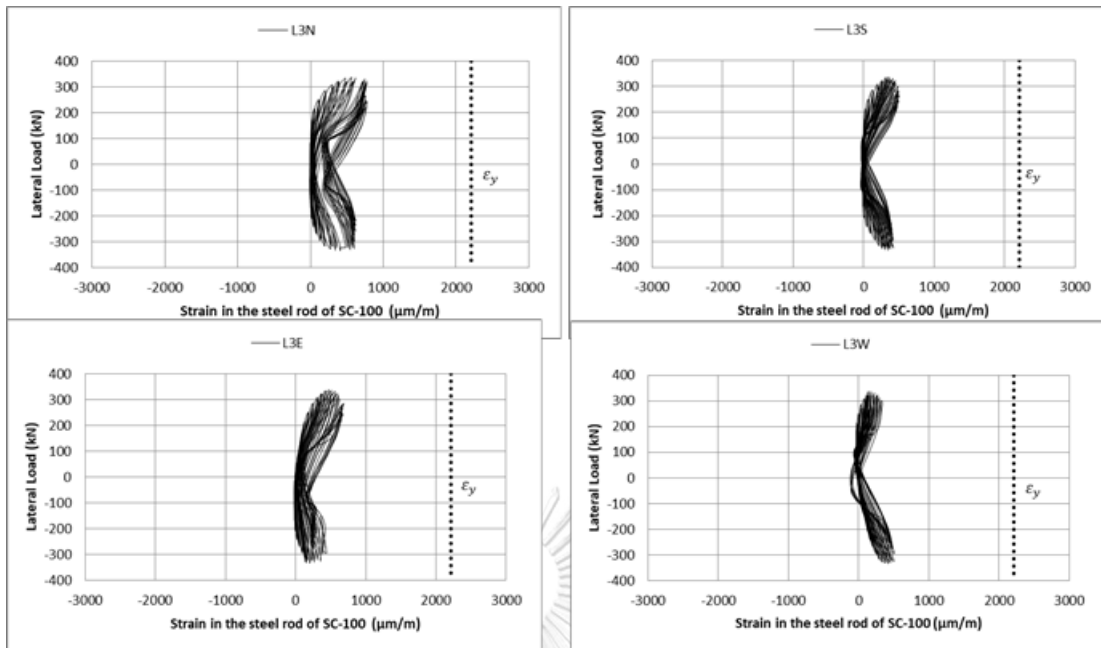
(a)
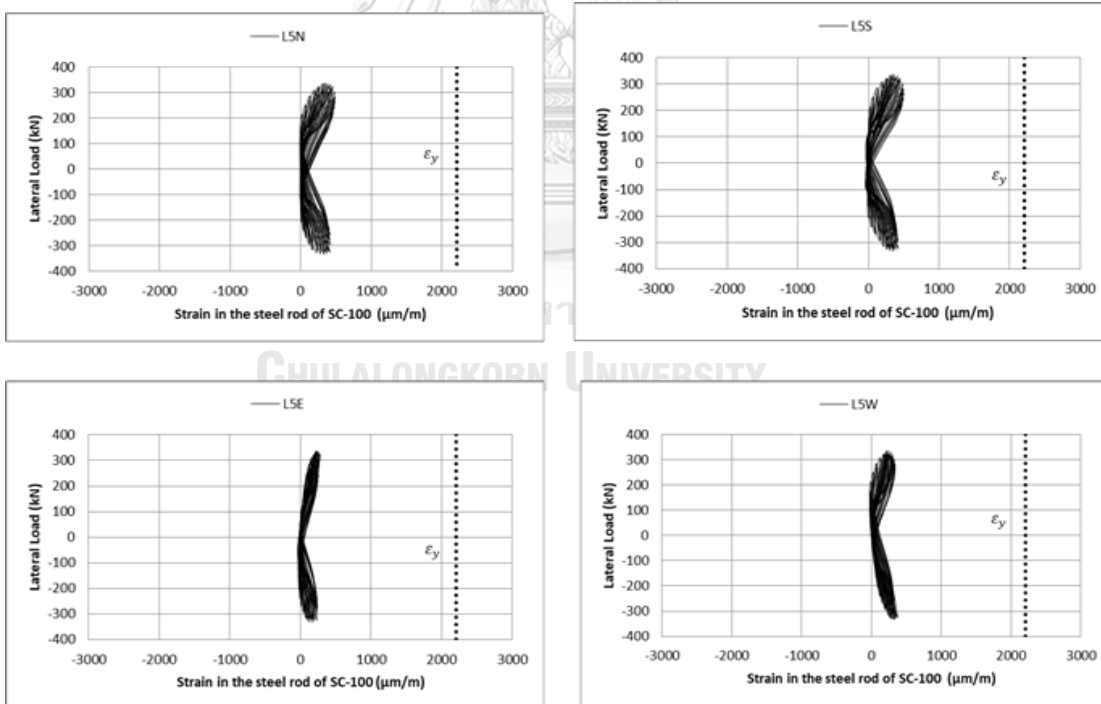
(b)
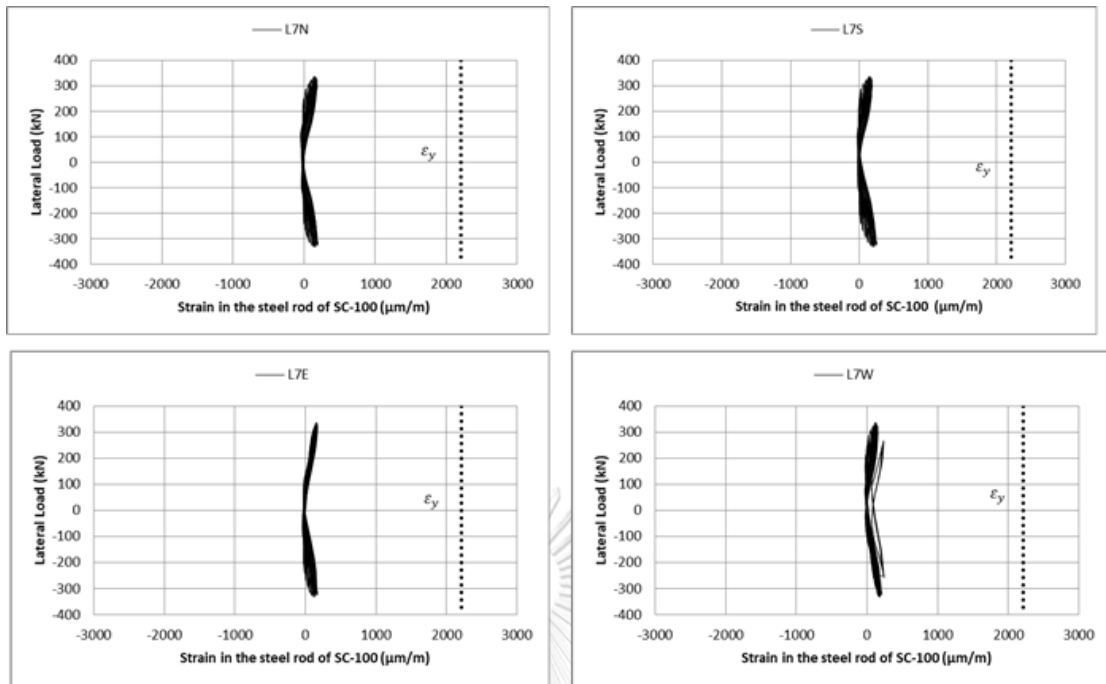
(c)

Figure 3.45 (a) Strain in the steel rods at level 3 of SC-100

(b) Strain in the steel rods at level 5 of SC-100

(c) Strain in the steel rods at level 7 of SC-100

CHAPTER 4

COMPARISON OF THREE SPECIMENS

4.1. Hysteretic Behavior and Damage Stages of Three Specimens

This section compared the hysteresis behavior of three specimens CC, SC-200 and SC-100. At 1.5% drift, many flexural cracks were appeared on the column specimen. In the first cycle of 2.5% drift, the lateral strength reached the peak strength of 280 kN and a diagonal shear crack developed clearly. The next cycle of 2.5% drift, the lateral strength started to drop. At 3% drift cycles, the lateral strength of the column continued to drop and finally the column failed by shear failure mode. The shear capacity at the 80% of the maximum load was about 224 kN.

SC-200 specimen is the strengthened column with the external steel cage 200 mm spacing of bars. The first flexural–shear crack appeared at second cycle of 1.5 % drift at elevation 400 mm and 600 mm. The maximum loading reached 340 kN at the loading cycle of 3% drift. At 5.5% drift, the cover concrete between the elevation of 100 mm and 300 mm significantly spalled off. At this stage, buckling of the longitudinal steel occurred clearly between 100 mm and 200 mm from the base of the column. When the loading cycle reached the final stage of 6.5% drift, the cover concrete totally damaged around the column between the lower portions of two steel rod collars. Finally, the column failed by flexure mode with spalling of concrete cover around the four faces of the specimen. Also, buckling of longitudinal reinforcement was occurred. The lateral strength at the 80% of the maximum load was 272 kN.

Whereas SC-100 specimen is the strengthened column with the external steel rod collars having 100 mm spacing. The peak loading of 335 kN reached at 3% drift and the next drift cycles the lateral load capacity decreased gradually. At 4% drift, crushing of the cover concrete were occurred on the west face of the column between the 100mm elevation from the base of the column. After the 4% drift, the later loading capacity is gradually decreased. At the 6% drift cycle, the cover concrete spalled off around 300 mm elevation from the base and also the buckling of the longitudinal steel

observed. At 6.5% drift, the lateral strength dropped continuously and the lateral loading cycles were stopped. The lateral load capacity at the 80% of maximum loading was 268 kN. The specimen SC- 100 failed by flexure. The maximum lateral load capacity increased when compared to the CC specimen.

In contrast, specimens SC-200 and SC-100 increased the lateral load capacity more than that of unstrengthened column CC. It can be said that additional transverse reinforcement by steel rod collars can considerably effect on increasing the shear capacity of the columns. Specimen SC-200 and SC-100 specimens indicated the good hysteresis performances and energy dissipation capacities. Moreover, the failure mode of SC-200 and SC-100 was dominated by flexure mode after strengthening the column by steel rod collars. When SC-200 and SC-100 specimens were compared, the maximum lateral load capacity was not quite much different. Instead, serious spalling of the cover concrete and buckling of the longitudinal steel were occurred between 100 mm and 300 mm elevation in SC-200 specimen than SC-100 specimen. The hysteresis behaviors of CC, SC-200 and SC-100 are shown in Figure 4.1. The envelope curve of the three specimens was shown in Figure 4.2. The damage stage at 1.5% drift is illustrated in Figure 4.3. The damage stage at maximum loading drift is illustrated in Figure 4.4. The damage stage at final stage of loading drift is illustrated in Figure 4.5.
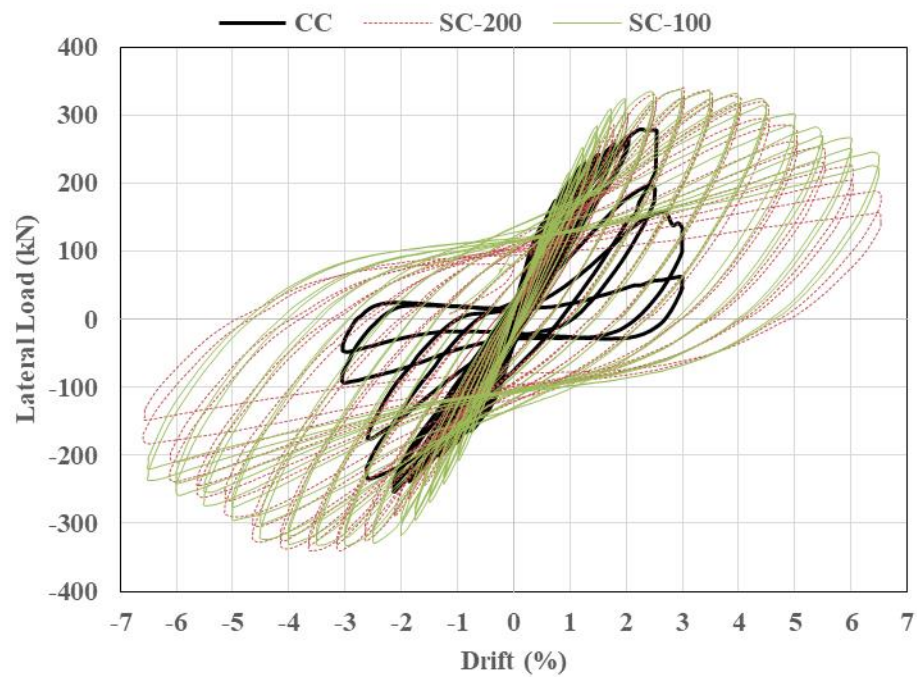
Figure 4.1 Comparison of hysteresis behaviour of CC, SC-200 and SC-100
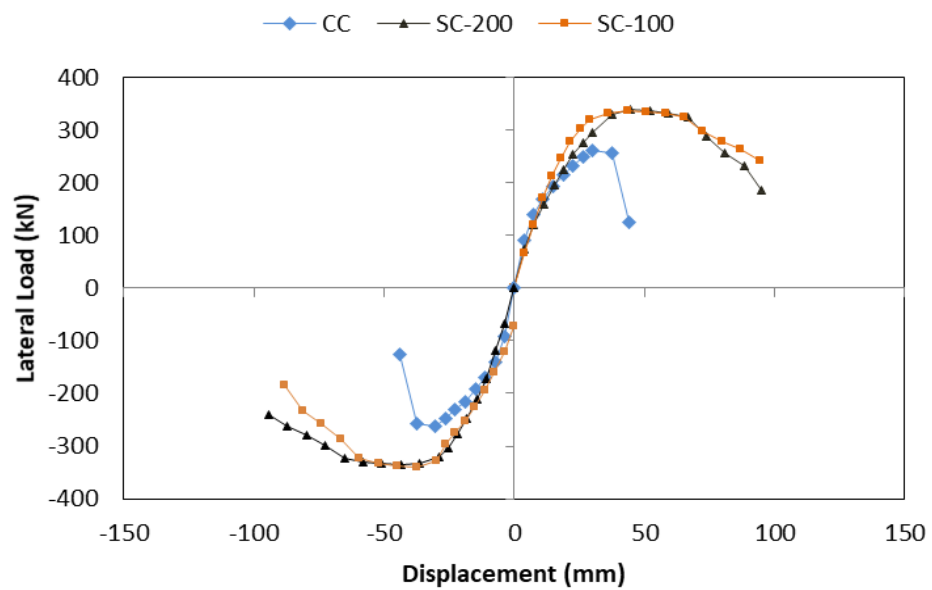
Figure 4.2 Envelope curve of CC, SC-200 and SC-100
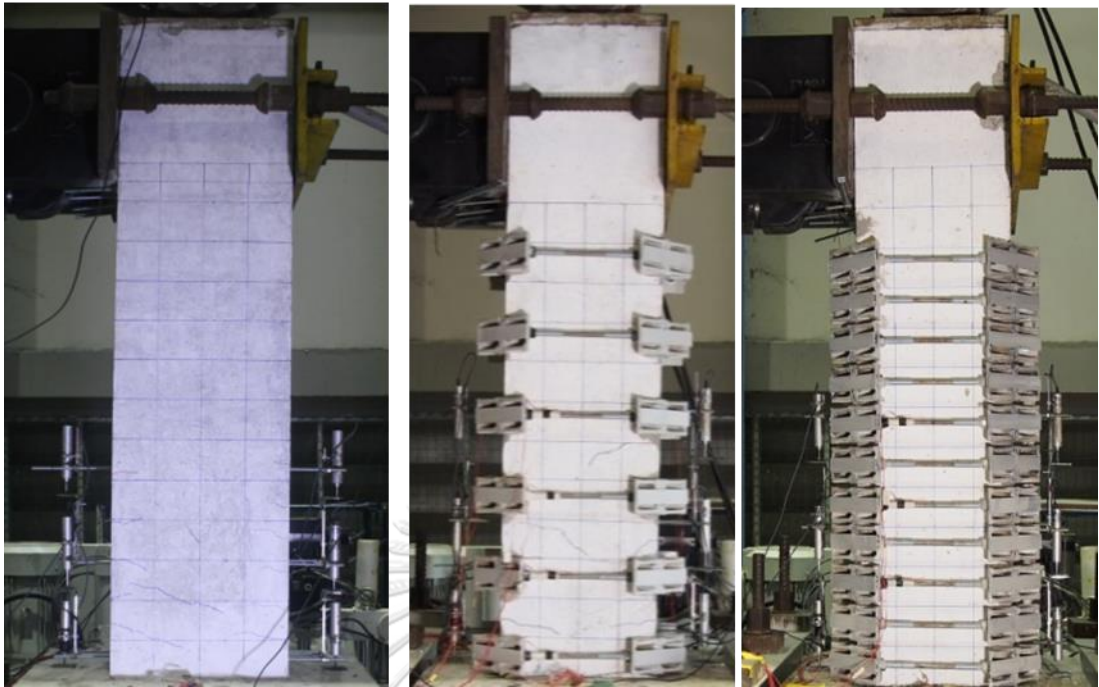
Figure 4.3 Damage stage at 1.5% drift
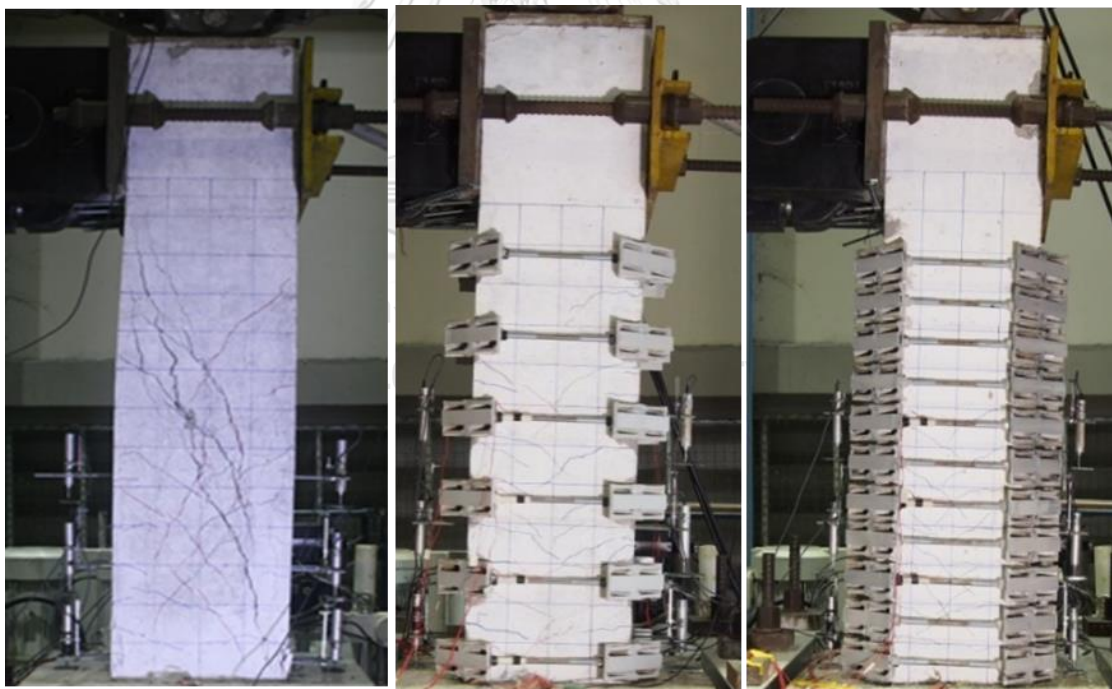
Figure 4.4 Damage stage at maximum loading drift

4.2. Displacement Ductility of the Columns

According to the (Park, 1988), the displacement ductility factor is defined as the maximum deformation divided by the corresponding deformation when yielding occurs. The displacement ductility factor defined for ideal elasto-plastic behavior is shown in Figure 4.5.
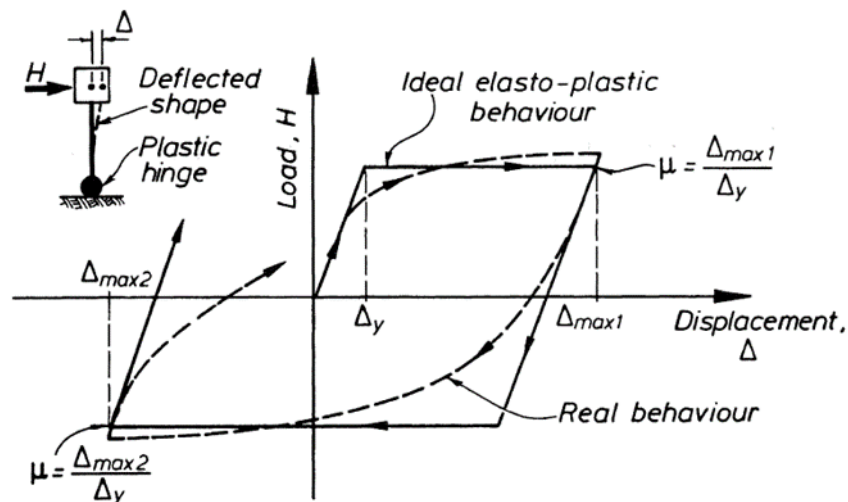
Figure 4.5 Displacement ductility (Park, 1988)

(Paulay and Priestley, 1992) identified the yield displacement was such that a secant was drawn to intersect the later load relationship at 75% of the maximum applied shear. Then, the line was extended to the intersection with a horizontal line corresponding to the maximum applied shear, and then projected onto the horizontal axis to get the yield displacement (Δ_y). This is shown in Figure 4.6. The slope of the idealized linear elastic response $K = \frac{S_y}{\Delta_y}$ used to quantify stiffness. Sy defines the yield or ideal strength Si of the member and ductility is defined by the ratio of the total imposed displacement at any instant to that at the onset of yield. The displacement ductility is

$$\mu = \frac{\Delta_{max}}{\Delta_y} \tag{4-1}$$
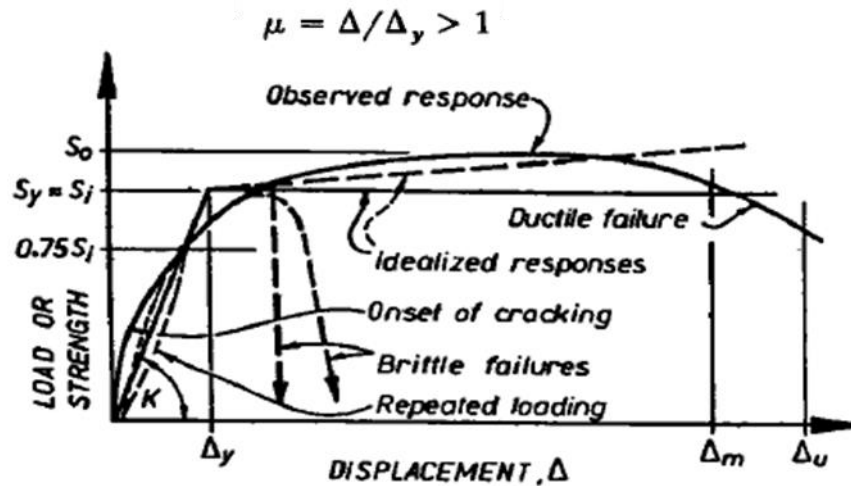
Figure 4.6 Typical load displacement relationship for a reinforced concrete element, (Paulay and Priestley, 1992)

In evaluating the column performance and studying the effects of different variables, ductility and toughness were defined by (Sheikh et al., 1994) as shown in Figure 4.7 and the displacement ductility factor (μ_Δ) can be calculated as

$$\mu = \frac{\Delta_2}{\Delta_1} \tag{4-2}$$
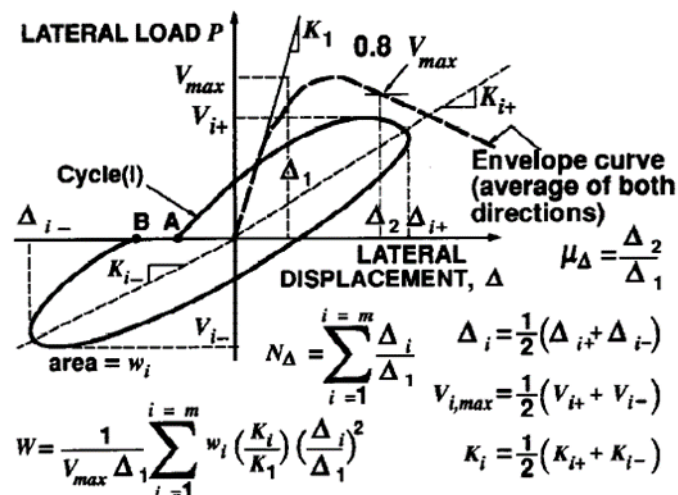
Figure 4.7 Section ductility factors element (Sheikh et al., 1994)

According to the (Sezen and Moehle, 2004), the yield displacement was defined such that a secant was drawn to intersect the later load relationship at 70% of the

maximum applied shear. Then, the line was extended to the intersection with a horizontal line corresponding to the maximum applied shear, and then projected onto the horizontal axis to get the yield displacement for those columns as shown in Figure 4.8. Displacement ductility is defined by the ratio of the ultimate displacement to yield displacement. The ultimate displacement was also defined as the displacement corresponding to the maximum measured displacement at which the applied shear dropped to 80% of the maximum applied shear
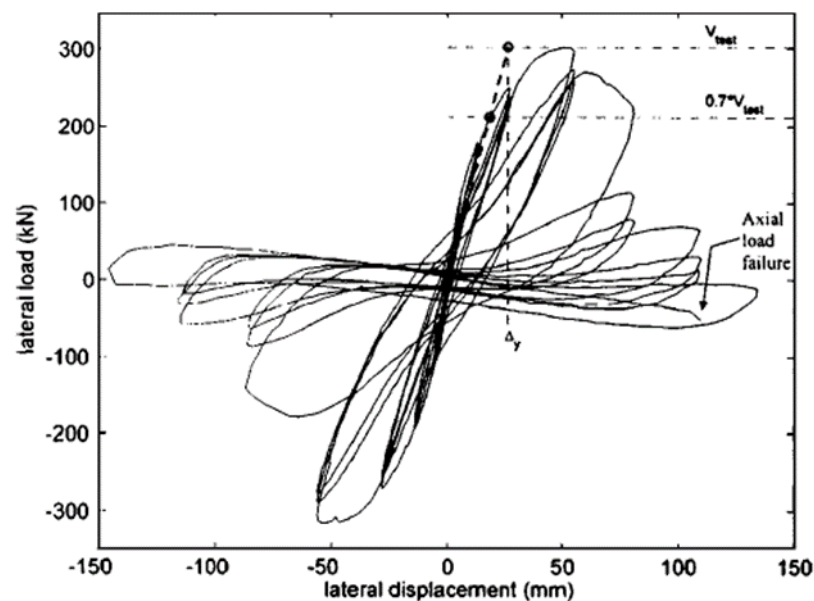
Figure 4.8 Load and Displacement Relation (Sezen and Moehle, 2004)

4.2.1. Displacement ductility of the specimens CC, SC-200 and SC-100

According to the previous literature review, the ductility was also defined as the ratio of the ultimate displacement to yield displacement in this study. Yield displacement was defined according to the Sezen (2004). The secant line was drawn to interest at the point of 70% of the maximum lateral load and extended to the maximum lateral load horizontal line. Then, the vertical line was drawn to the horizontal line to get the yield displacement.

The ultimate displacement was also defined as the displacement corresponding to the maximum measured displacement at which the applied shear dropped to 80% of the maximum applied shear. The ductility of SC-200 and SC-100 columns were calculated according to the Sezen's concept. However, the yield displacement for the

CC column was considered at the horizontal point that is drawn from the point of maximum loading because column CC was failed by shear before steel yielding according to the experimental test result. Looking at the values presented in the following Table 4.1, it was found that SC-200 and SC-100 exhibited the higher displacement ductility than that of CC specimen. It can be said that the external steel rod collars were effective for the shear critical column to be more ductile behaviour. Envelope curve with ductility of CC, .SC-200 and SC-100 are shown in Figure 4.9 (a), (b) and (c).

Table 4.1 Experimental results of lateral load capacity and displacement ductility

Specimens	CC	SC-200	SC-100
Maximum lateral load (kN)	280	340	335
Drift at maximum load (%)	2.5%	3%	3%
Yield displacement, Δ_y (mm)	37	29	24
Lateral load 80%of peak load (kN)	224	272	268
Drift at 80% of peak load (%)	2.7	5.4	5.8
Ultimate displacement, Δ_y (mm)	40	78	85
Displacement Ductility	1.1	2.7	3.5

จุฬาลงกรณ์มหาวิทยาลัย

CHULALONGKORN UNIVERSITY

(a)
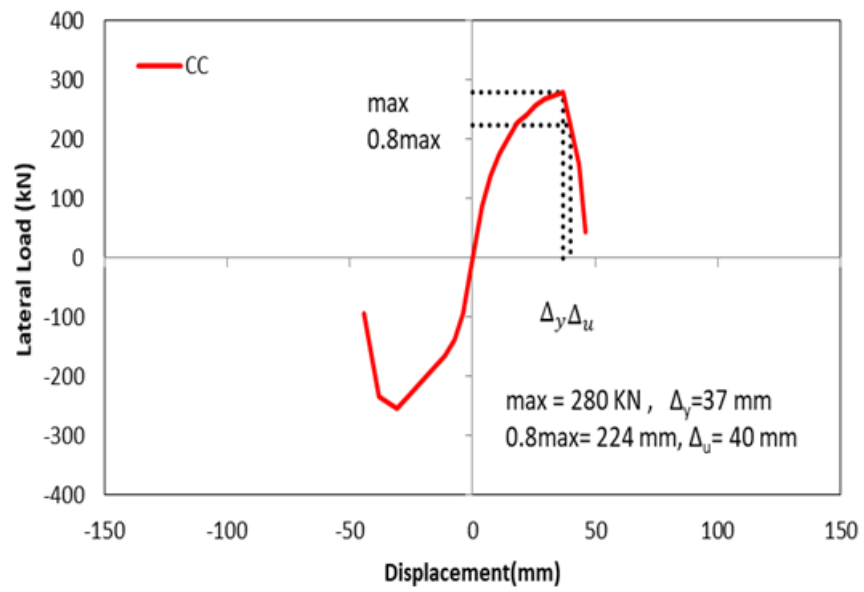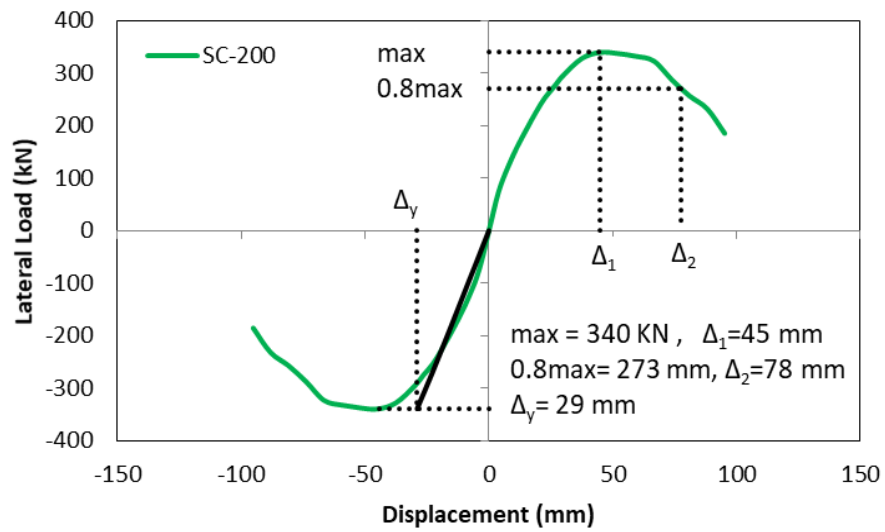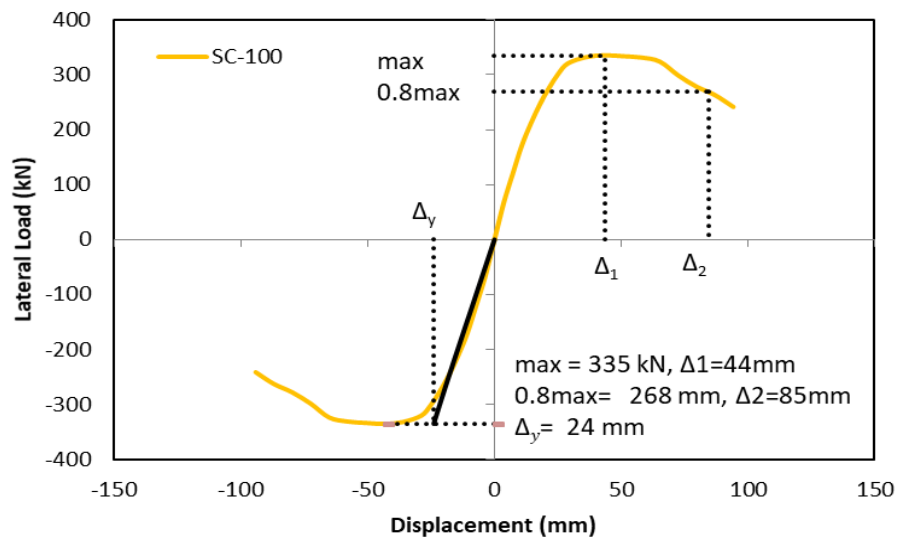
Figure 4.9 (a) Envelope curve with displacement ductility of CC

(b) Envelope curve with displacement ductility of SC-200

(c) Envelope curve with displacement ductility of SC-100

4.3. Energy Dissipation

The difference between the absorbed and lost energy is defined as the energy dissipation in each loading cycle. If the structural components are adequate in energy dissipation, they will not be suffering the serious failure during the earthquake. The higher the dissipated energy for a structural member is, the better it behaves during a seismic excitation. The energy dissipated in one cycle is the area under the cycle of loading. In this study, the area under the curve was calculated using the numerical method (Trapezoidal rule) as follows. The cumulative hysteretic dissipation energy was evaluated for all the tests, considering the area of each loading cycle and then the total energy was calculated as the sum of these parts. Figure 4.10 describes the dissipated energy for one loop.

$$Area = \frac{1}{2}\sum_{i=1}^{n}(y_{i+1} + y_i)(x + x_i) \qquad (4\text{-}3)$$

$$Energy\ dissipation = \frac{1}{2}Fd \qquad (4\text{-}4)$$

where, F is the lateral force (kN) and d is the displacement of the cycle (mm).
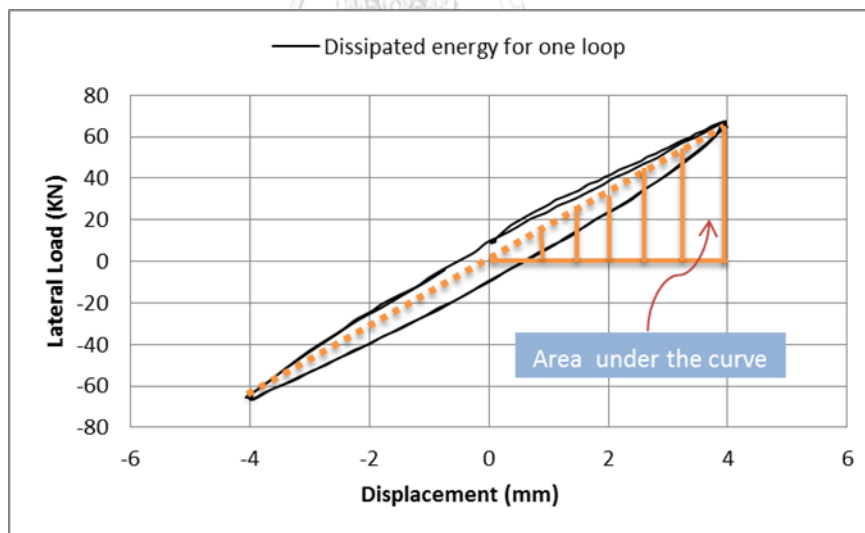
Figure 4.10 Energy dissipation for one loop

4.3.1. Energy Dissipation of CC, SC-200 and SC-100

Energy dissipation of three specimens is compared in this section. As expected, the specimen CC exhibited the lowest energy dissipation. At the 2.5% drift, the CC column reached the peak lateral load, diagonal shear crack developed and the energy dissipation was about 7.2 kN-m. Until 2.5% drift, the dissipation energy of their specimens was not quite different. On the other hand, after the 3% drift cycle, the energy dissipation trends were clearly different. After 3% drift, the CC cannot dissipate the energy anymore because the specimen failed by diagonal shear failure mode. At 3% drift, the dissipation of the energy capacity of CC, SC-200 and SC-100 were 8.5 kN-m, 10.2 kN-m and10. 4 kN-m respectively. The energy dissipation capacity of SC-200 and SC-100 more increased significantly after 3% drift than CC column. This is because SC-200 and SC-100 were strengthened by steel rod collars as additional confinement and this increased more energy dissipated capacity. In comparison of SC-200 and SC-100, SC-100 had a slightly higher energy dissipation capacity and this can be the effect of increasing confinement effect due to the steel rod collars. At 6.5% drift cycle, SC-100 reached the 25.8 kN-m energy dissipation capacities whereas the SC-200 dissipated energy of about 24.8 kN-m. On the other hand, the energy dissipation capacity of SC-100 was nearly 4% higher than that of SC-200. The cumulative dissipated energy for all specimens is compared in the Figure 4.11.
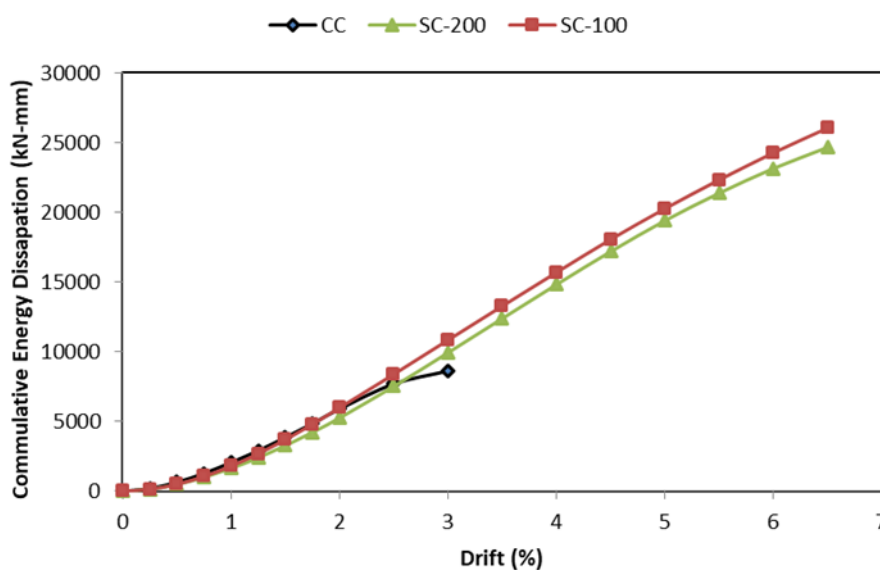
Figure 4.11 Cumulative energy dissipation of the specimens

4.4. Drift Components

This section provides drift capacity components based on experimental results. The lateral column displacement can be determined as the sum of the flexural, shear and yield penetration. Displacement transducers were attached to the column to measure the approximation of flexure, shear. Bar slip deformation is comprised in the flexural deformation calculation in this study. The linear displacement transducers setting up on the side of the columns of CC, SC-200 and SC-100 as shown in Figure 4.12.
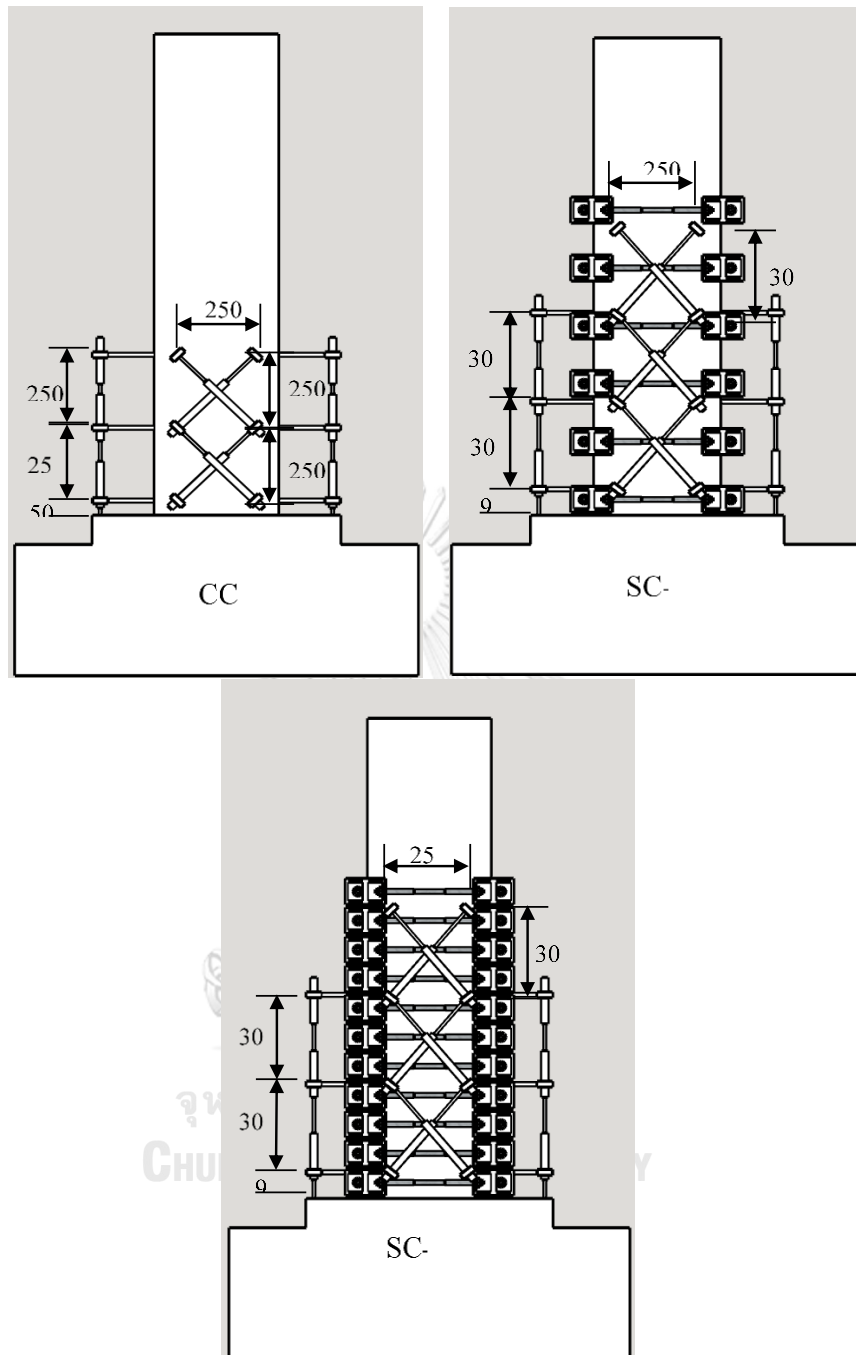
Figure 4.12 Location of the displacement transducers of CC, SC-200

and SC-100 (Unit –mm)

4.4.1. Flexural deformation

For flexural deformation, the column was divided into segments. Curvature between any two segments is calculated as the difference between measurements of vertical transducers attached to the sides of each segment divided by the product of horizontal and vertical dimension of each segment. This is illustrated in Figure 4.13.
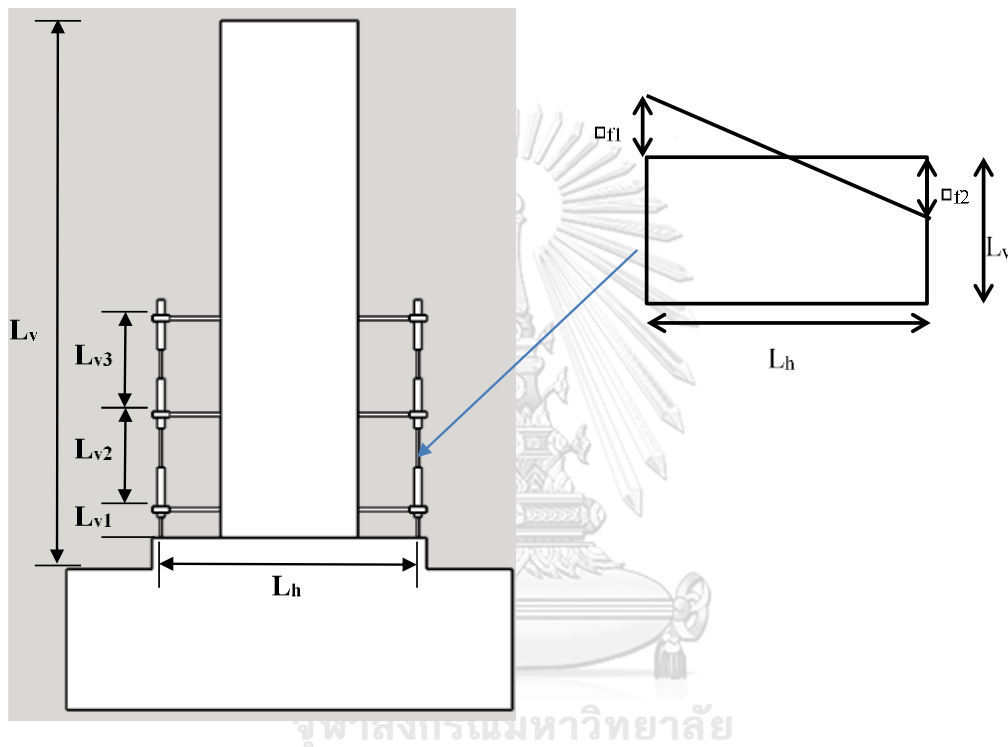
Figure 4.13 Flexural Deformation of the column

The vertical displacement transducers are used to measure the flexural displacement. The average curvature of the segment can be estimated as

displacement. The average curvature of the segment can be estimated as

$$\varphi = \frac{\theta_f}{L_v} \tag{4-5}$$

$$\varphi = \frac{\Delta_{f2} - \Delta_{f1}}{L_h} \cdot \frac{1}{L_v} \tag{4-6}$$

where,

L_h = horizontal distance between displacement transducer

L_v = vertical height per each segment

Δ_{f1}, Δ_{f2} = vertical displacement transducer measurement

The upper portion of the segment was considered as the linear and the curvature of the upper segment was calculated using

$$\varphi = \frac{1}{\rho} = \frac{d_\theta}{d_x} = \frac{M}{EI} = \frac{V \times L}{EI} \tag{4-7}$$

4.4.1.1. Flexural deformation of three specimens CC, SC-200 and SC-100

To measure the flexural deformation of CC specimen, six numbers of displacement transducers were mounted on the two sides of the specimens. The flexural deformations were shown with the graph of the moment curvature relationship. The curvature was the maximum at the lower level portion by at all drift cycles. The curvature at the upper segment did not increase too much. The curvature was gradually increased until the loading cycle reached to 2% drift. It gave the stable moment curvature relationship. However, when the loading cycles were increased to 2.5% drift, the curvature behavior was not stable. This was because the column nearly failed by shear failure mode. At first cycle of push 2.5% drift, the lateral strength reached the peak strength and then the column failed by shear. During the second cycle of 3% drift loading, the displacement transducer (namely FR1) at the level 1 could not capture the data anymore. Therefore, the data were recorded until before the displacement transducer removed. The curvature was the highest at the loading 3% drift after the shear failure occurred.

To measure the flexural deformation of the SC-200 specimen, six numbers of displacement transducers were mounted on both the sides of the specimens. The curvatures were the maximum at the lower level portion of all drift cycles. The curvatures at the any other levels did not increase too much. The curvature increased gradually until the 1% drift loading cycle from the beginning of the loading cycle. At 1% loading drift cycle, the curvature was about 0.05 (1/m). When the loading cycles reached to 2% drift, the curvature increased nearly double. At 3% drift, the lateral load reached the peak strength as well as the moment-curvature increased. At the first cycle

of 5 % drift displacement transducers at this level were removed because it was not able to record the data anymore.

To measure the flexural deformation of SC-100 specimen, six numbers of displacement transducers were mounted on both the sides of the specimens. The curvatures were the maximum at the lower level portion of all drift cycles. The curvatures at the any other levels did not increase too much. The curvature increased gradually until the 1% drift loading cycle from the beginning of the loading cycle. At the 1% drift cycle, it was about 0.05 (1/m). When the loading cycles reached to 2% drift, the curvature increased doubly. At 3% drift, the lateral load reached the peak strength as well as the moment-curvature increased. After the 3% drift, the lateral load capacity gradually decreased ,but the moment-curvatures were still increased because the SC-100 column still has the ductile behaviour for the post peak region. Therefore, at the 4.5% loading cycle, the curvature was increased too much. At the second cycle of 5 % drift, displacement transducers at the level 1 were removed because it was not able to record the data anymore. Comparison of the flexural deformation in some loading cycle of the columns CC, SC-200 and SC-100 are illustrated in Figure 4.14.
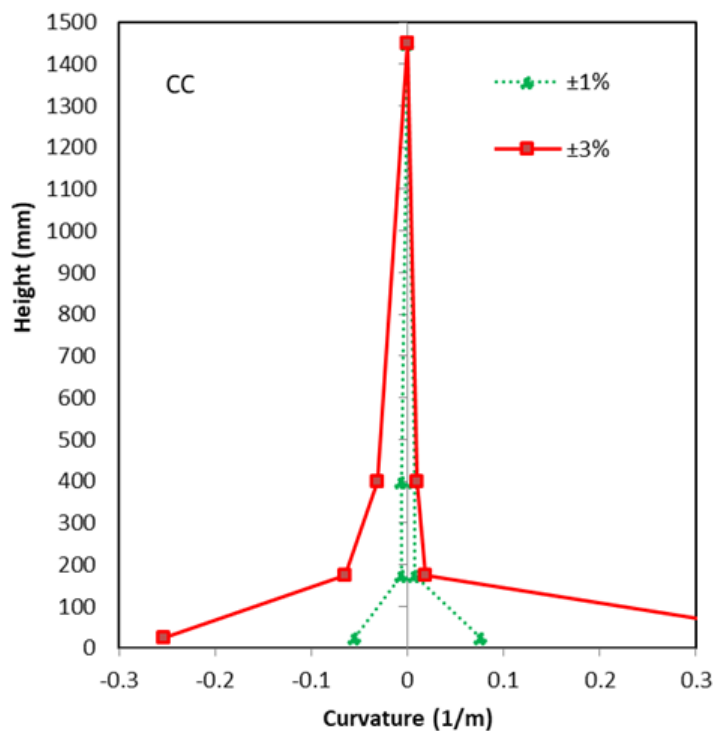
(a)
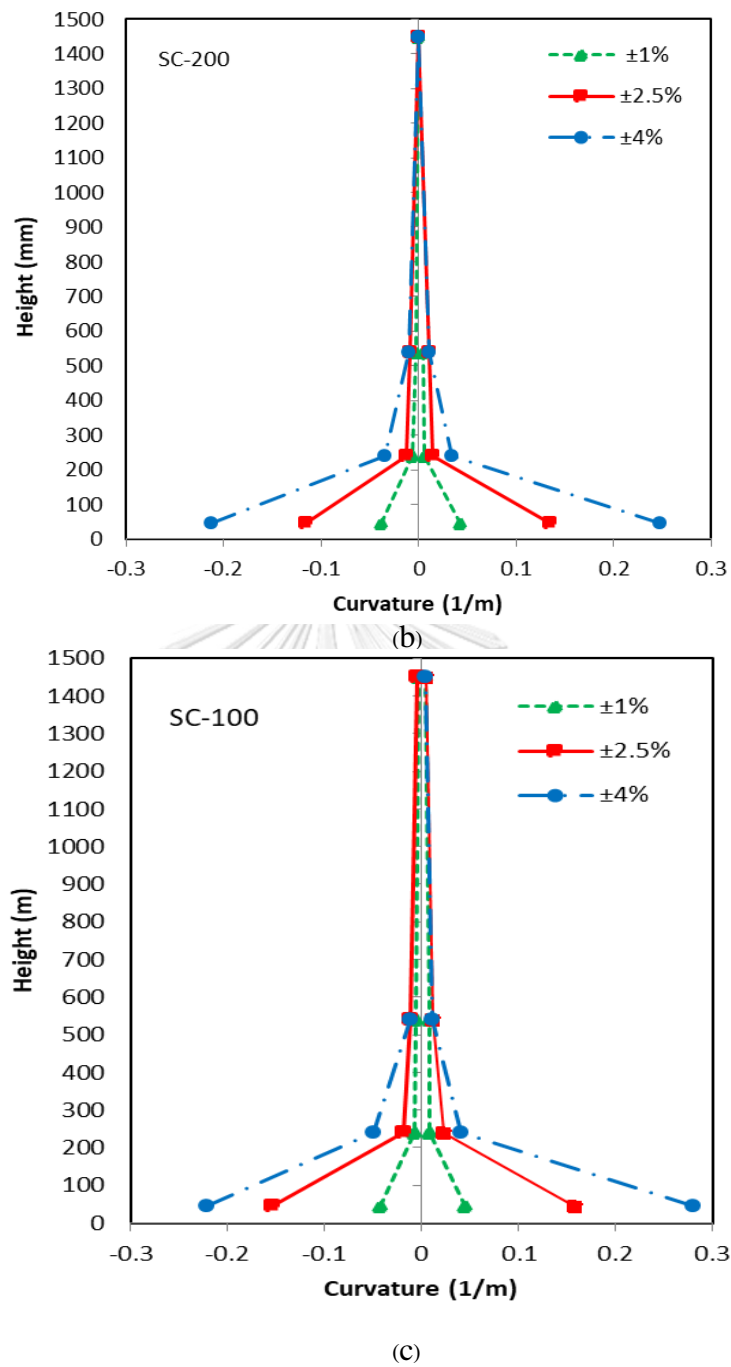
Figure 4.14 (a)Flexural deformation column, CC

(b) Flexural deformation of column, SC-200

(c) Flexural deformation of column, SC-100

4.4.2. Shear deformation of the columns

The shear forces cause shearing deformation. An element subject to shear does not change in length but undergoes a change in shape shown in Figure 4.15. The change in angle at the corner of an original rectangular element is called the shear strain and is expressed as Equation 4.8.
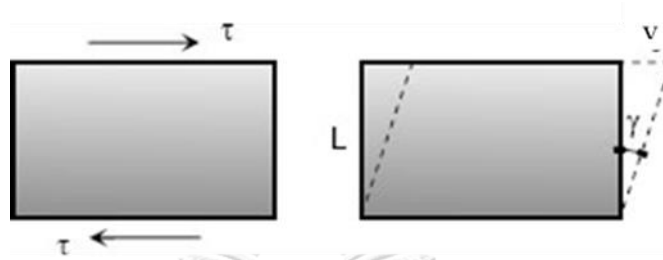
Figure 4.15 Shear deformation

$$\gamma = \frac{V}{L}$$
(4-8)

Where,

γ = change in angle and v = change in length

This concept can be applied in calculating the shear deformation of the experimental columns due to lateral cyclic loadings. In experimental columns, displacement transducers are installed diagonally to measure the shear deformation. Change in length of the diagonal distances was measured from the instruments. Then the change in horizontal distance is recalculated using the simple calculation. The shear deformation concept for the typical experimental column are shown in Figure 4.16.
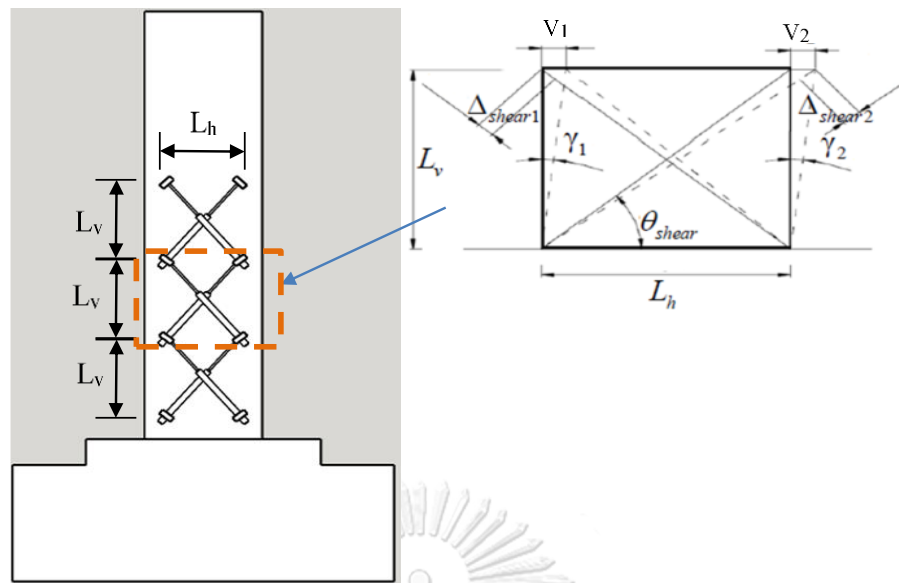
Figure 4.16 Illustration of shear deformation of typical column

Shear strain can be calculated as

$$\gamma = \frac{v}{L_V} \tag{4-9}$$

$$v_1 \cong \frac{\Delta_{shear1}}{cos\theta_{shear}} \tag{4-10}$$

$$v_2 \cong \frac{\Delta_{shear2}}{cos\theta_{shear}} \tag{4-11}$$

Equation (4-10) and (4-11) are substitute in Equation (4-12) to obtain the change in angle.

$$\gamma_1 = \frac{\Delta_{shear1}}{L_{V1} cos\theta_{shear}} \tag{4-12}$$

$$\gamma_2 = \frac{\Delta_{shear2}}{L_{V1} cos\theta_{shear}} \tag{4-13}$$

The average value of the rotation angles change can be obtained as follows;

$$\gamma = \frac{\gamma_1 + \gamma_2}{2} \tag{4-14}$$

$$\gamma = \frac{\Delta_{shear1} + \Delta_{shear2}}{2L_{V1} cos\theta_{shear}} \tag{4-15}$$

The total vertical top displacement due to shear can be calculated by summing the lateral deformation due to shear from every level as shown in Equation (4-16).

$$\Delta_{sh} = \sum \Delta_{shi} \qquad\qquad (4\text{-}16)$$

where,

Δ_{sh} = lateral top displacement due to shear forces

Δ_{shi} = average lateral displacement due to shear force calculated from every level of displacement transducer

In addition, the measured shear deformation Δ_{sh} can be estimated by Wibowo et al (2014) as follows;

$$\Delta_{sh} = \frac{\Delta_{shear1} + \Delta_{shear2}}{2} \sec \gamma = \frac{\Delta_{shear1} + \Delta_{shear2}}{2} \frac{\sqrt{L_v^2 + D^2}}{L_v} \qquad\qquad (4\text{-}17)$$

The relation between the lateral loads and the shear deformation are illustrated in Figure 4.17
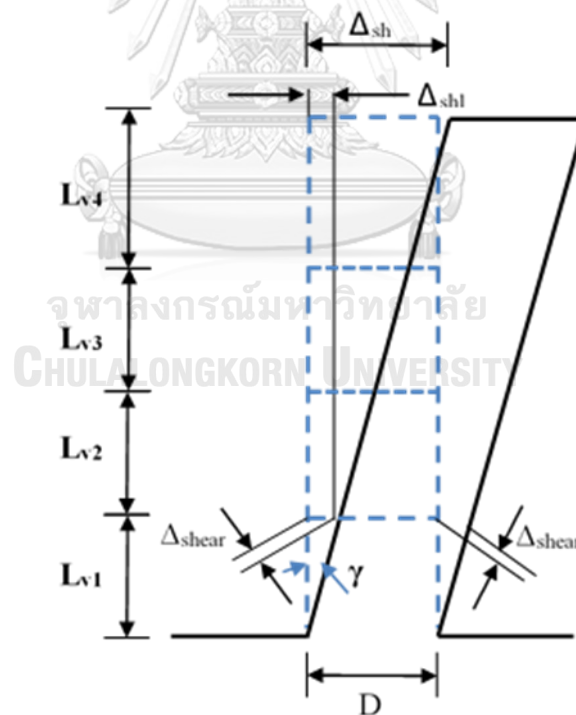
Figure 4.17 Illustration of top shear deformation of typical column

4.4.2.1. Shear deformation of the specimens of CC, SC-200 and SC-100

To measure the shear deformation, displacement transducers were mounted diagonally on the face of the tested column specimen. The placing and location of the location of the displacement transducers for all columns CC, SC-200 and SC-100 to capture the shear deformation are shown in Figure 4.18. Shear deformation is demonstrated as how much shear strain changed in all loading cycles during the test for all specimens.

In CC specimen, two levels of diagonal displacement transducers were installed to capture the shear deformation. The shear strain values were the highest in the second level. The higher the loading drift cycles, the more shear strains were occurred in the second level. The shear strain value was about 0.0011 rad until the end of the 1% drift and the shear deformation is not quite prominent. When the lateral loading was increased from 1.25% drift to until 2% drift, the shear strain value increased to 0.0044 rad. The shear deformation was prominent and it increased four times when compared to the beginning loading cycle. Thereafter, the shear deformation is unexpectedly increased about 0.012 rad when the displacement cycle is increased to 2.5% drift. At 2.5% drift, the lateral load capacity reached the peak value. At this stage, the diagonal shear crack started to initiate and later the CC specimen was dominated by shear failure mode. After the first cycle of 3% loading, namely right displacement transducer (SR1) at level 1 was removed because it could not capture the measured shear deformation any more.
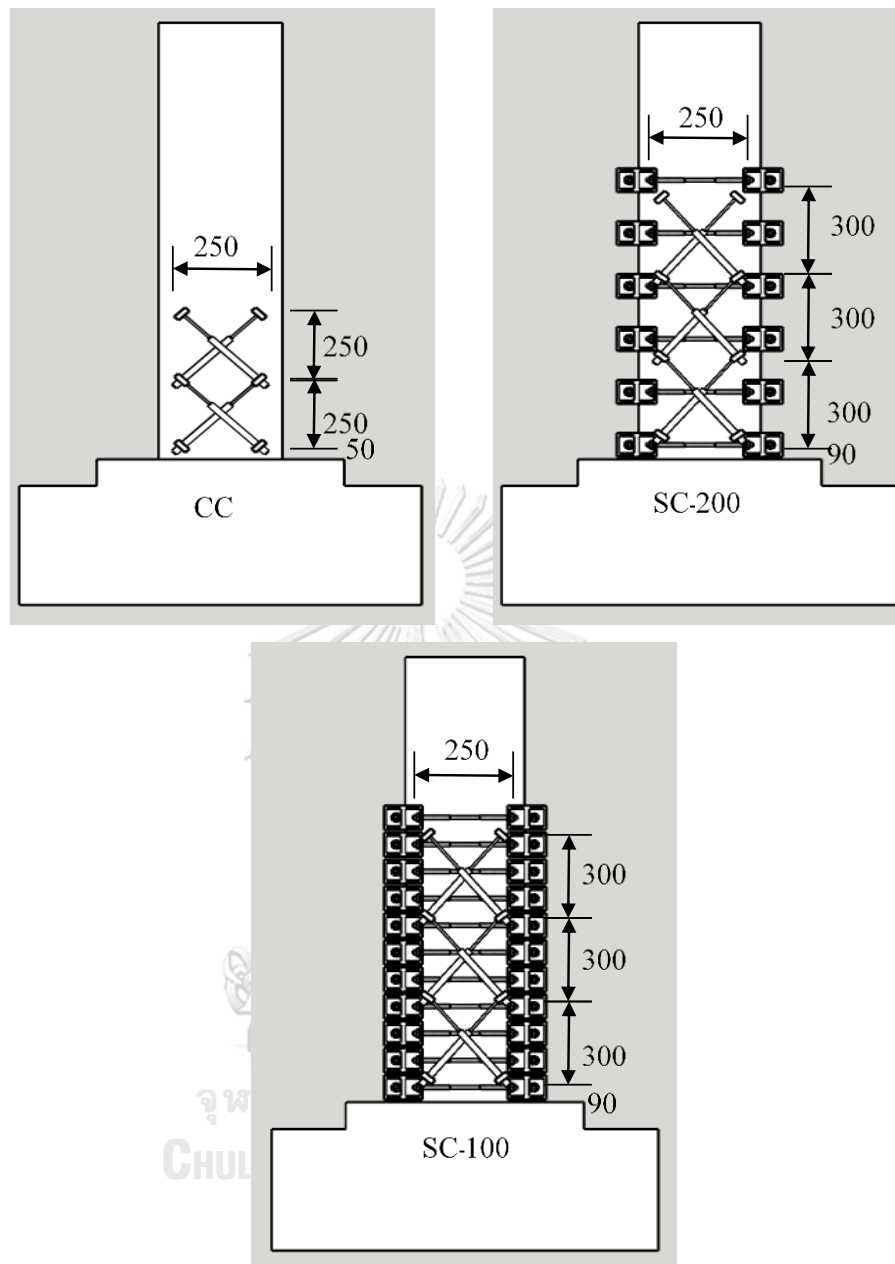
Figure 4.18 Location of displacement transducers to capture the shear deformation
(Unit in mm)

The shear deformation for CC is considered until before the SR1 removed. The shear deformation reached to 0.0311 rad at 3% drift loading cycles and then the column completely failed due to shear mode. Shear deformation of CC specimens at some loading cycles is presented in Figure 4.19.
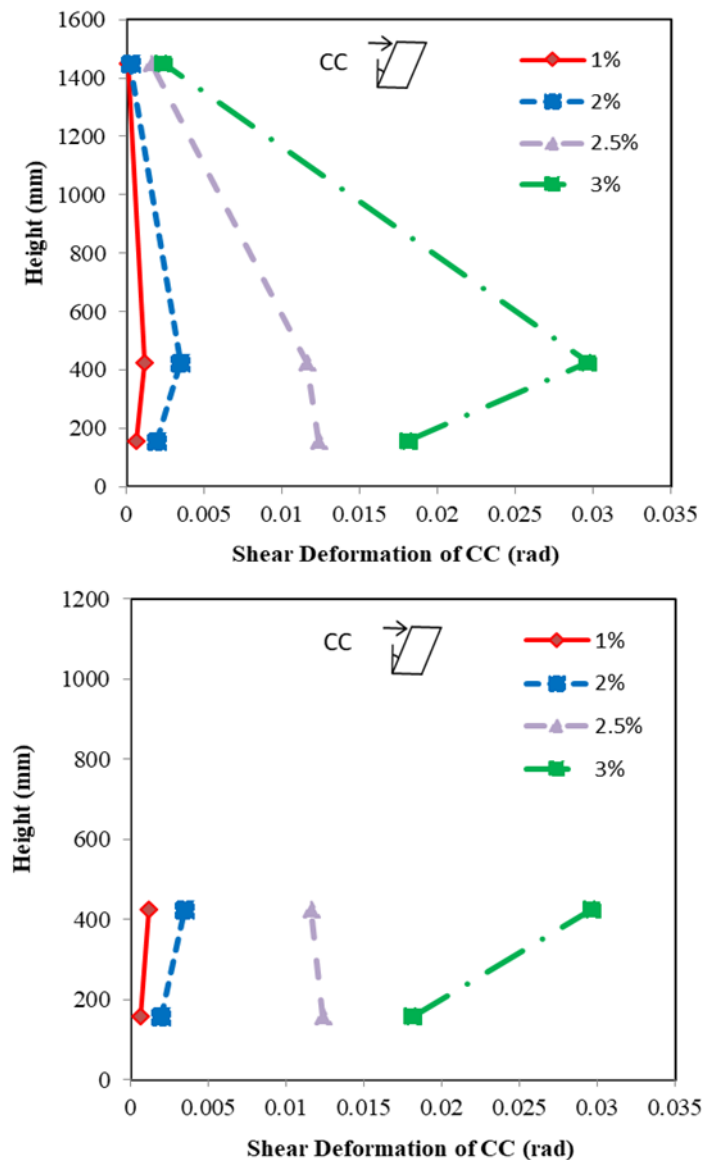
Figure 4.19 Shear deformation of the CC specimen along the height of the column

In the SC-200 specimen, the value of shear deformation reduced when compared to the CC specimen. Three levels of diagonal displacement transducers were installed to capture the shear deformation in the specimen. The shear strain value were maximum at the first level than any other upper levels. At 1% drift cycle, the shear deformation was about 0.0005 rad. However, at 2% drift cycle, the deformation reached about 0.002 rad and 0.003 rad at 3% drift. Then, the strain value a little bit increased to 0.006 rad at 4% drift loading cycle at the first level and the shear strain did not increase

too much in any other upper two levels. After the 4.5% drift cycle, the lateral load capacity decreased steadily as well as the shear strain value also declined at the loading cycles of 5%, 5.5%, 6% and 6.5% drift. At the first positive loading cycle of 6.5% drift, two diagonal displacement transducers at the first level namely, SL1 and SR1 were removed because it cannot capture the shear deformation any more. At this stage, the concrete cover spalled off at the plastic hinge region significantly and the longitudinal reinforcement buckled at around 300 mm from the base of the column specimen. Shear deformation of CC specimens at some loading cycles are presented in Figure 4.21.
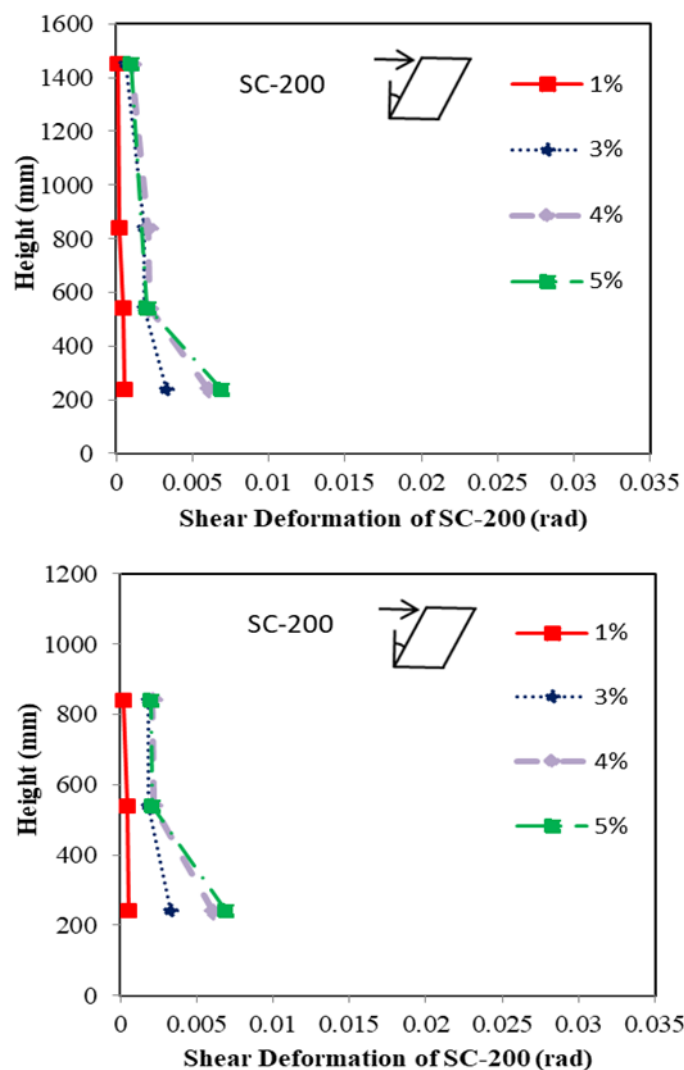
Figure 4.20 Shear deformation of the SC-200 specimen along the height of the column

In SC-100 specimens, three levels of diagonal displacement transducers were installed to capture the shear deformation of the specimen. In general, the shear deformations were the maximum at the first level. Until the end of the 1% drift, the shear strain only reached about 0.001 rad. At 2% drift cycle, the shear strain was about 0.003 rad and it was the peak strain in three levels. When the loading cycle is increased to 2.5% drift, the shear stains increased from 0.003 rad to 0.005 rad at the first level, whereas the shear deformation were not changed too much in any other two levels. The deformation reached 0.009 rad at the 4% drift loading cycle. After the 4% drift cycles, the shear deformations were not increased until the end of the loading cycles. In contrast the lateral load capacity of the SC-100 specimens was gradually decreasing at the later loading cycles. When SC-100 specimen compared to the CC specimen, the shear deformation in SC-100 specimen occurred less than that of CC specimen. This must be one of the benefits of additional shear reinforcement of steel rod collars. Shear deformation of CC specimens at some loading cycles is presented in Figure 4.21.

In conclusion, the CC specimen was the highest shear deformation in all three specimens and finally the CC specimen failed by shear. When the SC-100 specimen was strengthened by external steel rod collars, the deformation due to shear force was reduced significantly when it was compared to that of the CC specimen. This must be because of the benefit of the additional shear reinforcement of steel rod collars. Also the shear deformation was considerably reduced in the SC-200 specimen when it was compared to CC specimen. When the shear deformation of SC-100 and SC-200 were compared, shear deformation were higher at the first level in both specimens. At the first level, the shear deformation of SC-100 was a little bit higher than that of the SC-200 specimen. However, the shear deformation of SC-100 and SC-200 are almost the same in any other two levels.
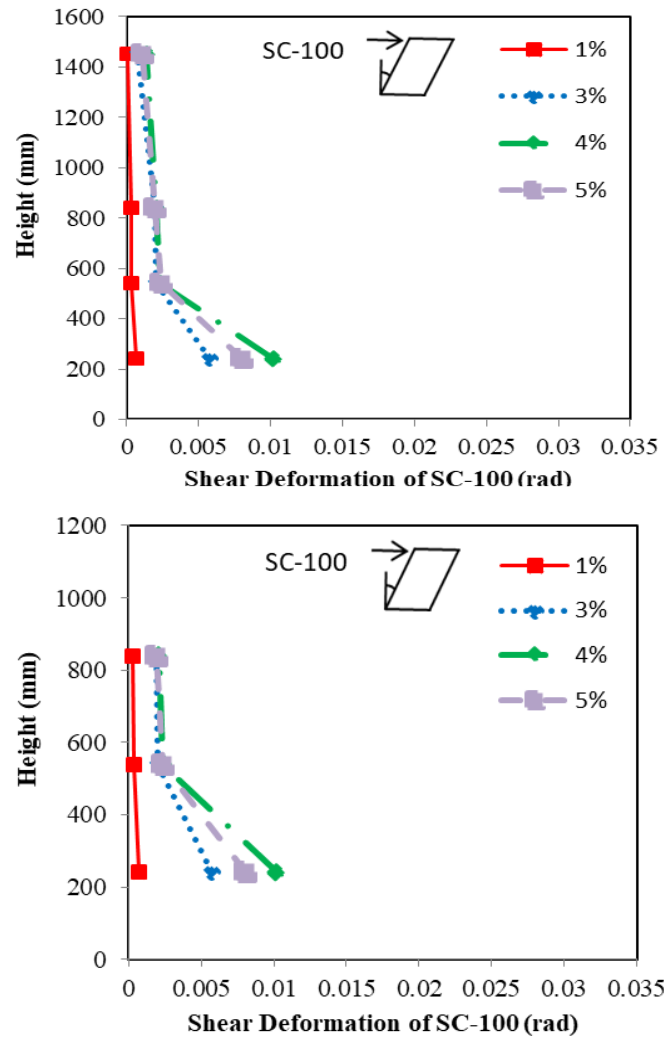
Figure 4.21 Shear deformation of the SC-100 specimen along the height of the column

CHAPTER 5

NUMERICAL MODELLING OF RC COLUMNS

5.1. Numerical Modelling in OpenSees

Two modelling strategies were applied to the numerical simulation of the unstrengthened column and strengthened columns. Both models are built using the OpenSees program

5.2. Checking the analytical model accuracy

Before analyzing the current research column, the analytical model of lumped plasticity model from the previous literature was checked with the experimental results of three columns that was tested by (Warakorn, 2008). Material properties for concrete and reinforcing steel are shown in Table 5.1. The columns were the cantilever column without lap splice bar. The difference between the three columns was the spacing of the transverse reinforcement and the diameter of the transverse reinforcement. Column dimension and cross section of the three columns are shown in Figure 5.1. Lumped plasticity model for the columns is shown in Figure 5.2. For unconfined concrete Concrete01 material model in OpenSees defined by Kent and Park (1971) was used. For confined concrete, Concrete02 material model in OpenSees defined by Mander (1988) was used. For longitudinal steel, Manigatopinto steel material model (Steel02 material model in OpenSees) was used.

Table.5.1 Properties of unconfined and confined concrete (Warakorn, 2008)

Type concrete	Ec (MPa)	fc1 (MPa)	Ɛ1 (m/m)	fc2 (MPa)	Ɛ2 (m/m)
Unconfined	27203	-33.5	-0.002	0	-0.0045
confined	27203	-34.6	-0.0025	7.1	-0.0053
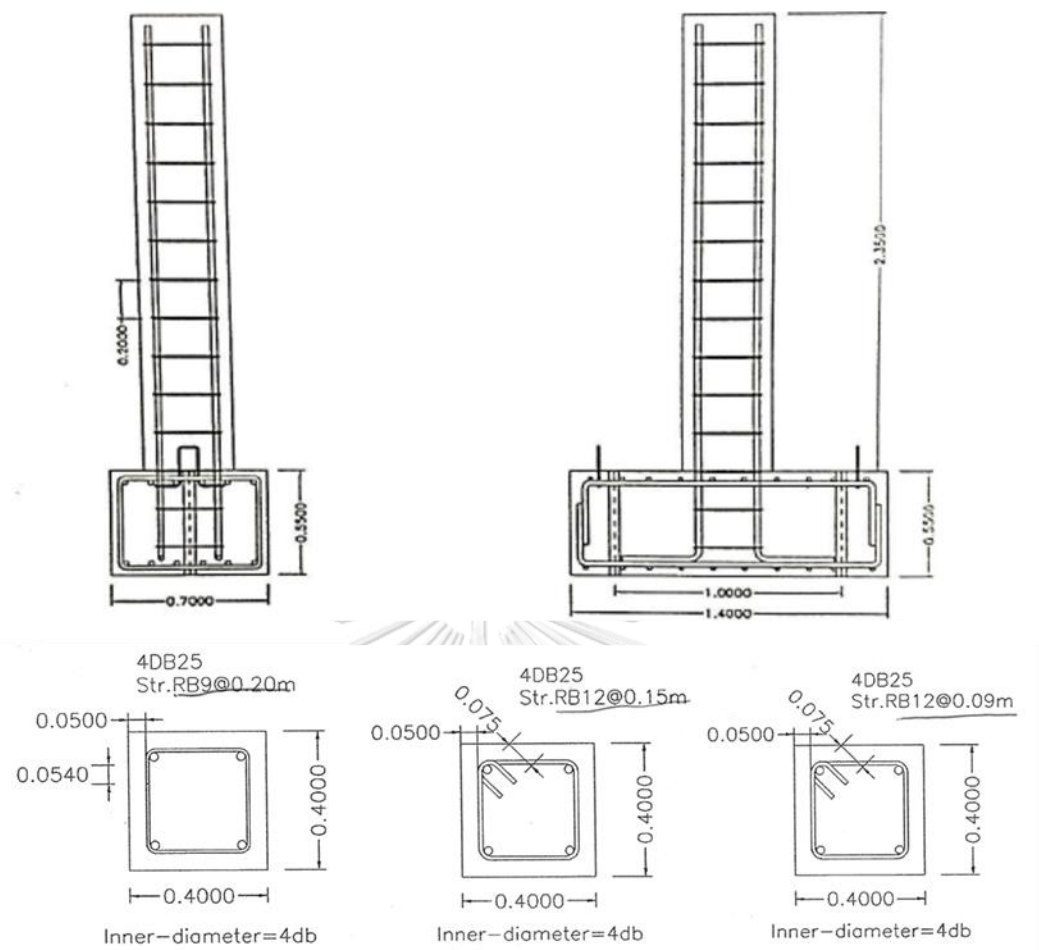
Figure 5.1 Column dimensions of the three columns (Warakorn, 2008)
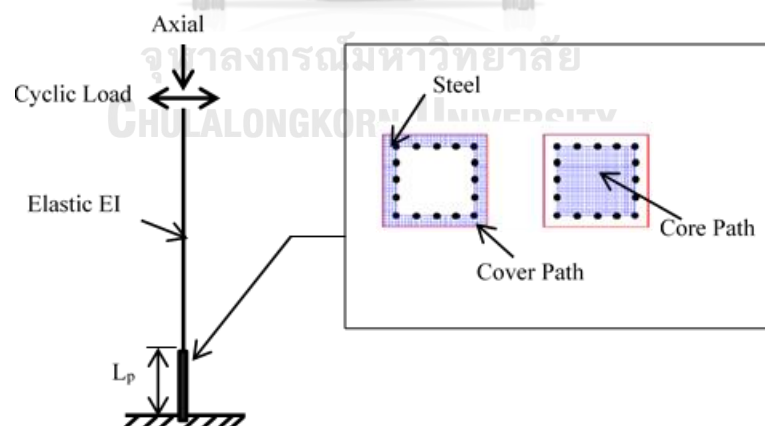
Figure 5.2 Lumped plasticity column model

After analyzing the columns in OpenSees, the hysteresis response of the three columns of the numerical results is compared with the experimental results. It was found that the hysteretic hoops from the analytical model were generally consistent with

the test results. The initial stiffness, maximum force and nonlinear flexural behaviors were accurately predicted. Experimental and analytical results for three specimens are shown in Figure 5.3.
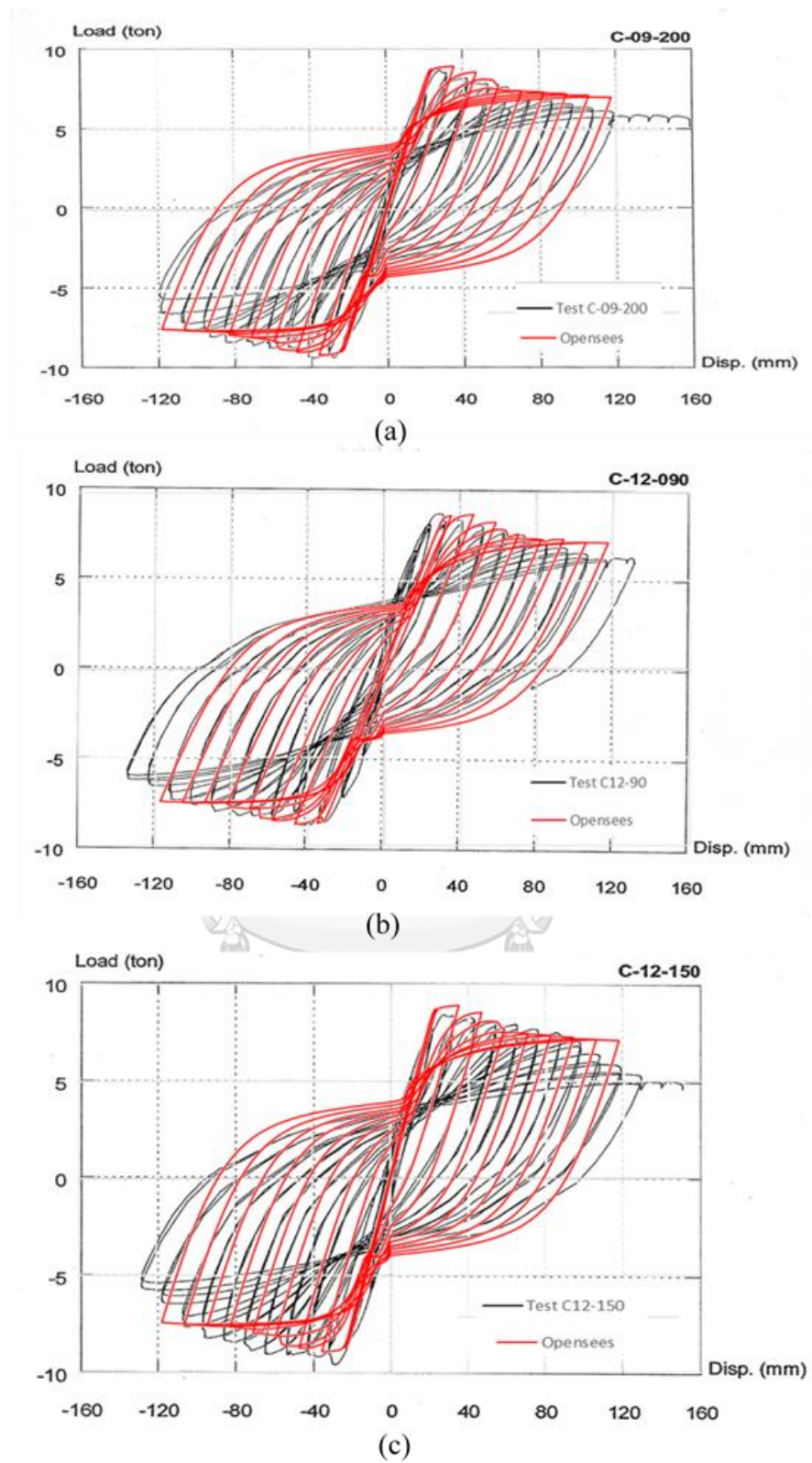
Figure 5.3 Comparison of experimental and analytical results of Warakorn 's test columns

5.3. Model of reinforced concrete components

The analysis of the reinforced concrete structure requires the accurate constitutive relationships of concrete and reinforcing steel especially for the fiber elements approach. The uniaxial constitutive relationships of both constitutive materials have to be assigned to each fiber element. In modelling the reinforced concrete columns, three uniaxial constitutive materials are needed to assign, such as unconfined concrete, confined concrete and longitudinal reinforcing steel.

5.3.1. Modelling of unconfined concrete

In all the columns modelling for CC, SC-200 and SC-100, the unconfined concrete fiber was assigned using the constitutive stress-strain relationships proposed by (Kent and Park, 1971) model. The Concrete01 material model in OpenSees was chosen to represent the Kant and Park material model. In uniaxial material model in OpenSees, concrete compressive strength at 28 days ($f_c^'$), concrete strain at maximum strength (ε_{co}), concrete crushing strength (f_{cu}) and concrete strain at crushing strength (ε_{cu}) need to be assigned. The ascending branch is represented by and ε_{co} by 0.002. The concrete crushing strength (f_{cu}) is represented by 20% of the maximum concrete strength and the concrete strain (ε_{cu}) is represented by the strain at crushing strength. The consecutive law for Kent and Park unconfined material model is demonstrated in Figure 5.4.
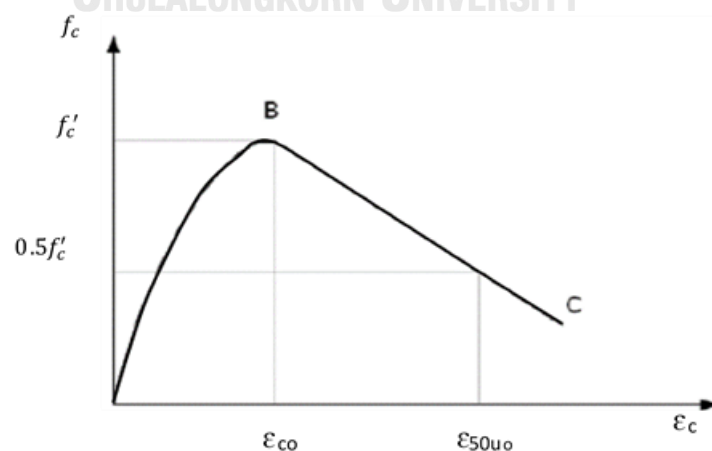
Figure 5.4 stress strain relationship of unconfined concrete (Kent and Park, 1971)

5.3.2. Modelling of confined concrete

(Mander et al., 1988) material model was used to represent the confined concrete model for CC, SC-200 and SC-100 columns' modelling. Concrete02 material was used to represent the (Mander et al., 1988) in OpenSees. The effective lateral confining stress for the square column section is calculated as,

$$f_l = k_e \rho_x f_y \quad , \quad f_l = k_e \rho_y f_y \tag{5-1}$$

$$\rho_x = \frac{nA_v}{sb_c} \quad , \quad \rho_y = \frac{nA_v}{sd_c} \tag{5-2}$$

$$k_e = \frac{\left(1 - \sum_{i=1}^{n} \frac{(w_i)^2}{6b_c d_c}\right)\left(1 - \frac{s-\phi}{2b_c}\right)\left(1 - \frac{s-\phi}{2d_c}\right)}{1 - \rho_{cc}} \quad ; \quad \rho_{cc} = \frac{nA_s}{b_c d_c} \tag{5-3}$$

where,

k_e = the confinement effectiveness coefficient

ρ_x , ρ_y = the confining steel volumetric ratio,

w_i = the clear distance between longitudinal bars

c = the clear cover, b_c is the horizontal spacing between centerlines of perimeter hoop

d_c = the vertical spacing between centerlines of perimeter of hoop

ρ_{cc} = the ratio of longitudinal reinforcements to the area of core section

A_s = the longitudinal reinforcement areas

A_v = the transverse reinforcement areas

n = the number of reinforcements

s = the vertical spacing between hoop

Ø = the diameter of transverse reinforcement

Concerning the strengthened confined concrete section with external steel-rod collars, some parameters need to be changed. Not only confinement ratio of the existing hoops but also the confinement ratio of the external steel rod collars needs to be considered. The confinement model for strengthened columns by (Montuori and Piluso, 2009), (Campione et al., 2017) is adopted to calculate the confinement

effectiveness coefficient for strengthened section (ke) and confining steel volumetric ratio for strengthened section (ρx, ρy). Model for identifying concrete confined by hoops and steel rod collars are shown in Figure 5.5
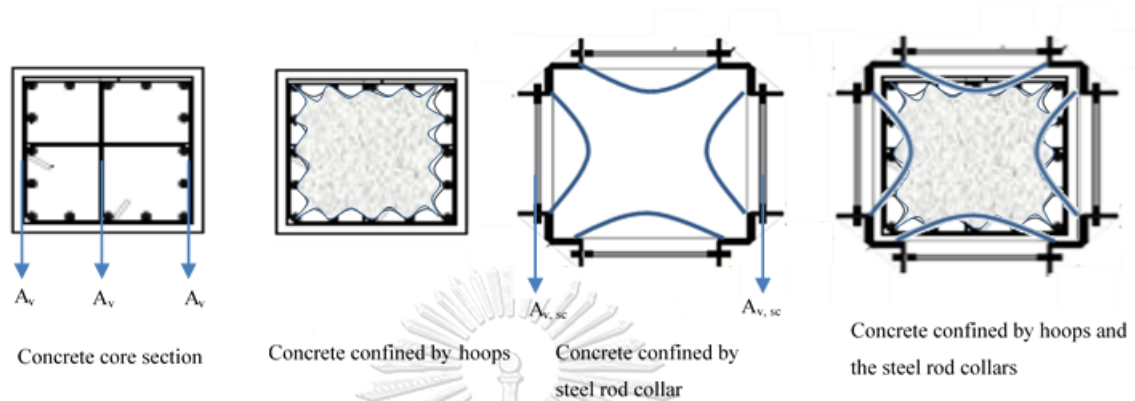
Figure 5.5 Model for identifying concrete confined by hoops and the steel rod collars

In particular, the yield strength of steel rods in strengthened section has to be assigned in place of steel yield strength in Equation (5-1) and the confining steel volumetric ratio of the steel-rod collars is calculated in Equation (5-4).

$$\rho_x = \frac{nA_{v,sc}}{sb} \quad , \quad \rho_y = \frac{nA_{v,sc}}{sd} \tag{5-4}$$

Then, the confinement effectiveness coefficient (k_e), confining steel volumetric ratio for confined by hoops and the steel rods collars (ρ_x , ρ_y) are described in Equation (5-5) and Equation (5-6).

$$k_e = \left(1 - \frac{s - \phi_{sc}}{2b}\right)\left(1 - \frac{s - \phi_{sc}}{2d}\right) \tag{5-5}$$

$$\rho_x = \frac{nA_v}{sb_c} + \frac{2A_{v,sc}}{sb} \quad , \quad \rho_y = \frac{nA_v}{sb_c} + \frac{2A_{v,sc}}{sd} \tag{5-6}$$

where,

b   = the width of the column section

d   = the depth of the column section,

Ø sc   = the diameter of external steel-rods

ρx, ρy = the confining steel volumetric ratio.

Then, the compressive strength of concrete (f_{cc}) and strain at maximum strength (ε_{cc}) and crushing strength (f_{cu}), concrete strain at crushing strength (ε_{cu}) are calculated following the (Mander et al., 1988) model. These values are assigned to the Concrete02 material model in OpenSees. The residual stress in the descending branch is considered at 20 % of f_{cc} defined by (Kent and Park, 1971) in order to relevant the real behaviour of the test columns.

$$f_{cc} = f_c' \left(2.254 \sqrt{1 + \frac{7.94 f_l}{f_c'}} - 2\frac{f_l}{f_c'} - 1.254 \right) \tag{5-7}$$

$$f_{ccu} = \frac{f_{cc}\left(\frac{\varepsilon_{ccu}}{\varepsilon_{cc}}\right) r}{r - 1 + \left(\frac{\varepsilon_{ccu}}{\varepsilon_{cc}}\right)^r} \quad ; \quad r = \frac{E_c}{E_c - E_{sec}} \quad ; \quad E_c = 5000\sqrt{f_c'} \quad ; \quad E_{sec} = \frac{f_{cc}}{\varepsilon_{cc}} \tag{5-8}$$

$$\varepsilon_{cc} = 0.002\left[1 + 5\left(\frac{f_{cc}}{f_c'} - 1\right)\right] \quad ; \quad \varepsilon_{ccu} = 0.004 + \frac{1.4\rho_{st} f_{yh} \varepsilon_{sm}}{f_{cc}} \tag{5-9}$$

where,

f_{cc} = the confined concrete strength

f_c' = the strength of unconfined concrete (compressive strength of the concrete)

f_l = the effective lateral confining stress

ρ_{st} = the confining steel volumetric ratio which are equal to $(\rho_x + \rho_y)$ for both

transverse reinforcement and steel cage rods

f_{yh} = the yield strength of transverse reinforcement

ε_{cc} = the confined concrete strain at maximum strength

ε_{ccu} = the confined concrete strain at crushing strength

ε_{sm} = the ultimate strain capacity of transverse reinforcement. Mander materl

model for confined concrete is shown in Figure 5.6 and concrete material properties

for tested columns CC, SC-200 and SC-100 is as shown in Table.5.2.
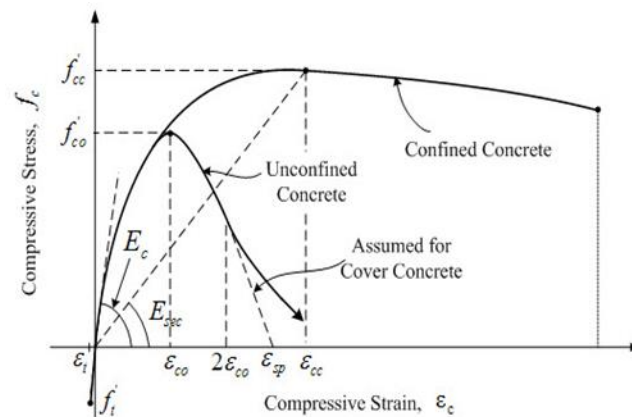
Figure 5.6 Stress strain relationship for confined concrete (Mander et al., 1988)

Table.5.2 Concrete material properties

Specimen	Materials	f_c' (Mpa)	ε_{cc}'	f_{cu}' (Mpa)	ε_{cu}'	λ	E_c
CC	Unconfined Concrete	31.5	0.002	0	0.0046	0.1	$5000\sqrt{f_c'}$
	Confined Concrete	32.7	0.0024	6.54	0.0086	0.1	$5000\sqrt{f_c'}$
SC-200	Unconfined Concrete	31.5	0.002	0	0.0046	0.1	$5000\sqrt{f_c'}$
	Confined Concrete	35.4	0.0032	7.08	0.0180	0.1	$5000\sqrt{f_c'}$
SC-100	Unconfined Concrete	31.5	0.002	0	0.0046	0.1	$5000\sqrt{f_c'}$
	Confined Concrete	37.9	0.004	7.58	0.0270	0.1	$5000\sqrt{f_c'}$

5.3.3. Modelling of reinforcing steel

The steel fiber was modeled by as uniaxial Giuffre-Menegotto-Pinto steel material with isotropic strain hardening, Steel02 material model in OpenSees was used to represent the Giuffre-Menegotto-Pinto steel material. For steel material model in OpenSees, yield strength of longitudinal steel (fy$_l$), initial elastic tangent (E$_0$), strain

hardening ratio (B_s), parameters to control the transition from elastic to plastic branches (R_0,R_1,R_2) and isotropic hardening parameters (a_1,a_2,a_3,a_4) are required to assign. Some parameters such as Ro, CR_1 and CR_2 were used as the recommended values from the OpenSees manual. Strain hardening ratio of longitudinal reinforcement (B_s) was the value of 0.01 (Huang and Kwon, 2015). In addition, the value of strain hardening ratio of 0.01 which was recommended in OpenSees uniaxial Material arguments. The value of steel yield strength was implemented from the tensile test of corresponding reinforcing steel. Concrete material properties and steel material properties for the specimens are presented in Table.5.3 and Giuffre-Menegotto-Pinto steel material is shown in Figure 5.7.
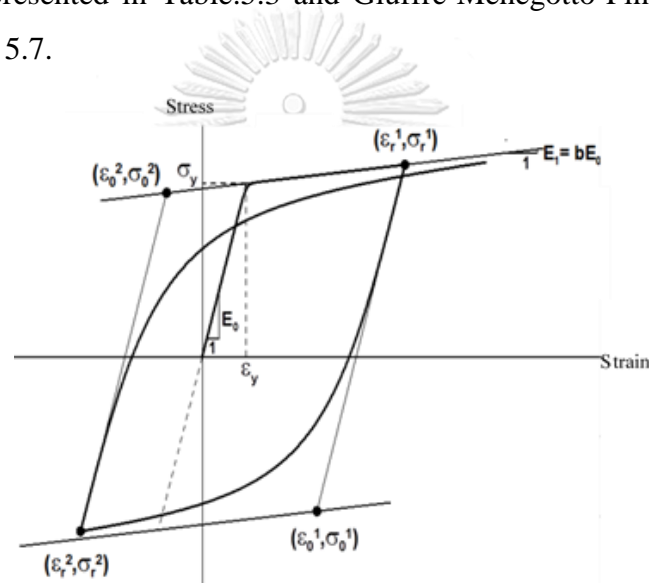
Figure 5.7 Giuffre-Menegotto-Pinto steel

Table.5.3 Steel material properties

CC, SC-100 and SC-200		f_{yl} (Mpa)	E_s (Mpa)	B_s	R_0	CR1	CR2
	Steel						
		514.85	200000	0.01	18	0.925	0.15

5.4. Structural Elements

In order to model the CC column, SC-200 and SC-100 columns, some structural elements are needed to consider in creating the forced-based beam column element model and lumped plasticity element model.

5.4.1 Rotational slip spring element

Contribution of the rotational slip was maintained at the elastic level to preserve the model uncertainty (K.Y. Liu et al., 2015). The elastic rotational stiffness recommended by Elwood and Eberhard was selected and the rotation stiffness K_{slip} was calculated as follows (Elwood and Eberhard, 2009).

$$K_{slip} = \frac{8\mu M_y}{d_b f_y \emptyset_y} \hspace{4cm} (5\text{-}10)$$

where,

d_b = the nominal diameter of the longitudinal reinforcement

f_{yl} = the yield strength of the longitudinal reinforcement

M_y = the yield moment

$\emptyset_y$ = the yield curvature

μ = the uniform bond stress along the embedded length.

The uniform bond stress suggested by the Elwood and Eberhard is $0.8\sqrt{f_c'}$. The yield moment and yield curvature were obtained from the moment curvature analysis of the column section using XTRACT program. The calculated value were simply assigned to the model and no calibration was done.

5.4.2 Shear spring element

A shear spring element was used to represent the behavior of CC column after the shear failure was detected. The shear spring was defined with the limit state material and the shear limit curve. The spring element are created using zero length element of OpenSees. To define the shear limit curve, it is important to define the slope of the third branch in the post failure backbone curve (K_{deg}) as shown in Figure 5.8. When the total response of the RC member reach the shear limit curve for the first time, the shear failure is detected and the backbone of the shear spring is redefined to include the shear degrading slope (K_{deg}) (Elwood, 2004).
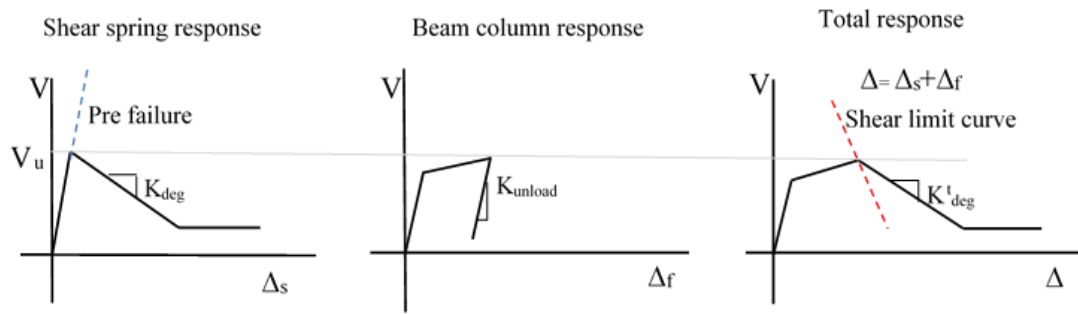
Figure 5.8 Shear spring with shear limit curve

When shear failure is detected, based on the intersection of the total response and the shear limit curve, the degrading slope for the total response, K^t_{deg} is estimated as follow

$$K^t_{deg} = \frac{V_u}{\Delta_a - \Delta_s} \tag{5-11}$$

where,

V_u = the ultimate capacity of the RC column

Δ_s = the calculated displacement at shear failure

Δ_a = the calculated displacement at axial failure

In this study, no axial failure occurred in the CC column. Therefore, displacement at axial failure was neglected. Drift capacity model proposed by Elwood and moehle (2005) was used to define the displacement at shear failure as follows.

$$\frac{\Delta_s}{L} = \frac{3}{100} + 4\rho_v - \frac{1}{40}\frac{v}{\sqrt{f'_c}} - \frac{1}{40}\frac{P}{A_g f'_c} \geq \frac{1}{100} \text{ (Mpa)} \tag{5-12}$$

where,

$\dfrac{\Delta_s}{L}$ = drift ratio at shear failure

ρ_v = transverse reinforcement ratio

v = nominal shear stress

To calculate the $K^t_{deg,}$ the ultimate shear capacity V_u of the column was calculated first. The shear capacity of the column was calculated by using (ACI 2011).

$$V_u = V_c + V_s \tag{5-13}$$

where,

V_c = the concrete contribution to shear strength

V_s = the steel contribution to shear strength.

Concrete contribution to shear was calculated as

$$V_c = 0.166\sqrt{f_c'}\left(1 + \frac{P}{13.8A_g}\right)bd \quad \text{(Mpa)} \quad (5\text{-}14)$$

where,

f_c' = the concrete compressive strength

A_g = the gross cross sectional area

P = the axial load

b = the width of the column section

d = the depth of the column section.

Steel contribution to shear strength V_s is calculated as

$$V_s = \frac{A_v f_{yh} d}{s} \quad \text{(Mpa)} \quad (5\text{-}15)$$

where ,

A_s = area of transverse reinforcement

f_{yh} = the yield strength of transverse reinforcement

s = the spacing of the transverse reinforcement

Since the shear spring and the beam column element are in series, the total flexibility is equal to the sum of the flexibilities of shear spring and the beam-column element. Hence, K_{deg} can be determined as follows,

$$K_{deg} = \left(\frac{1}{K_{deg}^t} - \frac{1}{K_{unload}}\right)^{-1} \quad (5\text{-}16)$$

where,

K_{unload} = the unloading stiffness of the beam column element

It depends on the boundary conditions of the column. In this study, for a cantilever column, K_{unload} is estimated as follows.

$$K_{unload} = \frac{3EI_{eff}}{L^3} \quad (5\text{-}17)$$

where,

EI$_{eff}$ = the effective flexural stiffness of RC column

L = the height of the RC column

Note that unloading stiffness K$_{unload}$ must be provided as the input parameter for the limit state material. Here, effective stiffness of the RC columns (EI$_{eff}$) is used 0.2 EI$_g$ which is recommended by (Elwood and Eberhard, 2009).

5.4.3 Plastic hinge length

The inelastic response of the element is a function of the plastic hinge length and the properties of the cross sections. (Huang and Kwon, 2015),(Bae and Bayrak, 2008) systematically evaluated the performance of different expressions and proposed a new analytical approach to estimate plastic hinge length. Nonlinear behaviour of the beam column element is confined to the plastic hinge length with a length lp in the lumped plasticity model. The axial load ratio, span depth ratio and the amount of longitudinal reinforcement are the main parameters in estimating the length of plastic hinge as follow.

$$\frac{L_p}{d} = \left[0.3\frac{P}{P_0} + 3\frac{A_s}{A_g} - 0.1 \right]\frac{L}{d} + 0.25 \geq 0.25 \quad (5\text{-}18)$$

$$P_0 = 0.85f_c'(A_g - A_s) + f_{yl}A_s \quad (5\text{-}19)$$

where,

A_s = the sectional area of the longitudinal reinforcement

L = the length of the column

d = the column section depth

P = the axial load

P$_o$ = the nominal axial load capacity

5.5. Modelling of Reinforced Concrete Columns

The specimen CC was the shear critical column and, therefore, forced based beam column model with shear spring was utilized to capture the shear failure of the column. Three elements such as a fiber beam column element, the rotational slip spring element and shear spring element were needed to model the shear critical column in OpenSees. Shear spring element was defined by using the limit state material with shear limit curve (Mazzoni et al., 2006). To capture the shear strength degradation, the shear spring with the rotational slip spring element were used in the zero length element at the end of the column.

5.5.1. Force based fiber beam column element

The column element in the CC column was modelled using the force-based fiber beam column element. The numerical element consists of a two-dimensional nonlinear beam-column with fiber section located at the integration points. Each section is subdivided into a number of fibers where each fiber is under uniaxial state of stress. In modeling the fiber section of the column, five integration points were used to efficiently compare the global response of the RC columns. Each section at the integration point was discretized into 20 core fibers and 20 cover fibers in both local x and z directions. The fiber section discretization imposes much less influence than the number of intermigration points on predicted global responses in OS-FBBC elements. Significant errors are only produced when very crude fiber meshes are used (Huang and Kwon, 2015). The CC specimen was modelled as four node element and each node has three degrees of freedom. Node 1 was fully fixed and node 4 was free end. The numerical element of the CC specimen was illustrated in Figure 5.9.
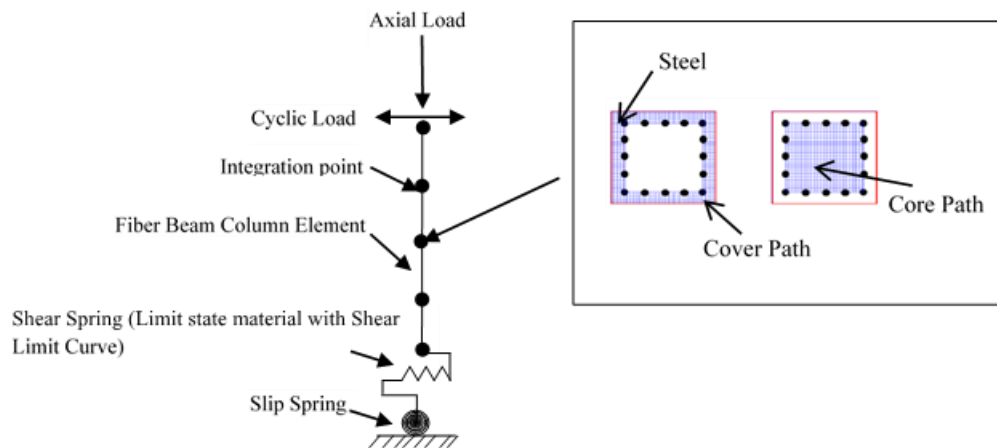
Figure 5.9 Numerical model for shear critical column

5.5.2. Numerical model of strengthened columns, SC-200 and SC-100

The strengthened columns SC-200 and SC-100 were modelled numerically by using the elastic element with plastic hinge model as shown in Figure 5.10. There were two reasons to choose the lumped plastic model for SC-100 and SC-200. The first one is that the strengthened column SC-100 and SC-200 were the flexural failure mode according to the test result, and so shear spring element was not included in the numerical model to capture the shear failure. The second one is that one of the researchers concluded for the numerical analysis of the flexural column that the lumped plasticity column model shows better performance, especially on the initial stiffness which will directly or indirectly affect the calculated peak force, absorbed energy as well as backbone (Huang, 2012). The elastic element with plastic hinge element is based on an integration method proposed by (Scott and Fenves, 2006). Nonlinear behavior of beam column element is confined to an assigned plastic hinge with a length Lp..The curvature distribution is linear above the plastic hinge and the curvature is calculated within the plastic hinge with moment curvature analysis of the force-based beam-column element. Plastic rotations are directly related to plastic curvature through the specified plastic hinge lengths. Each section at the integration point was discretized into 20 core fibers and 20 cover fibers in both local x and z directions. Node 1 was fully fixed and node 4 was free end.
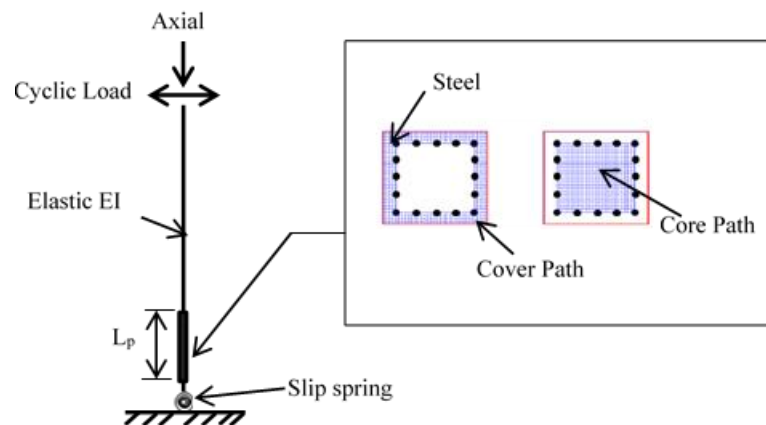
Figure 5.10 Lumped plasticity column model

5.6. Results of Numerical Analysis

This section shows the analysis result of CC, SC-200 and SC-100 columns and then compared the hysteresis behaviour was compared with the test results.

5.6.1. Analysis result of CC column

The specimen CC is the shear critical column, which is modelled using limit state material with shear limit curve. The limit state material with the shear limit curve model can approximately detect the shear failure surface of the shear critical column. During the analysis, the shear failure was well detected by the shear limit curve through the shear spring in the mode after the maximum lateral load reached. The shear behaviour is lumped on the spring. The shear failure was occurred before steel yielding during the analysis. Since CC column is shear critical column, the flexural contribution from fiber beam column element is very small. Therefore, concrete and reinforcing steel material model are still in the elastic region. However, the load deflection curve of the CC column is more interested in more general than the stress strain curve of materials in the analysis. Stress strain relationship of unconfined, confined and longitudinal reinforcement of CC column is shown in Figure 5.11. The analysis result of load displacement relationship is shown in Figure 5.12. When the analysis result and test result of the load displacement curve are compared, the strength degradation after the peak load of the model agrees with the test result. Therefore, it is seen that the behavior of the shear critical column (Specimen CC) can be captured well by the model with the

rotational slip spring and the shear spring. Even though the initial stiffness was a sight different with the experimental results, the post failure behaviour is well captured by the shear limit curve assigned in the shear spring. Comparison of load displacement relationship is shown in Figure 5.13.

(a)

(b)
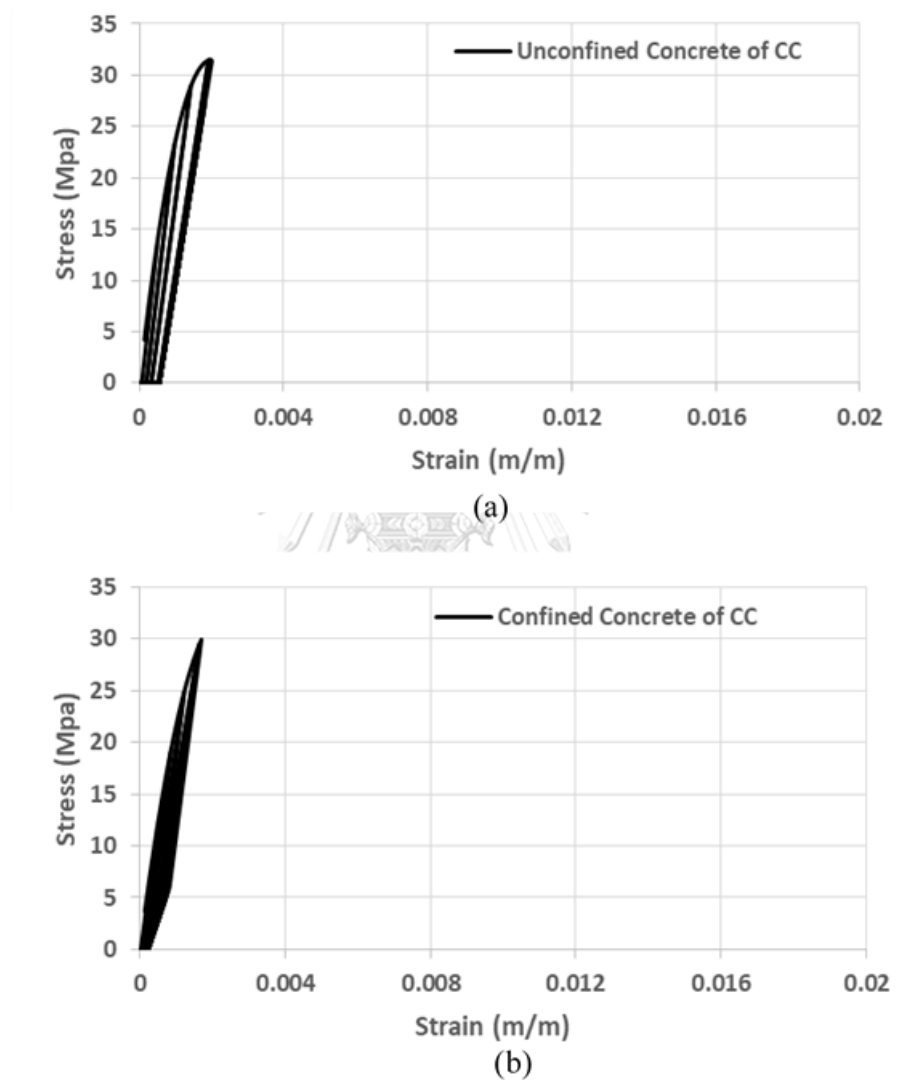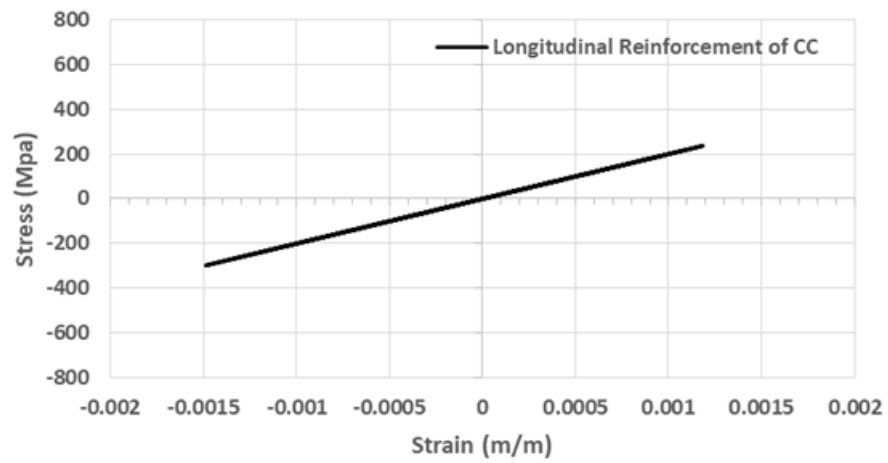
(c)

Figure 5.11 Stress-strain relationship of CC (a) Unconfined Concrete

(b) Confined Concrete (c) Longitudinal reinforcement
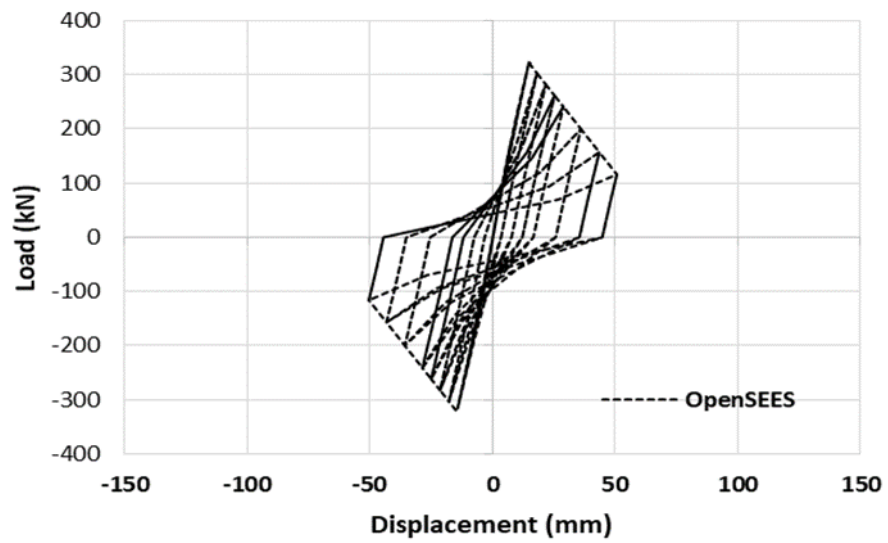
Figure 5.12 Analysis result of load displacement relationship of CC
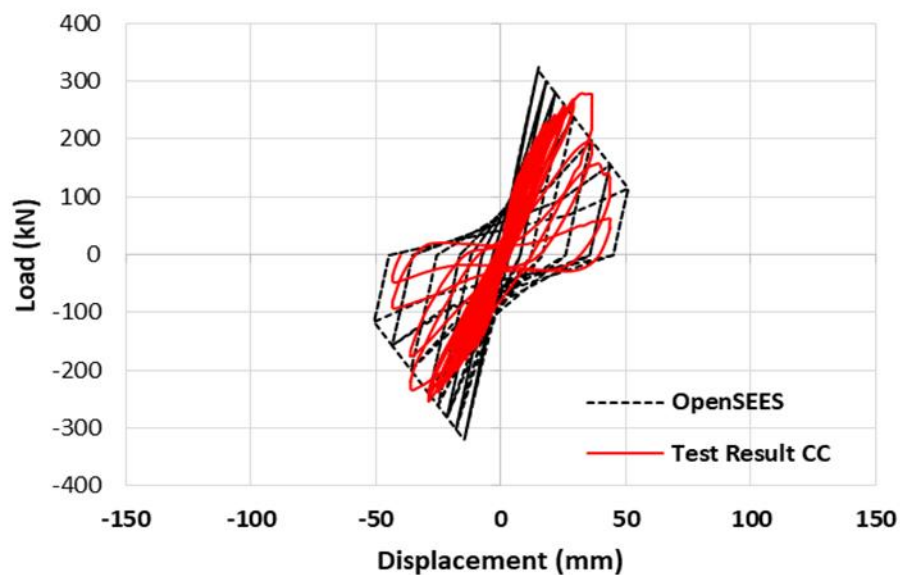
Figure 5.13 Comparison of analysis result and test result of CC

5.6.2. Analysis result of Strengthened column SC-200 and SC-100

The strengthened columns SC-200 and SC-100 were modelled numerically by using the elastic element with plastic hinge model. There were two reasons to choose the lumped plastic model for SC-200 and SC-100. The first one is that strengthened column SC-200 and SC-100 were the flexural failure mode according to the test result, and so the shear spring element was not included in the numerical model to capture the shear failure. The second one is that the numerical analysis of the lumped plasticity column model for flexural column showed better performance according to the literature. For the strengthened specimens which fail in flexure, the load-displacement relation from the analysis matches satisfactorily with that from the experiment. The fiber model can represent the actual behavior of the columns strengthened by the steel-rod collars. The confinement from the column ties and the steel-rod collars should be combined as used in this model to take into account the enhancement in confinement. Note that the hysteresis loops after the peak load which is mainly governed by steel reinforcement are different between the analysis and experiment. The improvement can be further investigated, one of which is the buckling of the longitudinal reinforcement.

Stress strain relationship of material model for SC-200 is shown in Figure 5.14. The analysis result of the load displacement relationship of SC-200 is shown in Figure 5.15. Comparison of load displacement relationship is shown in Figure 5.16. Stress strain relationship of material model for SC-100 is shown in Figure 5.17. The analysis result of the load displacement relationship of SC-200 is shown in Figure 5.18. Comparison of load displacement relationship is shown in Figure 5.19

Figure 5.14 Stress-strain relationship of SC-200 (a) Unconfined Concrete

(b) Confined Concrete (c) Longitudinal reinforcement

Figure 5.15 Analysis result of load displacement relationship of SC-200

Figure 5.16 Comparison of analysis result and test result of SC-200

Figure 5.17 Stress-strain relationship of SC-100 (a) Unconfined Concrete

(b) Confined Concrete (c) Longitudinal reinforcement

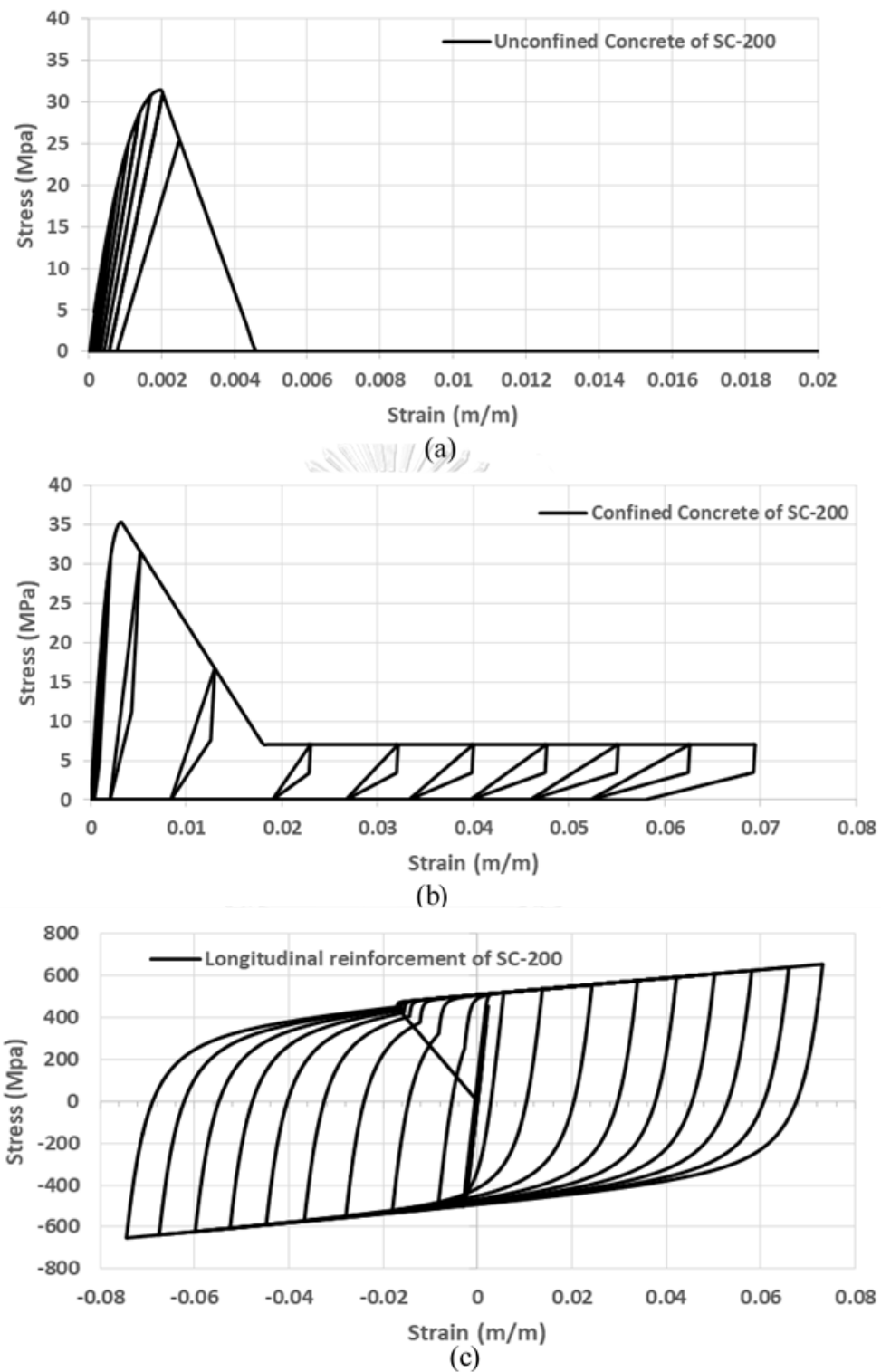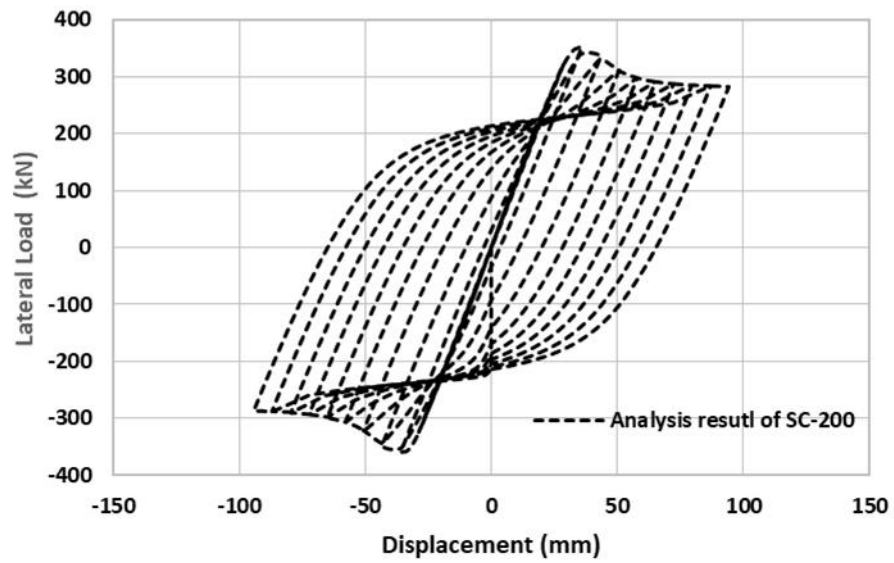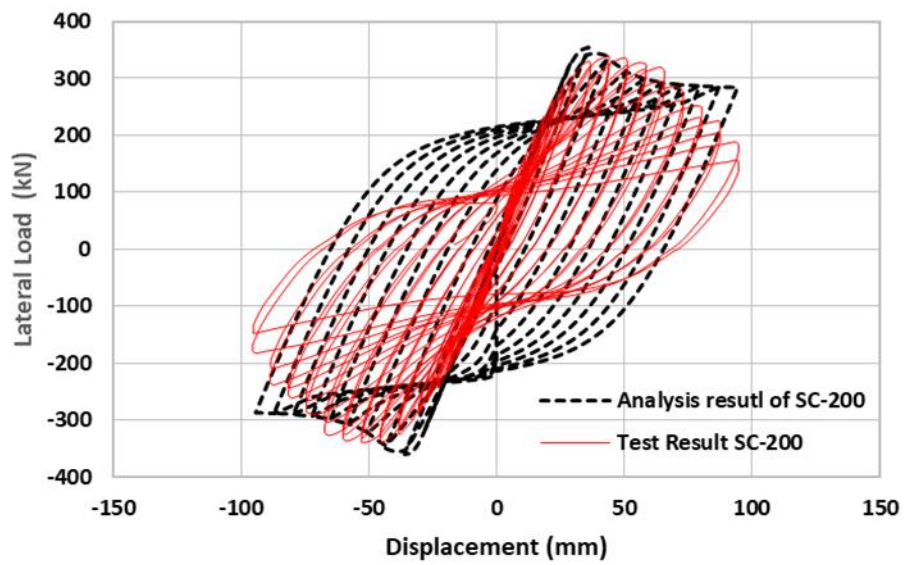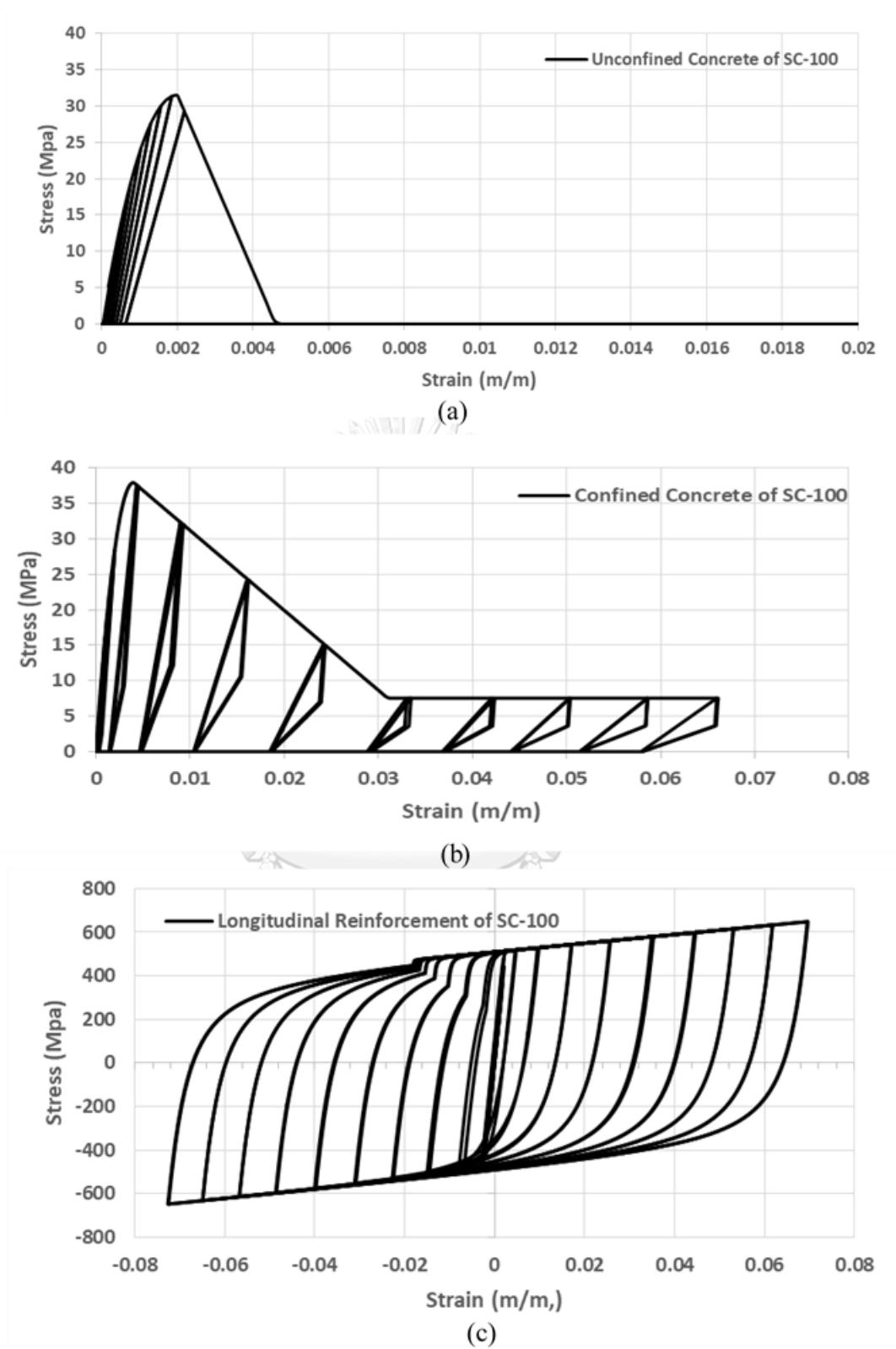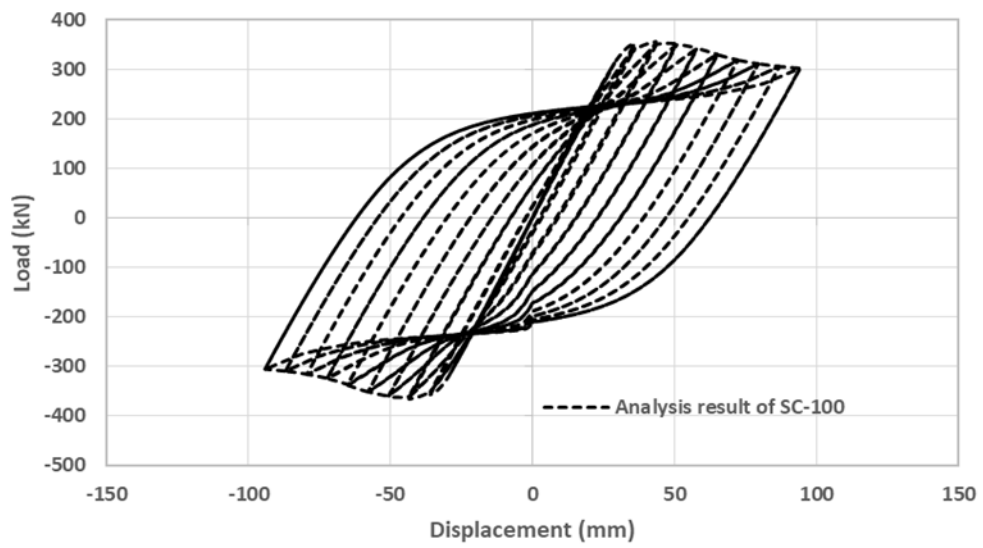Figure 5.18 Analysis result of load displacement relationship of SC-100
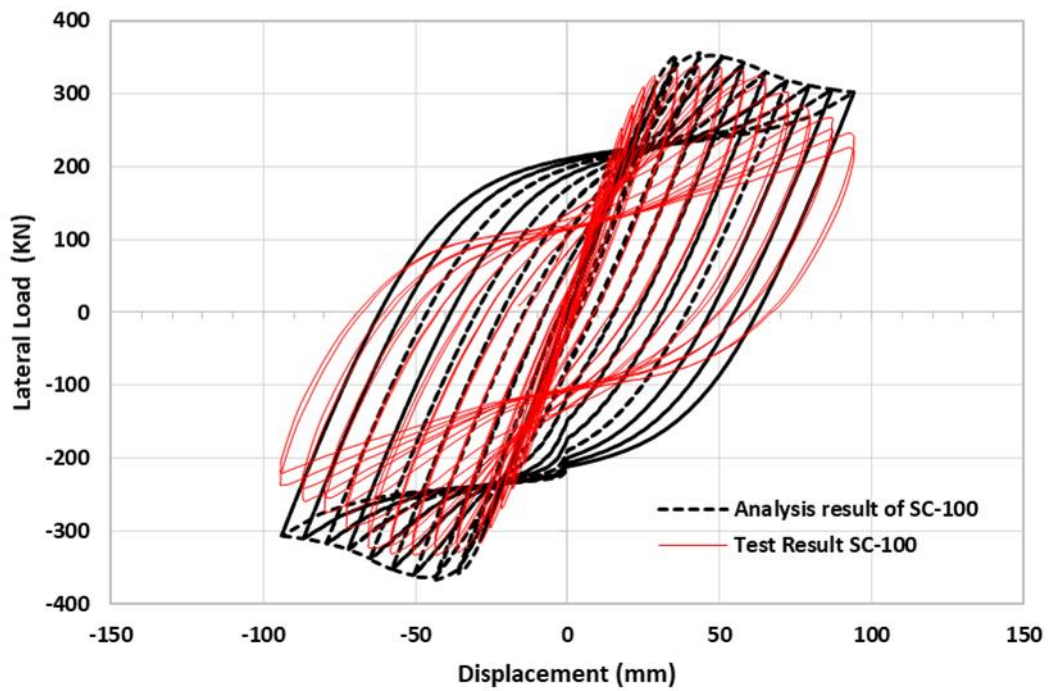
Figure 5.19 Comparison of analysis result and test result of SC-100

CHAPTER 6

CONCLUSIONS AND RECOMMENDATION

6.1. Conclusions

In this study, the effectiveness of steel-rod collars in the enhancement of shear critical columns is investigated by a series of experiment and analysis. The following conclusions are drawn based on the results of the experiment and analysis:

(1) The test on the controlled shear critical column (Specimen CC) shows that the column experiences the premature shear failure after reaching the maximum load. Shear cracks develop rapidly during strength degradation.

(2) Two columns with the same detailing are then strengthened by the steel-rod collars with different amounts of steel-rod collars (Specimens SC-200 and SC-100) to clarify the effectiveness of the steel-rod collars. Both strengthened specimens fail at the drift ratios larger than 5%, which are more than twice the drift capacity of the controlled specimen. After testing the column under constant axial load and cyclic loading, the unstrengthened column fails in shear while the strengthened columns fail in flexure and they have an increase in the lateral load capacity and the ductility. The percent increase in lateral load capacity and ductility ratio of SC-200 was 18 % and 59% than that of CC column, respectively. The increase in lateral load capacity and ductility ratio of SC-100 was 16% and 69% than that of CC column, respectively. Therefore, the lateral load capacities of the strengthened specimens are about 20% larger than that of the controlled specimen, respectively. The strengthened specimens have the stable hysteretic behaviors, higher ductility factors and higher energy dissipation than the unstrengthened column.

(3) Strains and shear deformations are also monitored during the test. The presence of steel-rod collars helps reduce the shear demand in the column ties by sharing shear forces as seen from the measured strains in the steel-rod collars because strain in the steel-rod did not reach the yield. Shear deformations can be significantly reduced and finally the strengthened specimens fail in flexure.

(4) Numerical analysis of the shear critical column (Specimen CC) shows that its

behavior can be captured well by the analytical model with the rotational slip spring and the shear spring, even though the initial stiffness in the numerical results is a slight difference in the test results.

(5) Numerical analysis of strengthening columns is also performed using the lumped plasticity fiber model. The fiber model can represent the actual behavior of the columns strengthened by the steel-rod collars. The confinement from the column ties and the steel-rod collars is combined as used in this model to take into account the enhancement in confinement. The initial stiffness, maximum load and backbone bone behaviour are quite consistent with the test results. Note that the hysteresis loops after the peak load which is mainly governed by steel reinforcement are different between the analysis and experiment.

In summary, strengthening the columns by steel-rod collar method is an effective method according to the experimental research of study. The failure behavior changes the shear dominated column to flexural dominated column after strengthening the column.

6.2. Recommendation for further study

According to the experimental results and analytical results, further study may involve the following things.

(1) Three specimens were tested in this study. Therefore, more experimental studies with various diameters of steel-rod and various sizes of steel collars should be done to prove strongly with much confirmation.

(2) The proposed steel caging method should be compared with other strengthening methods experimentally.

(3) The masonry infilled frame with shear deficient columns which are strengthened by steel-rod collars should be investigated experimentally in order to study the behaviour of the infilled masonry wall after strengthening the shear deficient columns.

(4) Finally, seismic analysis of the reinforced concrete building with and without masonry infilled wall with shear deficient columns which are strengthened by steel-rod collars should be studied.

REFERENCES

REFERENCES

Abedi, et al. (2010). Numerical study on the seismic retrofitting of reinforced concrete columns using rectified steel jackets. Asian *Journal of Civil Engineering (Building and Housing)*, 11(1).

Aboutaha, et al. (1999). Rehabilitation of shear critical concrete columns by use of rectangular steel jackets. *Structural Journal*, 96(1), 68-78.

Aci (2011). American Concrete Institute and International Organization for Standardization (2011). *Building code requirements for structural concrete (ACI 318-11) and commentary.*

Adam, et al. (2008). Experimental study of beam–column joints in axially loaded RC columns strengthened by steel angles and strips. *Steel Compos Struct*, 8(4), 329-342.

Adam, et al. (2007). Behaviour of axially loaded RC columns strengthened by steel angles and strips. *Steel and composite structures*, 7(5), 405.

Bae and Bayrak. (2008). Plastic hinge length of reinforced concrete columns. *ACI Structural Journal*, 105(3), 290.

Belal, et al. (2015). Behavior of reinforced concrete columns strengthened by steel jacket. *HBRC Journal*, 11(2), 201-212.

Berry and Eberhard. (2006). *Performance modeling strategies for modern reinforced concrete bridge columns* (Vol. 67).

Caltrans. (2011). *California Amendments to the AASHTO LRFD Bridge Design Specifications*. 4thEdition, California Department of Transportation, Sacramento, CA.

Campione, et al. (2017). Frictional effects in structural behavior of no-end-connected steel-jacketed RC columns: experimental results and new approaches to model numerical and analytical response. *Journal of Structural Engineering*, 143(8), 04017070.

Chai, et al. (1994). Analytical model for steel-jacketed RC circular bridge columns. *Journal of Structural Engineering*, 120(8), 2358-2376.

Chaiyapat. (2007). A survey configuration irregularities in typical multi-story concrete buildings in Thailand. *Master Thesis, Asian Institute of Technology, School of Engineering and Technology.*

Choi, et al. (2010). Behavior of Reinforced Concrete Columns Confined by New Steel-Jacketing Method. *ACI Structural Journal*, 107(6).

Choi, et al. (2013). Seismic performance of circular RC columns retrofitted with prefabricated steel wrapping jackets. *Magazine of Concrete Research*, 65(23), 1429-1440.

Del Vecchio, et al. (2013). Validation of numerical models for RC columns subjected to cyclic load. *COMPDYN*.

Elsamny, et al. (2013). Experimental study of eccentrically loaded columns strengthened using a steel jacketing technique. World Academy of Science, Engineering and Technology, *International Journal of Civil, Environmental, Structural, Construction and Architectural Engineering*, 7(12), 900-907.

Elwood. (2004). Modelling failures in existing reinforced concrete columns. *Canadian Journal of Civil Engineering*, 31(5), 846-859.

Elwood and Eberhard. (2009). Effective Stiffness of Reinforced Concrete Columns. *ACI Structural Journal*, 106(4).

Ghobarah, et al. (1997). Rehabilitation of reinforced concrete columns using corrugated steel jacketing. *Journal of Earthquake Engineering*, 1(04), 651-673.

Griffith, et al. (2005). Behaviour of steel plated RC columns subject to lateral loading. *Advances in Structural Engineering*, 8(4), 333-347.

Huang. (2012). Applicability criteria of fiber-section elements for the modelling of RC columns subjected to cyclic loading. *University of Toronto*.

Huang and Kwon. (2015). Numerical models of RC elements and their impacts on seismic performance assessment. *Earthquake Engineering & Structural Dynamics*, 44(2), 283-298.

Hussain and Driver. (2005). Experimental investigation of external confinement of reinforced concrete columns by hollow structural section collars. *ACI Structural Journal*, 102(2), 242.

Jsce. (2007). *Standard specification for design of concrete structures, structure performance verification*.

Kent and Park. (1971). Flexural members with confined concrete. *Journal of the Structural Division*.

Lin, et al. (2010). Seismic steel jacketing of rectangular RC bridge columns for the mitigation of lap-splice failures. *Earthquake Engineering & Structural Dynamics, 39(15)*, 1687-1710.

Liu, et al. (2011). Experimental Study on Short Concrete Columns with External Steel Collars. *ACI Structural Journal*, 108(3).

Liu, et al. (2015). Composed analytical models for seismic assessment of reinforced concrete bridge columns. *Earthquake Engineering & Structural Dynamics*, 44(2), 265-281.

Mander, et al. (1988). Theoretical stress-strain model for confined concrete. Journal of Structural Engineering, 114(8), 1804-1826.

Masri and Goel. (1996). Seismic design and testing of an RC slab-column frame strengthened by steel bracing. *Earthquake Spectra*, 12(4), 645-666.

Mazzoni, et al. (2006). OpenSees command language manual. *Pacific Earthquake Engineering Research (PEER) Center*, 264.

Montuori and Piluso. (2009). Reinforced concrete columns strengthened with angles and battens subjected to eccentric load. *Engineering Structures*, 31(2), 539-550.

Nagaprasad, et al. (2009). Seismic strengthening of RC columns using external steel cage. *Earthquake Engineering & Structural Dynamics*, 38(14), 1563-1586.

Park. (1988). Ductility evaluation from laboratory and analytical testing. Paper presented at the *Proceedings of the 9th world conference on earthquake engineering, Tokyo-Kyoto*, Japan.

Paulay and Priestley. (1992). Seismic design of reinforced concrete and masonry buildings.

Priestley, et al. (1994). Steel jacket retrofitting of reinforced concrete bridge columns for enhanced shear strength--Part 2: Test results and comparison with theory. *Structural Journal*, 91(5), 537-551.

Priestley, et al. (1994a). Seismic shear strength of reinforced concrete columns. *Journal of Structural Engineering*, 120(8), 2310-2329.

Rodrigues, et al. (2016). Numerical modelling of RC strengthened columns under biaxial loading. *Innovative Infrastructure Solutions*, 1(1), 6.

Scott and Fenves. (2006). Plastic hinge integration methods for force-based beam–column elements. *Journal of Structural Engineering*, 132(2), 244-252.

Sezen and Moehle. (2004). Shear strength model for lightly reinforced concrete columns. *Journal of Structural Engineering*, 130(11), 1692-1703.

Sheikh, et al. (1994). Confinement of high-strength concrete columns. *ACI Structural Journal*, 91, 100-100.

Suesuttajit,C. (2007). A survey configuration irregularities in typical multi-story concrete buildings in Thailand. *Master Thesis, Asian Institute of Technology, School of Engineering and Technology.*

Tanaka. (1990). Effect of lateral confining reinforcement on the ductile behaviour of reinforced concrete columns.

Tarabia and Albakry. (2014). Strengthening of RC columns by steel angles and strips. Alexandria *Engineering Journal*, 53(3), 615-626.

Tsai and Lin. (2002). Seismic jacketing of RC columns for enhanced axial load carrying performance. *Journal of the Chinese Institute of Engineers*, 25(4), 389-402.

Wang and Oh-Sung. (2014). Numerical study on flexural shear critical RC columns. *Second European Conference on Earthquake Engineering*

Wang and Su. (2012). Experimental investigation of preloaded RC columns strengthened with precambered steel plates under eccentric compression loading. *Advances in Structural Engineering*, 15(8), 1253-1264.

Wang, et al. (2017). Seismic behavior of preloaded rectangular RC columns strengthened with precambered steel plates under high axial load ratios. *Engineering Structures*, 152, 683-697.

Warakorn. (2008). Seismic Performance of reinforced concrete bridge columns in Thailand under cyclic loading. Ph.D. *Thesis,Dept. of Civil Engineering, Chulalongkorn University, Bangkok, Thailand.*

Xiao and Martirossyan. (1998). Seismic performance of high-strength concrete columns. *Journal of Structural Engineering*, 124(3), 241-251.

Xiao and Wu. (2003). Retrofit of reinforced concrete columns using partially stiffened steel jackets. *Journal of Structural Engineering*, 129(6), 725-732.

Ye, et al. (2002). Shear strength of reinforced concrete columns strengthened with carbon-fiber-reinforced plastic sheet. *Journal of Structural Engineering*, 128(12), 1527-1534.

VITA

NAME   Mrs. PHAWE SUIT THEINT

DATE OF BIRTH

PLACE OF BIRTH   Myeikthilar, Mandalay Division, Myanmar

INSTITUTIONS
ATTENDED
HOME ADDRESS   Mandalay,Myanmar